BOUNDARY LAYERS IN GEOPHYSICAL VORTICES

AND RELATED FLOWS

by

LANCE BODE

Thesis submitted for the degree of

Doctor of Philosophy

of the University of Edinburgh

University of Edinburgh, 1973.

CONTENTS

ACKNOWLEDGEMENTS

I wish to thank most sincerely my supervisor, Dr R.K. Smith, for the great amount of help and encouragement he has provided in the course of this work, and Dr L.M. Leslie for his invaluable assistance, particularly in the preparation of Chapter 3. I wish also to record my gratitude to Professor B.R. Morton at Monash University, and Professor A.G. Mackie at Edinburgh University, for the hospitality they and their departments have accorded me, and further, to Queensland University for their financial assistance in the form of a Foundation Travelling Scholarship. Finally, I must thank Mrs J. Speed for her patience and diligence in the typing of this thesis.

Chapter 1

A discussion of approximate methods for hurricane boundary layer calculations.

ABSTRACT

This chapter is basically a review and assessment of various approximate methods which have been developed in order to calculate the flow in the surface boundary layer of a hurricane. In particular we are concerned with two vertically integrated treatments - the momentum integral method of Smith and the Galerkin method of George. Also discussed in some detail, are the modified Oseén method of Carrier and the related work of Belcher, Burggraf and Stewartson, who investigate boundary layer flow on a flat disk under an imposed vortex.

It is demonstrated that there are certain basic defects in both the Galerkin and Oseén methods, which make them unsuitable for the treatment of hurricane boundary layers. By means of a regular perturbation analysis in the region of low Rossby number, additional support is lent to the use of the momentum integral method, although it is concluded that further work may be needed to give a more definitive answer to the question of its overall applicability.

1. Introduction

The principal aim of the work presented in this chapter is to investigate various methods which have appeared in the literature, for the description of motion in the frictional surface boundary layer of a hurricane or tropical cyclone. In particular, we shall consider in some detail, two different methods which are essentially vertically integrated treatments of the problem. The first is the momentum integral method of Smith (1968), which we shall henceforth denote by S, while the second is the method of weighted residuals, or Galerkin's method, introduced by Carrier and his co-workers (e.g., George 1970). The motive behind the development of the latter treatment is that its authors believed it would be a more accurate approximate method for solving the boundary layer equations associated with the flow, than the previously mentioned momentum integral method, which uses Ekman velocity profiles to model the vertical structure of the boundary layer flow.

The importance of the boundary layer in the overall description of hurricane-like flows has long been recognised, and has been discussed by a great many authors. In order to understand more fully the processes involved, we must firstly outline the basic features of a hurricane as a whole. Figure 1 is a schematical picture (as used in S) of the principal regions of a mature hurricane. The region which we shall be considering in detail is the narrow inflow region where the effects of friction are important, and whose height is of the order of a kilometre. The main vortex region where the swirling velocities are largest, has a height of the order of 10km, a radial extent of the order of 100km, and is a region of intense cumulus convection.

Other features include the well known eye, which is a comparatively calm, cloudless region around the axis of the storm where there is a slight downflow of air observed. Near the tropopause is the outflow region from the main vortex. Naturally the system is much more complicated than this simple picture would suggest; a more comprehensive description may be found in various publications, for instance those of Yanai (1964), Gray (1966) and Palmén and Newton (1969).

For purposes of the present study, we assume that the hurricane vortex can be represented by a steady axisymmetric inviscid vortex in the rotating frame of the earth, with the swirl (azimuthal) velocity as the sole horizontal velocity component. We refer to this as the outer flow. With this assumption of an axisymmetric vortex, we have neglected implicitly two basic properties of hurricanes: firstly, the Coriolis parameter f is assumed constant, whereas over the extent of the hurricane, f will vary considerably, thereby inducing asymmetry in the vortex motion; secondly, the vortex is assumed to be stationary, yet in fact the hurricane is only part of a much larger-scale atmospheric system, an essentially non-uniform flow which will also be important in producing asymmetry. Nevertheless, it is believed that the stationary, constant f model, does contain the principal factors of importance in such motions, necessary for the present study.

In the main vortex, under the above assumptions, there is a balance between the pressure-gradient and the centrifugal and Coriolis forces. This balance can be represented mathematically

by the gradient wind equation, which has the form

$$V_{gr}(R) = -\frac{Rf}{2} + \left[\left(\frac{Rf}{2}\right)^2 + \frac{R}{\rho}\frac{dP}{dR} \right]^{\frac{1}{2}} \qquad (1)$$

where V_{gr} is the swirl velocity, R is the radial coordinate, ρ is the density of air (assumed constant), P is the pressure and f, the Coriolis parameter is equal to $2\Omega \sin \emptyset$, Ω being the angular rotation rate of the earth and $\emptyset$ the local latitude. This flow is a solution of the Euler equations in a rotating frame for a system with no radial component of velocity and where the vertical velocity is a function of radius only. However this balance situation is altered as we approach the ground/sea surface, and the effect of friction becomes important.

In the frictional layer, the Coriolis and centrifugal forces are reduced, whereas the pressure field of the outer flow is transmitted virtually unchanged across the layer. Consequently there is a net pressure force in the boundary layer, and this drives an inflow, thereby inducing a meridional circulation in the vortex itself. In fact, this process is just the familiar "tea cup effect", so named, because as tea is stirred, it is observed that the leaves concentrate at the bottom of the cup around what might be imagined as the axis of rotation, having been transported towards the axis in an exactly analogous way to the above flow system.

It is clear that the surface boundary layer of a hurricane plays an essential role in the dynamics of the vortex, not only during the mature stage, but also in the growth and decay of such systems. A recent paper by Charney (1970) presents a clear account

of the mechanisms involved in the growth of a hurricane depression in the context of the theory of "conditional instability of the second kind" (CISK), first proposed by Charney and Eliassen (1949). A simplified version of Charney's description is as follows.

Firstly, hurricanes tend to form over the tropical oceans which act as a source of moisture, this moisture in turn acting as a convective driving mechanism through the release of latent heat of condensation. Now it is observed that the main driving of the convective motion in the storm occurs in the large cumulus cloud bands associated with the main vortex core. However, the scale of such motions is of the order of only 10 km, whereas that for the hurricane as a whole is of the order of 1000 km, and it is proposed that it is in fact the surface boundary layer which provides the link between these two dissimilar but obviously strongly coupled flow systems. In particular, the pattern of the secondary meridional circulation can be characterised by the vertical motion either into or out of the boundary layer. If we consider firstly the flow in the outer radial regions of the hurricane, we expect the inertial effects to play a minor role, and in the limit of zero Rossby number, the flow is of the classical Ekman type in which the vertical velocity at the 'top' of the boundary layer is proportional to the vertical component of relative vorticity of the outer flow (Lighthill 1966). Thus in the case of an outer flow with cyclonic vorticity, there is mass convergence and consequent upflow of (moist) air from the boundary layer into the main vortex, and the release of latent heat of condensation from this moist air increases the convective activity within the cumulus clouds. On

the other hand, when the outer flow is anti-cyclonic, there will be downflow of dryer air from above the boundary layer. This subsiding air is warmed adiabatically and the relative humidity decreased, thus inhibiting any tendency towards cumulus convection in these regions. Also, as pointed out by Charney, the release of latent heat of condensation in the cyclonic region will cause a lowering of the pressure there and a subsequent intensification of the vortex. Thus there exists a mechanism for the spontaneous growth of hurricane depressions over warm oceans, a mechanism which clearly, is strongly dependent on the behaviour of the surface boundary layer. The theory as presented by Charney (1971), considers the boundary layer to act as a simple Ekman layer when obtaining estimates of the intensification produced. However, in the inner radial region of the storm, the region where the upflow is observed to occur, it is the inertial terms which are dominant, and therefore the use of Ekman theory seems unlikely to provide realistic enough estimates of the subsequent convection resulting from the transport of moisture via the boundary layer into the main vortex. Thus there is considerable interest in obtaining a more accurate description of hurricane boundary layer flow, and this is the principal aim of the various methods which we intend to discuss in this Chapter. Ooyama (1969) has reported calculations for an extensive numerical model of a developing hurricane in which the boundary layer is also assumed to have a constant thickness.

In the present discussion of the various mathematical models used in the treatment of hurricane boundary layers, we consider only the simple idealised case of a constant eddy viscosity to model the turbulent structure within the boundary layer. However, we note

that treatments such as those of the momentum integral method of S, are sufficiently flexible to cope with more sophisticated models of boundary layer structure, as for instance in the work of the following chapter. It should be stressed, that in examining the interaction between the hurricane vortex and the boundary layer, we are assuming for the purposes of the model that a particular steady-state outer flow has been imposed, and that this will then drive motion within the boundary layer. From this, we proceed to calculate quantities which we have seen to play an important part in the overall description of the hurricane, such as the radial inflow, the boundary layer thickness and the vertical velocity at the top of the boundary layer. In the more interesting case of a developing hurricane system, the CISK theory makes it clear that we cannot realistically expect such a decoupling of the outer flow and the boundary layer. However it is anticipated that in an extended model, we can use the boundary layer equations as a diagnostic system to provide bottom boundary conditions for the outer flow. Charney (1970) has shown by dimensional arguments that the response time of the boundary layer flow is an order of magnitude less than that of the outer flow, and hence a steady treatment of the boundary layer is justified, since effectively it reacts instantaneously to any changes in the outer flow driving it. In this context, there are interesting laboratory experiments reported by Hide *et al.* (1968) which show the vital role the boundary layer plays in determining the resultant structure of the main vortex.

Earlier attempts at a mathematical treatment of the hurricane boundary layer problem were made by Haurwitz (1935) and later by

Rosenthal (1962) and Miller (1965). Their methods all involve a linearisation of the boundary layer equations, but as shown in S by a simple order of magnitude analysis using the continuity equation, certain terms which these authors considered negligible, are in fact of the same order as other terms retained in their final equations. The inadequacies of this line of approach led to the model developed in S and later extended by Leslie and Smith (1970). This particular momentum integral method is based on the assumption that for the purposes of describing the overall features of the boundary layer flow, Ekman velocity profiles provide a sufficiently realistic representation of the vertical structure over the entire radial extent, except of course at very small radii, where the boundary layer equations themselves no longer apply. Related work has been carried out by Kuo (1971) where despite some obvious errors and the use of a non-rotating frame, the basic equations he obtains are those of S. Power-law velocity profiles are also applied by Kuo to model the case of the turbulent boundary layer, this second approach being also adopted by Chi *et al.*(1969). However the use by Kuo of the radial scale functions of the flow obtained from the momentum integral equations to calculate more detailed velocity profiles, seems hardly likely to produce further information, and would appear to be completely outside the scope of momentum integral methods. The work of Barcilon (1968) is also closely related to that of S.

The method proposed by Smith and Smith (1965) is an expansion procedure in terms of a small parameter ε, representing the ratio of the boundary layer thickness to the effective radius of the vortex.

However, a number of basic defects in their method, both in the actual expansion and in the boundary conditions, have been detailed by Morton (1966). In fact, there have been a large number of works published in which the authors have alluded, in rather general terms, to similarities between hurricanes and their particular flow systems. Most of these are investigations of the boundary layer flow under an imposed vortex, and it is interesting to note the extent to which certain authors attribute properties of geophysical interest to the flows they happen to be studying, with often little thought towards the justification for doing so.

As mentioned previously, an alternative approach to the problem was suggested by Carrier, who believed that the results obtained by the above-mentioned authors by means of the momentum integral method, were not sufficiently accurate. In a series of papers by Carrier and his co-workers (George 1970; Carrier, Hammond and George 1971; Dergarabedian and Fendell 1972a,b) it was proposed that the method of weighted residuals (Galerkin's method) furnishes a more accurate description of motion in the hurricane boundary layer. However, we shall show that the approach adopted by these authors has certain inherent defects, and that *if* these could be allowed for, the results obtained with the Galerkin technique would differ very little from those of the simple and more mathematically tractable momentum integral method.

Soon after the development of this Galerkin procedure, Carrier (1971a,b) concluded, although for reasons different from those which we shall give, that the method fails to provide an adequate treatment

of the problem, and incorporated the idea of a modified Oséen method, further work along this line being conducted by McWilliams (1971). In these papers, contrary to the view of Charney (1970) given above, Carrier also came to the conclusion that a time-dependent analysis of the boundary layer is required in the treatment of a maturing hurricane, and proceeded to develop analysis along these lines.

A different line of approach has been adopted by Stewartson, Burggraf and Belcher (Burggraf *et al.* 1971; Belcher *et al.* 1972). These authors use r^{-n} profiles to represent the outer flow. With n in the range $|n| \leq 1$, they calculate numerical solutions of both the steady and time-dependent boundary layer equations for the flow over a non-rotating flat disk. Certain interesting flow features are obtained, and we shall make further comment on their results in a later section.

One important point which needs to be investigated if possible when discussing the momentum integral method of S, is the actual validity of using Ekman velocity profiles over the entire radial extent of the flow. This assumption is made on the grounds that Ekman profiles with appropriate scaling factors, provide perhaps the only physically realistic model of the vertical structure in the boundary layer of constant eddy viscosity, accompanied by the relative simplicity of the mathematical treatment which follows. However, it would appear that this is still the principal objection raised by various workers in the field, who feel that one should attempt solutions to the problem which provide more information than the radial scales of the motion obtained by the momentum integral

method. Accordingly, we have attempted by means of a perturbation analysis of the equations of motion for significantly different outer flows, to verify whether or not Ekman profiles are indeed a good assumption, at least in the outer radial regions of the hurricane system. Finally, we also consider slightly different formulations of the momentum integral method, which can arise when the nature of the boundary layer equations derived in S are investigated at the ground.

Since we shall be considering a number of different approaches to the problem in this chapter, we shall present firstly the discussion and theory relevant to these methods in various sections, and then finally present collectively the results of the computations performed in a single section.

2. The boundary layer equations

To describe the motion in the surface boundary layer of a hurricane, we define a cylindrical coordinate system (R, θ, Z) fixed in the frame of the rotating earth, with corresponding velocity components (U,V,W). As previously discussed, it is assumed that the earth is locally flat, the Coriolis parameter f is constant and the flow in the boundary layer is steady and axisymmetric, being driven from above by a steady, two-dimensional potential vortex. Under these assumptions, the full boundary layer momentum equations, valid except for small values of the radius, have the following form in the rotating reference frame:

$$U\frac{\partial U}{\partial R} + W\frac{\partial U}{\partial Z} + \frac{V_{gr}^2 - V^2}{R} + f(V_{gr} - V) = K\frac{\partial^2 U}{\partial Z^2},$$

$$U\frac{\partial V}{\partial R} + W\frac{\partial V}{\partial Z} + \frac{UV}{R} + fU = K\frac{\partial^2 V}{\partial Z^2},$$

together with the equation of continuity,

$$\frac{1}{R}\frac{\partial}{\partial R}(RU) + \frac{\partial W}{\partial Z} = 0.$$

As is well known, these equations are derived from the Navier-Stokes equations in a rotating frame, under the assumption that

$$\frac{\partial^2}{\partial R^2}, \quad \frac{1}{R}\frac{\partial}{\partial R} \ll \frac{\partial^2}{\partial Z^2},$$

and that the pressure P is transmitted unchanged from the outer flow across the extent of the boundary layer. Here, the outer flow (various forms of which will be discussed later) is represented by $V_{gr}(R)$ and K is the constant coefficient of eddy viscosity.

At large values of the radius we expect the flow to be approximately geostrophic; that is, the magnitude of inertial forces is negligible compared with the Coriolis and pressure-gradient forces, or alternatively, the Rossby number is effectively zero. We can therefore fix a radial scale R_g, the 'geostrophic radius' of the order of 1000 km, at which V_{gr} has the value V_g. The value of R_g is chosen such that the local Rossby number is sufficiently small for the Ekman solution to be a reasonable representation of the actual flow system there. The natural vertical scale at R_g is the Ekman thickness $Z_g = (K/f)^{\frac{1}{2}}$.

If we now non-dimensionalise the variables as follows:

$$V_{gr} = V_g v_{gr}, \quad U = V_g u, \quad V = V_g v, \quad R = R_g r, \quad Z = Z_g z$$

and $W = (V_g Z_g / R_g)w$, where the scaling for W can be seen to arise in a natural manner from the equation of continuity, the above equations assume the form

$$Ro\ (u\frac{\partial u}{\partial r} + w\frac{\partial u}{\partial z} + \frac{v_{gr}^2 - v^2}{r}) + (v_{gr} - v) = \frac{\partial^2 u}{\partial z^2}, \quad (2)$$

$$Ro\ (u\frac{\partial v}{\partial r} + w\frac{\partial v}{\partial z} + \frac{uv}{r}) + u = \frac{\partial^2 v}{\partial z^2}, \quad (3)$$

$$\frac{1}{r}\frac{\partial}{\partial r}(ru) + \frac{\partial w}{\partial z} = 0, \quad (4)$$

where $Ro = V_g/(fR_g)$ is a Rossby number defined by the scales at the geostrophic radius.

As representative vertical boundary conditions, we apply no-slip conditions at the earth's surface and match the flow at the top of the boundary layer to the outer flow. That is

$$\left.\begin{array}{ll} z=o & : \quad u=v=w=o \\ z=\infty & : \quad u=o, v=v_{gr}, w=w_{gr}, \quad \frac{\partial u}{\partial z} = \frac{\partial v}{\partial z} = 0 \end{array}\right\} \quad (5)$$

In the following chapter, we shall show that these boundary conditions can be relaxed to provide a more realistic termination of the boundary layer at the ground or sea surface. Also, the boundary conditions at infinity are clearly not all independent, the zero stress situation ($\partial u/\partial z = \partial v/\partial z = 0$) arising automatically, since u and v are independent of z there.

The two momentum equations above can be modified to a form more suitable for approximate integral treatments, by adding each to the continuity equation (4) multiplied by Ro.u and Ro.v respectively,

to obtain

$$Ro\left[\frac{1}{r}\frac{\partial}{\partial r}(ru^2) + \frac{\partial}{\partial z}(uw) + \frac{v_{gr}^2 - v^2}{r}\right] + (v_{gr} - v) = \frac{\partial^2 u}{\partial z^2}, \quad (6)$$

$$Ro\left[\frac{1}{r^2}\frac{\partial}{\partial r}(r^2 uv) + \frac{\partial}{\partial z}(vw)\right] + u = \frac{\partial^2 v}{\partial z^2}, \quad (7)$$

2.1 The Ekman solution

This well known exact solution of the equations of motion applies for conditions of (approximate) geostrophy; that is, the Rossby number Ro in equations (2) and (3) is effectively zero. Using the boundary conditions (5), we obtain the solution

$$(u,v) = \left(-e^{-z/\sqrt{2}}\sin\frac{z}{\sqrt{2}},\ 1-e^{-z/\sqrt{2}}\cos\frac{z}{\sqrt{2}}\right).$$

In solving the boundary layer equations, we shall employ the Ekman solution as the outer boundary condition at r=1, the geostrophic radius.

The vertical velocity at the top of the boundary layer can be readily obtained by vertically integrating the equation of continuity (4) to obtain

$$w_e(r) = w(r,\infty) = -\frac{1}{r}\frac{d}{dr}\left(r\int_0^\infty u\,dz\right),$$

which, when the above Ekman profile for u is substituted, leads to

$$w_e = \frac{1}{\sqrt{2}r}\frac{d}{dr}(rv_{gr}) \quad (8)$$

This expression states that the upflow is proportional to the relative vorticity of the outer flow. Physically we have the situation that if the outer flow is cyclonic, say, the vertical component of vorticity above the boundary layer is greater than f, the local background vorticity. However, because of the no slip boundary condition, this value is reduced to f at z=o, and hence vorticity is being diffused into the ground. Yet if the flow is steady, this diffusion must necessarily be compensated for by stretching of the vortex lines in the boundary layer through the vertical upflow velocity given above.

2.2 Solution for large z

A further solution to equations (2) and (3) has been obtained by Carrier *et al.* (1971), who considered the asymptotic behaviour for large z.

If we let $z\to\infty$, then $u\to\hat{u}$, $(v_{gr}-v)\to\hat{v}$ and $w\to(w_{gr}+\hat{w})$, where all quantities denoted by $(\hat{})$ are assumed small with respect to unity and $w_{gr}(r) = w(r,\infty)$ is of order unity. On linearising equations (2) and (3), we obtain

$$\mathrm{Ro}\left(w_{gr}\frac{\partial\hat{u}}{\partial z} + \frac{2v_{gr}}{r}\hat{v}\right) + \hat{v} = \frac{\partial^2\hat{u}}{\partial z^2} ,$$

$$\mathrm{Ro}\left(u\,v'_{gr} - w_{gr}\frac{\partial\hat{v}}{\partial z} + \frac{\hat{u}v_{gr}}{r}\right) + \hat{u} = -\frac{\partial^2\hat{v}}{\partial z^2} ,$$

where the dash denotes differentiation with respect to r. To simplify, substitute $p = r\hat{u}$, $q = r\hat{v}$, $\varepsilon = \mathrm{Ro}\,w_{gr}$, $\alpha = 1+2\,\mathrm{Ro}\,v_{gr}/r$ and $\beta = 1+\mathrm{Ro}(rv_{gr})'$ to obtain from the above two equations

$$\varepsilon \frac{\partial p}{\partial z} + \alpha q = \frac{\partial^2 p}{\partial z^2},$$

$$\varepsilon \frac{\partial q}{\partial z} - \beta p = \frac{\partial^2 q}{\partial z^2},$$

Eliminating q, say, yields the characteristic equation

$$\lambda^2(\lambda-\varepsilon)^2 + \mu = 0,$$

with $\mu = \alpha\beta$, which has the solutions

$$\lambda = \frac{\varepsilon \pm \sqrt{\varepsilon^2 \pm 4i\sqrt{\mu}}}{2}$$

If the small quantity ε of order Ro is neglected with respect to μ, we have $\lambda^4 = -\mu$ and the resulting boundary layer profiles are of the general form $e^{-\lambda z}(\cos \lambda z, \sin \lambda z)$, leading to a boundary layer thickness scale (at *large* z) of

$$\lambda = \frac{\sqrt{2}}{\mu^{\frac{1}{4}}} = \sqrt{2} \Big/ \left\{ \left[1 + 2 \frac{\mathrm{Ro}\ v_{gr}}{r} \right] \left[1 + \mathrm{Ro} \frac{(r\ v_{gr})'}{r} \right] \right\}^{\frac{1}{4}}. \qquad (9)$$

This is equivalent to the result deduced by Carrier *et al.* whose expression for μ with different scaling (see Section 4) is $\mu = (1 + \frac{\Psi}{x})(1 + \Psi_x)$.

---

3. The momentum integral method

As stated earlier, the particular momentum integral method which will be considered here, was introduced by Smith (1968) - denoted by S - in order to provide a relatively simple but also physically realistic method of determining the scales of flow within the hurricane

boundary layer, by taking into consideration all the nonlinear terms. This is accomplished by assuming that for the purposes of determining the overall scales of the motion, the vertical structure of the horizontal velocity components in the boundary layer can be represented with sufficient accuracy by suitably scaled Ekman profiles.

If we neglect the influence of the small inertial effects at the geostrophic radius (r=1), the exact velocity profiles there are the Ekman profiles of Section 2.1, where in the non-dimensional form of the equations, $\sqrt{2}$ is the vertical scale thickness of the boundary layer. At values of the radius smaller than unity, we might expect that because of the increasingly important contribution from the inertial terms, this scale height of $\sqrt{2}$ will change, and also that the Ekman suction will differ from that of the classical relationship (8). Because of this, the scale of the radial inflow velocity will differ from its geostrophic value of unity, whereas on the other hand, it is reasonable to assume that the swirl velocity in the boundary layer remains in scale with the imposed swirl $v_{gr}(r)$. In other words, we can introduce a boundary layer scale thickness $\delta(r)$ and an amplitude coefficient $E(r)$ for the radial velocity component, with boundary conditions of $\delta=\sqrt{2}$ and $E=1$ at $r=1$ to satisfy the (approximately) geostrophic flow which applies there.

The flow in hurricane boundary layers is characterised by a horizontal/vertical length scale ratio of the order of a thousand, in which case we can expect a slow variation of the boundary layer scales with radius. In such situations, with a suitable choice of velocity profiles, the momentum integral method should provide an adequate description of the overall quantitative characteristics

of the motion. On the other hand, its value in the treatment of the boundary layers of narrow vortices such as tornadoes (where the horizontal and vertical length scales are comparable), as for instance by Rott and Lewellen (1966) and Chi *et al.* (1969) is indeed questionable. The simplest profiles suggested are clearly the Ekman profiles as used in S.

The use of this representation, particularly at small values of the radius, has been questioned by a number of authors, yet it has more to justify itself than mere mathematical convenience. Extensive measurements by Crawford (1971) of the velocity components in the laminar boundary layer associated with a concentrated draining vortex are shown to resemble very closely scaled Ekman profiles which are also presented. Similar measurements have been reported by Ying and Chang (1970), except that the boundary layer is in this case turbulent and has a similar structure to that obtained by Cham and Head (1969). In the latter paper, the authors treat both theoretically and experimentally the case of a turbulent boundary layer on a rotating disk. Their theory, which is in fact a momentum integral treatment, shows close agreement with the experimental results. The turbulent velocity profiles of Cham and Head differ very little from those obtained by Smith (1969) or by the author in the following chapter. In the latter work, the characteristics of the flow in the frictional sublayer near the ground are incorporated by matching a logarithmic wind profile to an Ekman profile. Extensive numerical computations by Deardorff (1972) also appear to be consistent with the above view, but we shall defer any further quantitative investigation of the validity of the method until Section 6.

In line with the above discussion, we now assume velocity profiles in the boundary layer as in S, following Mack (1962), of the form

$$\left.\begin{aligned} u(r,\eta) &= v_{gr}(r)\ E(r)\ f(\eta)\ , \\ v(r,\eta) &= v_{gr}(r)\ g(\eta)\ , \end{aligned}\right\} \qquad (10)$$

where $\eta = z/\delta$ and f and g are the Ekman profiles of Section 2.1:

$$\left.\begin{aligned} f(\eta) &= -\ e^{-\eta}\ \sin\eta \\ g(\eta) &= 1 - e^{-\eta}\ \cos\eta \end{aligned}\right\} \qquad (11)$$

On substituting these profiles into equations (6) and (7), integrating vertically across the boundary layer and using the boundary conditions (5), we obtain the following pair of ordinary differential equations for E and δ:

$$\mathrm{Ro}\left[(r\ v_{gr}^{2}\ E^{2}\ \delta)'\ I_1 + v_{gr}^{2}\ \delta\ I_2\right] + r\ v_{gr}\ \delta\ I_3 = -\frac{r\ v_{gr}}{\delta}\ E\ f'(0),$$

$$\mathrm{Ro}\left[(r^{2}v_{gr}^{2}E\delta)'\ I_4 - rv_{gr}(rv_{gr}E\delta)'I_5\right] + r^{2}v_{gr}\ E\delta I_5 = -\frac{r^{2}v_{gr}}{\delta}\ g'(0),$$

with the vertical velocity at the top of the boundary layer being obtained by integration of the continuity equation:

$$w_{gr} = -\frac{I_5}{r}\,(rv_{gr}\ E\delta)'\ .$$

The dash denotes ordinary differentiation with respect to r, while the momentum integrals are

$$\left.\begin{aligned} I_1 &= \int_0^\infty f^2\, d\eta = \frac{1}{8} \quad , \; I_2 = \int_0^\infty (1-g^2)d\eta = \frac{5}{8} \quad , \\ I_3 &= \int_0^\infty (1-g)d\eta = \frac{1}{2} \quad , \; I_4 = \int_0^\infty fg\, d\eta = -\frac{3}{8} \quad , \\ I_5 &= \int_0^\infty f\, d\eta = -\frac{1}{2} \quad . \end{aligned}\right\} \tag{12}$$

The above three equations for E, δ and w_{gr} can be converted to a form more suitable for numerical treatment, where the dependent variables are E^2, $E\delta^2$ and w_{gr}, namely

$$\frac{1}{E^2}(E^2)' = -\frac{2}{r\tilde{v}^2}\left[(r\tilde{v}^2)' - S_2\,\tilde{v}(r\tilde{v})'\right] - \frac{2}{E^2}\left(\frac{S_1}{r} + \frac{S_5}{\tilde{v}}\right) + \frac{2S_6}{\tilde{v}} - \frac{2(S_3+S_4)}{\tilde{v}\,E\delta^2} \quad , \tag{13}$$

$$\frac{1}{E\delta^2}(E\delta^2)' = \frac{1}{r\tilde{v}^2}\left[(r\tilde{v}^2)' - 3\,S_2\,\tilde{v}(r\tilde{v})'\right] + \frac{1}{E^2}\left(\frac{S_1}{r} + \frac{S_5}{\tilde{v}}\right) - \frac{3S_6}{\tilde{v}} + \frac{S_3+3S_4}{\tilde{v}\,E\delta^2} \quad , \tag{14}$$

$$W_{gr} = -\frac{I_5}{Ro\;\delta}\left\{S_4 + E\delta^2\left[\frac{(1-S_2)}{r}(r\tilde{v})' - S_6\right]\right\} \quad , \tag{15}$$

with $\tilde{v} = Ro\; v_{gr}$ and

$$S_1 = \frac{I_2}{I_1} \quad , \quad S_2 = \frac{2I_4 - I_5}{I_4 - I_5} \quad , \quad S_3 = \frac{f'(0)}{I_1} \quad , \quad S_4 = -\frac{g'(0)}{I_4 - I_5} \quad ,$$

$$S_5 = \frac{I_3}{I_1} \quad , \quad S_6 = \frac{I_5}{I_4 - I_5} \quad .$$

The flexibility of this method permits immediate extension to cases where K is a function of both r and z and where the momentum integrals themselves are functions of the radius, as well as to a variety of vertical velocity profiles and surface boundary conditions.

A slight adjustment to the given values of E and δ at r=1 (E=1, $\delta=\sqrt{2}$) must be calculated to allow for the small but finite effect of ageostrophy. This is accomplished by requiring that the radial derivatives of E^2 and $E\delta^2$ in equations (13) and (14) be zero at r=1 for a given outer flow $v_{gr}(r)$, and ensures subsequent stability of the numerical integration, the method used being the familiar Runge-Kutta-Gill routine.

4. The Galerkin method

As stated in the Introduction, the use of the method of weighted residuals, or Galerkin's method, was suggested by Carrier as an improvement on momentum integral techniques for the hurricane boundary layer problem.† The mathematical development of the method involves considerable work and we shall merely outline the procedure,

---

† Part of the motivation for their study was claimed to be the unsatisfactory results obtained by Anderson (1966) for flow in a Ranque-Hilsch tube using the momentum integral method. However, Anderson in fact claims (see e.g., xv and p. 76) that his use of the momentum integral method provides a reasonably accurate description of the overall flow characteristics when compared with the results obtained from full finite-difference calculations.

details of which can be found in the thesis of George (1970). It would be possible to derive Galerkin equations analogous to those obtained by George from (6) and (7), but for convenience we shall adopt his scaling. Here the following non-dimensional variables are introduced:

$$\Psi = \frac{RV_{gr}}{\Psi_o}, \quad \psi = \frac{RV}{\Psi_o}, \quad \phi = \frac{RU}{\Psi_o}, \quad z = \frac{Z}{(K/f)^{\frac{1}{2}}},$$

$$w = \frac{W}{(Kf)^{\frac{1}{2}}}, \quad x = \frac{R^2 f}{2\Psi_o},$$

where Ψ_o is a characteristic dimensional circulation of the outer flow, for example $\Psi_o = R_1 V_{gr}(R_1)$ where R_1 is the radius of maximum swirl velocity. In this non-dimensional form, the boundary layer equations (2) and (3) and the equation of continuity (4) become

$$\phi\phi_x + w\phi_z + \frac{1}{2x}(\Psi^2 - \psi^2 - \phi^2) + (\Psi - \psi) = \phi_{zz}, \qquad (16)$$

$$\phi\psi_x + w\psi_z + \phi = \psi_{zz}, \qquad (17)$$

$$\phi_x + w_z = 0, \qquad (18)$$

with subscripts denoting partial differentiation.

An unusual feature of this particular scaling is that it results in all terms in the equations being of order one, in contrast with the form of the equations (2) and (3) where the importance of the Rossby number is apparent, and which also suggests a perturbation scheme with Ro as the expansion parameter. Furthermore, the use of the variable 'x' as the new radial coordinate effectively

concentrates the new coordinate system near the origin. From the numerical point of view, this increases the possibility of instabilities developing, since it is near the origin that the radial gradients of the governing terms in the equations are largest.

The Galerkin method involves basically the expansion of the unknown functions $\phi(r,z)$ and $\psi(r,z)$ in terms of a complete orthonormal set of functions. The properties of these base functions are then used to reduce the original partial differential equations to a set of coupled ordinary differential equations. The method has been used by several authors to treat boundary layer problems, for instance Finlayson and Scriven (1966), Bethel (1968) and MacDonald (1970), all of whom have emphasized the importance of a judicious choice of base functions. Following George, we let

$$\left.\begin{aligned} \phi &= \sum_{n=1}^{\infty} a_n(x)\ \omega_n(x,z), \\ \psi &= \Psi\left[1-e^{-\lambda(x)z}\cos\ \lambda(x)z\right]+\psi', \end{aligned}\right\} \qquad (19a)$$

where $\psi' = \sum_{n=1}^{\infty} b_n(x)\ \omega_n(x,z)$,

and from the continuity equation (18),

$$w(z) = -\frac{\partial}{\partial x}\int_0^z \sum_{n=1}^{\infty} a_n(x)\omega_n(x,\zeta)d\zeta.$$

In practice, the summations are taken to a fixed number N of terms at which the series are judged to have converged. In order to satisfy the boundary conditions at z=o and the limiting conditions (5) as $z\to\infty$, as well as to be consistent with the physical situation, the following set of base functions was proposed by George:

$$\omega_n(x,z) = \sum_{k=1}^{n} g_{nk}\, e^{-[k\lambda(x)z]} \sin [k\lambda(x)z], \qquad (n=1,2,\ldots,N) \tag{19b}$$

the normalising condition being

$$\int_0^{\infty} \omega_m \omega_n dz = \frac{H_n \delta_{mn}}{\lambda(x)} ,$$

where δ_{mn} is the Kronecker delta and the normalising coefficients g_{nk} and H_n are given by George (1970).

The function $\lambda(x)$ has been earlier introduced in Section 2.2, where it was obtained as the asymptotic scale height of the boundary layer for large z. Dergarabedian and Fendell (1972b) in fact suggest the two possible forms,

$$\lambda = [\mu(x)]^{\rho/4}/\sqrt{2} \qquad (\rho=0 \text{ or } 1) \tag{19c}$$

in the expression for the base functions. With $\rho=0$, we have the simple Ekman case in which the scale height is $\sqrt{2}$, while for $\rho=1$, for the type of outer flows we shall be considering (see Section 7), the effect is to reduce this scale height as $x \to 0$. In other words, George's method involves specifying *a priori* a particular form of the boundary layer thickness, this form being obtained from a linearised analysis of the equations of motion for *large* z, and dependent only upon the characteristics of the outer flow, without reference to the equations themselves. On the contrary, we can expect this approach to have limited applicability, since it is the inertial terms in the boundary layer equations which will be the dominating effect at small values of the radius.

The physical meaning of the particular expansions above, used

by George for the functions ϕ and ψ' can now be seen. Firstly, the function ψ' provides a measure of the variation of the azimuthal velocity component from the Ekman form; ϕ and ψ' are expressed as weighted combinations of Ekman-like profiles, the scale heights of which have been predetermined as $\sqrt{2}/(n\mu^{\rho/4})$ $(n=0,1,2,\ldots;\ \rho=0 \text{ or } 1)$. By contrast, in the momentum integral method of S, the azimuthal velocity component is assumed to be Ekman-like; that is, $\psi' \equiv 0$. Furthermore, even if this assumption is made here, it appears to be impossible to introduce the analogous concept of a combination of boundary layer thicknesses to be determined from the equations, since the Galerkin method depends upon the linear form of the expansions for ϕ and ψ' in terms of the unknown coefficients a_n and b_n.

These simple observations suggest that difficulties may arise in the computations, but for the present we shall discuss the remaining details in the development of the method. Further consideration of the choice of profiles is deferred until Section 6.

The two boundary layer equations (16) and (17) can be written in the shorthand form $L_i(\phi,\psi,w\,;\ x,z)=0$, with $i=1$ or 2. The principle of the Galerkin technique is to minimise the residuals obtained when the series for ϕ and ψ' are substituted into the equations; this can be shown to be equivalent to requiring

$$\int_0^\infty L_i(\phi,\psi,w\,;\ x,z)\ \omega_n(x,z)\,dz = 0, \qquad (i=1,2;\ n=1,2,\ldots,N)$$

with the properties of the orthonormal base functions ω_n being used to simplify the 2N equations obtained. The resulting details are comparatively straightforward, but involve extremely large amounts

of algebraic manipulation. The final set of ordinary differential equations derived by George (1970) for the coefficients a_n and b_n is, in matrix form,

$$P\dot{\underline{a}} = \underline{U}, \qquad Q\dot{\underline{b}} = \underline{V} - R\dot{\underline{a}}, \tag{20}$$

where the dot denotes differentation with respect to x, $\underline{a}$ and $\underline{b}$ are column vectors of length N representing the unknown a_n and b_n. Two of the typical matrices P and $\underline{U}$ are given by

$$P_{\beta\alpha} = a_i \overset{(15)}{E}_{i\alpha\beta}$$

$$U_\beta = -\lambda^2 a_i \overset{(1)}{E}_{\beta i} - \frac{\dot{\lambda}}{\lambda} a_i a_j \overset{(16)}{E}_{ij\beta} + \frac{1}{2x}(a_i a_j + b_i b_j) \overset{(2)}{E}_{ij\beta}$$

$$+ (1 + \frac{\Psi}{x}) b_\beta H_\beta - \frac{\Psi}{x} b_i \overset{(7)}{E}_{i\beta} - (1 + \frac{\Psi}{x})\frac{\Psi}{2} \overset{(1)}{E}_{\beta 1} + \frac{\Psi^2}{2x} \overset{(8)}{E}_\beta$$

where the Einstein summation convention has been employed.* The E-quantities are detailed in George's thesis, a typical example being

$$\overset{(2)}{E}_{mnp} = \sum_{i=1}^{m} g_{mi} \sum_{j=1}^{n} g_{nj} \sum_{k=1}^{p} g_{pk} \overset{(2)}{T}_{jik},$$

where

$$\overset{(2)}{T}_{n\ell p} = \int_0^\infty e^{-(n+\ell+p)\zeta} \sin n\zeta \sin \ell\zeta \sin p\zeta \, d\zeta$$

---

*There is a slight error in the form of U_β in George's thesis, where the term involving $\overset{(8)}{E}_\beta$ has been written as $\frac{\Psi^2}{4x} \overset{(8)}{E}_\beta$ instead of as above. However a number of numerical calculations with various outer flows have shown that the effect of the error in this term is minimal.

$$= \frac{1}{8}\left[\frac{p+n-l}{p^2+n^2+l^2+2pn} - \frac{p-n+l}{p^2+n^2+l^2+2pl} - \frac{p+n-l}{p^2+n^2+l^2+2nl} - \frac{1}{p+n+l}\right].$$

The numerical solution of the above equations, given a particular outer flow $\Psi(x)$ is in many respects similar to that used in the momentum integral method. At the 'outer edge' of the vortex, Ekman flow specifies the boundary conditions, i.e., $a_1 = -\Psi$ and $a_r = b_s = 0$ ($r>1$, $s\geq 1$). As in the momentum integral method, these values must be adjusted slightly to allow for small ageostrophic effects and the equations are then integrated radially inwards by a Runge-Kutta-Gill routine.

5. Other approaches to the problem

Although it is our intention to concentrate on the two methods outlined in Sections 3 and 4, there are a number of different approaches which have been pursued in the literature, and we shall comment briefly on two of the more notable of these, as well as show how application of a constraint on the momentum integral equations of S, can lead to a slightly different formulation of the problem.

5.1 The work of Stewartson *et al.*

In two papers by Stewartson, Belcher and Burggraf (Burggraf *et al.* 1971; Belcher *et al.* 1972), a different line of approach from that of previously mentioned work is adopted, with only general inferences being drawn about applicability to hurricane—like flows. These authors investigate the flow in the viscous boundary layer of a flat disk, above which is imposed an outer circulation.

The method involves transforming the boundary layer equations to a new coordinate system, based on certain similarity solutions which had been previously obtained, and a full finite-difference treatment of the resulting equations is then used to determine the flow structure under the vortex. The 'generalised vortex' which they employ to represent the outer flow, has the swirl velocity V proportional to a power of the radius; specifically, $V(r)=r^{-n}$. The first paper deals with the steady potential vortex (n=1), while in the second, four values of n in the range $|n|\leq 1$, $(n=-1,0,\frac{1}{2},1)$ are investigated. Except for the potential vortex, where the flow direction is everywhere inwards, flow reversal is experienced within the boundary layer, and to cope with this, a time-dependent approach is necessary in order to overcome the numerical difficulties which arise.

In the case of the potential vortex, certain distinctive and unusual features are revealed. For *small* radius, a two-level boundary layer structure is apparent. The inner layer, whose thickness is proportional to r, is dominated by viscosity. At the outer edge of this layer, in the limit $r\to 0$, the radial inflow velocity u, is equal to V, while the azimuthal velocity remains small. Above this inner layer, the flow is effectively inviscid, with v adjusting to the flow in the outer vortex and u tending rapidly to zero. This two-level structure means that for the potential vortex, there is no similarity solution valid at small r. For the cases of n=-1 (solid body rotation) and n=0 ($V\equiv 1$) it is found that the boundary layer has a single thickness, in line with successful similarity solutions which have been previously obtained.

In fact, it is proposed in the second paper, that there is a number n_o=0.1217, such that similarity solutions exist only if $n<n_o$. When $n=\frac{1}{2}$, the boundary layer exhibits a most unusual extension of the potential vortex behaviour, consisting of an infinite number of inviscid layers, each pair of which is separated by a comparatively thin shear layer in which viscous effects are important. Furthermore, in the outer regions of the boundary layer, the radial velocity develops very considerable 'overshoots', whereas near the ground, the shape of the profiles is largely independent of r. This clearly suggests the influence of the particular form of the outer flow on the resulting boundary layer velocity profiles, and is relevant to our discussion of Section 6.

It is evident that a considerable number of interesting and relevant results have emerged from these two papers. However, in attempting to assess this work within the context of hurricane boundary layers, it should be noted (i) that the motion is in a non-rotating frame, (ii) that it is clearly an oversimplification to represent a hurricane vortex by a simple flow such as $V=r^{-n}$ and (iii) that their solutions are started at the edge of the disk (r=1) from similarity profiles derived previously by Stewartson and not from Ekman profiles. Therefore, notwithstanding the value of the results obtained, one should be cautious in interpreting the flows as being of direct geophysical interest.

5.2 The modified Oseen method

Shortly after the appearance of the paper by Carrier *et al.* (1971)

in which the Galerkin technique was presented, a further two works were published by Carrier (1971a,b), in which a new method was introduced. In the opinion of Carrier, the Galerkin method of George (1970) is considered unsatisfactory except for large radius, the principal reason being that for small radius, the base functions used by George are unable to resolve the type of structure found by Stewartson *et al.*, discussed above in Section 5.1 (see Dergarabedian and Fendell 1972a,b, for a more detailed version of this criticism). In Section 4 above, we also express the opinion that the Galerkin method is suitable only for large radius - in our view however it is the method itself and not the particular profiles used which account for this, since there is no possible way in which the relevant boundary layer thickness scale can be *predicted*.

In Carrier (1971a) the modified Oseen method is presented for two very simple swirl profiles above the boundary layer. The method has the advantage that it involves very little computational effort, at least for the outer flows discussed by Carrier. McWilliams (1971) is reported to have extended the method to a wider range of outer flows, but to date we have been unable to procure a copy of his work. Basically, the method involves neglecting the vertical convective terms in the boundary layer equations; for instance, the term $w\frac{\partial u}{\partial z}$ is assumed negligible with respect to $u\frac{\partial u}{\partial r}$. The remaining inertial terms are then linearised in the manner of Oseen's method (see Carrier 1965 for a more detailed account).

The assumptions made by Carrier are indeed rather far reaching if they were to apply to hurricane boundary layers in general, as is suggested. However, a simple dimensional analysis via the continuity

equation, casts considerable doubt on the validity of such an approach, since the terms $w\frac{\partial u}{\partial z}$ and $u\frac{\partial u}{\partial r}$ can be shown to be of the same order of magnitude. We have also performed a simple calculation to be discussed in Section 7, which we believe shows clearly that these two convective terms are of the same order of magnitude for the entire radial extent of the boundary layer. Carrier (1971b) also describes a time-dependent formulation for the boundary layer of a developing hurricane; see Introduction.

5.3 Variations on the momentum integral method

In this section we shall be investigating certain features of the momentum integral method of S which we feel are worthy of attention. The problem arises when we investigate the behaviour of the boundary layer equations (2) and (3) at z=0, when the velocity profiles (10) are substituted for u and v. At z=0, we have u=v=w=0, f"(0) = 2 and g"(0) = 0. Equation (3) can be seen to be satisfied identically, whereas from equation (2) we obtain

$$Ro\ \frac{v_{gr}^2}{r} + v_{gr} = \frac{v_{gr}\,E}{\delta}\ f''(0)$$

Thus it would appear that for the radial velocity profile to be compatible with the radial equation of motion, at least at z=0, we require

$$E = \frac{\delta^2}{2}\ \left(1 + Ro\ \frac{v_{gr}}{r}\right). \qquad (21)$$

Clearly this relationship now reduces the number of parameters from two to one, whereas we still have the two boundary layer equations (2) and (3). This suggests that three parameters are needed initially,

but firstly we shall proceed with the present situation.

A similar example of this type of over-specification arises in integrated equations for plume models (Morton 1971), and the same type of behaviour has been reported by Mack (1963) for boundary layer flow over a flat disk. In a sense it can be considered as arising from the assumption of separable solutions (10) without any real mathematical justification, the main motivation for the momentum integral method being its relative simplicity, while the integrated velocity profiles are meant to provide a physically realistic, *not* an exact description of the scales of motion. One of the objections raised by Carrier (personal communication) to the momentum integral method of S (as well as to the Galerkin method) was that the maximum radial inflow velocity it predicts at certain radii, can exceed the swirl velocity above the boundary layer, a situation which he believed to be physically unrealistic. In this context however, it is interesting to note that in the limit $r \to 0$, an asymptotic solution obtained by Belcher *et al.* (1972) for the case $V = r^{-\frac{1}{2}}$, does in fact permit the magnitude of u to exceed V. In the light of the relationship (21) one is led to believe that the original formulation of S may well be too loosely constrained, allowing the development of excessive radial velocities.

At this stage we shall merely develop the modified momentum integral equations, and reserve any conclusions for Sections 7 and 8.

The two velocity profiles (10) become, by way of equation (21) above,

$$\left.\begin{aligned} u(r,\eta) &= \frac{\delta^2 v_{gr}}{2}\left(1 + Ro\,\frac{v_{gr}}{r}\right) f(\eta) \\ v(r,\eta) &= v_{gr}\, g(\eta) \end{aligned}\right\} \qquad (22)$$

Since E is now a function of δ, the relationship (21) having been obtained from the radial momentum equation (2), we employ the azimuthal equation to solve for δ. As in Section 3, we substitute the profiles (22) into equation (7) and integrate across the boundary layer from z=0 to ∞. Using the boundary conditions (5) and the values of the integrals (12), the following equations for δ and w_{gr} are obtained:

$$\frac{d\delta}{dr} = \frac{4r\,(\delta^4\chi - 4) - Ro\,\delta^4\,(\Gamma\chi' - 2\Gamma\chi)}{3Ro\,\Gamma\delta^3\chi}\,, \qquad (23)$$

$$w_{gr} = -\frac{1}{4r}\,(\Gamma\delta^3\chi)'\,, \qquad (24)$$

where $\chi=(1+Ro\ v_{gr}/r)$ and $\Gamma=r\ v_{gr}$ is the dimensionliss circulation of the outer flow. Equation (23) is of the form $\delta' = \Gamma(r,\delta)$ and hence as before, it can be solved numerically by the Runge-Kutta-Gill routine, subject to the boundary conditions of $\delta = \sqrt{2}$ at $r = 1$.

In the above discussion, the number of parameters is effectively reduced from two to one. A different approach can be made however, by introducing distinct boundary layer thickness scales for the radial and azimuthal velocity profiles. Cooke (1952) has adopted this method for solving the flow in a vortex chamber, while in the present context, at least some support is lent by the work of Stewartson *et al.*, cited in Section 5.1, who observe such a two-level behaviour in certain of their numerical solutions. The concept has also been employed by MacDonald (1966) to obtain entry profiles in a rotating pipe. In the present case, application of the compatibility condition (21) results in two parameters to be calculated from the two integrated equations of motion. As boundary layer

profiles, we now have

$$u(r,z) = v_{gr}(r)E(r)f(\frac{z}{\delta}) \ ,$$

$$v(r,z) = v_{gr}(r)g(\frac{z}{\Delta}) \ ,$$

where $\delta(r)$ and $\Delta(r)$ are the radial and azimuthal boundary layer thicknesses respectively. From (21), we can write

$$\left.\begin{aligned} u(r,\eta) &= \frac{\delta^2 v_{gr}}{2}\ (1+Ro\frac{v_{gr}}{r})f(\eta) \ , \\ v(r,\xi) &= v_{gr}g(\xi) \ , \end{aligned}\right\} \qquad (25)$$

where $\eta=z/\delta$ and $\xi=z/\Delta$. The velocity profiles f and g are those used previously, but with their respective vertical scalings, namely

$$f(\eta) = -e^{-\eta}\sin\eta \ ,$$

$$g(\xi) = 1-e^{-\xi}\cos\xi.$$

For convenience, we introduce the parameter $\kappa(r)$, defined by $\delta=\kappa\Delta$, and therefore $\xi=\kappa\eta$, the azimuthal velocity profile being written now as

$$v(r,\eta,\kappa) = v_{gr}\ g(\kappa\eta). \qquad (25')$$

Thus the momentum integrals involving g are functions of κ:

$$I_1 = \frac{1}{8} \ , \ I_2 = \frac{5}{8\kappa} \ , \ I_3 = \frac{1}{2\kappa} \ , \ I_4 = -\frac{\kappa(1+\kappa+\kappa^2)}{2(1+\kappa)(1+\kappa^2)} \ , \ I_5 = -\frac{1}{2} \ ,$$

which, as they must, reduce to those of S - equation (12) - when $\kappa=1$, i.e., $\Delta=\delta$.

Using the values of these intergrals, we obtain the following two simultaneous momentum integral equations for δ and κ:

$$\frac{d\delta}{dr} = \frac{4\, v_{gr}\left[4r(\kappa\chi-1)-5Ro\, v_{gr}\right] - \kappa\delta^4 Ro(r v_{gr}^2 \chi^2)'}{5\kappa\delta^3 Ro\, r\, v_{gr}^2 \chi^2} = F(r,\delta,\kappa), \quad (26)$$

$$\frac{d\kappa}{dr} = \frac{\delta^3 Ro\left[\Gamma'\psi\delta\chi + \Gamma\phi(3F\chi + \delta\chi')\right] - r(\delta^4\chi - 4\kappa)}{\delta^4 Ro\Gamma\chi P}, \quad (27)$$

where

$$\phi = \frac{1}{(1+\kappa)(1+\kappa^2)}, \quad P = (1+2\kappa+3\kappa^2)/\phi^2, \quad \psi=(1-\kappa(1+\kappa+\kappa^2))/\phi$$

Here, w_{gr} is calculated again from equation (24).

As before, the numerical solution is obtained by the Runge-Kutta-Gill routine, subject to the boundary conditions at r=1, of $\delta=\sqrt{2}$ and $\kappa=1$, that is, equal boundary layer thicknesses at the geostrophic radius, consistent with the Ekman flow assumed.

6. Examination of boundary layer profiles

In this section, we shall attempt to assess the validity of assuming Ekman velocity profiles for the vertical structure of the boundary layer, in momentum integral calculations. In effect, what we are concerned with here is an investigation of the basic formulation of such momentum integral methods, using the idealised situation of a constant eddy viscosity from which Ekman profiles arise. For this case we obtain a regular perturbation solution in the region of low Rossby number, that is, in the outer radial regions of the flow. In spite of the fact that normal hurricane boundary layers progress through regions of small, order one and finally large Rossby numbers as we advance radially inwards, it is felt nevertheless, that considerable information can be obtained from the present approach.

In Chapter 2 we go on to extend the momentum integral method to one using velocity profiles which are believed provide a more realistic representation of the flow structure, than the case of constant eddy viscosity envisaged here. But before doing this, it is clearly advantageous to investigate just how well the method can cope with the present more simple situation.

6.1 Possible effect of outer flow on profiles

We have noted earlier that a number of authors have had misgivings about the use of Ekman profiles in S, and indeed the following simple example, although necessarily speculative, should serve to illustrate that even in regions of low Rossby numbers where we expect the Ekman solution to be a good approximation, the velocity profiles may well be affected to a marked extent by the properties of the outer flow.

Consider the situation as illustrated in the sketch below, in which we have a dimensionless outer (inviscid) flow $V=V(r)$, arising from the balance between the radial pressure-gradient and the centrifugal (and Coriolis in a rotating frame) forces. Disruption of this balance by the no slip condition at the ground, gives rise to a *net* inward motion in the surface boundary layer. Consider parcels of air 1 and 2 at radial positions r_1 and r_2 ($r_2>r_1$) as shown, above the effective region of influence of the boundary layer.

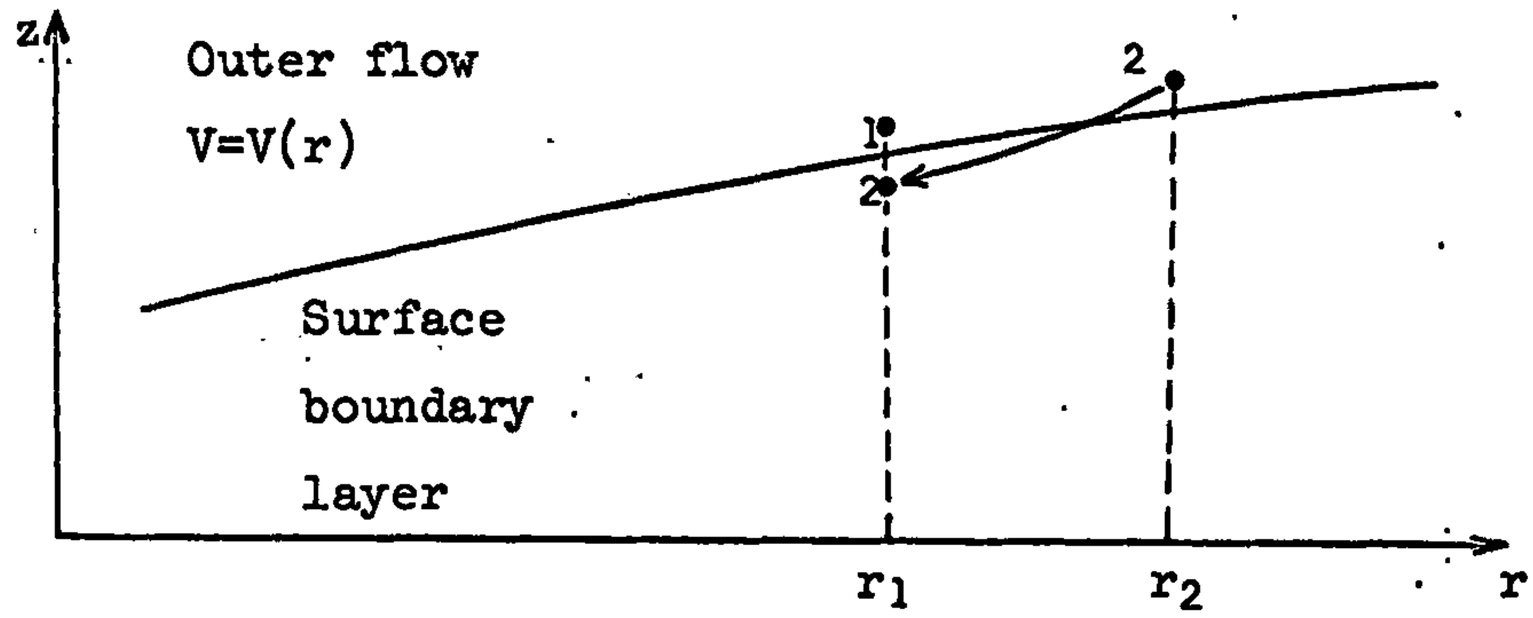

The respective circulations of these parcels are $\Gamma_1(r_1)=r_1V_1(r_1)$ and $\Gamma_2(r_2)=r_2V_2(r_2)$. In the hurricane boundary layer context it is reasonable to expect that under Ekman suction, parcel 2 could be drawn into the boundary layer and thence transported inward to radial position r_1. If we assume for the moment that it is only the *outer*, effectively inviscid region of the boundary layer which is affected by this process, then angular momentum is approximately conserved, very little being lost to the boundary by viscous dissipation. Thus $\Gamma_2(r_1)=\Gamma_2(r_2)$, or alternatively, $V_2(r_1)=r_2V_2(r_2)/r_1$. The outward centrifigal acceleration on 1 is $\beta_1 = V_1^2(r_1)/r_1$, which under balance conditions, equals the negative radial pressure gradient. The outwards acceleration on 2 at r_1 is

$$\beta_2 = \frac{V_2^2(r_1)}{r_1} = \frac{r_2^2 V_2^2(r_2)}{r_1^3},$$

and this leads therefore to the following possible cases, first derived by Rayleigh (1916):

Stable : 2 tends to return to r_2 if $\beta_2 > \beta_1$; i.e., $\Gamma_2^2 > \Gamma_1^2$;

Neutral : 2 tends to remain at r_1 if $\beta_2 = \beta_1$; i.e., $\Gamma_2^2 = \Gamma_1^2$;

Unstable: 2 tends to accelarate inward if $\beta_2 < \beta_1$; i.e., $\Gamma_2^2 < \Gamma_2^2$.

Thus in the stable case for example, Γ^2 increases monotonically with r, and if V>0, this is equivalent to $\Gamma'>0$. In a rotating frame, $\mathbf{V}=V(r)+rf/2$, where $\mathbf{V}$ and V are measured in inertial and rotating frames respectively. Hence

$$\Gamma(r) = r\mathbf{V} = rV + \frac{r^2 f}{2},$$

and to model the various types of outer flow we set $(r\mathbf{V})'=\varepsilon$, a suitably small number which is positive, zero or negative for the respective cases of stability, neutrality and instability. If as in previous sections, we scale velocity such that V(1)=1, this leads to the outer flow

$$V(r) = \varepsilon + \frac{1-\varepsilon+f/2}{r} - \frac{rf}{2}. \qquad (28)$$

Since f is taken to be 5×10^{-5}, the actual difference between the V profiles in the rotating and non-rotating frames is negligible.

Physically, what we might anticipate on the basis of the Rayleigh criterion, is that in the case of stability ($\varepsilon>0$), say, the fluid particles experience a restoring force, acting against the overall tendency of inward radial motion in the boundary layer. Accordingly, it is conceivable that the velocity profiles may become distorted to the extent that Ekman profiles will in fact be a poor representation of the actual vertical structure of the boundary layer flow. Further support to this simple contention is given by the results of Belcher *et al.* (1972) discussed in Section 5.1. Their generalised vortices, except for the potential vortex which has neutral stability, are all stable outer flows, and the radial velocity profiles exhibit often considerable overshoots. These occur however, only in the *outer*

region of the boundary layer, the flow near the ground appearing to be effectively insensitive to the form of the imposed vortex. It is the investigation of the possibility of this type of behaviour, which may have an important bearing on the range of applicability of momentum integral methods, that will concern us subsequently in this section.

It must be stressed here, that we are looking to the momentum integral method to provide realistic *overall scales* of the motion in the hurricane boundary layer, namely for the radial inflow velocity and the boundary layer thickness; nowhere is it asserted that these Ekman profiles reproduce the flow details with any great accuracy. Indeed, both from the results of Belcher *et al.* (1972) and the heuristic reasoning associated with the Rayleigh stability criterion, it may well be rather unrealistic to do so.

6.2 The perturbation equations

We use here the scaling of Section 2, which immediately transforms the boundary layer equations to a form suitable for a low Rossby number expansion scheme. The boundary layer equations, together with the continuity equation are, from Section 2,

$$\mathrm{Ro}\left[u\frac{\partial u}{\partial r} + w\frac{\partial u}{\partial z} + \frac{V^2 - v^2}{r}\right] + (V-v) = \frac{\partial^2 u}{\partial z^2},$$

$$\mathrm{Ro}\left[u\frac{\partial v}{\partial r} + w\frac{\partial v}{\partial z} + \frac{uv}{r}\right] + u = \frac{\partial^2 v}{\partial z^2},$$

$$\frac{1}{r}\frac{\partial}{\partial r}(ru) + \frac{\partial w}{\partial z} = 0,$$

where $V=V(r)$ is the outer flow. The velocity components are expanded in a power series of the (small) Rossby number Ro, as

$$\underline{u} = (u,v,w) = \underline{u}_o + Ro\,\underline{u}_1 + \ldots \qquad (29)$$

On substituting for $\underline{u}$ in the above equations and equating terms with equal powers of Ro, a system of regular perturbation equations is obtained. The zeroth order equations are clearly those for zero Rossby number, in other words, the Ekman equations:

$$V - v_o = \frac{\partial^2 u_o}{\partial z^2},$$

$$u_o = \frac{\partial^2 v_o}{\partial z^2},$$

where the boundary conditions are

$$z=0: \quad u_o = v_o = 0,$$

$$z=\infty: \quad u_o = 0, \quad v_o = V.$$

The solution for u_o and v_o is well known, and has been already discussed in Section 2.1. To obtain it, we set $W_o = u_o + iv_o$ and $W_g = U+iV = iV$, where $i^2=-1$ and U, the radial component of the outer flow, is zero. The solution obtained, which satisfies the above boundary conditions, is

$$W_o = iV\left(1-e^{-(\frac{1+i}{\sqrt{2}})z}\right),$$

or $u_o = Vf(\zeta)$, $v_o = Vg(\zeta)$, where f and g are the Ekman profiles (11):

$$f(\zeta) = -e^{-\zeta}\sin\zeta,$$

$$g(\zeta) = 1-e^{-\zeta}\cos\zeta,$$

and for convenience, we set $\zeta = z/\sqrt{2}$. Also by integration of the zeroth order continuity equation, we find

$$w_o = -\sqrt{2}\,\frac{(rV)'}{r}\,F_o(\zeta)\,,$$

where $F_o = -\frac{1}{2}(g-f)$. Therefore, we have the familiar Ekman result (8) for the outflow velocity at the top of the boundary layer,

$$w_o(r,\infty) = \frac{(rV)'}{\sqrt{2}r}\,,$$

The first order equations, obtained by equating coefficients of Ro, are

$$\frac{\partial^2 u_1}{\partial z^2} + v_1 = V_o,$$

$$\frac{\partial^2 v_1}{\partial z^2} - u_1 = -U_o,$$

where

$$-U_o = u_o\frac{\partial v_o}{\partial r} + w_o\frac{\partial v_o}{\partial z} + \frac{u_o v_o}{r}\,,$$

$$V_o = u_o\frac{\partial u_o}{\partial r} + w_o\frac{\partial u_o}{\partial z} + \frac{V^2 - v_o^2}{r}\,,$$

and the boundary conditions are

$u_1 = v_1 = 0$ at $z=0$ and as $z\to\infty$.

The solution is obtained in an identical manner to the zero order case, and we arrive at

$$W_1 = u_1 + iv_1$$

$$= \left[U_o + \frac{V^2}{r}f(\zeta)\right] + i\left[V_o - \frac{V^2}{r}\left[1-g(\zeta)\right]\right],$$

where from above, it can be shown that

$$-U_o = V\frac{(rV)'}{r}\left[fg + \frac{1}{2}(g-f)\dot{g}\right],$$

$$V_o = V\left[V'f^2 + \frac{(rV)'}{2r}(g-f)\dot{f} + \frac{V}{r}(1-g^2)\right],$$

the dot denoting differentiation with respect to ζ. For later convenience, we express the first order expansions as

$$\left.\begin{aligned} u &= u_o + Ro\,u_1 = Vf_*(\zeta), \\ v &= v_o + Ro\,v_1 = Vg_*(\zeta), \end{aligned}\right\} \tag{30}$$

where it is clear that

$$\left.\begin{aligned} f_* &= f + Ro\left\{\frac{V}{r}f - \frac{(rV)'}{r}\left[fg + \frac{1}{2}(g-f)\,\dot{g}\right]\right\}, \\ g_* &= g + Ro\left\{V'f^2 + \frac{(rV)'}{2r}(g-f)\dot{f} + \frac{V}{r}g(1-g)\right\}. \end{aligned}\right\}$$

The expansion (29) is valid for small Rossby numbers only, and hence we need to ensure that the local Rossby number, equal to RoV/r, remains small. The typical value assumed here for Ro is 0.05 and thus for a potential vortex (which will remain a reasonable approximation to the outer flows (28) as ϵ is varied), the local Rossby number increases from 0.05 at r=1 to only 0.2 at $r=\frac{1}{2}$. However this value is increasing quadratically, and hence the expansion scheme ultimately becomes invalid.

6.3 Comparison with momentum integral procedure

We have stated above that we wish to compare the perturbation analysis with the momentum integral method of S, as a means of

determining the viability of employing Ekman profiles for hurricane boundary layer calculations. To this end, we can form integrals such as

$$I_{1*} = \int_0^\infty f_*^2(z)\, dz.$$

If we wish to use these integrals to make meaningful comparisons, we clearly need to extract quantities E_* and δ_* analogous to the radial velocity and boundary layer thickness scales defined by (10). With this in mind, it is natural to set

$$I_{1*} = \sqrt{2} \int_0^\infty f_*^2(\zeta)\, d\zeta = E_*^2 \delta_* J_1 ,$$

$$I_{2*} = \sqrt{2} \int_0^\infty \left[1-g_*^2(\zeta)\right] d\zeta = \delta_* J_2 ,$$

$$I_{3*} = \sqrt{2} \int_0^\infty \left[1-g_*(\zeta)\right] d\zeta = \delta_* J_3 , \qquad (31)$$

$$I_{4*} = \sqrt{2} \int_0^\infty f_*(\zeta) g_*(\zeta)\, d\zeta = E_* \delta_* J_4 ,$$

$$I_{5*} = \sqrt{2} \int_0^\infty f_*(\zeta)\, d\zeta = E_* \delta_* J_5 ,$$

where J_1 to J_5 are meant to correspond to the *constant* momentum integrals I_1 to I_5 defined in (12). The calculation of the above integrals is detailed in the Appendix.

However, it is only the integrals I_{1*} to I_{5*} which we can obtain here, not the more relevant quantities E_*, δ_* and J_1 to J_5. Nevertheless, if the momentum integral formulation of (10), (11) and (12) can be accurately expressed by (31), then there are certain

quantities which should (hopefully) be natural invariants. The simplest of these are

$$C_1 = \frac{I_{3*}}{I_{2*}} , \quad C_2 = \frac{I_{4*}}{I_{5*}} , \quad C_3 = \frac{1}{4} \frac{I_{4*}\, I_{5*}}{I_{1*}\, I_{2*}} , \quad C_4 = \frac{1}{3} \frac{I_{4*}\, I_{5*}}{I_{1*}\, I_{3*}} , \tag{32}$$

and from (12), the appropriate Ekman values for these 'invariants' are 0.8, 0.75, 0.6 and 1.0 respectively.

Furthermore, should these quantities C_1 to C_4 can be found to be approximately constant, both with radius and the stability parameter ε, we can then obtain meaningful measures of E_* and δ_*. For example, we can define

$$\left.\begin{aligned} E_*^{(1)} &= -4I_{1*}/I_{5*} , \quad E_*^{(2)} = -I_{5*}/I_{3*} , \\ E_*^{(3)} &= -\tfrac{5}{4}I_{5*}/I_{2*} , \quad E_*^{(4)} = -3I_{1*}/I_{4*} , \end{aligned}\right\} \tag{33}$$

and so on. With quantities such as these, we are in a position to make a direct comparison between the momentum integral and perturbation solutions, provided of course that we are able to demonstrate via (32) that there is originally real justification in applying the former method.

Details of the relevant calculations follow in Section 7.

7. Results

In the following discussion we present details of certain calculations arising from the various techniques which have been outlined in this chapter. Table 1 provides a convenient summary of the cases which have been treated, together with the corresponding nomenclature used

in the diagrams.

In the calculations which have been performed, we have used for the form of the swirling flow above the hurricane boundary layer, the profile obtained in S, together with two of the profiles presented by George (1970).

The profile of S is a solution of the gradient wind equation (1), and is obtained by assuming that the pressure in the hurricane vortex is given by

$$P(R) = P_c + (P_g - P_c)e^{x(b-R_m/R)} ,$$

where P_c and P_g are the pressures at the centre and the geostrophic radius respectively, and x is chosen so that the maximum velocity occurs at $R=R_m$, with $b=R_m/R_g$. Specifically, this leads to the profile

$$\tilde{v} = -\frac{r}{2} + \left[(\frac{r}{2})^2 + \frac{mxb}{r} e^{xb(1-r^{-1})}\right]^{\frac{1}{2}} , \qquad (34)$$

where $m = (P_g - P_c)/(\rho R_g^2 f^2)$. According to the scaling of Section 2, $v_{gr} = 1$ at $r=1$, and hence from (34),

$$Ro = -\frac{1}{2} + (\frac{1}{4} + mxb)^{\frac{1}{2}} , \qquad (35)$$

and x can be shown to satisfy the equation

$$mx(x-1)^2 e^{x(b-1)} - (2-x)b^2 = 0 \qquad (1<x<2).$$

The particular physical parameters used to represent the hurricane vortex, are $P_c = 940$ mb, $P_g = 1000$ mb, $R_g = 1000$ km, $R_m = 40$ km,

ρ = 0.0012 gm/cc and $f = 5\times10^{-5}$ sec^{-1}, with the constant eddy viscosity $K = 5\times10^{4}$ cm^{2} sec^{-1}. The dimensional form of this profile (34) is sketched in Figure 2(a); the flow is effectively solid body rotation near the centre with the velocity rising to a maximum value of approximately 43 m/sec at $R=R_m$, falling to about 4 m/sec at $R=R_g$. The Rossby number Ro, calculated from (35), is approximately 0.0776.

Two of the swirling profiles of George (1970) which are also used in the present calculations, were obtained on much more of an *ad hoc* basis than that used in S. With reference to the scaling of Section 4, they can be written as

$$\Psi = \begin{cases} 4\left[\left(\frac{x}{x_1}\right)^{\frac{1}{2}} - \frac{x}{x_1}\right] & x_o < x \leq x_1 = 4x_o \\ 1 & 0 < x \leq x_o \end{cases} \qquad (36)$$

and

$$\Psi = \begin{cases} e^{-x^{0.1}} & x \geq 1 \\ Ax^{0.1} + Bx + Cx^2 & 0 < x \leq 1 \end{cases} \qquad (37)$$

where the constants A, B and C are obtained by imposing continuity of Ψ, $d\Psi/dx$ and $d^2\Psi/dx^2$ at x=1. If we scale according to the vortex of S, then we can set $\Psi_o = R_g V_g$ and hence x_1 in equation (36), which corresponds to the geostrophic radius, is equal to 1/(2Ro). Profiles of V_{gr} corresponding to the above Ψ profiles are presented in Figure 2(b).

As far as the physics of the situation is concerned, these

two profiles are rather less satisfactory than that of S, since they exhibit no core structure near the centre. Furthermore, profile I which is the principal one used by George, tends to *zero* at the geostrophic radius. Accordingly, although extensive calculations were also performed with George's profiles, we have judged it preferable to use the profile of S - Figure 2(a) - in presenting the results which follow.

Figure 3 shows the variation with radius of the boundary layer thicknesses predicted by the momentum integral method of S and the two modified methods of Section 5.3. One noticeable feature is that in the case of two boundary layer thicknesses (S3), the radial boundary layer is seen to 'erupt' near the centre, as must happen in the real situation. However, this behaviour may be merely an artifact of the method used and we are unable to make any further comment at this stage. In this same figure, we also plot the function $1/\lambda(x)$, defined by equations (9) and (19c) with $\rho=1$, for the swirling profile of Figure 2(a). We see that it has roughly the form of the boundary layer thicknesses *predicted* by the momentum integral methods, thus fortuitously providing the base functions (19b) used in the Galerkin method with a realistic thickness scale. It can be seen that in the outer half of the vortex, these boundary layer thicknesses remain effectively constant near the Ekman value of $\sqrt{2}$, and hence it can be expected that Ekman flow will provide a reasonable approximation of the overall flow details in this region.

In Figure 4, the variations of the maximum radial velocity component $U_{max}=E(r)V_{gr}(r)f_{max}$ with radius, are given for the three

momentum integral methods, together with the Ekman result, $V_{gr}f_{max}$. Here, f_{max} is the maximum magnitude of the radial Ekman profile (11) which equals $e^{-\pi/4}/\sqrt{2}$. In Figures 5(a) to (d), we show the profiles of w_{gr}, the dimensionless outflow from the boundary layer for Ekman flow, the three momentum integral methods and for selected calculations with the Galerkin method.

As a result of Figures 4 and 5 we can now make several general observations. Firstly, as expected from Figure 3, the classical Ekman results for U_{max} and w_{gr} agree quite closely with the momentum integral calculations in the outer half of the vortex. The results obtained for w_{gr} from the Galerkin method, are rather less consistent, both in this outer region, and also closer to the centre. In the outer region - Figure 5(b) - it is the Galerkin method with N=3,ρ=0 (G2) which agrees closely with the method of S. In this particular case, we have three terms in the expansions (19a), in which the thickness scales of the base functions are *constant* with radius, being equal to $\sqrt{2}$, $\sqrt{2}/2$ and $\sqrt{2}/3$. However it can be seen in Figure 5(d), that as the centre is further approached, the real problems of the Galerkin method become apparent: Curve G3 the case when the scale thicknesses of the base functions are multiples of $1/\lambda$, is seen to be well behaved for all radii, although at small r it does predict a w_{gr} considerably smaller than S1. This behavious is not altogether surprising, since we have seen in Figure 3, that the function $1/\lambda$ calculated directly from the swirling velocity above the boundary layer, exhibits the same overall behaviour as the δ's calculated from the various momentum integral method - approximately $\sqrt{2}$ for large r, followed by a rapid decrease as the centre is

approached. However when the base functions have a constant scale thickness (G1, G2), the calculations become unstable at small r and the situation is merely worsened if more terms are included in the expansions (19a): the point at which the singularity occurs changes from r=0.022 for N=1, to r=0.096 for N=3.

Further details of the Galerkin solutions which may help to explain the situation, are presented in Figure 6, where we show the variation with radius of the expansion coefficients a_1 and a_2 for the cases G2 and G3, together with the form of Ψ corresponding to the swirl profile of S - Figure 2(a). At large radius the Ekman solution holds approximately; that is, $a_1 = -\Psi$, $a_i = O(i>1)$. Now if we consider the expansions (19a) to be meaningful, then we expect a_2 to remain small with respect to a_1, but as seen from Figure 6, this is not the case. For case G2, $a_2 > a_1$ at small radius, and this is followed by instability as r is further decreased. We presume therefore that the system is singular at small r but this has not been investigated, since we believe it is because the Galerkin method is basically inconsistent with the physics of the boundary layer that the above problems arise. Firstly, the assumption of a constant thickness scale of $\sqrt{2}$ especially at small radius, is at variance with the results of both the momentum integral methods (Figure 3) and those of Stewartson *et al.* discussed in Section 5.1. Secondly, although it leads to a well behaved system of equations, the alternative assumption of the $1/\lambda$ scale, arising as it does from a linear analysis at large z, cannot possibly be considered as

representative of the overall description of the motion in the boundary layer.† Thus, although the Galerkin method does at first appear to offer an improved treatment of the hurricane boundary layer, it is clear from the above discussion, that at most, it can be applied only in regions where Ekman flow itself is a good approximation.

In Section 5.2 we discussed the modified Oseen method of Carrier (1971a) and deduced simply by examination of the continuity equation, that the basic assumption of neglecting the term $w\frac{\partial u}{\partial z}$ with respect to $u\frac{\partial u}{\partial r}$, could not be justified. In Figure 7, we show the ratio of the maximum magnitudes of these two terms as obtained from the momentum integral method S1, and which clearly supports our original criticism.

In Figures 8 and 9, we present certain results from the first order perturbation analysis of the boundary layer equations, as discussed in Section 6. In Figure 8 are shown the curves of the functions $C_i(\varepsilon,r)$ defined by (32), the values of the stability parameter ε being 0, + 4Ro and - 4Ro. These curves give to some extent, an indication of the applicability of the momentum integral method since we have also indicated the constant values they would assume, if Ekman profiles were an exact representation of the structure

---

†One practical disadvantage of the method is the amount of computation necessary: the computer time for N=1 is roughly twice that of the momentum integral method S1, while increasing N by one, leads to an order of magnitude increase in the time required!

of the boundary layer. In the region considered, the Rossby number ranges from 0.05 at r=1 to 0.220 and 0.274 at r=0.45 for the plus and minus curves respectively, and it is somewhat encouraging to note that in one instance (C_4), it is the curve with the lower Rossby number which differs the most from the constant Ekman value. Figure 9 gives the functions $E_*^{(1)}$ to $E_*^{(4)}$ defined by (33) with $\varepsilon=0$. These are analogous to the radial velocity amplitude coefficient E(r) associated with the momentum integral methods, and which are also shown for comparison.

As a result of the calculations detailed above, we are now in a position to make an overall assessment of the various methods discussed in this chapter. Firstly, we have demonstrated that neither the Galerkin method nor the modified Oseen method is capable of providing a realistic description of the motion. This therefore leaves the momentum integral method as being still the only practical method applicable to hurricane boundary layer flows, with some additional justification being provided by Figure 8. On the other hand, it is also doubtful as to whether any real advantage has been gained by the introduction of the alternative momentum integral methods of Section 5.3 It was believed that use of the constraint (21) would lead to a formulation predicting smaller radial velocities in the boundary layer. However, it can be seen from Figure 4, that although this is effected for case S2, the values obtained for the second case S3 are larger than those obtained from the original momentum integral method S1. In fact the results of the perturbation analysis in Figure 9, suggest that the radial velocities obtained from the momentum integral methods may in all cases be too low.

8. Conclusions

The results of the work performed in this chapter suggest that at present, the momentum integral method is the only really practical and efficient method for treating the hurricane boundary layer. By contrast, the methods introduced by Carrier and his co-workers contain obvious and vital defects in their basic formulation. Nevertheless it is also felt that a more extensive study is needed should it be thought necessary to obtain more stringent tests of the applicability of the momentum integral method. This suggests that calculations similar to those of Stewartson *et al.* of Section 5.1 be performed, but modelling a system more directly applicable to geophysical flows.

Provided Ekman velocity profiles are suitable for this simple case of constant eddy viscosity (and we believe that they are), it opens the way for a number of significant extensions. Firstly, more realistic boundary layer parameterisations, such as the one to be discussed in Chapter 2, can be used with confidence over the entire radial range of the vortex. Secondly, we can use the momentum integral method as a diagnostic in more comprehensive numerical models of developing hurricanes, as discussed in the Introduction, with the method being adapted to take into account the three-dimensional nature of the outer flow.

APPENDIX

As the simplest example of the integrals (31) associated with the perturbation solution of Section 6, we calculate I_{5*}, where from (30) and (31),

$$\frac{I_{5*}}{\sqrt{2}} = \int_0^\infty f_*(\zeta)\, d\zeta$$

$$= (1+\mathrm{Ro}\frac{V}{r})\int f\, d\zeta - \mathrm{Ro}\,\frac{(rV)'}{r}\int \left[fg+\frac{1}{2}(g-f)\dot{g}\right] d\zeta$$

$$= (1+\mathrm{Ro}\frac{V}{r})(-\frac{1}{2}) - \mathrm{Ro}\,\frac{(rV)'}{r}\,(-\frac{3}{8}+\frac{1}{2}\cdot\frac{3}{4})$$

i.e., $I_{5*} = -\sqrt{2}\frac{X}{2}$,

where $X = 1 + \mathrm{RoV}/r$. In similar fashion, we find

$$I_{1*} = \sqrt{2}\left[\frac{1}{8}X^2 + \mathrm{Ro}X\,\frac{(rV)'}{30r} + \frac{13}{480}\left(\mathrm{Ro}\,\frac{(rV)'}{r}\right)^2\right]$$

$$I_{2*} = \sqrt{2}\left[\frac{5}{8} - \frac{\mathrm{Ro}}{60}\left(22\,\frac{(rV)'}{r} + 9V'\right) - \frac{\mathrm{Ro}^2}{240}\left(19\left\{\frac{(rV)'}{r}\right\}^2 + 4\frac{V}{r}\left(\frac{V}{r} - 2V'\right)\right)\right]$$

$$I_{3*} = \sqrt{2}\left[\frac{1}{2} - \frac{1}{4}\,\mathrm{Ro}\,\frac{(rV)'}{r}\right]$$

$$I_{4*} = \sqrt{2}\left[-\frac{3}{8}X - \frac{\mathrm{Ro}}{40}X\left\{2\,\frac{(rV)'}{r} + \frac{V}{r}\right\} + \frac{3}{40}\,\mathrm{Ro}\frac{(rV)'}{r} - \frac{\mathrm{Ro}^2}{8}\,\frac{(rV)'}{r}\left\{\frac{(rV)'}{12r} - \frac{V}{5}\right\}\right]$$

Case	Method	Equations
E	Classical Ekman results	8,11
S1	Momentum integral method - Smith (1968)	13,14,15
S2	Modified momentum integral method: one independent parameter (δ)	23,24
S3	Modified momentum integral method: two independent parameters (δ,Δ)	26,27
G1	$N=1,\rho=0$	9,19,20
G2	Galerkin method - George(1970): $N=3,\rho=0$	
G3	$N=3,\rho=1$	

Table 1. Details of the methods used in the boundary layer calculations discussed, together with the shorthand notation which denotes these cases in the diagrams.

Figure Captions

Figure 1. Sketch of the principal features of the mature hurricane - after Smith (1968).

Figure 2. Profiles of V_{gr} representing the flow in the hurricane vortex above the boundary layer: (a) obtained by Smith (1968) - equation (34); (b) obtained by George (1970) - equations (36), (37).

Figure 3. Profiles of $\delta(r)$, the non-dimensional boundary layer thickness for the cases E,S1,S2 and S3 together with the *a priori* boundary layer scale $1/\lambda$, used in the Galerkin method of George (1970).

Figure 4. Profiles of U_{max}, representing the maximum radial velocity attained in the boundary layer, for the cases E,S1,S2 and S3.

Figure 5. Profiles of w_{gr}, the dimensionless outflow from the top of the boundary layer for the cases E,S1,S2,S3,G1,G2 and G3.

Figure 6. Radial variation of the ratio of the maximum magnitudes of $u\frac{\partial u}{\partial r}$ and $w\frac{\partial u}{\partial z}$, calculated from the momentum integral method S1.

Figure 7. The coefficients a_1 and a_2 obtained from the solution of the Galerkin equations, together with the Ψ-profile corresponding to Figure 2(a).

Figure 8. Variation with radius r and stability parameter ε of the functions C_1 to C_4 defined by (32). The values of ε are 0, + 4 Ro and - 4 Ro, as indicated by the plus and minus signs. The constant Ekman values for Ro=0 are indicated at r=1.

Figure 9. The functions $E_*^{(1)}$ to $E_*^{(4)}$ defined by (33), with ε=0. Comparison curves of the functions E(r) from the momentum integral methods are also shown.

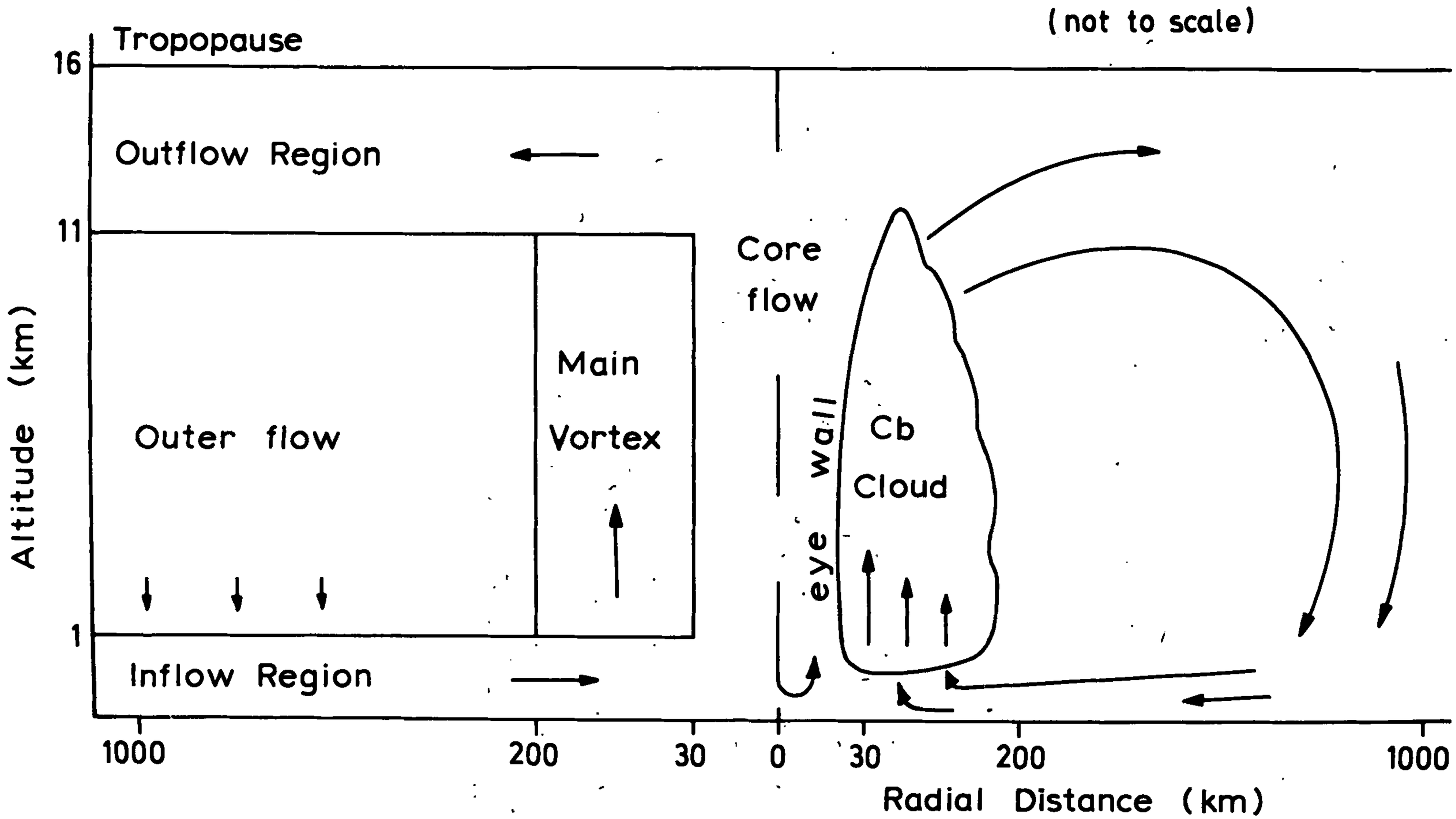
(not to scale)
Tropopause
16
Outflow Region
11
Outer flow
Main
Vortex
Inflow Region
1
Altitude (km)
Core
flow
eye wall
Cb
Cloud
1000
200
30
0
30
200
1000
Radial Distance (km)

Figure 1

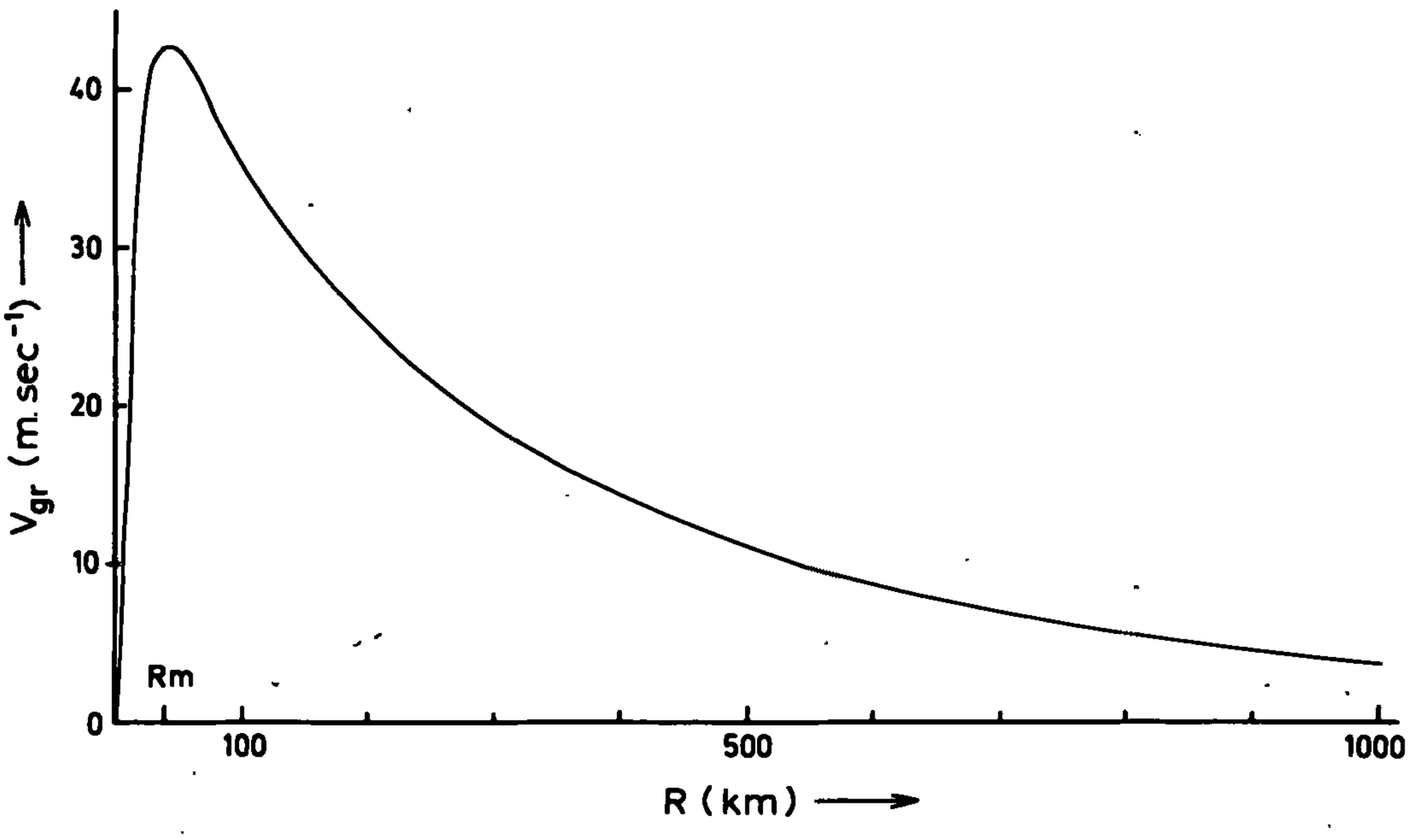

Figure 2(a)

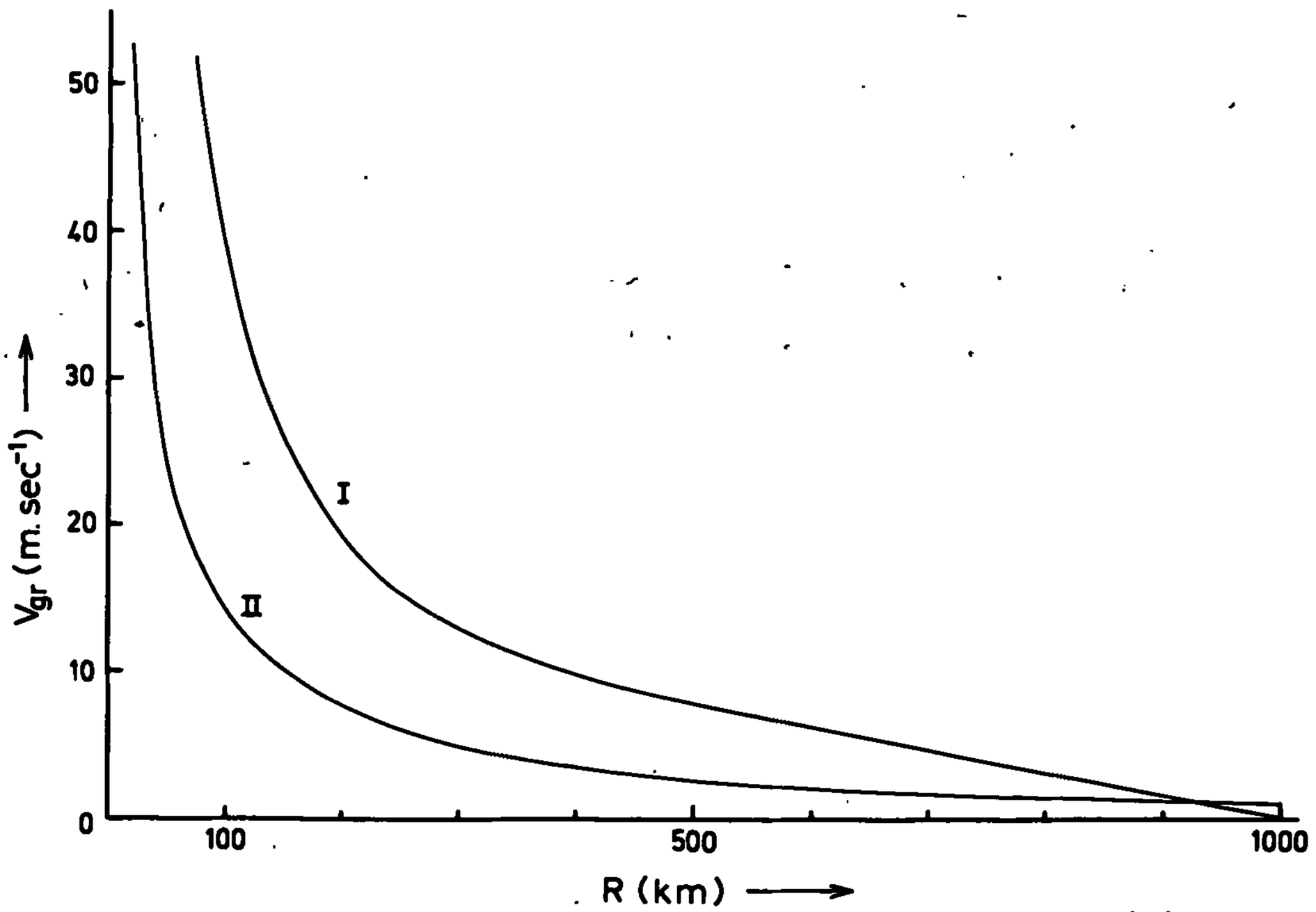

Figure 2(b)

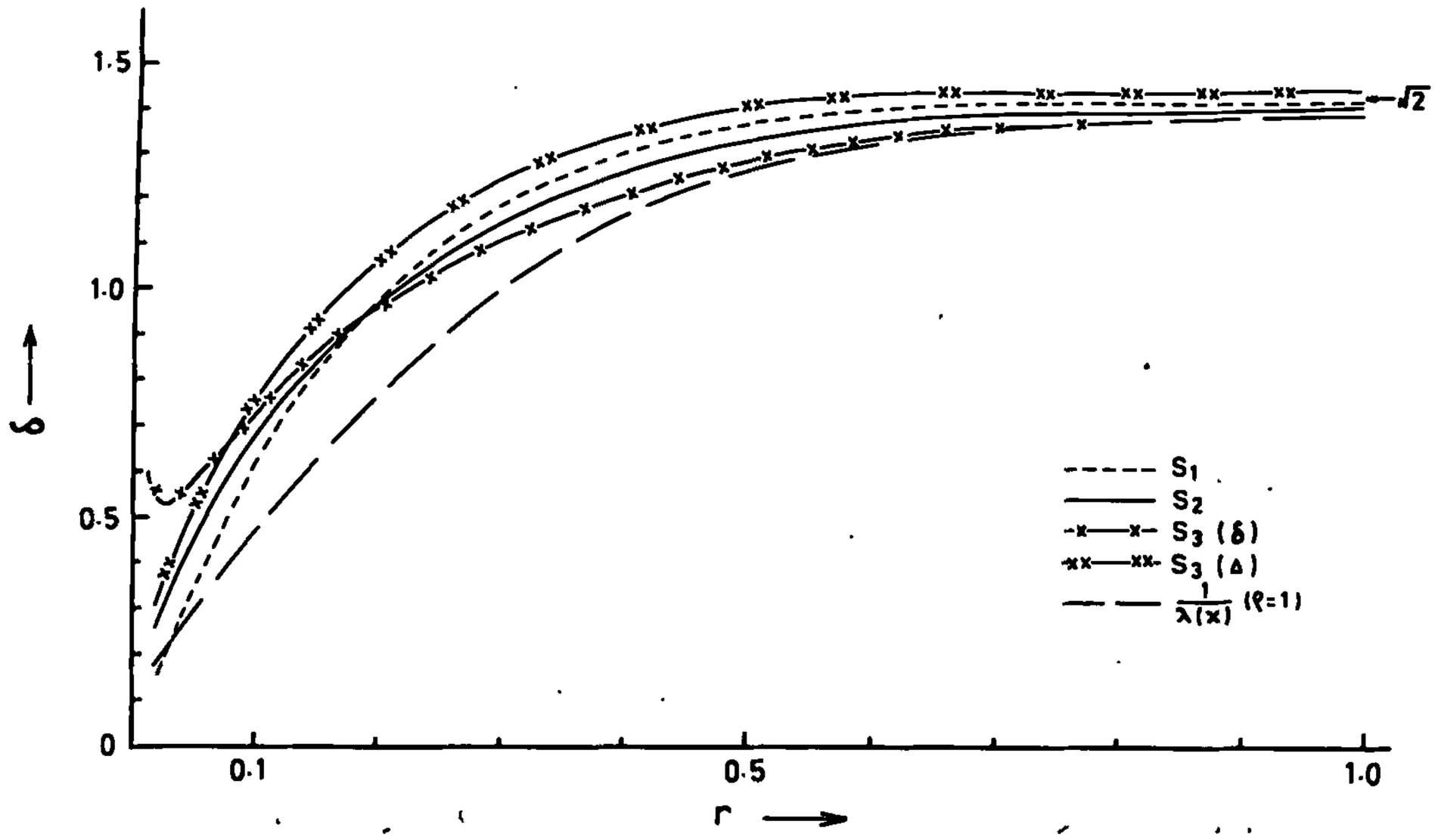

Figure 3

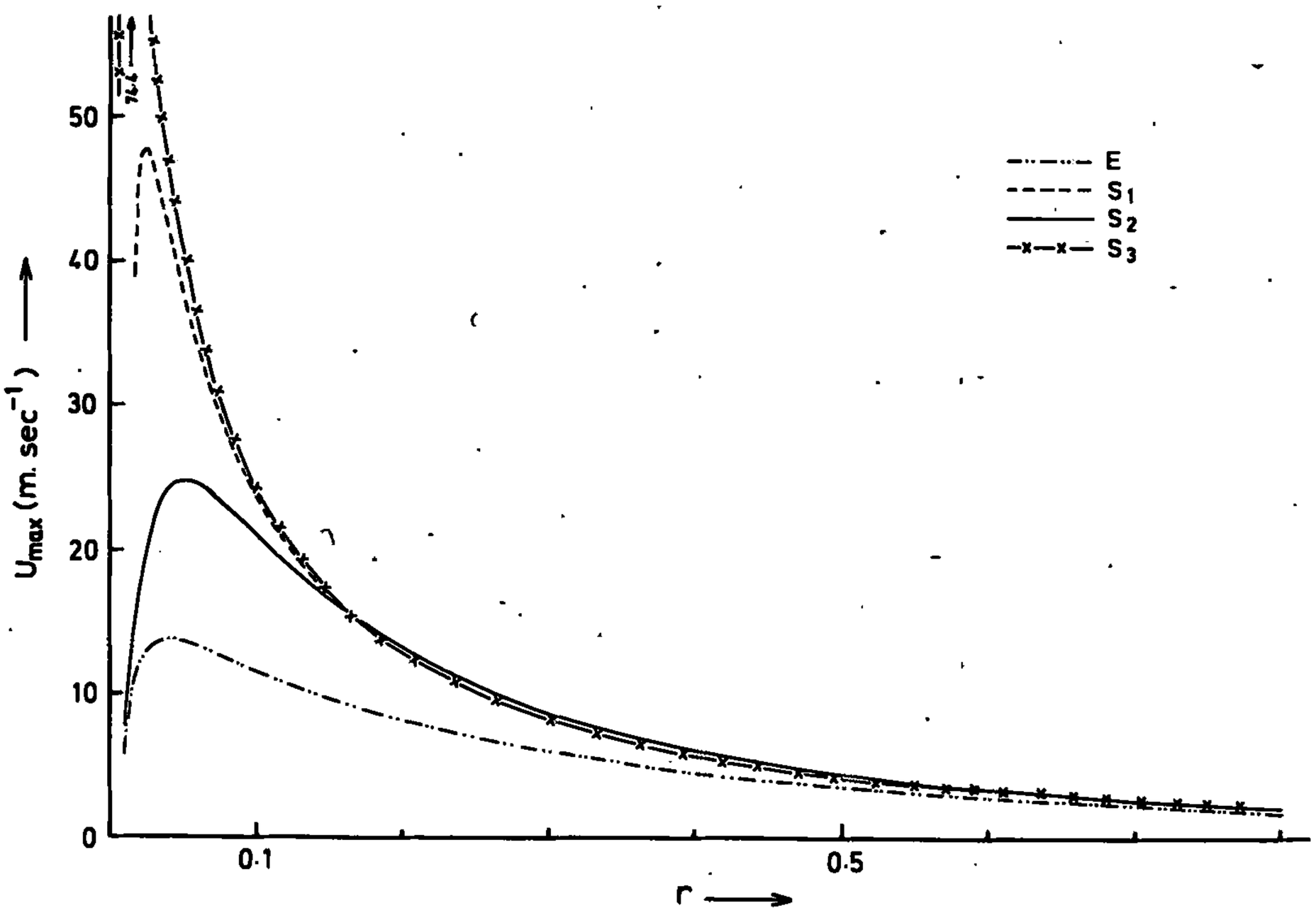

Figure 4

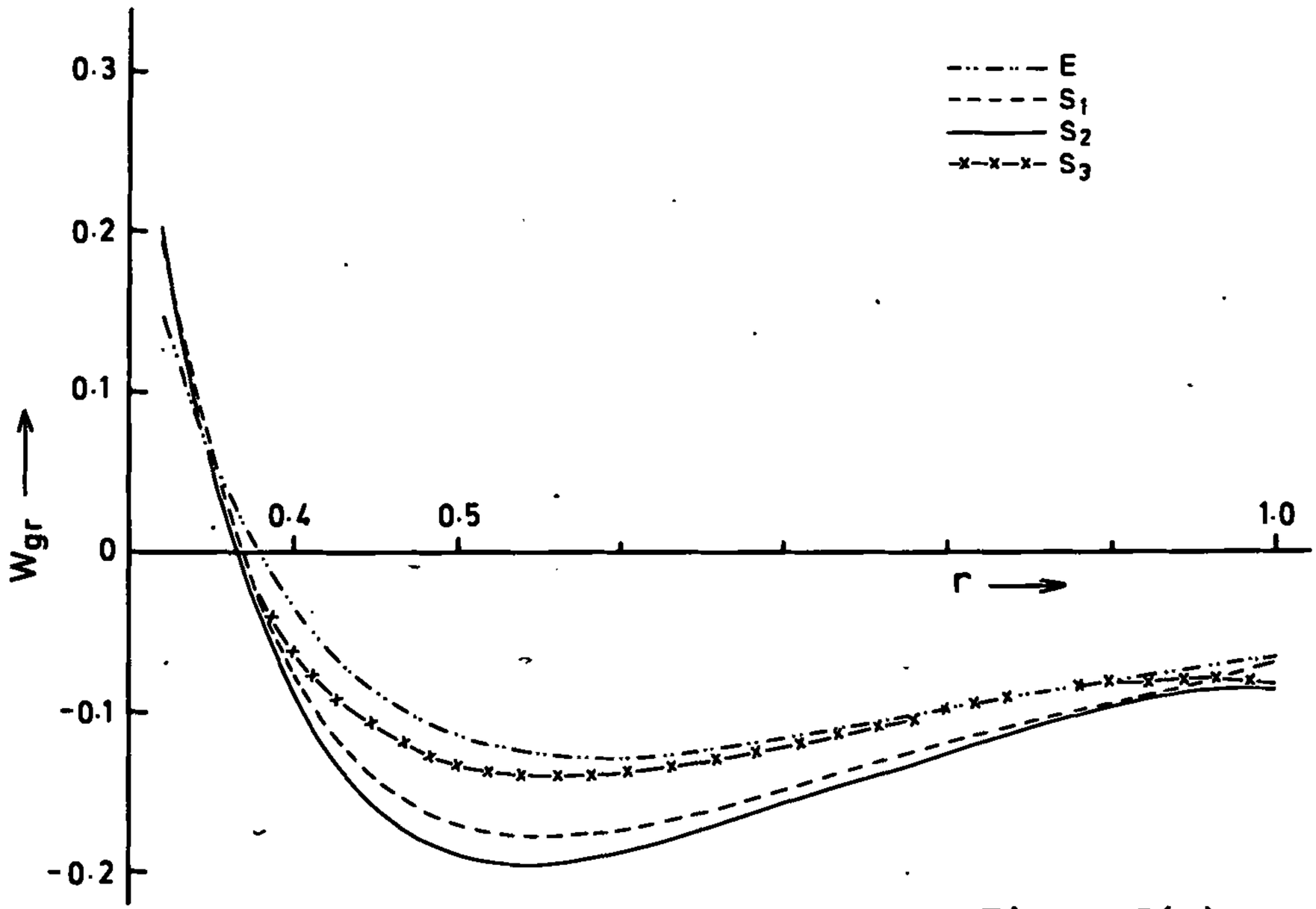

Figure 5(a)

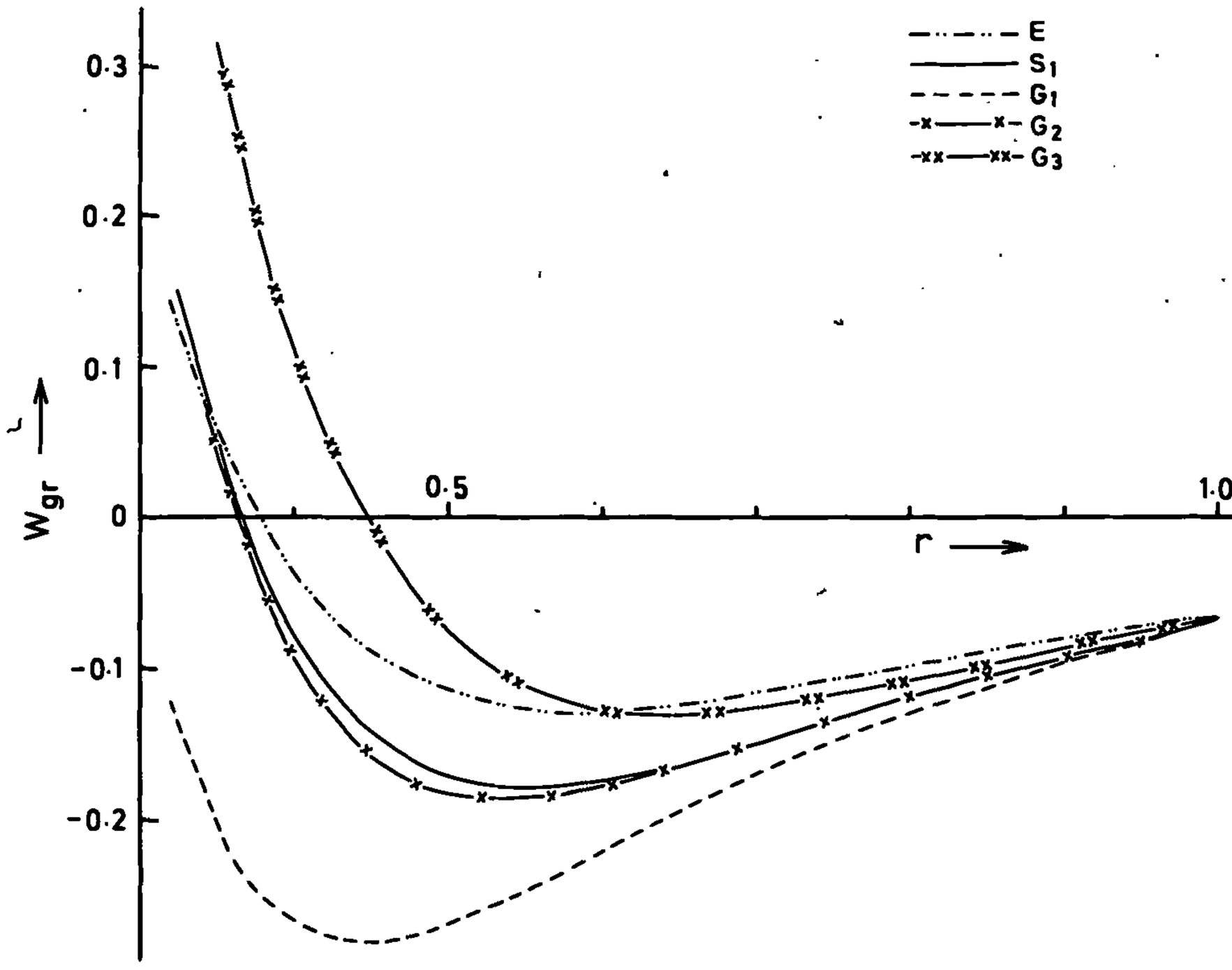

Figure 5(b)

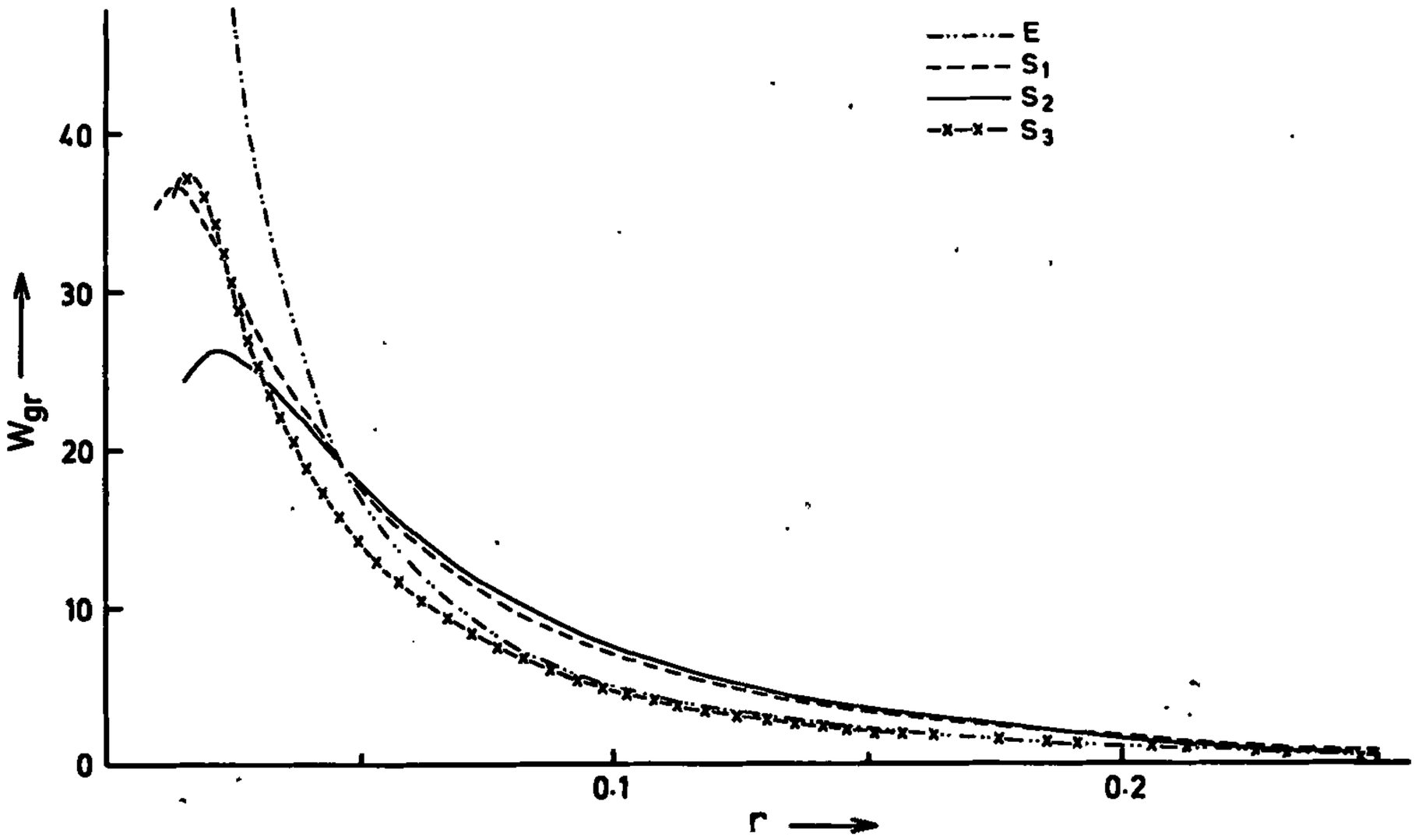

Figure 5(c)

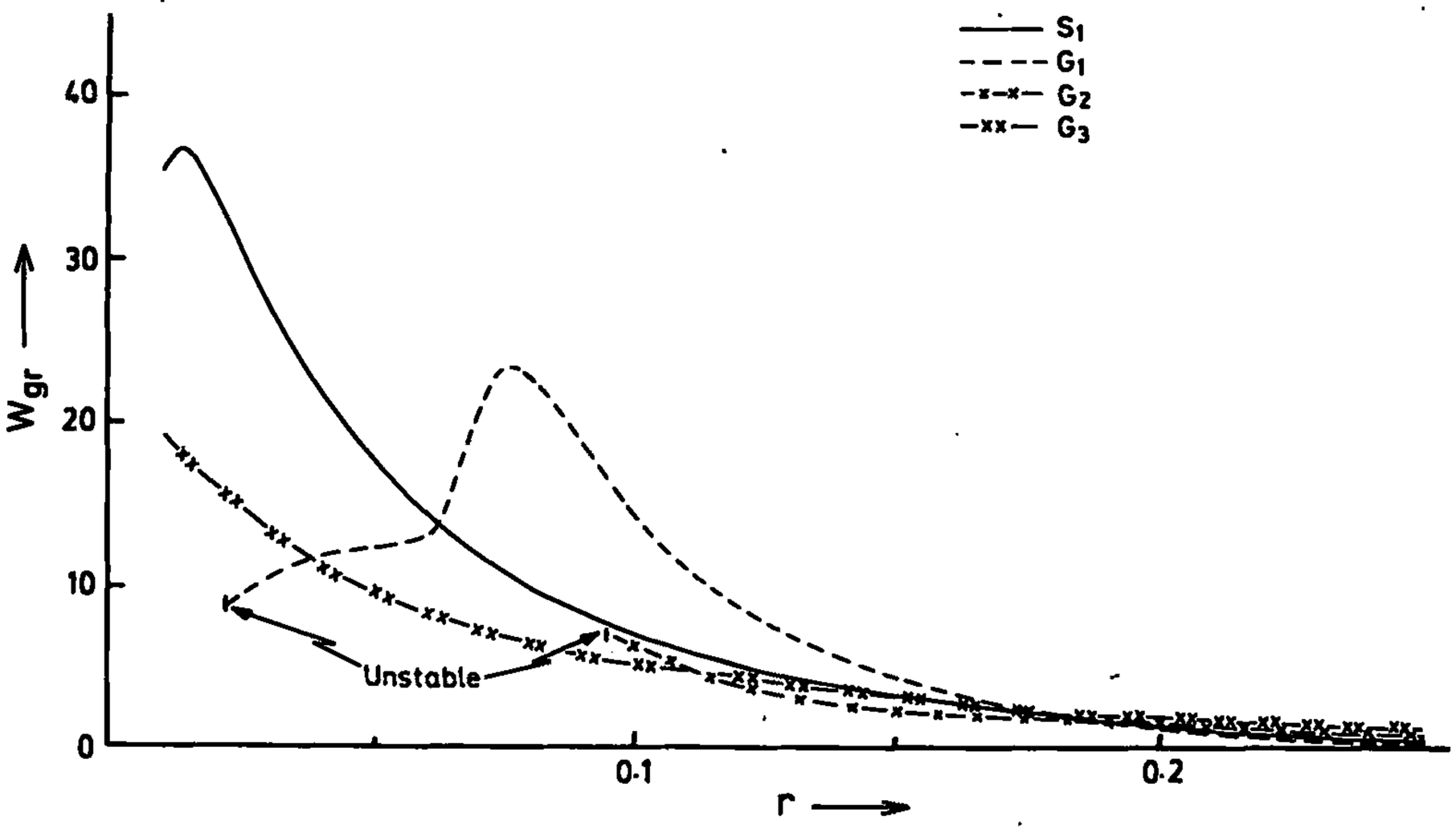

Figure 5(d)

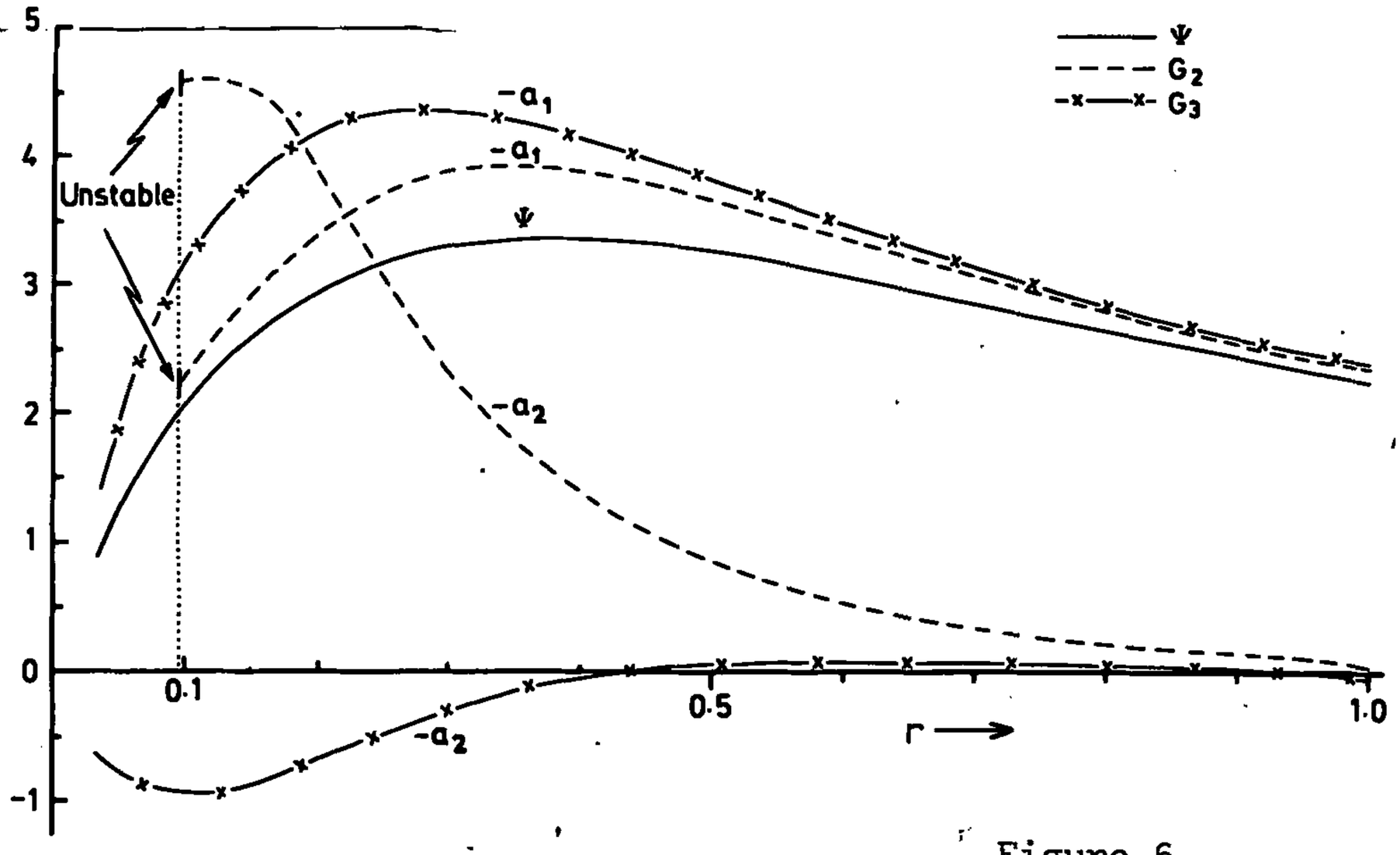

Figure 6

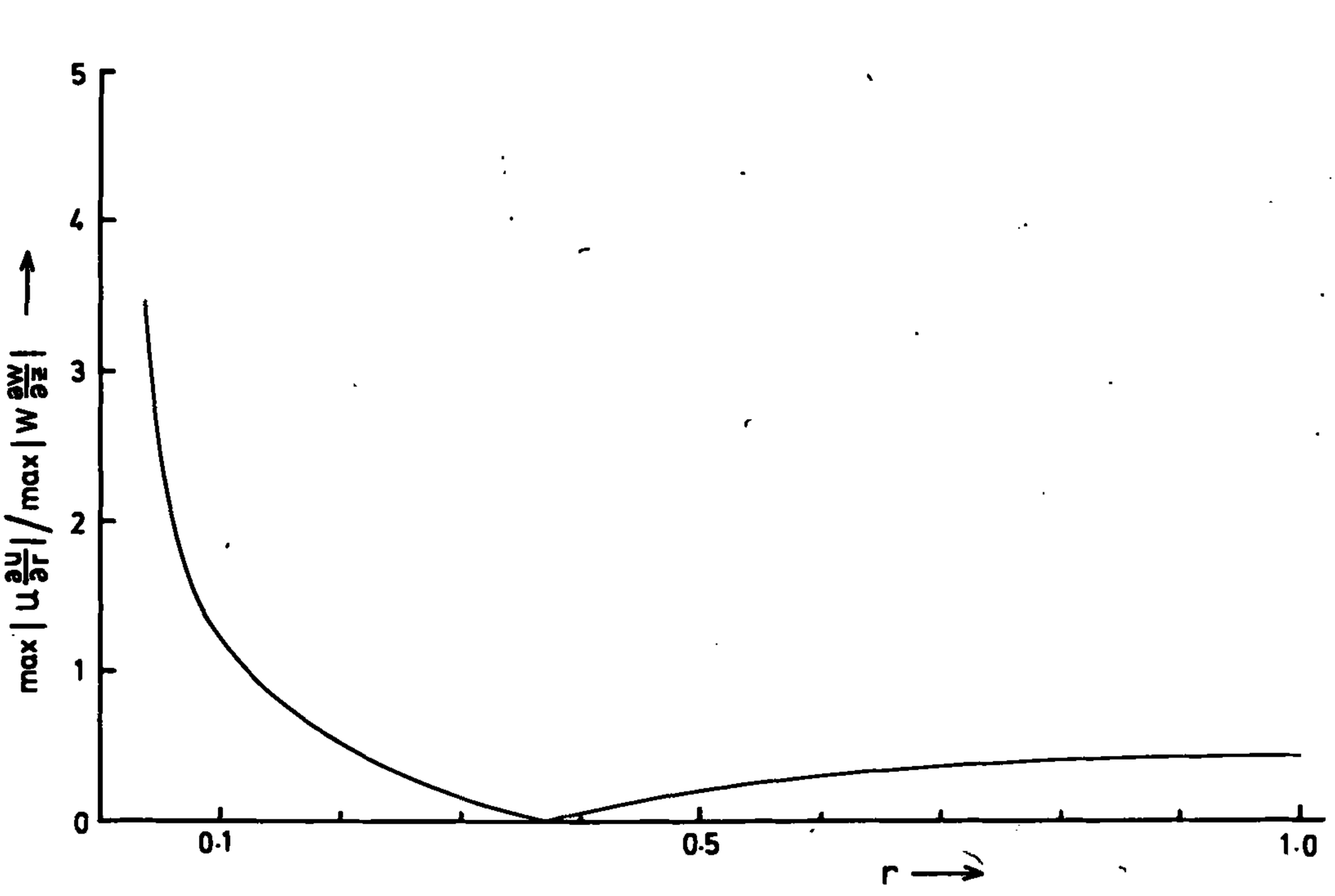

Figure 7

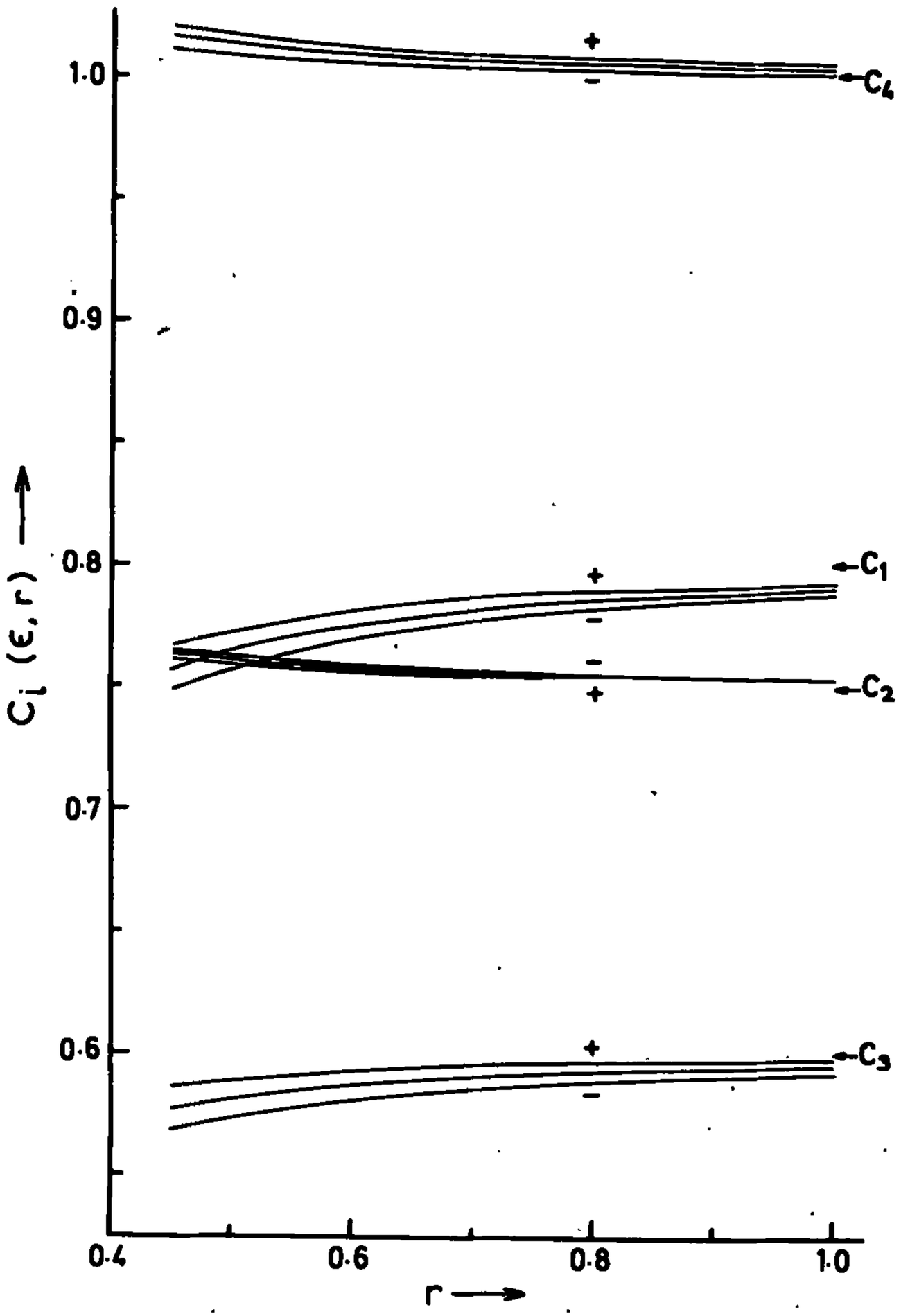

Figure 8

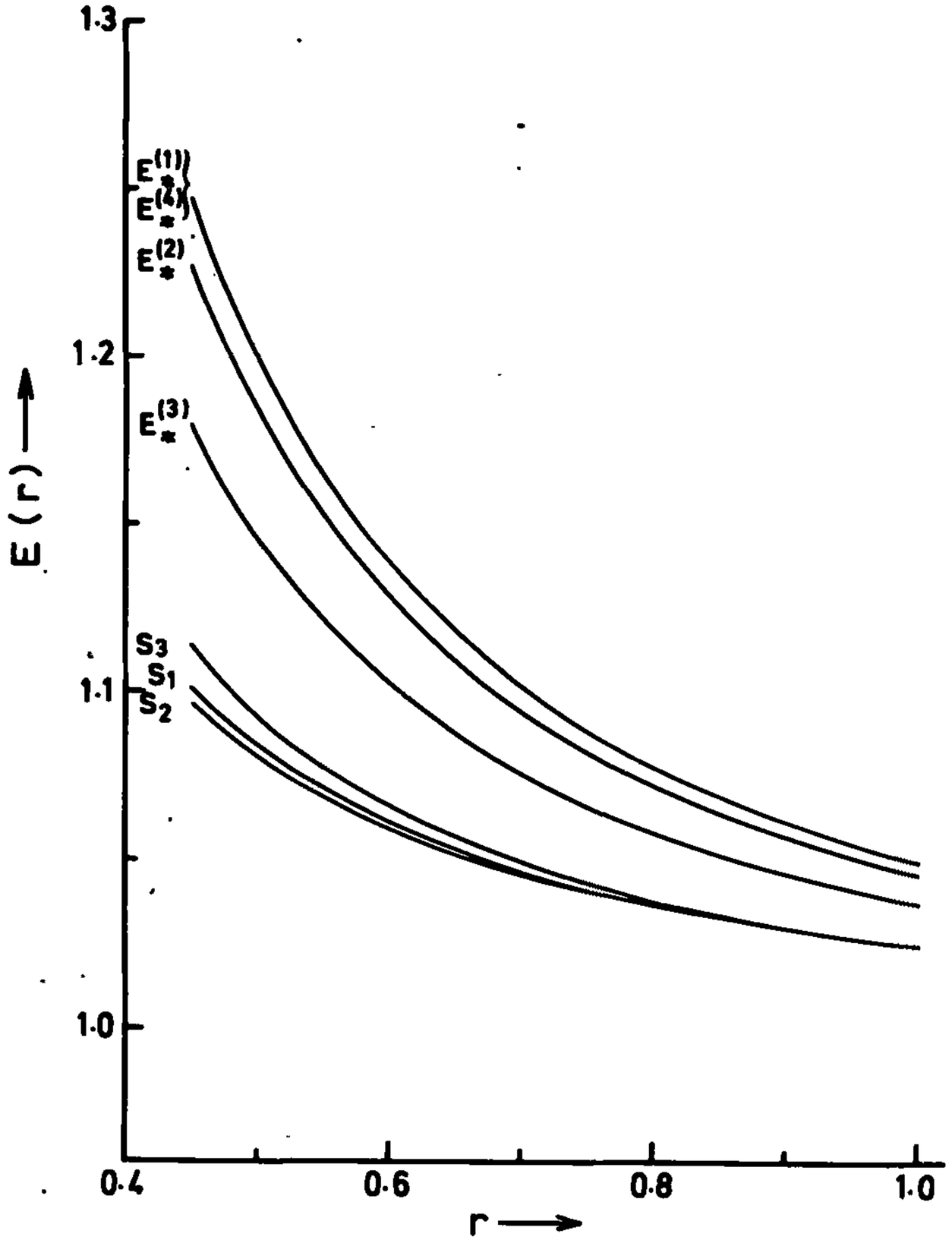

Figure 9

Chapter 2

A parameterisation of the neutral atmospheric boundary layer, with application to momentum integral calculations.

ABSTRACT

The work in this chapter consists of two sections. In Section A, a relatively simple two-layer parameterisation of the neutral atmospheric boundary layer is developed. It comprises the well known logarithmic sublayer near the surface, matched to an Ekman layer which adjusts to the geostrophic wind V_g. The model is self-consistent, requiring only the specification of the universal relationship between the surface Rossby number $V_g/(fZ_o)$ and the geostrophic drag coefficient U_*/V_g, where f is the Coriolis parameter, Z_o is a length scale characterising the physical roughness of either the land or sea surface, and U_* is the friction velocity: two such relationships are investigated. Thus for a given V_g and f, the system is completely defined by specification of the surface roughness length Z_o. In spite of the simplicity of the model, it predicts results which compare favourably with the more sophisticated model of Lettau for the Leipzig and Scilly wind profiles.

In Section B, the velocity profiles obtained from the first section are incorporated in a momentum integral method to determine the flow in the surface boundary layer of an idealised hurricane. The particularly simple analytic form of these profiles makes them ideal for such a treatment. It is shown that the effective role of the frictional sublayer is to provide bottom boundary conditions for the Ekman layer in such calculations. Also investigated are the effects of various refinements to the momentum integral method.

Introduction

The work to be discussed in this chapter falls into two distinct sections. In Section A we develop a relatively simple, but also physically significant parameterisation of the neutral atmospheric boundary layer (henceforth referred to as the ABL). In Section B, the velocity profiles and the turbulent structure of the ABL obtained from this model, are used to study the properties of the surface boundary layer of a hurricane by means of the momentum integral method developed by Smith (1968), henceforth denoted by S.

Attempts to model the turbulent structure of the ABL by means of an eddy viscosity distribution $K_m(Z)$, have been made by many authors beginning with Taylor (1915). Recent reviews which cover this work include those of Zilitinkevich, Laikhtmann and Monin (1967), Hanna (1969) and Monin (1970). In Section A we propose to show that an eddy viscosity of the form

$$K_m(Z) = \begin{cases} kU_*Z & , \ Z \leq H \\ kU_*H & , \ Z > H \end{cases} \qquad (1)$$

first suggested by Yudin and Shvets (1940), provides a satisfactory description for many purposes of the structure of turbulence in model studies. Strong vortical flows for example, such as large-scale hurricanes will tend to strongly constrain the flow in the boundary layer. Furthermore, the dominating effect of the shear-induced turbulent mixing over that of convective processes in such motions, make the assumption of neutral stability a good approximation. Here k is Kármán's constant (approx. 0.4) and U_*, known as the 'friction velocity' is related to the surface stress $\underline{\tau}_o$ and the

density ρ, by

$$|\underline{\tau}_o| = \rho U_*^2 .$$

The value of the intermediate altitude H in equation (1) is not specified *a priori*, but is found from the model itself.

It is well known experimentally, that for approximately neutral conditions, the mean velocity profile in the thin sublayer of the ABL extending over the first few tens of metres is logarithmic (see e.g., Priestley (1959), Ch. 3). In this layer the stress has the constant value $\underline{\tau}_o$ and hence there is no spiralling of the wind with height. These conditions may be shown to be compatible with an eddy viscosity proportional to height, namely

$$K_m = kU_*Z.$$

Above this sublayer the behaviour of the eddy viscosity is less certain; in fact the use of K_m at all has been questioned rather critically by Kraus (1968). However it is generally accepted that above the sublayer, K_m increases more slowly to a maximum value at a height of the order of a few hundred metres, and then decreases very gradually to a residual 'Austausch', not necessarily zero, of the free atmosphere at the so-called gradient wind level. This type of behaviour was first proposed by Mildner (1932) in his analysis of the famous Leipzig wind profile. Similar conclusions were reached by Bujatti and Blackadar (1957), from their numerical model of diurnal wind variations.

Single-layer numerical models of K_m which have reproduced this behaviour most accurately include those of Blackadar (1962) and

Lettau (1962). The models of both these authors use an appropriate mixing length involving a universal constant which they are required to specify *a priori*. The form of the eddy viscosity proposed by Blackadar, is

$$K_m(Z) = \left(\frac{kZ}{1 + kZ/\lambda}\right)^2 \cdot \left(\frac{\partial^2 U}{\partial Z^2} + \frac{\partial^2 V}{\partial Z^2}\right)^2$$

Models very similar to Blackadar's are those of Wagner (1966) and Estoque (1967). Here U and V are the horizontal velocity components and λ is the empirically determined parameter, related to the magnitude V_g of the geostrophic wind above the ABL, and the Coriolis parameter f, by $\lambda = 0.00027V_g/f$. A model whose results agree closely with those of Lettau (1962) is that of Ohmstede and Appleby (1964). Both express K_m as the product of a mixing length (determined from the Leipzig wind profile) and U_*. The form obtained by Lettau is

$$K_m(Z) = \frac{kU_*Z}{\left[1 + 4\left(\frac{Z}{X_1}\right)^{5/4}\right]}$$

where the parameter X_1 is called the 'scale height of the boundary layer' and is of the order of several hundred metres. Its form is deduced by an analogy of the ABL flow with turbulent flow in straight ducts. Certain results of the present model will be compared with Blackadar's and Lettau's. - However both these models, because of their inherent non-linearity, require considerable numerical computation for each set of dynamical parameters specified. Hence they tend to be too unwieldy in the case of hurricane boundary layer calculations for example, where such a parameterisation must be performed many times in the course of integrating the boundary

layer equations numerically. The main purpose of Section A is to show that the simple model proposed there for K_m, yields results in quite good agreement with those of Blackadar and Lettau, yet that the amount of computation required is comparatively minimal.

A significant advance in the study of the turbulent structure of the ABL was made by Rossby and Montgomery (1935) in their well known paper, where they formulated a two-layer model. In the frictional sublayer, $Z \leq H$, they adopt the condition of constant stress leading to the non-spiralling logarithmic profile; this is combined with a second profile for $Z \geq H$, the theory for which had been developed in an earlier paper by Rossby (1932). Here the mixing length l (with K_m proportional to l^2) decreases linearly from its value at H, to zero at the gradient wind level H_1, the resultant wind profile being a logarithmic spiral with constant shear. However, in order to obtain more acceptable agreement with observed behaviour, it is found necessary to postulate a residual Austausch at H_1 of 50 gm cm^{-1} sec^{-1}. Their theory agrees well with available experimental measurements and in order to close the system, an additional empirical constant equal to 0.065 is specified.

The particular eddy viscosity model used in the present work was proposed initially by Yudin and Shvets (1940) and is reviewed in Chapter 2.6 of the book by Laikhtmann (1964). This model comprises a constant stress sublayer, which is 'patched' to a constant eddy viscosity Ekman layer at some intermediate height H, to be determined by the model. Thus in the sublayer the velocity profile is logarithmic, and this is matched at Z = H to an Ekman

spiral, by requiring that velocity and stress be continuous there. The actual details of the model of Yudin and Shvets differ from the present in that they solved the equations of motion in the sublayer (with $K_m = kU_*Z$) to obtain Hankel function solutions (see Ellison 1956). The form of K_m used in the present model has a similar structure to that proposed by Smith (1969), namely

$$K_m(Z) = K(1-e^{-aZ}) \text{ , with } a = kU_*/K$$

Here, for small Z, K_m is approximately kU_*Z, while for large Z it tends to the constant value K. However, obtaining the velocity profiles involves rather laborious manipulation of hypergeometric series.

What might be considered the most obvious deficiency of the present model is the fact that K_m is constant above the sublayer, contrary to the generally accepted behaviour discussed above. It has been claimed, for instance by O'Brien (1970), that in formulating a model it is necessary for the residual value of K_m at the gradient wind level to be small (or zero) in order to 'insulate' the ABL from the free atmosphere above it. However we contend that this condition imposes an unnecessarily strong constraint on the system — the Ekman profiles obtained for the region of constant K_m above the sublayer are such that the wind stress tends rapidly to zero, and within only a few Ekman scale heights, we attain the geostrophic motion of the free atmosphere. In fact the particular description proposed by O'Brien, although having the advantage of mathematical simplicity is too loosely constrained, requiring the specification of *four* parameters for closure. Moreover, there

are a number of advantages in the present model, the principal one being that the system is parameterised so that we require just *one* relationship to be specified *a priori*. This is the universal relationship between the 'geostrophic drag coefficient' $C_d = U_*/V_g$ and the surface Rossby number $Rs = V_g/(fZ_o)$, introduced by Rossby and Montgomery (1935), where the quantity Z_o, whose significance will be discussed later, is known as the 'surface roughness length.' A number of authors have investigated the derivation of a formula linking these two dimensionless quantities, and in the survey by Hanna (1969), several such works are discussed. In the present study we use firstly the relationship derived by Blackadar (1962) for neutral stability. Also used is the semi-empirical formula of Kazanskii and Monin (1961), with the experimentally determined constants A and B being taken from the recent and very extensive measurements of Clarke (1970). In the latter case we can tentatively extend the analysis to non-neutral conditions. A further advantage of the present model is the relatively small amount of computation required to solve the system, given a set of dynamical parameters. In contrast with the model of, for example Blackadar, who is required to solve a pair of coupled differential equations, we are required to solve a single transcendental equation, a simple matter numerically. Also, the velocity profiles can be expressed in a concise analytical form and hence are immediately applicable to momentum integral calculations.

These momentum integral calculations form Section B of the present work. They are used to obtain the gross structure of the boundary layer of an idealised hurricane, in which the turbulent

structure of the boundary layer has been obtained from the parameterisation of Section A. A discussion of hurricane boundary layer calculations and the use and justification of the particular momentum integral method employed, is presented in the previous chapter.

A - PARAMETERISATION

1. The equations of motion

We consider motion in the ABL under the usual assumptions that the mean flow is steady and horizontal, and that the density of the air is constant with height. In a Cartesian coordinate system (X,Y,Z), the equations which we obtain from the Navier — Stokes equations under the above assumptions, are

$$\left.\begin{aligned} -f(V-V_g) &= \frac{d}{dZ}\left(K_m \frac{dU}{dZ}\right) , \\ f(U-U_g) &= \frac{d}{dZ}\left(K_m \frac{dV}{dZ}\right) , \end{aligned}\right\} \qquad (2)$$

where f is the Coriolis parameter ($f = 2\Omega \sin \phi$, Ω being the angular rate of rotation of the Earth about its axis and ϕ the latitude), Z is the vertical coordinate, (U(Z), V(Z)) are the horizontal wind velocity components in the ABL, (U_g, V_g) is the (constant) geostrophic wind above the boundary layer and K_m is the coefficient of eddy viscosity. A derivation of equations (2) may be found in most standard meteorological texts (e.g. Haltiner and Martin (1957), p. 233). The convention we adopt for representing physical variables is that dimensional quantities are denoted by block letters and non-dimensional quantities by lower case script.

We introduce the complex velocity representation for equations (2) by setting

$$W = U+iV \quad \text{and} \quad W_g = U_g+iV_g$$

to obtain the single equation

$$if(W-W_g) = \frac{d}{dZ}(K_m \frac{dW}{dZ}) \qquad (3)$$

2. The frictional sublayer

As stated in the Introduction, the complex velocity profile in the frictional sublayer ($Z \leq H$) will have the well known and experimentally confirmed logarithmic form (e.g. Priestley (1959), Ch.3),

$$W_1 = e^{i\gamma} \frac{U_*}{k} \ln(\frac{Z}{Z_o}) \qquad (4)$$

where γ is the angle which the surface wind makes with the X-axis, and the other quantities have been previously defined. The roughness length Z_o is actually a constant of integration obtained from the derivation of (4). The size of Z_o is generally an order of magnitude less than the actual physical roughness elements at the earth's surface, and it has its physical significance as a length scale for the eddies produced by these roughness elements. The value of Kármán's constant k, has long been accepted as approximately 0.4, although recent detailed analysis by Tennekes (1968) and Businger *et al.* (1971) question the use of this value and suggest $k = 0.34$ and 0.35 respectively. However it is felt that in order to link the present work with the many other models of the ABL, we must continue to use the value of 0.4.

By assuming the shear stress to be constant, the left side of equation (3) is neglected. It can be seen, however, that this is legitimate provided that $fV_gH \ll U_*^2$, and it is found that this condition is satisfied by the numerical parameters introduced on page 69.

3. The Ekman layer

In the Ekman layer ($Z \geq H$) where K_m has the constant value $K=kU_*H$, we obtain the relevant velocity profiles by solving equation (3). If we further specify the Y-axis to be in the direction of the isobars, then we require the geostrophic wind to have no X-component. Thus the upper boundary condition is

$$W \to iV_g \quad \text{as } Z \to \infty.$$

The solution of equation (3) under this condition is a generalised Ekman spiral of the form

$$W_2 = iV_g \left\{ 1 - P \exp\left[-\left(\frac{1+i}{\sqrt{2}}\right)\frac{Z}{Z_g} + i\alpha \right] \right\} , \qquad (5)$$

where $Z_g = (K/f)^{\frac{1}{2}}$ is the Ekman scale thickness. P and α are constants for a particular set of dynamical conditions.

4. The patching process

The two wind profiles W_1 and W_2 thus obtained are matched at the intermediate altitude H, by requiring continuity of velocity and stress there. At Z=H, the following two conditions hold for the velocity profile W_1 and its vertical derivative:

$$\sigma \frac{dW_1}{dZ} = W_1 , \qquad (6a)$$

$$K \left| \frac{dW_1}{dZ} \right| = U_*^2 , \qquad (6b)$$

where $\sigma = H \ln(\frac{H}{Z_o})$. On applying equation (6a) to the Ekman profile

W_2 at Z=H, we obtain after some simplification,

$$P\left(1 + \frac{\sigma}{Z_g} e^{i\pi/4}\right).\exp\left[-\left(\frac{1+i}{\sqrt{2}}\right)\frac{H}{Z_g} + i\alpha\right] = 1 \qquad (7)$$

To simplify this further let

$$1 + \frac{\sigma}{Z_g} e^{i\pi/4} = Qe^{i\beta},$$

the inverse relationships being clearly

$$Q = \left[(\sigma+\sqrt{2}Z_g)^2 + \sigma^2\right]^{\frac{1}{2}} /(\sqrt{2}Z_g),$$

$$\beta = \tan^{-1}\left(\frac{\sigma}{\sigma+\sqrt{2}\,Z_g}\right). \qquad (8)$$

Therefore, in terms of P and β, equation (7) is

$$P.Q.\ \exp\left[-H/(\sqrt{2}Z_g)\right].\exp\left[i(\alpha + \beta - H/(\sqrt{2}Z_g))\right] = 1.$$

Taking the modulus and argument respectively of this equation leads to

$$P = \frac{\exp\ H/(\sqrt{2}Z_g)}{Q} \qquad (9)$$

$$\alpha = \frac{H}{\sqrt{2}Z_g} - \beta \qquad (10)$$

It is also a simple matter to show from equations (4) and (6a) that the angle γ' which the surface wind makes with the isobars (i.e. the Y-axis), since $\gamma' = \pi/2 - \gamma$, is

$$\gamma' = \beta - \pi/4 \qquad (11)$$

Furthermore the cross-isobaric volume flux F may be obtained from equation (2) thus:

$$F = \int_{Z_o}^{\infty} U \, dZ = R\left(\int_{Z_o}^{\infty} (W-W_g) dZ \right)$$

$$= -R\left[\frac{iK_m}{f} \frac{dW}{dZ} \right]_{Z_o}^{\infty}$$

Thus,

$$F = - \frac{U_*^2 \sin \gamma}{f} \qquad (12)$$

where $R(\ )$ denotes the real part of a complex expression.

Thus it is seen, that given the appropriate set of dynamical parameters (V_g, f, U_*, Z_o) for a particular physical situation, the quantities P, α, γ' and F may be calculated immediately from equations (9-12) as functions of H only. In order to solve for H, we make use of the second matching condition - equation (6b). This yields, when applied to the profile W_2 at Z = H,

$$\frac{kH}{Z_g} = \frac{U_*}{V_g} Q$$

Squaring this and substituting for Q from (8) gives

$$2(kH)^2 = \left(\frac{U_*}{V_g} \right)^2 \left[(\sigma + \sqrt{2} Z_g)^2 + \sigma^2 \right]$$

We now introduce the surface Rossby number Rs and the geostrophic drag coefficient C_d, which were defined in the Introduction, and for convenience, let $\theta = \ln(H/Z_o)$. As a result of these substitutions, the above equation can be written as

$$\left(\frac{k}{C_d} \right)^2 = k.Rs.C_d.e^{-\theta} + (2k.Rs.C_d.e^{-\theta})^{\frac{1}{2}} \theta + \theta^2 \qquad (13)$$

It is now a relatively simple matter to solve this equation numerically - in our case by the Newton-Raphson method - to yield θ and hence H. This value of H is a function of Rs and C_d, that is, a function of the given dynamical parameters V_g, f, U_*, and Z_o. Finally, through the various relations 9 to 12 we obtain P, α, γ and from these the velocity profiles of equations (4) and (5).

5. The relationship, $C_d = C_d(Rs)$

As mentioned in the Introduction, the present model still requires the specification of one *a priori* relationship, namely the functional dependence of C_d $(=U_*/V_g)$ on Rs $(=V_g/(fZ_o))$. The idea that the parameters V_g, f, U_* and Z_o are not all independent, was first suggested by Rossby and Montgomery (1935). Indeed it is reasonable to expect that the magnitude of the surface stress $|\underline{\tau}_o|$ (and hence $U_* = (|\underline{\tau}_o|/\rho)^{\frac{1}{2}}$) will be related to the surface roughness characteristics represented by Z_o.

For the present model we employ two such relationships, the first being that derived by Blackadar (1962) in his single-layer model of the structure of the ABL. This is represented graphically by curve I of Figure 1. The second such functional form of $C_d = C_d(Rs)$ is the semi-empirical implicit expression,

$$\ln(Rs) = B - \ln(C_d) + \left[\left(\frac{k}{C_d}\right)^2 - A^2\right]^{\frac{1}{2}} \qquad (14)$$

The above equation has recently been the subject of attention by a number of workers. Kazanskii and Monin (1961) were the first to derive this expression from the equations of motion. Blackadar and co-workers employ what they call the principle of 'Rossby number similarity' to link the frictional sublayer with the Ekman regime by asymptotic analysis, to obtain equation (14) - Blackadar and Tennekes (1968), Blackadar and Panofsky (1969). A similar technique is used also by Csanady (1967, 1972).

Following the derivation of equation (14), much interest has been focussed on obtaining accurate measurements of the parameters A and B, but on the whole, there is little consistency amongst the various values reported (see e.g. Table 2 of Zilitinkevich *et al.*, 1967). The most detailed and entensive measurements which have been carried out to date are those reported by Clarke (1970). The values obtained for A and B in conditions of neutral stability are 4.6 and 1.0 respectively, although measurements of B are subject to considerable experimental scatter. The parameters A and B are in fact, universal functions of the stability of the ABL; that is, $A=A(\mu)$ and $B=B(\mu)$, where μ is a suitable stability parameter defined by $\mu=kU_*/(fL)$, L being the Monin-Obhukov length (Monin and Obhukov 1954). The corresponding plot of C_d as a function of Rs, is given as curve II in Figure 1.

Therefore we have the possibility that the analysis can be extended immediately to conditions other than those of neutral stability. However caution must be exercised in doing this since (i) the velocity profile in the frictional sublayer contains a

linear term in Z/L as well as the logarithmic contribution as we move away from neutral conditions ($L=\infty$), and (ii) we must consider whether or not the assumption of an Ekman profile above the frictional sublayer is justified for such cases. Condition (i) could be quite easily incorporated, and from a brief survey of the literature it would appear that (ii) is also justifiable. For example, various Russian experiments as reported by Zilitinkevich *et al.* (1967) as well as the work of Tennekes (1970) and Clarke (1970) indicate for all classes of stability, the existence of at least a rudimentary Ekman spiral. This is also confirmed in the extensive three-dimensional, time-dependent numerical simulations of the turbulent processes in the ABL recently performed by Deardorff (1972), for both neutral and unstable cases.

6. Results.

The profiles of U and V are presented in Figures 3 and 4 respectively. They are compared with the simple Ekman profiles and those obtained by the parameterisation of Smith (1969). The dynamical parameters used in the calculation of these profiles are U_*=0.3 m sec^{-1}, Z_o = 1 cm, f=5x10^{-5} sec^{-1} and V_g = 10 m sec^{-1}, and the value of Kármán's constant is 0.4. As expected, the U and V profiles for the present model are very similar to those of Smith. It can be seen, that in contrast with the Ekman profiles, both models predict significant inflow in the thin layer close to the ground, yet the total inflow over the entire boundary layer is little more than one half that of the Ekman layer. The ratios

of the cross-isobaric volume fluxes, F (present model) given by equation (12), F_s (Smith) and F_e (Ekman) are

$$F/F_s = 1.016 \quad \text{and} \quad F/F_e = 0.586.$$

The respective cross-isobaric angles of the surface wind for the particular dynamical parameters used in this case are

$$\gamma' = 15.3^\circ, \quad \gamma'_s = 19.5^\circ, \quad \gamma'_e = 45^\circ$$

The results of these calculations demonstrate the similarities in the wind structure of the present model and that of Smith (1969). However, the latter has the disadvantage that the calculations involve the use of hypergeometric functions, which make this particular parameterisation rather unwieldy if used repeatedly, as for instance in conjunction with the momentum integral method of the following section.

In Figure 2 we detail the curves for the variation of γ', the cross-isobaric angle of the surface wind, as a function of the surface Rossby number. These are calculated using the (C_d , Rs) curves in Figure 1 of both Blackadar (K_I) and Clarke (K_{II}), and as expected, the two results are in close agreement over most of the range. These cases are compared with corresponding results obtained by the two-layer model of Rossby and Montgomery (1935) and with the single-layer models of Blackadar (1962) and Lettau (1962), as well as the one value found by Smith (1969).

Lettau (1962) has used certain experimental observations as a test of the validity of his single-layer model. The particular observations he used are those of the 'Leipzig' and 'Scilly' wind

profiles, the dynamical parameters measured at these two locations being:

Leipzig (Oct 20, 1931): V_g = 17.51 m sec^{-1}, f=1.14x10^{-4} sec^{-1}, estimated Z_o = 30 cm (over land);

Scilly Isles (Jan 4, 1951): V_g = 12.19 m sec^{-1}, f=1.11x10^{-4} sec^{-1}, estimated Z_o = 0.03 cm (over ocean).

The value of k used by Lettau is 0.4, and his theoretical and experimental results are presented in Table 1 along with the results calculated from the present model, using drag curve I of Figure 1. As can be seen from the table, the present two-layer model exhibits good agreement between theory and observation and compares very favourably with the theoretical calculations of Lettau. Moreover, little computational effort has been involved in these present calculations, unlike the case of the more complicated numerical model used by Lettau.

B - MOMENTUM INTEGRAL TREATMENT.

1. The integrated equations

The momentum integral treatment which we adopt in this section, for the problem of motion in the boundary layer of an idealised hurricane, is essentially the method developed in S and extended to a wider class of problems by Leslie and Smith (1970). The velocity profiles obtained from the parameterisation of the ABL in Section A, are suitable for such a treatment, since they are expressed in an analytical form, such that the momentum integrals which arise are convergent. However it is apparent from Section A, that these velocity profiles are dependent on V_g (in the present context, the swirling velocity above the boundary layer) in such a way that the resulting momentum integrals are not in general constant. This is in contrast with both the above — mentioned treatments which ignore radial variations in the momentum integrals. Only a brief explanatory outline of the method is given below; a more comprehensive discussion can be found in Chapter 1.

The eddy viscosity K_m is both radially and vertically dependent, and to this end we set

$$K_m = K_g.\kappa(r,z),$$

where $K_g = kU_*H$, evaluated at the geostrophic radius R_g. After non-dimensionalisation of the various physical variables with respect to their relevant scales at R_g, the boundary layer equations, combined with the equation of continuity, have the form given by equations (6) and (7) of Chapter 1.

In obtaining the integrated equations of motion appropriate to the present model, care must be exercised in the choice of the lower limit of integration. In the method of S, as outlined in the previous chapter, this limit is the ground, allowing the condition of no slip which applies there, to be used to simplify the integrated equations. However in the present case, the velocity profile in the frictional sublayer ($Z_o \leq Z \leq H$) is obtained on a semi-empirical basis, with the matched upper Ekman profile being a solution of the zero Rossby number equations which hold approximately at the geostrophic radius. To illustrate the result of this procedure, consider the integrated radial, say, Ekman equation, which can be expressed in dimensional terms from equation (2), as

$$f \int_{Z_1}^{\infty} (V - V_g)\, dZ = K_m \left[\frac{dU}{dZ}\right]_{Z=Z_1}$$

The term on the right is τ_1/ρ, where τ_1 is the radial stress component at $Z = Z_1$. Now we know from Section A, that this is constant in the sublayer, having the value $U_*^2 \cos\gamma$ from $Z = Z_o$ to $Z = H$, whereas the integral on the left will clearly vary over this range. Thus it is evident that we must specify this lower limit Z_1 to be H, not Z_o, and this arises simply because the logarithmic profile in the sublayer is not in fact consistent with the Ekman equations. We see therefore, that the role of the frictional sublayer is effectively to provide bottom boundary conditions at $Z = H$ for the Ekman layer, the stress at the bottom of the layer being equal to the constant value below this height. Since these boundary conditions are now not as simple

as the no slip conditions at Z=0, the momentum integral equations will consequently contain several terms not present in the original formulation of S.

Upon integrating the boundary layer equations (6) and (7) of Chapter 1, from z=h to ∞ in the normal manner, we obtain

$$\mathrm{Ro}\left[\frac{d}{dr}\left(r\int_h^\infty u^2\,dz\right) + r\left[uw\right]_h^\infty + \int_h^\infty (v_{gr}^2 - v^2)\,dz\right]$$

$$+ r\int_h^\infty (v_{gr} - v)\,dz \quad = -r\left[\kappa\frac{\partial u}{\partial z}\right]_{z=h}, \qquad (15)$$

$$\mathrm{Ro}\left[\frac{d}{dr}\left(r^2\int_h^\infty uv\,dz\right) + r^2\left[vw\right]_h^\infty + r^2\int_h^\infty u\,dz\right]$$

$$\pm -r^2\left[\kappa\frac{\partial v}{\partial z}\right]_{z=h} \qquad (16)$$

where $\mathrm{Ro}=V_g/(fR_g)$ is the appropriate Rossby number for the flow at the geostrophic radius R_g, V_g is the (dimensional) geostrophic velocity there, f is the Coriolis parameter, u and v are the radial and azimuthal velocity components in the axisymmetric coordinate system (r,z), and $v_{gr}(r)$ is the dimensionless swirling flow imposed above the boundary layer.

$$w_{gr}(r) = -\frac{1}{r}\frac{d}{dr}\left(r\int_{z_o}^\infty u\,dz\right) \qquad (17)$$

is the dimensionless vertical velocity at the top of the boundary layer, obtained by integration of the continuity equation. As the dimensional scales of r,z,u,v,w and v_{gr}, we have taken $R_g, Z_g, V_g, V_g, Z_g V_g/R_g$ and V_g respectively, where $Z_g = (K_g/f)^{\frac{1}{2}}$ is the Ekman scale thickness of the boundary layer at the geostrophic radius.

Following S, we assume boundary layer velocity profiles of the form

$$\left.\begin{aligned} u(r,z) &= v_{gr}(r)\ E(r)\ f(\eta), \\ v(r,z) &= v_{gr}(r)\ g(\eta), \end{aligned}\right\} \quad (18)$$

where $\eta = z/\delta(r)$, δ being a non-dimensional variable which characterises the boundary layer thickness, while $E(r)$ is the amplitude coefficient of the radial velocity. The vertical structure of the boundary layer velocity components is given by $f(\eta)$ and $g(\eta)$, which in the present case are obtained from the parameterisation of the boundary layer in Section A.

In the first instance, we assume that the momentum integrals are radially independent, whereupon, if the profiles (18) are substituted into (15),(16) and (17), we obtain the following three equations for E, δ and w_{gr}:

$$\mathrm{Ro}\left[\frac{d}{dr}(r v_{gr}^2 E^2 \delta) I_1 + \bar{f}\ E\ v_{gr}\ \frac{d}{dr}(r v_{gr} E \delta) I_* + v^2 \delta I_2\right]$$

$$+ r\ v_{gr}\ \delta\ I_3 = -\lim_{\eta \to h\sqrt{2}} \frac{\kappa(r,\sqrt{2}\eta)\ r v_{gr}\ E\ f'(\eta)}{\delta}, \quad (19)$$

$$\mathrm{Ro}\left[\frac{d}{dr}(r^2 v_{gr}^2 E\delta) I_4 - r v_{gr}(I_5 + (1-\bar{g}) I_*)\frac{d}{dr}(r\ v_{gr}\ E\delta)\right]$$

$$+ r^2\ v_{gr}\ E\ \delta\ I_5 = -\lim_{\eta \to h\sqrt{2}} \frac{\kappa(r,\sqrt{2}\eta) r^2\ v_{gr}\ g'(\eta)}{\delta}, \quad (20)$$

$$w_{gr} = -\frac{(I_5 + I_*)}{r}\ \frac{d}{dr}(r\ v_{gr}\ E\delta) \quad (21)$$

where $I_1 = \int f^2 d\eta$, $I_2 = \int (1-g^2) d\eta$, $I_3 = \int (1-g) d\eta$

$I_4 = \int fg \, d\eta$, $I_5 = \int f \, d\eta$ (22a)

the limits of integration being $\eta = h/\sqrt{2}$ to ∞. The dash denotes differentiation with respect to η. We also define

$$I_* = \int_{z_o/\sqrt{2}}^{h/\sqrt{2}} f \, d\eta \quad , \tag{22b}$$

while $\bar{f}$ and $\bar{g}$ are the values of the profiles at the interface of the two layers. For convenience, we set

$$I_6 = \bar{f} \, I_* \quad , \; I_7 = I_5 + (1-\bar{g}) I_* \tag{22c}$$

On choosing E^2, $E\delta^2$ and W_{gr} as the dependent variables, equations (19) to (21) reduce after considerable manipulation, to a form more suitable for numerical solution:

$$\frac{1}{E^2} \frac{d}{dr}(E^2) = -\frac{2}{r\tilde{v}^2}\left[\frac{d}{dr}(r\tilde{v}^2) - (S_2 - S_7)\tilde{v}\frac{d}{dr}(r\tilde{v})\right] - 2\left[\frac{1}{E^2}\left(\frac{S_1}{r} + \frac{S_5}{\tilde{v}^2}\right) + \frac{S_6}{\tilde{v}^2}(1+S_*) + \frac{S_3 + S_4(1+S_*)}{\tilde{v}\, E\delta^2}\right] , \tag{23}$$

$$\frac{1}{E\delta^2}\frac{d}{dr}(E\delta^2) = \frac{1}{r\tilde{v}^2}\left[\frac{d}{dr}(r\tilde{v}^2) - (3S_2 - S_7)\tilde{v}\frac{d}{dr}(r\tilde{v})\right] + \frac{1}{E^2}\left(\frac{S_1}{r} + \frac{S_5}{\tilde{v}^2}\right) + \frac{S_6}{\tilde{v}^2}(3+S_*) + \frac{S_3 + S_4(3+S_*)}{\tilde{v} E\delta^2}\Bigg] \tag{24}$$

$$W_{gr} = -\frac{(I_5+I_*)}{Ro\,\delta}\left\{S_4 + E\delta^2\left[\frac{(1-S_2)}{r}\frac{d}{dr}(r\tilde{v}) + S_6\right]\right\} , \tag{25}$$

where $\tilde{v} = R_o v_{gr}$, and

$$S_1 = \frac{I_2}{I_1} \quad , \quad S_2 = \frac{I_7 - 2I_4}{I_7 - I_4} \quad , \quad S_3 = \lim_{\eta \to h\sqrt{2}} \frac{\kappa(r,\sqrt{2}\eta)\ f'(\eta)}{I_1} \ ,$$

$$S_4 = \lim_{\eta \to h/\sqrt{2}} \frac{\kappa(r,\sqrt{2}\eta)\ g'(\eta)}{I_7 - I_4} \quad , \quad S_5 = \frac{I_3}{I_1} \ , \ S_6 = \frac{I_5}{I_7 - I_4} \ ,$$

$$S_* = \frac{I_6}{I_1} \quad , \quad S_7 = \frac{S_* I_4}{I_7 - I_4} \ .$$

In deriving (23) to (25), we use the expression (21) to obtain w_{gr}; that is, we take into account the contribution to w_{gr} arising from the logarithmic sublayer as well as from the matched Ekman layer, whereas we have seen that the derivation of the momentum integral equations must necessarily involve only the Ekman layer. Since w_{gr} is obtained diagnostically, there is no inconsistency here. If the contribution from the sublayer is in fact neglected (i.e., $I_* = 0$, and hence S_6, S_7 and S_* are all identically zero), the equations reduce to the form derived by Leslie and Smith (1970) - see Chapter 1, Section 3.

The second situation arises when we take into consideration the radial variation of the momentum integrals. In this case it can be shown that the relevant equations, analogous to (23), (24) and (25), are

$$\frac{1}{E^2}\frac{d}{dr}(E^2) = -\frac{2}{r\tilde{v}^2}\left[\frac{d}{dr}(r\tilde{v}^2) - (S_2 - S_7)\tilde{v}\frac{d}{dr}(r\tilde{v})\right] - 2\left[\frac{1}{E^2}\left(\frac{S_1}{r} + \frac{S_5}{\tilde{v}}\right)\right.$$

$$\left. + \frac{S_6}{\tilde{v}}(1+S_*) + \frac{S_3 + S_4(1+S_*)}{\tilde{v}E\delta^2} + S_8 - S_9(1+S_*)\right] \qquad (23')$$

$$\frac{1}{E\delta^2}\frac{d}{dr}(E\delta^2) = \frac{1}{r\tilde{v}^2}\left[\frac{d}{dr}(r\tilde{v}^2) - (3S_2-S_7)\tilde{v}\frac{d}{dr}(r\tilde{v})\right] + \frac{1}{E^2}\left(\frac{S_1}{r} + \frac{S_5}{\tilde{v}}\right)$$

$$+ \frac{S_6}{\tilde{v}}(3+S_*) + \frac{S_3+S_4(3+S_*)}{\tilde{v}E\delta^2} + S_8 - S_9\,(3+S_*), \qquad (24')$$

$$w_{gr} = -\frac{(I_5+I_*)}{Ro\ \delta}\left\{S_4+E\delta^2\left[\frac{(1-S_2)}{r}\frac{d}{dr}(r\tilde{v})+S_6+\tilde{v}(S_{10}-S_9)\right]\right\} \qquad (25')$$

where the extra terms which have been introduced, are

$$S_8 = \frac{(I_1 + I_6)'}{I_1}, \quad S_9 = \frac{(I_7 - I_4)'}{I_7 - I_4}, \quad S_{10} = \frac{(I_5+I_*)'}{I_5+I_*}.$$

For convenience, as well as for purposes of comparison, the form which we use for v_{gr}, representing the swirling flow in the hurricane vortex above the boundary layer, is that obtained in S, and also discussed in Section 7 of the previous chapter, namely

$$\tilde{v}(r) = -\frac{r}{2} + \left[\left(\frac{r}{2}\right)^2 + \frac{mxb}{r}\ e^{xb(1-r^{-1})}\right]^{\frac{1}{2}} \qquad (26)$$

where $m = (P_g-P_c)/(\rho R_g^2 f^2)$. Here P_c and P_g are the pressures at the vortex centre and geostrophic radius respectively, ρ is the (constant) air density, $b=R_m/R_g$ and x, chosen so that the maximum swirling velocity above the boundary layer occurs at $R=R_m$, satisfies the equation

$$mx(x-1)^2\ e^{x(b-1)} - (2-x)b^2 = 0.$$

The physical parameters which scale the hurricane are also identical to those of Chapter 1, namely P_c=940 mb, P_g=1000 mb, R_g=1000 km, R_m=40 km, ρ=0.0012 gm cm^{-3} and $f=5\times10^{-5}$ sec^{-1}. As a result, Ro is approximately 0.0776, and a plot of V_{gr} as a function of R is shown in Figure 2 of Chapter 1.

2. The velocity profiles

As stated previously, the profiles $f(\eta)$ and $g(\eta)$ which we use to evaluate the momentum integrals, are those obtained in Section A - the parameterisation of a two-layer atmospheric boundary layer. We have, therefore

$$f(\eta) = \begin{cases} f_1(\eta) \quad , \quad z_o \leq z \leq h, & \text{i.e., } \dfrac{z_o}{\sqrt{2}} \leq \eta \leq \dfrac{h}{\sqrt{2}} \quad , \\ f_2(\eta) \quad , \quad z \geq h, & \text{i.e., } \eta \geq \dfrac{h}{\sqrt{2}} \quad , \end{cases}$$

and similarly for the g - profiles g_1 and g_2. Hence the integrals (22) can be expressed in the form

$$I_1 = \int_{h/\sqrt{2}}^{\infty} f_2^{\,2}(\eta)\, d\eta \quad , \quad I_* = \int_{z_o/\sqrt{2}}^{h/\sqrt{2}} f_1(\eta)\, d\eta \quad ,$$

etc., where on non-dimensionalising equations (4) and (5) with respect to the scales at the geostrophic radius, we have

$$\begin{aligned} f_1(\eta) &= \frac{u_* \cos\gamma}{k\, v_{gr}} \ln\left(\frac{\sqrt{2}\eta}{z_o}\right) , \\ g_1(\eta) &= \frac{u_* \sin\gamma}{k\, v_{gr}} \ln\left(\frac{\sqrt{2}\eta}{z_o}\right) , \\ f_2(\eta) &= Pe^{-\eta/z_{gr}} \sin\left(\frac{\eta}{z_{gr}} - \alpha\right) , \\ g_2(\eta) &= 1 - Pe^{-\eta/z_{gr}} \cos\left(\frac{\eta}{z_{gr}} - \alpha\right). \end{aligned} \tag{27}$$

The parameter z_{gr} in the profiles above, arises because the eddy viscosity (and hence the local Ekman scale thickness) is radially dependent:

$$z_{gr} = \frac{Z_{gr}}{Z_g} = \left(\frac{U_* H}{U_{*g} H_g}\right)^{\frac{1}{2}}$$

The calculation of the momentum integrals (22) from the profiles (27) is mathematically straightforward, but also rather tedious, and the details are given in the Appendix.

3. The numerical solution

The differential equations (23) and (24) are integrated radially inwards from r=1 using a standard fourth order Runge-Kutta-Gill routine to obtain E^2 and $E\delta^2$, and hence E, δ and w_{gr} at each radial step. As described in Chapter 1, the Ekman starting values of $E=1$ and $\delta=\sqrt{2}$ at the geostrophic radius (r=1) are adjusted slightly so that their derivatives are exactly zero. That is, we prescribe geostrophic flow at r=1, the adjustment in the starting values, necessary for numerical stability, being due to the small but non-zero contributions from the inertial terms in the equations of motion.

At each radial step, using the given values of Z_o and f, we calculate v_{gr} from (26), and hence the surface Rossby number $Rs = V_g v_{gr}/(fZ_o)$. From the value of this parameter, we obtain the geostrophic drag coefficient C_d, either from the graphical relationship of Blackadar (1962) or from equation (14) using Clarke's (1970) values for the parameters A and B. We can now effect the boundary layer parameterisation of Section A at this particular radius, to obtain the velocity profiles (4) and (5), and finally the momentum integrals (22) needed to solve the two differential equations.

Thus it can be seen, that as well as requiring that the

parameterisation procedure be physically realistic, it is also preferable that it should involve as little computation as possible, owing to the large number of times it must be repeated. This requirement would be even more essential should one wish to extend the present boundary layer technique to time-dependent flows, and therefore tends to rule out the use of finite-difference numerical models of the ABL, such as those of Blackadar (1962) and Lettau (1962).

4. Results

In Figures 5 to 8 we present the results of various calculations arising out of this section. In all of these calculations, we have a choice of using curves I or II in Figure 1, which are the graphs of $C_d = C_d(Rs)$ obtained by Blackadar (1962) and Clarke (1970) respectively. However, as anticipated, these two relationships give very similar results (less than 1% variation for all radii), and for the purpose of graphical representation, it has been decided (arbitrarily) to use the relationship I of Blackadar.

Figures 5(a) and (b) give the profiles of W_{gr}, the vertical velocity through the top of the boundary layer, as a function of the radial position R for a number of different situations. One detail which is immediately obvious, is the effect of taking account of the terms S_8, S_9 and S_{10} in the equations. With Z_o constant at 0.1 cm, the maximum upflow for case A, in which the radial derivatives of the momentum integrals are set to zero (i.e., S_8, S_9, S_{10}=0), is 51.06 cm sec^{-1} at 20 km, as against 57.54 at 15 km for case B ($S_8, S_9, S_{10} \neq 0$). This difference is most apparent at small radius

where the convective terms are dominant. On the other hand, the region of slow downflow in the outer extent of the vortex extends inwards to 397 km for case A, whereas in B, the upflow is delayed until R=284 km. Also considered is the case of allowing Z_o to to vary in some way as a function of the swirl velocity, to model, although naively, the increased roughness of the sea surface in regions of high wind speed. As can be seen when we set Z_o=0.1 $v_{gr}(r)$ cm for case A, there is considerable enhancement of the upflow velocity, particularly at small radius.

We have shown earlier, that in deriving the momentum integral equations, the effective role of the frictional sublayer is to provide bottom boundary conditions for the matched Ekman layer. However we do incorporate the contribution of the sublayer to the vertical velocity via the integral I_* - equation (22b). In Figure 5(b), we see by setting I_* = 0, that this contribution, although negligible for R>200 km, clearly affects the scales of the motion at small radius. The final curve in Figure 5(b), drawn principally for purposes of comparison, is W_{gr} for the situation modelled in S of a constant eddy viscosity throughout the boundary layer, equal to 5×10^{4} m^2 sec^{-1}.

Figure 6 shows the variation of the maximum radial inflow velocity U_{max} as a function of radius. From (18), $U_{max} = EV_{gr}f_{max}$, f_{max} being the magnitude of the maximum value of $f_2(\eta)$, the vertical profile of the radial velocity. The curves drawn are for Z_o=0.1 cm (cases A and B) and Z_o=0.1 v_{gr} cm (case A), together with that for constant eddy viscosity. It can be seen that one result

of the present parameterisation is to reduce substantially the magnitude of the inflow velocities below the values obtained for constant eddy viscosity, which are considerably higher than observed in hurricanes (Miller 1965). In Figure 7, the profiles of the boundary layer scale thickness δ, for Z_o = 0.1 cm (cases A and B) are presented, together with the result for constant eddy viscosity.

In Figure 8, the radial dependence of K_{max}, the constant value of the eddy viscosity in the Ekman region above the sublayer is shown. This emphasises one of the principal advantages of the model, namely its ability to determine the turbulent structure of the boundary layer itself, given the relevant parameters (V_{gr}, Z_o, f) for a particular physical situation. Unlike the results obtained by Leslie and Smith (1970) with the somewhat similar parameterisation of Smith (1969) - see Introduction - δ does not at first increase rapidly as we advance radially inwards. This is due to our use of the parameter z_{gr} which takes account of the increase in K_m (Figure 8), and thus keeps δ in scale.

From the above results, we see that the maximum inflow velocities are considerably smaller than those obtained using Ekman profiles with a constant eddy viscosity. In this context we refer to Section A, where it is seen that although the profiles of the model are characterised by large velocities near the ground, the actual radial volume flux is little more than half that of the full Ekman layer. The results of Figures 5 and 6 further indicate that the radial inflow velocity is much less sensitive to radial variations in the boundary layer structure than the vertical upflow, in accord with the results of Leslie and Smith (1970).

Conclusions

We have presented in this chapter a simple two-layer parameterisation of the atmospheric boundary layer, which depends only upon the universal relationship $C_d=C_d(Rs)$ between the surface Rossby number and the geostrophic drag coefficient. In spite of its relative simplicity and approximate nature, the model is shown to be effective, in that it reproduces the main atmospheric features and compares favourably with the predictions of more sophisticated parameterisations.

The main benefit of this model lies in the analytic nature of the velocity profiles, allowing it to be incorporated into a momentum integral method to determine the flow in the boundary layer of a hurricane. The profiles are similar to those used by Leslie and Smith (1970) but involve elementary functions only, so that the resulting momentum integrals can be calculated analytically rather than by the more approximate method necessary in the latter. It is found, in agreement with Leslie and Smith, that the predictions of the momentum integral method are sensitive to radial variations in the surface roughness length Z_o, but apart from this, we are unable to directly compare our results with theirs since they were obliged to prescribe an eddy viscosity distribution. However by our use here of the relationship $C_d=C_d(Rs)$, the eddy viscosity can be calculated from the model itself.

It has also been demonstrated that allowance should be made for the radial variation in the momentum integrals themselves. This effect, together with that for changes in Z_o, are most noticeable in the profiles of W_{gr}, the vertical outflow from the boundary layer,

and hence must be taken into account if possible, since it is W_{gr} which provides a measure of the mass transfer from the boundary layer into the main vortex. The values obtained for W_{gr} appear to be lower than the approximate 1/m/sec measured by Gray (1966). On the other hand we have noted how critically this depends on Z_o, about which very little information has actually been obtained in the regions of intense wind speeds.

One query which should be raised, concerns the validity of using the (C_d,Rs) curves for high wind speeds, even though they cover the range of surface Rossby numbers encountered. For instance, Kraus (1972) has suggested that there may be a complete disruption of the boundary layer at such high wind speeds due to violent surface motions, and where the spray itself may also play an active role in the momentum transfer processes. On the whole however, the model has been shown to be both realistic and capable of incorporating detailed observational data, should this become available, and as such, we believe that it constitutes an advance in the treatment of such problems.

APPENDIX - THE MOMENTUM INTEGRALS.

As the simplest examples, we consider

$$I_5 = \int_{h/\sqrt{2}}^{\infty} f_2(\eta)\, d\eta \quad \text{and} \quad I_* = \int_{z_o/\sqrt{2}}^{h/\sqrt{2}} f_1(\eta)\, d\eta$$

where $$f_1(\eta) = \frac{u_* \cos\gamma}{k\, v_{gr}} \ln\left(\frac{\sqrt{2}\eta}{z_o}\right)$$

$$f_2(\eta) = -Pe^{-\eta/z_{gr}} \sin\left(\frac{\eta}{z_{gr}} - \alpha\right)$$

Thus,

$$I_5 = -P \int_{h/\sqrt{2}}^{\infty} e^{-\eta/z_{gr}} \sin\left(\frac{\eta}{z_{gr}} - \alpha\right) d\eta$$

$$= -\frac{Pz_{gr}}{2} e^{-\Omega}\left[\cos(\Omega-\alpha) + \sin(\Omega-\alpha)\right],$$

and

$$I_* = \frac{u_* \cos\gamma}{k\, v_{gr}} \int_{z_o/\sqrt{2}}^{h/\sqrt{2}} \ln\left(\frac{\sqrt{2}\eta}{z_o}\right) d\eta$$

$$= \frac{u_* \cos\gamma}{\sqrt{2}k\, v_{gr}}\left[h\left(\ln\frac{h}{z_o} - 1\right) + z_o\right],$$

where for convenience we have set $\Omega = h/(\sqrt{2}\, z_{gr})$. In a similar manner we calculate the integrals I_1 to I_4, to obtain

$$I_1 = \frac{P^2 z_{gr}}{8} e^{-2\Omega}\left[2 + \sin\left[2(\Omega-\alpha)\right] - \cos\left[2(\Omega-\alpha)\right]\right],$$

$$I_2 = Pz_{gr} e^{-\Omega}\left[\cos(\Omega-\alpha) - \sin(\Omega-\alpha)\right] - \frac{P^2 z_{gr}}{8} e^{-2\Omega}\left[2 + \cos\left[2(\Omega-\alpha)\right]\right.$$

$$\left. - \sin\left[2(\Omega-\alpha)\right]\right],$$

$$I_3 = \frac{P z_{gr}}{2} e^{-\Omega} \left[\cos(\Omega-\alpha) - \sin(\Omega-\alpha)\right],$$

$$I_4 = -\frac{P z_{gr}}{2} e^{-\Omega}\left[\cos(\Omega-\alpha)+\sin(\Omega-\alpha)\right]+\frac{P^2 z_{gr}}{8} e^{-2\Omega}\left[\cos\left[2(\Omega-\alpha)\right]+\sin\left[2(\Omega-\alpha)\right]\right].$$

As expected, these expressions reduce to those obtained in I, if we use the variables corresponding to the case of a single Ekman layer extending to the ground:- $P=z_{gr} = 1$; $\alpha=h = z_o=0$. Also,

$$S_3 = \lim_{\eta\to h/\sqrt{2}} \frac{K(r,\sqrt{2}\eta)\, f'(\eta)}{I_1} = \frac{V_g Z_g \sqrt{2}\, u_*^2 \cos\gamma}{K_g v_{gr} I_1},$$

$$S_4 = \lim_{\eta\to h/\sqrt{2}} \frac{K(r,\sqrt{2}\eta)\, g'(\eta)}{I_7 - I_4} = \frac{V_g Z_g \sqrt{2}\, u_*^2 \sin\gamma}{K_g v_{gr} (I_7 - I_4)};$$

In evaluating the variables S_8, S_9 and S_{10} of Section B, we require the radial derivatives of several of the above integrals. However, this operation which would involve much tedious calculation can be avoided, simply by using finite - difference approximations to these derivatives. For example,

$$\frac{dI_1(r)}{dr} = \frac{1}{\Delta r}\left[I_1\left(r+\frac{\Delta r}{2}\right) - I_1\left(r-\frac{\Delta r}{2}\right)\right],$$

with accuracy of the order of $(\Delta r)^2$, Δr being the radial increment used in the numerical solution of equations (23) and (24). Since the method used (Runge-Kutta-Gill) already required the values of the integrals in increments of $\Delta r/2$, very little additional effort is need to incorporate this device into the computer program.

Table Captions

Table 1: Comparison of certain theoretical results of the present model with both theoretical and experimental results presented by Lettau (1962), for the Leipzig and Scilly wind profiles.

Figure Captions

Figure 1. The curves used to obtain the geostrophic drag coefficient C_d, as a function of the surface Rossby number Rs. Curve I is taken from Blackadar (1962); II is obtained from equation (14), the constants A and B being those measured by Clarke (1970).

Figure 2. Calculate values of γ', the cross-isobar angle of the surface wind, as a function of Rs for the present model using the curves of Blackadar (K_I) and Clarke (K_{II}) in Figure 1. These are compared with the relationships of Rossby and Montgomery (1935) - R, Blackadar (1962) - B, and Lettau (1962) - L, together with a single value calculated by Smith (1969) - *.

Figure 3. Vertical velocity profiles of U, for the Ekman layer (E), the model of Smith (1969) - (S), and the present model (K). The parameters used are V_g=10 m sec^{-1}, f= $5x10^{-5}$ sec^{-1}, U_* = 0.3 m sec^{-1} and Z_o = 1 cm. The

value of k is assumed to be 0.4.

Figure 4. Vertical velocity profiles of V; legend as for Figure 3.

Figure 5. Profiles of the vertical velocity W_{gr} through the top of the boundary layer as a function of radius.

a) (i) Z_o = 0.1 cm, (S_8,S_9,S_{10}) = 0

(ii) Z_o = 0.1 cm, (S_8,S_9,S_{10}) ≠ 0

(iii) Z_o = 0.1 $v_{gr}(r)$ cm, (S_8,S_9,S_{10}) = 0

b) (i) Z_o = 0.1 cm, $(S_8,S_9,S_{10})=0$

(ii) Z_o = 0.1 cm, $I_*=0$ $(S_8,S_9,S_{10})=0$

(iii) K_m = const = 5×10^4 $m^2 sec^{-1}$ $(S_8,S_9,S_{10})=0$

Figure 6. Profiles of the maximum radial inflow velocity.

(i), (ii), (iii) - As in Figure 5(a).

(iv) - As in Figure 5(b), (iii).

Figure 7. Profiles of δ, the non-dimensional scale thickness of the Ekman layer.

(i), (ii) - As in Figure 5(a)

(iii) - As in Figure 5(b), (iii).

Figure 8. The eddy viscosity $K(r) = kU_*H$, the constant value in the Ekman region of the boundary layer, for Z_o=0.1 cm (S_8=S_9=S_{10}=0), as a function of the radial position. For reference, the value $K_m=5\times10^4$, used for comparison results, is depicted.

Table 1.

Quantity	Leizeig (over land)			Scilly (over ocean)		
	Observed	Lettau (1962)	Present work	Observed	Lettau (1962)	Present work
γ'(deg.)=angle between surface wind and isobars	26.1	27.7	23.9	13.9	17.3	13.7
τ_o (dynes cm^{-2}) = surface stress	5.31	5.65	5.09*	0.92	1.13	1.07*
Z_m(m.)= height at which eddy viscosity is maximum	235	223	Z>64	100	102	Z>38
K_{max} (cm^2 sec^{-1}) = maximum eddy viscosity	144,700	205,000	171,000	28,000	41,000	47,000
Z_y(m.)=level of maximum cross-isobar wind component	250	274	293	70	75	115
Z_g(m)=level at which cross-isobaric wind first equals zero	1,070	1,200	1,140	480	534	574

* : Use made of curve I in Figure 1.

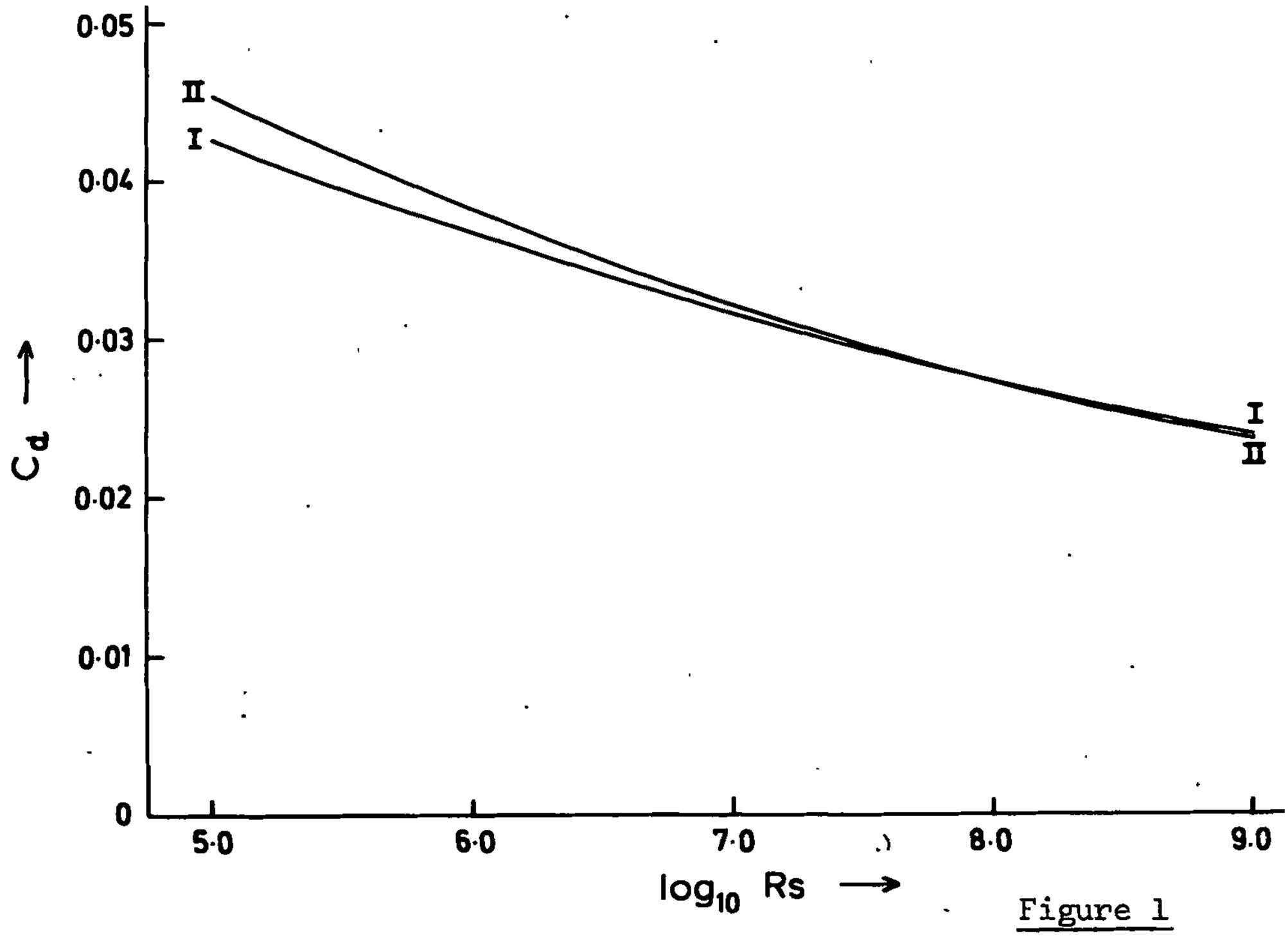

Figure 1

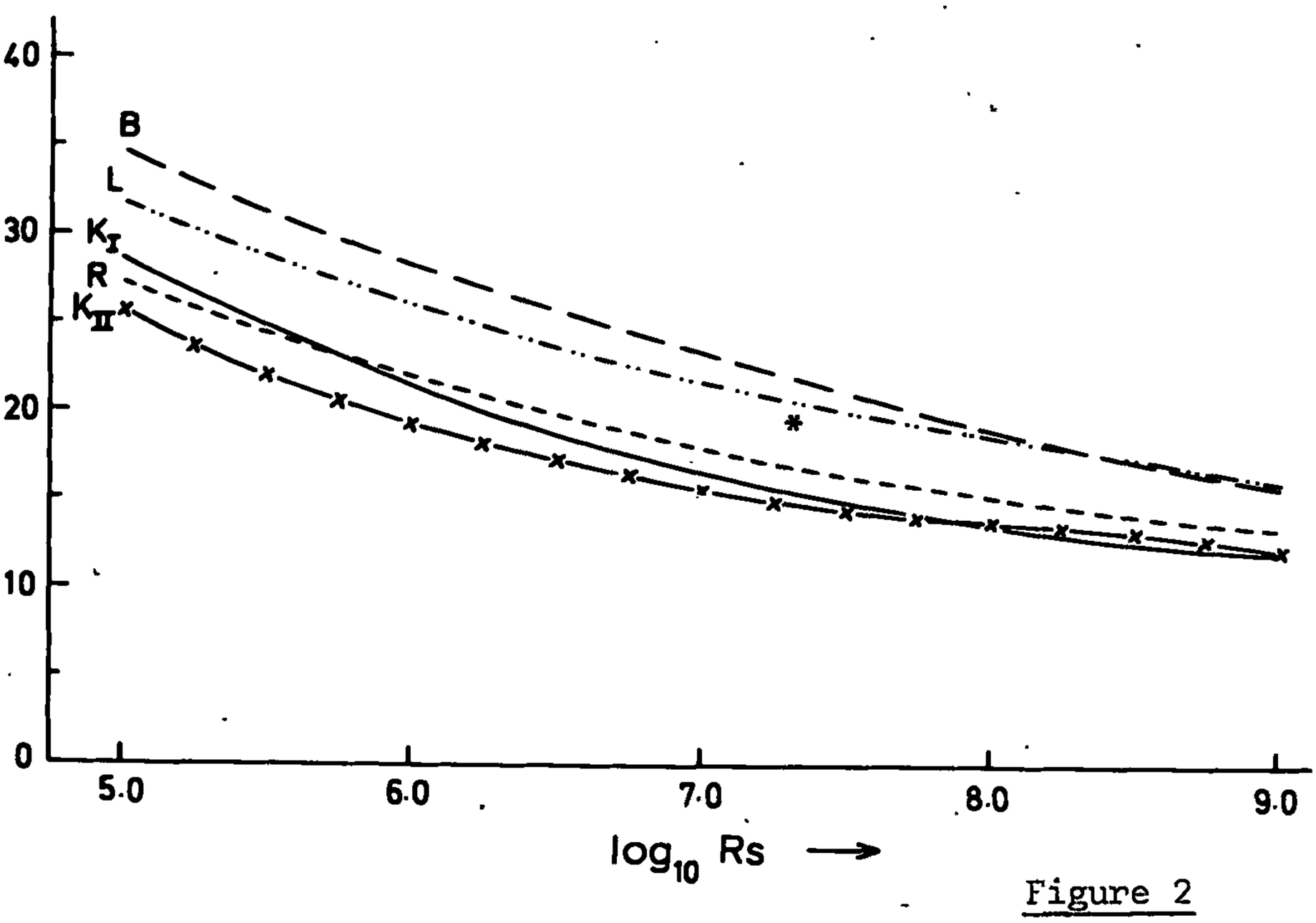

Figure 2

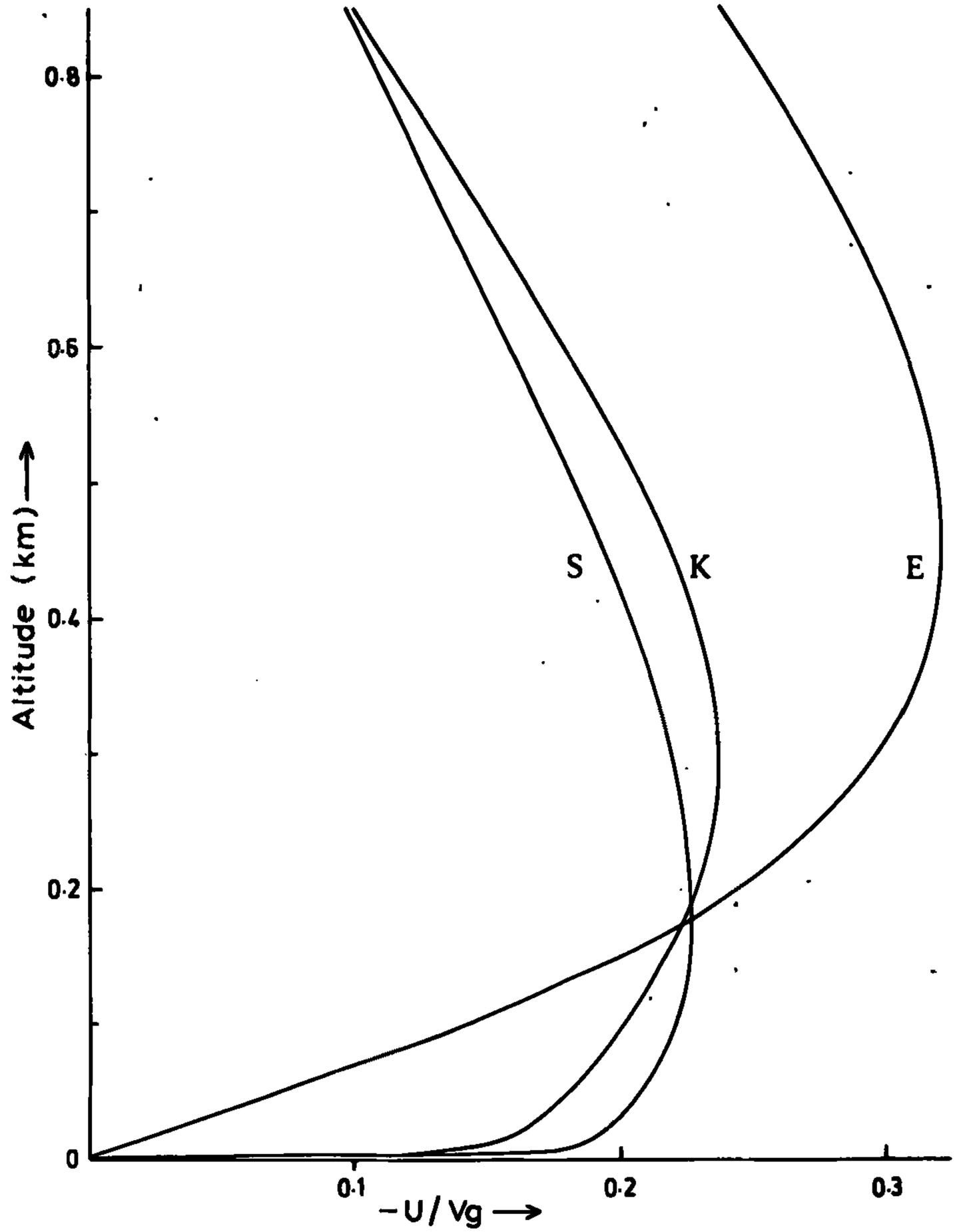

Figure 3

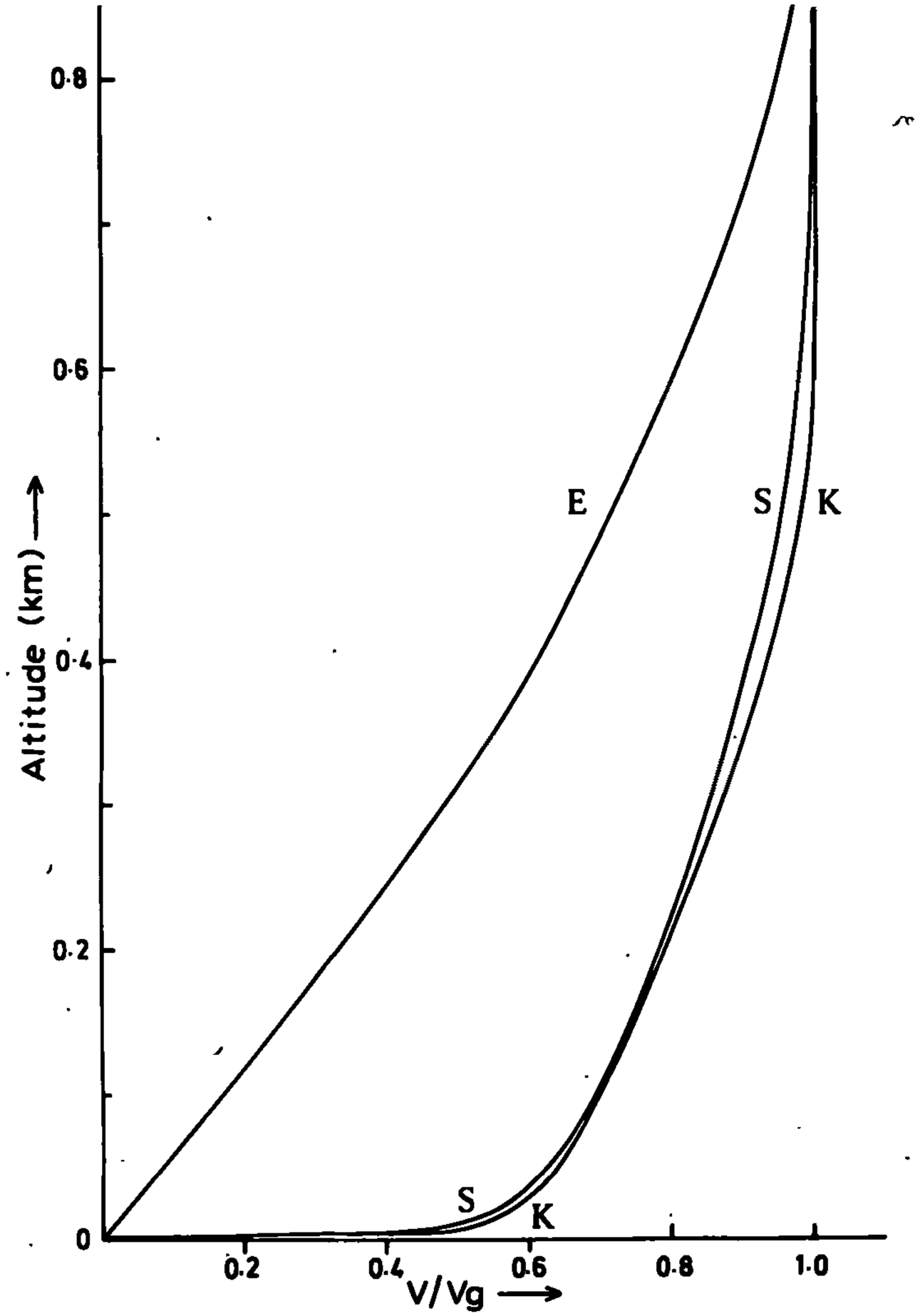

Figure 4

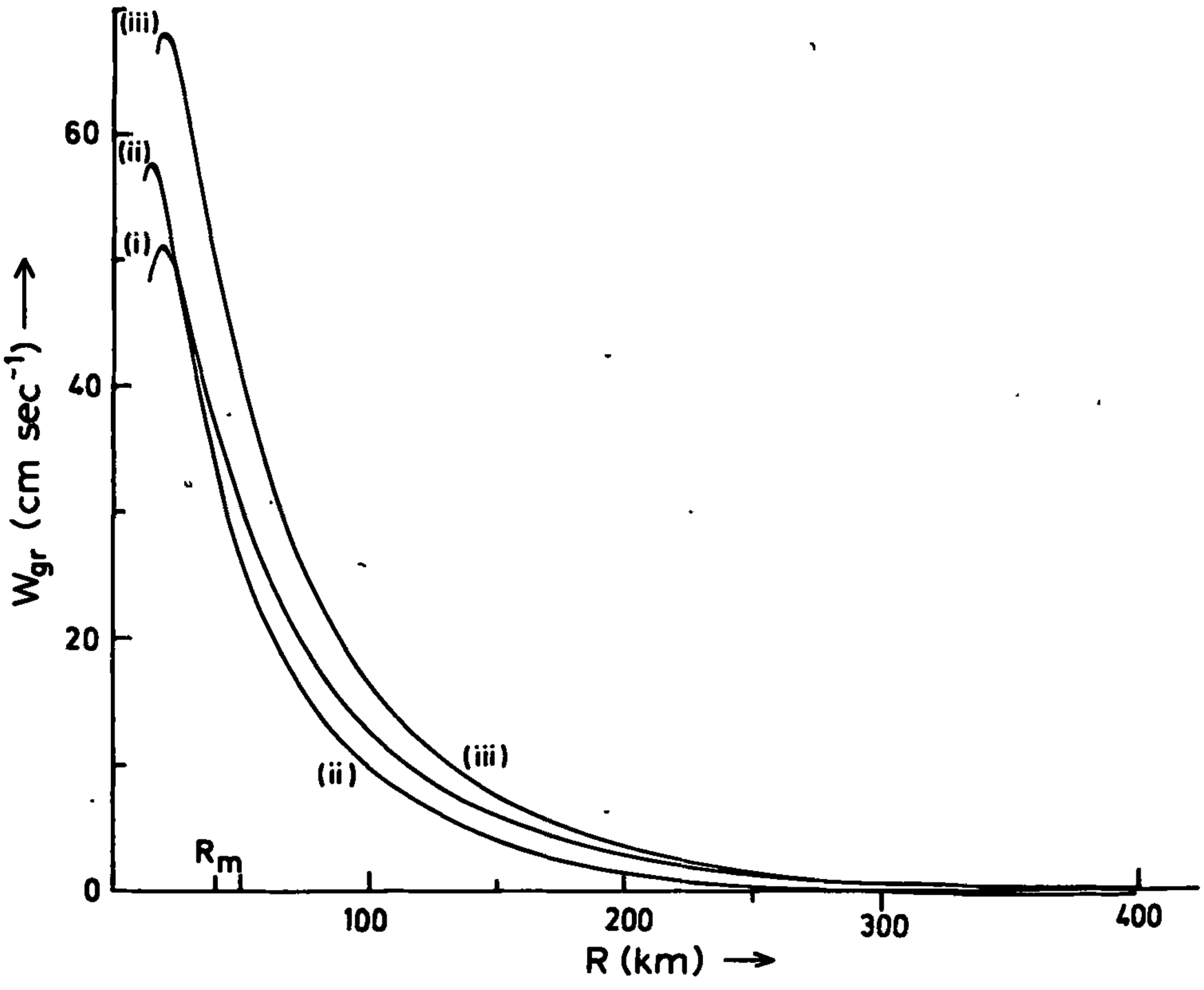

Figure 5(a)

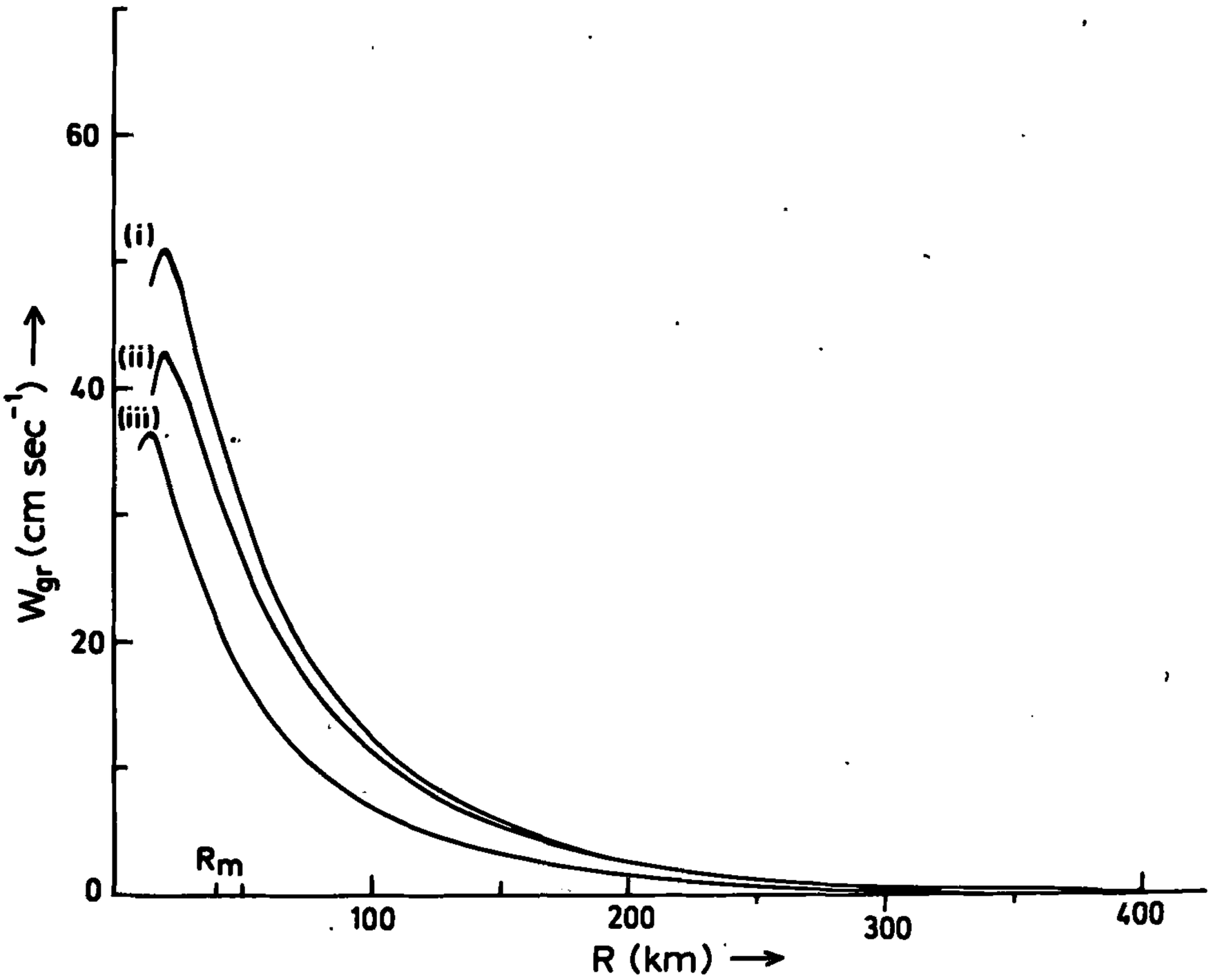

Figure 5(b)

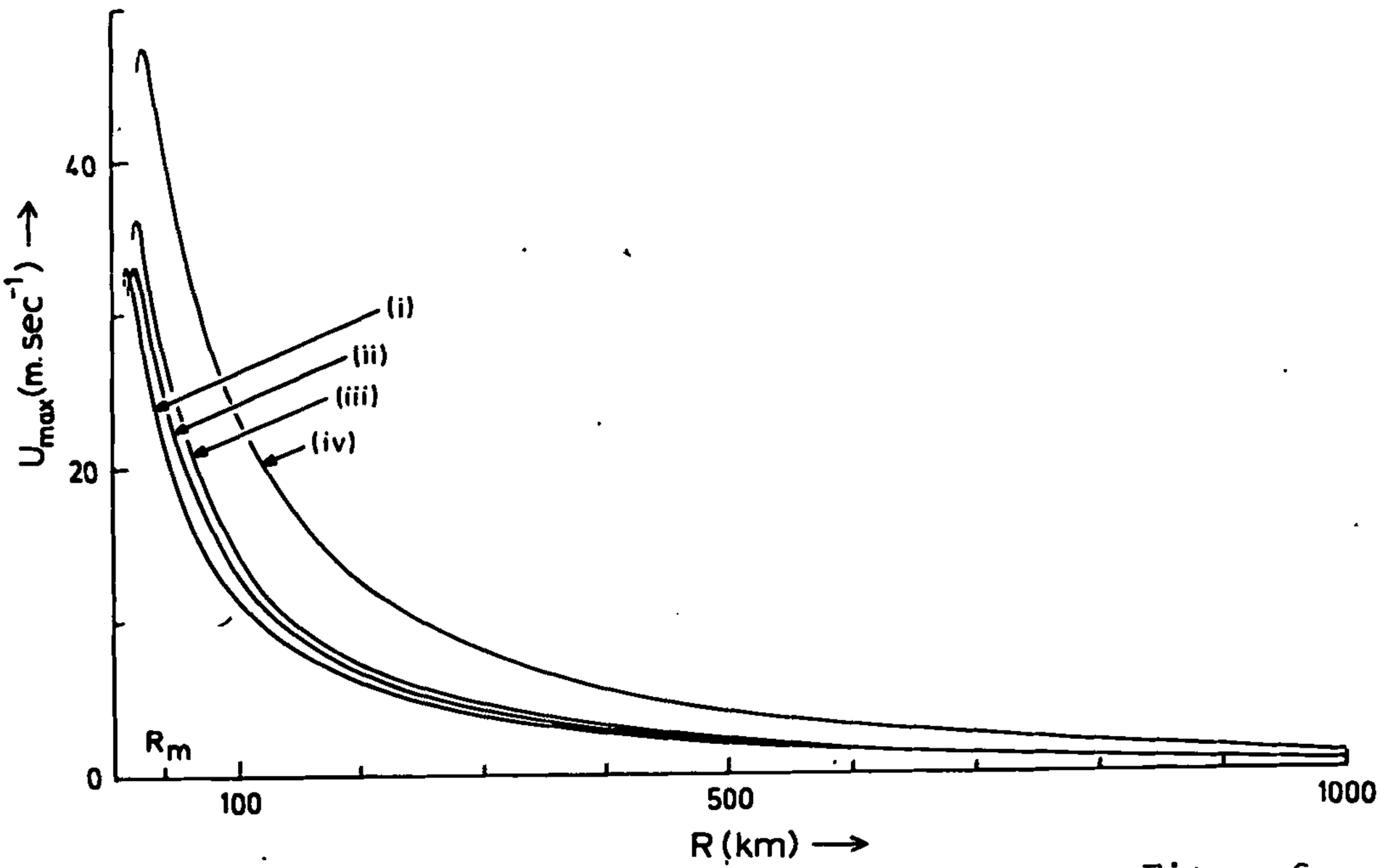

Figure 6

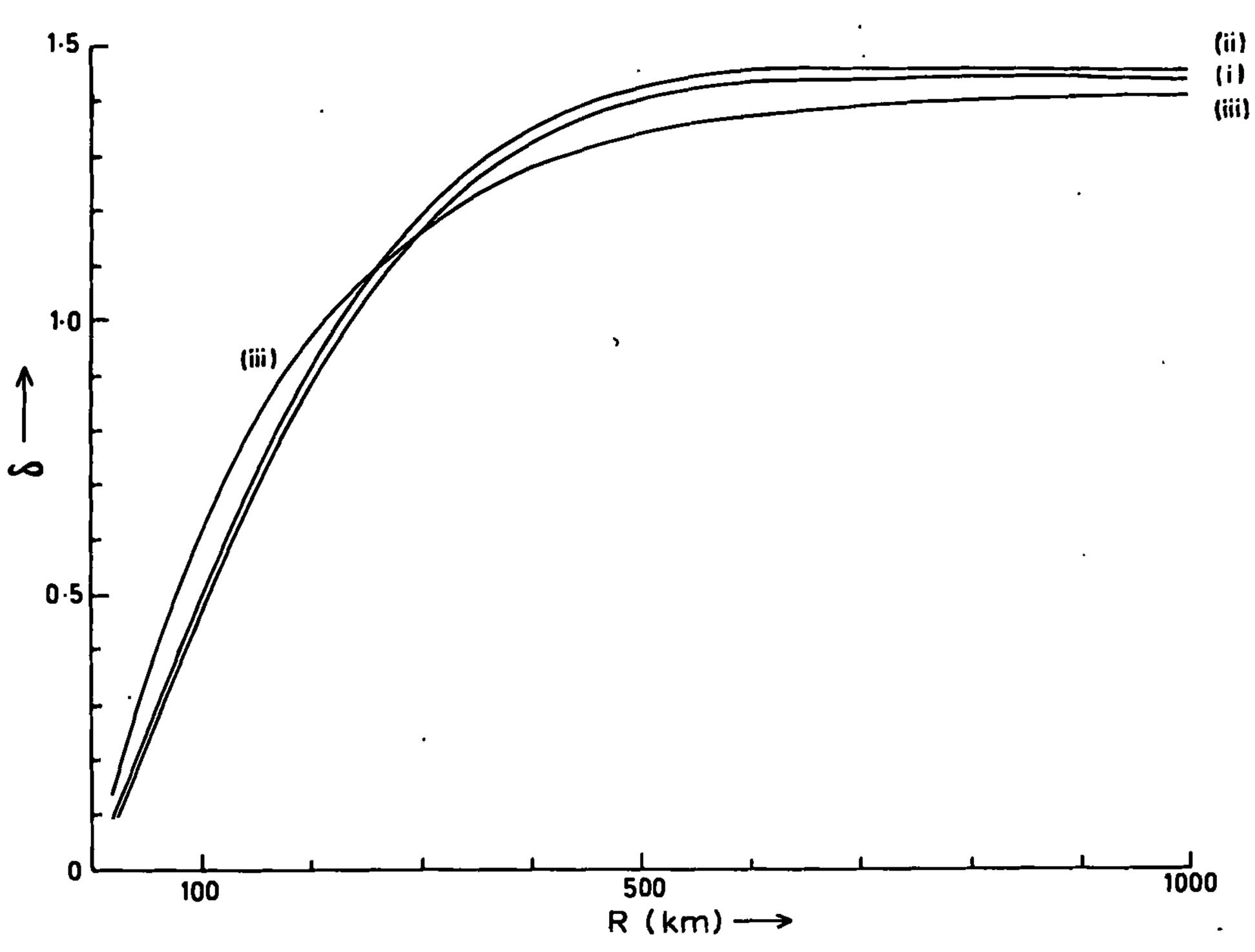

Figure 7

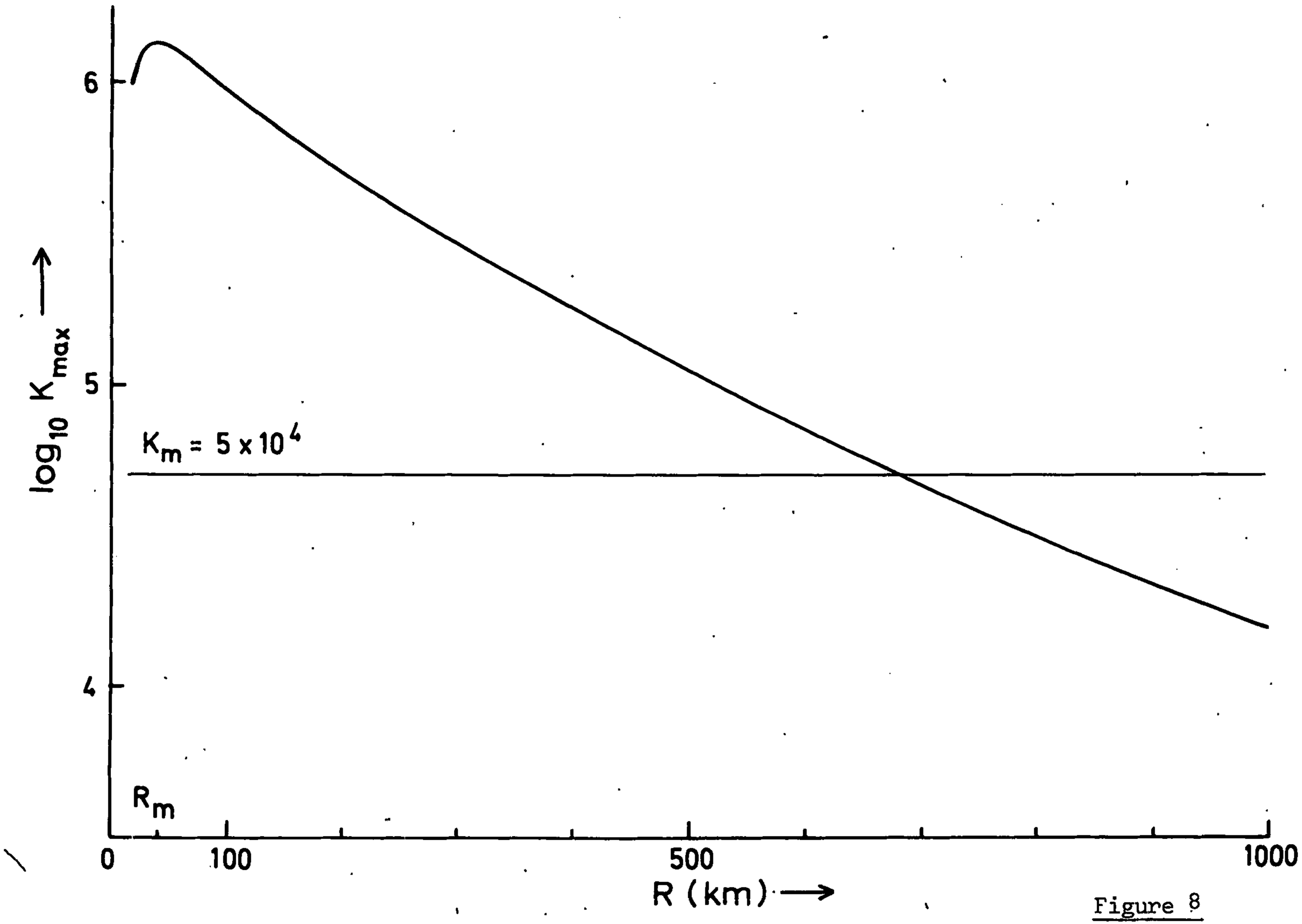

Figure 8

Chapter 3

On boundary effects in models of concentrated vortices - a numerical study.

ABSTRACT

In recent years, considerable interest has been focussed on the modelling of flows with concentrated vorticity, as a means to a possible greater understanding of tornadoes and waterspouts. Much of this effort has been involved with the development of realistic experimental, and to some extent, numerical models of such systems, but progress has been hampered by the almost complete lack of consideration given to the effects on the flow of boundary constraints. In such models there are both physical, and non-physical (artificially imposed) boundaries. By the former, we mean the bottom boundary, with which we would like to model the effect of the earth or ocean surface. Examples of the latter are the side of a rotating tank or the boundary of a computational domain; both of which place on the flow constraints that are clearly not present in the case of atmospheric vortices.

The aim of the work in the present chapter† is to evaluate the effect of both types of boundaries, and to this end, a number of numerical experiments have been performed. This study is an extension of that initiated by Leslie, and is based on the experimental model of Turner and Lilly, in which a vortex is produced in a rotating tank of water, by means of gas bubbles released along the axis of rotation. The results clearly indicate the extent to which these boundaries govern the flow, and point to the importance of such considerations (which to date have been largely neglected) in the development of concentrated vortex models.

---

†Preliminary results were presented to the Euromech 41 Conference, University of East Anglia, 18-21 September, 1973.

1. Introduction

During recent years, particularly in the past decade or so, there has been considerable interest in modelling flows with concentrated vorticity, as a means to a possible greater understanding of the mechanisms involved in convective atmospheric vortices such as tornadoes, waterspouts, and to some extent, dust devils. These investigations are both mathematical (either by analytical or numerical methods) and experimental. Unfortunately, one of the principal shortcomings of this work is due to the lack of consideration given to boundary effects, and the way in which such boundaries affect the development and structure of the vortices generated.

In both the numerical and experimental models, these boundaries may be either physical (such as the bottom boundary meant to simulate the earth or ocean surface) or artificially imposed, non-physical boundaries. In numerical models, the latter arise since we are required to solve the equations of motion in a finite region, a vastly different situation from that enjoyed by the atmosphere. Laboratory simulations tend also to suffer from this defect, although models which use air as the medium can be made considerably less constrained than those in which the vortices are generated in water, by permitting flow through the boundaries. Thus, in developing numerical models of concentrated vortices (and also those in the laboratory), we should endeavour to consider two aspects in the treatment of boundary effects: firstly, we would like information on the effect of the physically significant boundaries, such as the different constraints imposed on fully developed atmospheric vortices

by various bottom boundary conditions; secondly, we should attempt to assess the effect of the non-physical boundaries on the flow, and to minimise these effects if possible.

The work to be discussed in this chapter concerns the simulation of concentrated tornado-like vortices by numerical integration of the Navier-Stokes equations in a rotating cylindrical coordinate system. It extends the study initiated by Leslie (1971) - henceforth denoted by L. The physical system upon which this model is based, is principally the laboratory experiments reported by Turner and Lilly (1963) and later by Turner (1966). Here, fluid in a rotating cylinder is convectively driven from an initial state of solid body rotation, in a meridional circulation by means of gas bubbles released on the axis, in the upper third of the cylinder; these gas bubbles are either carbon dioxide released by nucleation from soda water contained in the cylinder, or else are air bubbles released from a pipe on the axis into the water. Under certain conditions, it is found that a narrow axial vortex can be produced, in which the angular rotation rate of the fluid is many times that of the rotating tank. In the numerical studies of L, the drag force of the gas bubbles driving the circulation is simulated by means of an applied body-force distribution along the upper third of the axis. The choice of parameters for which vortices are formed is critical, although some guidance in resolving this problem is obtained from theoretical results of Morton (1969).

The principal interest in the numerical model of L was to determine such a combination of the relevant parameters - the

driving force and the background rotation - which would result in vortex formation. The vortex obtained 'grows' downwards from the driven region towards the bottom of the tank, whereupon it interacts with the bottom boundary and further amplification of the vortex is observed. In L, a comparison is made between two boundary conditions, these being no slip and zero stress, imposed at the *upper* boundary of the tank. Amplifications (the ratio of the maximum angular velocity of the fluid to that of the cylinder) of 29 and 22 respectively are found. Whereas the main motive in this particular study was to show that such vortex motions could be simulated numerically, the present study concentrates on the effects that the imposed boundaries have on these flows, as well as on a more detailed examination of the characteristics of the flow fields obtained.

A considerable volume of work has been published on concentrated vortex motions, the principal reason being as mentioned above, the interest shown in analogous meteorological phenomena. The more notable of such treatments are discussed below. The experimental models of Turner and Lilly (1963) and Turner (1966), outlined above, have certain features in common with tornadoes and waterspouts: both are rapidly rotating flows driven convectively from above (by Cumulus convection in the tornado and waterspout), and both draw on the background vorticity of the rotating coordinate system, although in the case of atmospheric vortices, some mechanism is also required for a pre-concentration of the background vorticity in order for them to be physically capable of forming in the time-scale observed (see e.g., Morton (1966), Lilly (1969) and Gray

(1969) for relevant details). Furthermore, in both systems, the region of strong rotation is observed to grow downwards, as evidenced by the descent of the characteristic funnel cloud associated with both tornadoes and waterspouts.†

We have yet to consider the importance of the bottom boundary and the interaction between it and the vortex core region. However for the moment, we defer any further discussion on this point and concentrate on the literature relevant to the flow in the vortex core. For an earlier, more comprehensive review of the mechanisms involved in geophysical vortices, see Morton (1966) and also Kessler (1970).

A particular class of solutions to the Navier-Stokes equations in an axisymmetric cylindrical coordinate system was obtained by Burgers (1948). The system has circulation $\Gamma_\infty = \lim_{r\to\infty} (2\pi r v)$ imposed at large radius. An exact solution is obtained through the assumption of constant vertical divergence D, leading to horizontal and vertical velocities proportional to radius and height respectively. The zonal (swirling) velocity profile has the form $v(r) = \frac{\Gamma_\infty}{2\pi r}\left[1-e^{-(r/\sigma)^2}\right]$, where the constant $\sigma=2(\nu/D)^{\frac{1}{2}}$, ν being the kinematic viscosity. In the steady-state represented by this solution, there is a balance between amplification of vorticity by vertical stretching and the loss to the boundaries by radial diffusion of the vortex lines. The characteristic radial length scale of the vortex core σ, is a function

---

†This funnel cloud is no more than an isobaric surface; it is formed of water droplets which condense out when the dynamic pressure in the intensifying vortex falls below the saturated vapour pressure of the surrounding environment.

of D and ν and provides a measure of the relative strengths of these two opposing effects. This profile for v(r) has the form of solid body rotation, $v = \left(\frac{\Gamma_\infty}{2\pi\sigma^2}\right) \cdot r$ at small r, and the form of a potential vortex, $v = \frac{\Gamma_\infty}{2\pi r}$ as r tends to infinity. It is therefore similar to the Rankine combined vortex which has been frequently used in simplified tornado treatments (e.g., Dergarabedian and Fendell 1970). The Burgers solution was obtained independently by Rott (1958, 1959) who extended the analysis to time-dependent flows and also calculated pressure and temperature profiles. Quite naturally, there are a number of problems which arise in such a simplified treatment: the radial and vertical velocity fields are unbounded at large distances and, more importantly, the zonal velocity field has no vertical dependence. Hence, only *inviscid* boundary conditions can be satisfied at the ground, whereas in the real situation, the vortex lines must terminate in the boundary layer adjacent to the ground and not in the ground itself.

The Burgers vortex can be called a 'one-celled' solution since there are no separation streamlines in the interior of the flow. A 'two-celled' solution of similar form has been presented by Sullivan (1959) and by Donaldson and Sullivan (1960). Here, there is a cell of reversed circulation adjacent to the axis, and the model is proposed as being more representative of the flow in an atmospheric vortex, since there is a considerable body of evidence to suggest axial downflow in tornado cores (e.g., Hoecker 1960). Moreover, this appears to be an inherent property of waterspouts, according to measurements by Golden (1973). This solution suffers from the same basic defects as those noted above for the Burgers vortex.

Extensions of the results of Donaldson and Sullivan to multi-celled vortices are calculated by Bellamy-Knights (1970,1971), but this line of approach cannot really be taken as providing a more realistic model of tornadoes and waterspouts.

Considerable impetus to the study of concentrated vortices on the laboratory scale was provided by the experiments of Long (1956), in which fluid is withdrawn axially from a hole in the bottom of a rotating cylinder of water. For a given sink strength, the resulting flow is found to depend strongly on Ω, the angular velocity of rotation of the tank. At small values of Ω, the flow is largely unaffected by the background rotation and varies only slightly from the potential sink flow observed for zero rotation. However as Ω is progressively increased, the flow towards the sink is drawn from an ever decreasing region around the vertical axis of the cylinder, until eventually this region consists of a narrow vortex core in which large zonal velocities are observed. Two further papers by Long (1958, 1961) are concerned with an examination of this vortex flow obtained. In the subsequent experimental setup, the fluid is withdrawn from the top of the rotating cylinder and replaced at the outer wall. The observed conical shape of the vortex obtained led Long to seek a similarity solution in the variable $x = r/z$, with the circulation at large radius and the 'flow force'†

---

†This is the name given to the integrated quantity $\mathbf{F} = 2\pi\int_0^\infty (p+\rho w^2)r\,dr$. Morton (1969) shows that $\mathbf{F}$ is conserved for strongly rotating core flows, and is therefore a more significant quantity than the flux of axial momentum. This is due to the strong pressure-coupling of the axial and zonal velocity fields.

as constants of the motion. A significant property of the solution is that zonal and axial velocity scales are of comparable magnitude in the core region, while radial inflow there is much smaller. However, as pointed out by Long, this similarity solution is incapable of representing the observed flow except at large distances from the ground; further difficulties regarding the relevance of Long's solution are noted by Morton (1969).

Extensions of the experimental work initiated by Long have been reported by Shih and Pao (1971) and by Pao and Shih (1973). Their study is mainly concerned with the selective withdrawal phenomenon first demonstrated by Long (1956) and not so much with the more extreme case leading to the formation of concentrated vortices. In the first of these two papers they describe experiments in which three successive stages in the time evolution of the selective withdrawal process are observed: (i) a short period of potential flow towards the sink, followed by (ii) selective withdrawal in which the flow characteristics are primarily inviscid until (iii) the region of withdrawal extends to the bottom boundary, at which point viscous effects are judged to influence more strongly the flow in the axial core region. The second paper is basically concerned with developing an inviscid theory of the second stage (selective withdrawal) in terms of a blocking wave propagated upstream from the sink. Theoretical extensions of Long's similarity solution are due to Pao and Long (1966) for the case of a magnetohydrodynamically driven vortex, and to Pao and Kao (1969). However, the solution obtained by Pao and Kao clearly corresponds to a *low* Rossby number (i.e., rotationally dominated) system, and therefore is not

appropriate to the present discussion: the crucial role of the Rossby number will be clarified in due course. Their final system of equations, obtained via Oseen and boundary layer approximations, neglects the contribution of the centrifugal terms, whereas it can be shown by dimensional analysis (e.g., Morton 1969), that these terms are essential to strongly rotating core flows. This leads Pao and Kao to seek a similarity solution resembling that of Herbert (1965) for a weak jet along the axis of a strongly rotating fluid, in which the core radius varies as $(\nu z/\Omega)^{1/3}$.

The flow development observed by Shih and Pao (1971) above, parallels that reported in L. The initial motion is inflow towards the bottom of the forcing region, followed by the establishment of an approximate centrifugal/pressure-gradient balance, provided the values of the body-force and background rotation are compatible. This balance tends to inhibit further radial entrainment in this region, and hence the flow is constrained to develop axially until it interacts with the bottom boundary. At the ground, the boundary conditions in a real situation disrupt this dynamical balance, inducing large radial inflow velocities in the boundary layer adjacent to the ground. The basic processes involved in the formation of this type of concentrated vortex are now apparent, the foremost requirement being that the parameters governing the system must be suitable for the initial vortex development along the axis. Radial convergence, most of which occurs in the boundary layer adjacent to the ground in the mature state, entrains fluid radially inwards, and in so doing the fluid rotates faster. At the axis, the flow becomes principally vertical,

with the local vertical component of vorticity being intensified through vertical stretching of vortex lines by the divergent velocity field.

Thus in considering the growth of concentrated vortices, we require firstly a suitable criterion for the existence of such flows, and secondly, we need also to determine the role played by the bottom boundary. For a flow such as that of Long (1958), the two essential flow parameters are the Rossby number measuring the ratio of inertial to Coriolis forces, and the Reynolds number measuring the ratio of inertial to viscous forces. Long found that the type of flow obtained could be described in terms of a Rossby number, $\varepsilon = Q/(2\pi\Omega b^3)$, where Q is the volume flux of the sink, b is the radius of the tank and Ω is its angular velocity. Vortex flows were observed for ε less than 0.02. However, such a low value would suggest that this vortex is completely dominated by the effects of rotation, but as pointed out by Morton (1969), the appropriate length scale for vortex core flows is not b, but the sink radius b_o, and therefore it appears that Long's critical Rossby number could be three, or even four orders of magnitude larger than the value given. Thus these vortices are in fact rather high Rossby number flows: the background rotation provides the source of vorticity, but has little influence on the resulting structure. In the paper by Morton (1969), two relationships are shown to be necessary for the formation of concentrated sink vortices. Firstly, the flow force (defined earlier in a footnote) is required to be of the same order as the background circulation, and secondly the Reynolds number, with length scale based on the

core radius, must be large. This second criterion states that although the Rossby number may be appropriate for concentrated vortex flows, the vertical stretching of vortex lines must not be dominated by radial diffusion. Two criteria for vortex formation are also proposed by Dergarabedian and Fendell (1967), but these conditions both ultimately concern the second question of the balance of vertical stretching and radial diffusion. In the experiments of Turner and Lilly (1963) and Turner (1966), the effect of rotation is such that the return flow occurs within the interior of the cylinder and is not controlled by the boundaries. This has led Morton (1966) to suggest that the Rossby number of these experiments may well be too low for realistic simulation of convective atmospheric vortices. However the situation in these experiments differs notably from those of Long (1958), since in the latter, the fluid is removed at the sink and then replaced at the walls, whereas in the Turner/Lilly experiments, no such external control is exerted.

With respect to the second question of the influence of the bottom boundary on the structure of such vortices, there is indeed very little published work in this area, and it is one of the aims of this chapter to examine the vortex flow resulting from various bottom boundary conditions. This bottom boundary condition can in general be formulated in terms of a drag coefficient C_d, in which the stress at the surface is equal to C_d times the square of the velocity there. This permits us to range from a no slip condition ($C_d = \infty$) such as would apply in the laminar laboratory model of Turner (1966), to an idealised stress-free situation ($C_d = 0$) which

is associated for example, with the Burgers vortex. We also expect this formulation to extend to atmospheric vortices, with a large drag coefficient modelling the turbulent boundary layer of the tornado, and C_d being considerably smaller for the yielding surface condition associated with the waterspout.

With respect to the question of the influence of the bottom boundary on the vortex, Brooks (1951) advanced the opinion that surface frictional effects act in a purely dissipative manner, in stating that it is the atmospheric conditions above and not boundary layer friction which is a chief factor in determining the relative strengths of tornadoes and waterspouts, since otherwise, waterspouts would be the stronger, contrary to observed behaviour. He illustrates this by noting that waterspouts usually disapper when they pass over land. Golden (1971) also refers to some of his observations, in which a waterspout which reached the shore was soon reduced to a large dust devil. The view of Brooks is further supported by laboratory experiments of Dessens (1969,1972) who observed that increased friction in the bottom boundary layer (provided by physical roughness elements) led to a reduction in the intensity of the vortex obtained. On the other hand, it may be argued that a no slip bottom boundary condition, by virtue of the enhanced convergence it induces in the boundary layer, *may* in fact have the opposite effect, since this added radial convergence results in correspondingly greater vertical divergence along the axis, leading to further stretching of vortex lines, and hence intensification of the vortex produced. Numerical experiments of Davies-Jones and Vickers (1971) appear nevertheless to be in accord with Brooks'

argument, rather than with the alternative mechanism. Their system is similar to that of L, except that the driving is provided by buoyancy forces, rather than an applied body-force distribution.

For a number of years, considerable effort has been made by Chang and his co-workers at the Catholic University of America, into principally experimental studies of tornado-like vortices. Their experimental setup, as reported by Chang (1969) and by Ying and Chang (1970), has certain basic similarities to that of Long (1958). Fluid is withdrawn from a narrow sink on the axis at the top of a cylindrical tank; the working fluid in their case is air, and the radial constraint is reduced by drawing the air radially into the main chamber through a gauze screen. The source of vorticity is provided by rotation of this screen at radial distance b, which imposes a given tangential velocity on the injected air. At the operating Reynolds numbers of the experiments, the flow is observed to have considerable turbulent development in the boundary layer. Detailed measurements with hot-wire anemometry are given by Wan and Chang (1972), who examine the flow at two different Rossby numbers, arguing that the flow depends only upon scales determined by the sink strength Q, the *sink* radius b_o, and Γ_∞, the outer circulation induced by the screen. If we calculate their Rossby numbers in terms of Long's modified definition, $\varepsilon = Q/(2\pi\Omega b_o^3)$ with $\Omega = \Gamma_\infty/(2\pi b^2)$, we find values of approximately 191.6 and 8.5 respectively for the two cases they discuss. In the first, they obtain a single-celled vortex coupled strongly to the bottom boundary, and which they are able to compare favourably with measurements by Hoecker (1960) of observed tornadoes. In the second case at the lower Rossby number, the effect of background

rotation is much more predominant, and the flow is confined largely to a region near the axis, with a cell of reversed axial flow being observed.

Experiments performed by Ward (1972) have certain similarities to those of Chang *et al.* noted above. Ward, however, sought to remove the constraint introduced by a fixed sink width, by imposing the upflow over a large radial extent, the air being withdrawn by a fan through a fine mesh screen at the top of the chamber. This screen is used in order to 'decouple' the vortex flow from the fan convection, although the fact that this now imposes *zero* swirling velocity at large height could well mean that atmospheric conditions are not in fact simulated to the extent claimed. The apparent interest in this work is in observing the occurrence of tornado phenomena such as multiple vortices and suction spots. Crawford (1971) also reports experiments similar to those of Long cited above for a rotating cylinder of water. However in the case of Crawford, the bottom boundary is not permitted to rotate with the tank (a property also of the experiments of Chang *et al.* and Ward) and under certain conditions, the flow exhibits turbulence in the bottom boundary layer. This phenomenon has also been observed in the laboratory by Turner (personal communication) who found that flows in which the bottom boundary is inhibited from rotating with the tank are much more likely to develop instabilities than in the case of a rotating boundary, in which only laminar flow is observed.†

---

†Very recently reported experimental vortex studies are those of Fitzjarrald (1973) and Kaiser (1973).

Because of the complicated nature of these vortex flows, in which the equations of motion have to describe a number of important flow regions with widely differing properties (vortex core, terminating boundary layer, outer flow region), it is not surprising that there has been a proliferation of similarity solutions, in order to reduce the equations to more manageable forms. Both Gutman (1957) and Kuo (1966) present similarity solutions in which the vortex is driven by buoyancy forces. Kuo obtains both one- and two-celled solutions, while that of Gutman is two-celled. Both Morton (1966) and Lilly (1969) point out a number of defects in the systems proposed by these two authors, noting that their solutions are similar to the Burgers vortex, and that the existence of a cold downdraft in the two-celled solutions can be precluded on physical grounds; Kuo (1967) attempts to overcome some of these problems by calculating modified solutions which are bounded for large radius. In the 1966 paper, the vortex obtained by Kuo, which satisfies inviscid bottom boundary conditions, is matched to a boundary layer at the ground. However it needs to be emphasised that in this situation, the boundary layer is not able to interact with the vortex, being merely driven passively by it, and hence this approach can in no way provide information as to the effect of the bottom boundary on the vortex core.

Following an approach developed by Gol'dshtik (1960), Serrin (1972) has proposed a similarity solution in which the bottom no slip boundary condition is incorporated. Certain interesting flow solutions are demonstrated to be possible, and these solutions are compared with the flow observed near the bottom of tornado and

waterspout cores. However, we believe there are a number of important difficulties which arise in comparing Serrin's model with actual tornadoes and waterspouts: (i) The flow is not driven convectively in any meridional circulation pattern as atmospheric vortices are, but is generated by imposing a line vortex of strength C along the axis adjacent to the ground; it is the condition of no slip at the ground which is then able to set up the secondary circulation. (ii) In using a model such as this, we encounter the added problem, that any flow system based on a line vortex has infinite kinetic energy, infinite angular momentum and more importantly, in this particular instance *infinite flow force* **F** (defined in the footnote on p.94). This last condition arises, since it is shown that the pressure is given by

$$\frac{p}{\rho} = \frac{\Pi}{r^2} + \text{const}, \text{ and } \Pi \to -\frac{1}{2}C^2 \text{ as } r \to 0.$$

(iii) In Morton (1969), it is established that for viscous swirling core flows,

$$\frac{V}{W} \sim \frac{\Gamma_\infty}{\nu}\left[\frac{F}{\rho\nu^2}\right]^{-\frac{1}{2}} \quad (= \eta, \text{ say}), \qquad (1)$$

and for *strong* vortices, $V \sim W$; that is, $\eta \sim 1$. Here, V and W are the respective scales of the swirling and axial velocities, Γ_∞ is the circulation outside the core region, and the symbol '$\sim$' indicates quantities of the same order of magnitude. In Serrin's model, Γ_∞ is finite, but **F** is infinite. Hence $\eta=0$, implying that the solution represents a *weak* vortex, with no coupling between the swirling and axial velocity fields. (iv) In connection with (iii), it is observed that near the axis, the isobars are apparently

vertical. However in general, vortex core flows exhibit progressive radial spread due to viscous (or turbulent) diffusion. Associated with this process is an adverse axial pressure gradient, not evident in Serrin's solution, tending to oppose the convective driving; it is this mechanism which can lead to the formation of an axial stagnation point, and ultimately, axial flow reversal.

(v) There is no evidence of the characteristic thin inflow boundary layer adjacent to the ground, as found in tornadoes. (vi) Serrin's vortex has in fact no natural radial length scale, and thus it cannot hope to represent the flow in the viscous core adjacent to the axis. Furthermore, it is evident that the velocity fields are unbounded at the axis, and thus to obtain a meaningful solution, Serrin's vortex would have to be matched to an inner solution capable of representing the flow in the core region.

A buoyancy driven vortex solution has been also proposed by Fendell and Coats (1967), in which the model is largely based on that of a laminar plume. However their similarity solution requires the background angular momentum to increase as the square root of the height, a condition which is too great a constraint for their model to have any real physical applicability. A much earlier, well known study is that of Einstein and Li (1955) who obtained simple vortex solutions by specifying the axial velocity to be either zero or very small. However their study has no real relevance to concentrated vortices, since it has been demonstrated by a number of authors (e.g., Morton 1966, 1969; Turner (1966) and L) that strong axial flow is an essential feature of such phenomena.

However similarity solutions, by their very nature, are at most able to represent a single feature of the flow, for example the vortex core. In this particular case, the solution then suffers by being unable to cope with the interaction between the core and the boundary layer. Other similarity solutions invariably suffer from similar such defects, in spite of the frequent claims made that good representations of convective atmospheric vortices are provided. One work which does attempt a more comprehensive treatment is that of Barcilon (1967a,b), who models a dust devil by dividing the flow into a number of regions - surface boundary layer, vortex core, bottom corner region and outer potential vortex - to be subsequently matched. The system is driven by a heated bottom boundary, accompanying experiments being also performed. Unfortunately, the author is unable to successfully match these regions, and hence no further progress can be made with this potentially promising approach.

One other area apart from geophysical vortices, which has prompted work in the field of narrow concentrated vortices is that of flow in vortex chambers. Here the fluid is injected tangentially at the outer wall of the cylinder and expelled axially, much as in the case of Chang's work cited above. Lewellen (1962) approaches this problem via a perturbation expansion in terms of a small Rossby number, his method therefore being particularly valid for cases in which the imposed circulation exerts a considerably influence on the vortex flow. Lewellen's procedure is utilised for the case of a confined convectively driven vortex by Turner (1966), who matches this vortex solution to the boundary layer solution of Rogers and

Lance (1960) for flow on a rotating disk, the aim being to demonstrate the close coupling between the two flow regimes. Lewellen's method is also used by Rosenzweig, Lewellen and Ross (1964) in association with a momentum integral treatment of the surface boundary layer, but unfortunately they appear unable to obtain close agreement with accompanying experiments. Granger (1966) develops an expansion procedure in terms of an inverse radial Reynolds number for the vortex core, yet notes various defects of this approach in a second paper (Granger 1972) in which the method proposed is a generalised similarity solution. There are disadvantages in this approach also, since apart from neglecting the terminating boundary layer, the assumption is made that the effective radius of the viscous core (as measured by the radius of maximum zonal velocity) is constant, and furthermore, this particular constant must be determined experimentally! However we have already shown in connection with Serrin's solution, that this property is not typical of strongly rotating viscous core flows.

Except for the work of L and that of Davies-Jones and Vickers (1971), there are few fully numerical models of concentrated vortices reported. Wilkins, Sasaki and Schauss (1971) attempt to simulate an atmospheric vortex by the release of a thermal (or two successive thermals) from the ground in a rotating frame. Inviscid bottom boundary conditions only, can be specified in their model and hence they are unable to obtain the characteristic strong radial inflow adjacent to the ground. Chaussee (1972) claims to have produced thermally driven vortices numerically, but

the flow he obtains is characterised by weak vertical motions, whereas we have already seen that this property is not typical of concentrated vortices. Wipperman, Berkofsky and Szilinsky (1969) present numerical studies in which a tornado-like vortex is generated in a cylinder with a rotating lid. Unfortunately, there is a serious defect in their numerical procedure, as noted by Leslie, Morton and Smith (1970), in that the vertical vorticity component is generated falsely, by their imposition of the condition of strong rotation ($\partial p/\partial r = \rho v^2/r$) at *all* time, resulting in a steady state being reached in a time less than the period of rotation of their lid! Textor, Lick and Farris (1969) attempt to obtain steady numerical solutions to a vortex chamber problem, but the shortcomings of their numerical method prevents them from examining all but low Reynolds number flows. Harlow (personal communication) has reported numerical work corresponding to the experiments of Wan and Chang (1972) and Ward (1972), but to date we have yet to receive details of this work.

From analysis of the measurements of Hoecker (1960) for a real tornado,† and those of Chang (1969) for a laboratory vortex, Lilly (1969) argues the use of an alternative radial length scale for tornado-like vortices. Instead of the Burgers scale discussed above: $\sigma = 2(\nu/D)^{\frac{1}{2}}$, Lilly proposes a scale proportional to $(\Gamma_\infty/D)^{\frac{1}{2}}$. He then develops an inviscid treatment of the vortex flow, satisfactory results being claimed except for the region in

---

†It has been noted by Morton (1966) that considerable caution must be exercised in assessing the results of Hoecker (1960), owing to certain questionable features in the methods employed to obtain wind velocities, such as the neglect of centrifugal effects on the large debris used as markers of the flow field.

the immediate vicinity of the axis, where friction is expected to play an important role. Lilly proposes that his analysis of observed vortex motions suggests that earlier theories, in which the vortex is considered as principally a balance between vertical flow divergence and radial diffusion, are inconsistent with observed behaviour and it is in fact the boundary layer drag which is the factor of prime importance. This is indeed one of the main points which we propose to consider in the present study.

From the above discussion, it is clear that there are many aspects of tornado-like vortices which remain to be considered in a more comprehensive manner. In a large number of the treatments reviewed in this section, the analysis has been incomplete, and in some cases of little relevance to the actual flows under investigation. The question of the influence of the bottom boundary has received scant attention, in spite of the vital role it obviously plays in coupling the narrow axial vortex region to the outer flow. On the other hand, it is also apparent that the problems involved in resolving the more important features of the vortex flows are indeed of considerable magnitude, and therefore it is often more feasible to concentrate on only a few of the many relevant aspects of this system. To this end, we hope in the present study to be able to clarify to some extent the role of the bottom boundary and to investigate the importance of the constraints which are associated with the imposition of boundaries in the flow regime.

2. Equations of motion

In Figure 1(a) we present the essential features of the system under study. It consists of a right circular cylinder of radius R_* and height Z_* which rotates about its vertical axis with angular velocity Ω. A cylindrical coordinate system $(R,\emptyset,Z)$ is fixed in the rotating cylinder as shown, with corresponding velocity components (U,V,W). The flow is driven by an applied body-force of magnitude F, situated along the axis and of radial extent R_c. Axisymmetry of the flow is assumed, a sketch of the relevant features in the (R,Z) plane being given in Figure 1(b).

The Navier-Stokes equations for time-dependent, axisymmetric incompressible flow in a rotating cylindrical coordinate system, with an imposed vertical body-force F, together with the continuity equation, have the form

$$\frac{\partial U}{\partial T} + U\frac{\partial U}{\partial R} + W\frac{\partial U}{\partial Z} - (2\Omega + \frac{V}{R})V = -\frac{1}{\rho}\frac{\partial P}{\partial R} + \nu\left[\frac{\partial^2 U}{\partial Z^2} + \frac{\partial}{\partial R}\left(\frac{1}{R}\frac{\partial}{\partial R}(RU)\right)\right], \quad (2)$$

$$\frac{\partial V}{\partial T} + U\frac{\partial V}{\partial R} + W\frac{\partial V}{\partial Z} + (2\Omega + \frac{V}{R})U = \nu\left[\frac{\partial^2 V}{\partial Z^2} + \frac{\partial}{\partial R}\left(\frac{1}{R}\frac{\partial}{\partial R}(RV)\right)\right], \quad (3)$$

$$\frac{\partial W}{\partial T} + U\frac{\partial W}{\partial R} + W\frac{\partial W}{\partial Z} = F - \frac{1}{\rho}\frac{\partial P}{\partial Z} + \nu\left[\frac{\partial^2 W}{\partial Z^2} + \frac{1}{R}\frac{\partial}{\partial R}\left(R\frac{\partial W}{\partial R}\right)\right], \quad (4)$$

$$\frac{\partial}{\partial R}(RU) + \frac{\partial}{\partial Z}(RW) = 0, \quad (5)$$

where ρ is the fluid density, ν the kinematic viscosity, both assumed constant, and T is the time. The dynamic pressure P is related to the total pressure P_* by

$$P = P_* + \rho g Z - \frac{1}{2}\rho R^2\Omega^2.$$

Equations (2) to (5) are non-dimensionalised as follows. As the length scale we choose R_c, the radial extent of the applied body-force distribution, following Morton (1969) and Wan and Chang (1972). A representative velocity scale can be incorporated by defining $W_* = (F.R_c)^{\frac{1}{2}}$, and as the natural time scale we have $T_* = R_c/W_*$. We thus define the following dimensionless variable denoting them by lower case letters:

$$\left.\begin{aligned} (U,V,W) &= W_*(u,v,w) \quad , \quad (R,Z) = R_c(r,z) \\ T &= T_* t \quad , \quad P = \rho W_*^2 p, \end{aligned}\right\} \qquad (6)$$

and in non-dimensional terms, the tank dimensions are given by $r_* = R_*/R_c$ and $z_* = Z_*/R_c$, with the dimensionless radius of the driven region being $r_c = 1$. In dimensionless form, equations (2) to (5) can be expressed as

$$\frac{\partial u}{\partial t} + u\frac{\partial u}{\partial r} + w\frac{\partial u}{\partial z} - \left(\frac{1}{\varepsilon} + \frac{v}{r}\right)v = -\frac{\partial p}{\partial r} + \frac{1}{R}\left[\frac{\partial^2 u}{\partial z^2} + \frac{\partial}{\partial r}\left(\frac{1}{r}\frac{\partial}{\partial r}(ru)\right)\right], \qquad (7)$$

$$\frac{\partial v}{\partial t} + u\frac{\partial v}{\partial r} + w\frac{\partial v}{\partial z} + \left(\frac{1}{\varepsilon} + \frac{v}{r}\right)u = \frac{1}{R}\left[\frac{\partial^2 v}{\partial z^2} + \frac{\partial}{\partial r}\left(\frac{1}{r}\frac{\partial}{\partial r}(rv)\right)\right], \qquad (8)$$

$$\frac{\partial w}{\partial t} + u\frac{\partial w}{\partial r} + w\frac{\partial w}{\partial z} = f - \frac{\partial p}{\partial z} + \frac{1}{R}\left[\frac{\partial^2 w}{\partial z^2} + \frac{1}{r}\frac{\partial}{\partial r}\left(r\frac{\partial w}{\partial r}\right)\right], \qquad (9)$$

$$\frac{\partial}{\partial r}(ru) + \frac{\partial}{\partial z}(rw) = 0, \qquad (10)$$

where the applied body-force, after non-dimensionalisation is f, of unit strength. The two dimensionless parameters appearing in the above equations are the Rossby number

$$\varepsilon = \frac{W_*}{2\Omega R_c} \qquad (11)$$

and the radial Reynolds number

$$R = \frac{W_* R_c}{\nu} \quad . \tag{12}$$

We now reduce the number of equations from four to three, and by doing so, obtain equations which are more suitable for numerical treatment. The stream function ψ is defined by

$$u = -\frac{1}{r}\frac{\partial \psi}{\partial z} \quad , \quad w = \frac{1}{r}\frac{\partial \psi}{\partial r} \quad , \tag{13}$$

ensuring that continuity (10) is satisfied identically. The zonal vorticity component is

$$\zeta = \frac{\partial u}{\partial z} - \frac{\partial w}{\partial r} \tag{14}$$

Equations (7) and (9) are cross-differentiated to eliminate pressure, and the three momentum equations for u, v and w reduce to two prediction equations for ζ and v, together with a diagnostic equation for ψ, obtained from the definitions (13) and (14), thus:

$$\frac{\partial \zeta}{\partial t} + J(\zeta/r) = -\frac{\partial f}{\partial r} + \frac{\partial v}{\partial z}\left(\frac{1}{\epsilon} + \frac{2v}{r}\right) + \frac{1}{R}\left[\frac{\partial^2 \zeta}{\partial z^2} + \frac{\partial}{\partial r}\left(\frac{1}{r}\frac{\partial}{\partial r}(r\zeta)\right)\right] \quad , \tag{15}$$

$$\frac{\partial v}{\partial t} + \frac{1}{r} J(v) = \frac{1}{r}\frac{\partial \psi}{\partial z}\left(\frac{1}{\epsilon} + \frac{v}{r}\right) + \frac{1}{R}\left[\frac{\partial^2 v}{\partial z^2} + \frac{\partial}{\partial r}\left(\frac{1}{r}\frac{\partial}{\partial r}(rv)\right)\right] \quad , \tag{16}$$

$$\frac{\partial}{\partial r}\left(\frac{1}{r}\frac{\partial \psi}{\partial r}\right) + \frac{1}{r}\frac{\partial^2 \psi}{\partial z^2} = -\zeta \quad , \tag{17}$$

where

$$J(\theta) = \frac{\partial \psi}{\partial r}\frac{\partial \theta}{\partial z} - \frac{\partial \psi}{\partial z}\frac{\partial \theta}{\partial r} \tag{18}$$

is the Jacobian shorthand notation for the convective terms, θ being a typical flow variable. If required, the pressure p can be recovered from the Poisson equation,

$$\frac{1}{r}\frac{\partial}{\partial r}\left(r\frac{\partial p}{\partial r}\right)+\frac{\partial^2 p}{\partial z^2}=\frac{\partial f}{\partial z}-2\left[\frac{\partial u}{\partial z}\frac{\partial w}{\partial r}-\frac{\partial u}{\partial r}\frac{\partial w}{\partial z}-\left(\frac{u}{r}\right)^2\right]+\frac{1}{r}\frac{\partial}{\partial r}\left[r\left(\frac{1}{\varepsilon}+\frac{v}{r}\right)v\right],$$

obtained by taking the divergence of the momentum equations.

3. Boundary conditions

We shall consider in turn the conditions imposed on the four boundaries of the computational domain, depicted in Figure 1(b).

(i) r=0: Symmetry at the axis of rotation implies that

$u=v=\frac{\partial w}{\partial r}=\frac{\partial p}{\partial r}=0$, and in terms of ζ, v and ψ, we have

$$\zeta = v = \psi = 0. \tag{19}$$

(ii) z=0: Three different boundary conditions can be specified:

(A) one of no slip, (B) a yielding surface with non-zero stress and (C) a stress-free surface; in all cases this bottom boundary is assumed flat. The boundary condition at z=0 can be expressed in a general form involving the drag coefficient C_d, where if the velocity at this boundary is $\underline{u}_o = (u_o, v_o, 0)$, we have in dimensionless form

$$\frac{\partial \underline{u}_o}{\partial z} = \mathbf{R}\, C_d |\underline{u}_o| \underline{u}_o . \tag{20}$$

Cases A, B and C correspond to C_d infinite, finite and zero respectively. In terms of ζ, v and ψ, the boundary conditions in the various cases are

$$\text{A:} \qquad \zeta = -\frac{1}{r}\frac{\partial^2 \psi}{\partial z^2}, \quad v = \psi = 0; \tag{21a}$$

$$\text{B:} \qquad \zeta = \mathbf{R} C_d |\underline{u}_o| u_o, \quad \frac{\partial v}{\partial z} = \mathbf{R}\, C_d |\underline{u}_o| v_o, \quad \psi=0; \tag{21b}$$

$$\text{C:} \qquad \zeta = \frac{\partial v}{\partial z} = \psi = 0. \tag{21c}$$

For case B, the boundary condition (21b) is discussed in more detail in Section 4(d).

On the boundaries $r=r_*$ and $z=z_*$, two possible situations are envisaged - one in which the flow is entirely contained within a rotating cylinder, and the second in which we attempt to provide a more realistic model of the atmospheric situation by removal of the constraints imposed by these boundaries; this is accomplished by allowing the fluid to flow freely through the boundaries of the computational region.

In the first case, the relevant boundary conditions at $r=r_*$ are no slip, while at the upper surface we can model either a no slip lid or a free surface (assumed horizontal). These cases are labelled α and β respectively. In preliminary numerical experiments, the effect of an imposed boundary, particularly at the upper surface, was clearly apparent in the computed fields. Physically, the model simulates a narrow rotating jet of fluid convected along the axis, which interacts with a fixed upper surface. It is this situation which is found to lead to the appearance of oscillations near the upper surface, notably in the vorticity and radial velocity fields, and particularly at large Reynolds numbers. We model this second type of boundary condition by assuming that the height z_* of the computational region is sufficient for the flow there to be effectively vertical. The advantages of this stratagem are twofold: firstly, the oscillatory motion is removed, and perhaps more importantly, the system is more realistic as far as comparisons with atmospheric vortices are concerned. This case is denoted by γ. At the side boundary

$r=r_*$ we can impose either a no slip condition or one in which the boundary constraint is removed, corresponding to radial flow only; these are denoted by a and b respectively. Hence, the appropriate boundary conditions are

(iii) $r=r_*$:

$$a: \quad \zeta = -\frac{1}{r}\frac{\partial^2 \psi}{\partial r^2}, \quad v = \psi = 0; \tag{22a}$$

$$b: \quad \frac{\partial \zeta}{\partial r} = \frac{\partial v}{\partial r} = \frac{\partial \psi}{\partial r} = 0. \tag{22b}$$

(iv) $z=z_*$:

$$\alpha: \quad \zeta = -\frac{1}{r}\frac{\partial^2 \psi}{\partial z^2}, \quad v = \psi = 0; \tag{23a}$$

$$\beta: \quad \zeta = \frac{\partial v}{\partial z} = \psi = 0; \tag{23b}$$

$$\gamma: \quad \frac{\partial \zeta}{\partial z} = \frac{\partial v}{\partial z} = \frac{\partial \psi}{\partial z} = 0. \tag{23c}$$

We also specify the cases of a non-rotating and a rotating tank, denoting them by the indices 1 and 2 respectively. Thus, for example, a rotating tank with no slip on all boundaries, will be specified by Aaα2, and so on.

4. Numerical method

Following L, we obtain firstly the finite-difference analogues of the differential equations (15) to (17), whereupon the difference equations corresponding to the two prediction equations (15) and (16) are solved by the explicit leapfrog scheme. The diagnostic equation resulting from (17) is solved by a direct Fourier method,

in contrast with Successive Overrelaxation used in L.

(a) *Finite-difference operations.* The difference equations are solved on a square mesh defined in the (r,z) plane with equal grid spacing h in both coordinate directions. The number of mesh points in the radial and vertical directions are I+1 and J+1 respectively, and hence the region of integration is specified by

$$r_i = ih \qquad (i=0,1,2,\ldots,I),$$
$$z_j = jh \qquad (j=0,1,2,\ldots,J), \tag{24}$$

where $h = r_*/I = z_*/J$, as denoted in Figure 2. The position coordinates of the flow variables are denoted by a pair of subscripts and their time development by a superscript. For example, $v^n_{i,j}$ represents the finite-difference approximation to the zonal velocity field at the point (r_i,z_j) defined above in (24), at time $n\Delta t$, where Δt is the time increment used in integrating the prediction equations (n=0,1,2,...).

The simplest finite-difference formulation, that of a constant mesh spacing in both coordinate directions is chosen here. However, since we are considering flows whose structure is expected to be concentrated more in the regions adjacent to the boundaries of the computational domain (in particular the axial core and bottom boundary layer), there is a case for use of a non-uniform mesh distribution as formulated for example by Davies-Jones and Vickers (1971) in their model of a thermally driven vortex. Unfortunately there are a number of unresolved problems associated with the use

of non-uniform grids for time-dependent problems. Indeed an examination of the flow fields calculated by Davies-Jones and Vickers indicates the existence of a number of physically spurious interactions which have occurred in the course of their computations.

(b) *The difference equations.* In the notation of Lilly (1965), we define the averaging operator $\bar{\theta}^{x}$ and the difference operator $\delta_x\theta$ for a given flow variable θ, where x can be any of r, z or t whose mesh spacing is Δx:

$$\bar{\theta}^{x} = \frac{1}{2}\left[\theta(x + \frac{\Delta x}{2}) + \theta(x - \frac{\Delta x}{2})\right] ,$$

$$\delta_x\theta = \frac{1}{\Delta x}\left[\theta(x + \frac{\Delta x}{2}) - \theta(x - \frac{\Delta x}{2})\right] . \qquad (25)$$

Using these operators, we express equations (15) to (17) in their corresponding finite-difference form:

$$\delta_t\bar{\zeta}^{t} + J_A(\zeta/r) = -\delta_r\bar{f}^{r} + \frac{1}{\varepsilon}\delta_z\bar{v}^{z} + \frac{1}{r}\delta_z\overline{(v^2)}^{z} + \frac{1}{R}\left[\delta_{zz}\zeta + \delta_r\left(\frac{1}{r}\delta_r(r\zeta)\right)\right]_{lag} , \qquad (26)$$

$$\delta_t\bar{v}^{t} + \frac{1}{r}J_A(v) = \frac{1}{r}\delta_z\bar{\psi}^{z}\left(\frac{1}{\varepsilon} + \frac{v}{r}\right) + \frac{1}{R}\left[\delta_{zz}v + \delta_r\left(\frac{1}{r}\delta_r(rv)\right)\right]_{lag} , \qquad (27)$$

$$-\zeta = \delta_r\left(\frac{1}{r}\delta_r\psi\right) + \frac{1}{r}\delta_{zz}\psi , \qquad (28)$$

where the particular form of the Jacobian J_A is now discussed.

(c) *Stability requirements.*

(i) Conservative difference schemes: In theory, the problem of solving the above system (26) to (28) numerically, is comparatively straightforward. However, when such equations were first being considered in the initial development of numerical weather prediction models, it was observed that instabilities developed in the computed

fields (Phillips 1959). This difficulty arises because the usual difference form of the Jacobian (18),

$$J_1(\theta) = \delta_r\bar{\psi}^r.\delta_z\bar{\theta}^z - \delta_z\bar{\psi}^z.\delta_r\bar{\theta}^r ,$$

is unable to conserve certain integral constraints such as mean and mean-squared vorticity and the meridional and zonal kinetic energies, necessary in the real fluid (assuming dissipation is neglected). The source of these instabilities is the inability of the finite-difference mesh to resolve disturbances longer than a certain critical wavelength (Haltiner 1971); these disturbances then interact with other waves to produce a cascade of energy into the smaller wavelengths. This process, called 'aliasing' continues with ever-increasing amplification until the computations become unstable.

One way to overcome this problem is to use a dissipative difference scheme which damps out the troublesome wavelengths. But Arakawa (1966) has pointed out that this becomes unnecessary if one uses difference approximations to the Jacobians which conserve the necessary integral constraints, thus ensuring computational stability. Arakawa introduced three forms of the Jacobian, J_1 (defined above), J_2 and J_3, which are equivalent for an incompressible fluid:

$$J_2(\theta) = \delta_r\overline{(\psi\delta_z\bar{\theta}^z)}^r - \delta_z\overline{(\psi\delta_r\bar{\theta}^r)}^z ,$$

$$J_3(\theta) = -\delta_r\overline{(\theta\delta_z\bar{\psi}^z)}^r + \delta_z\overline{(\theta\delta_r\bar{\psi}^r)}^z .$$

It can be shown that these three forms conserve the quantities $\langle\theta\rangle$, $\langle\theta^2\rangle$ and $\langle\theta\psi\rangle$, where $\langle\ \rangle$ denotes an integrated average over a given area.

When θ is the vorticity, for example, the three Jacobians conserve mean vorticity, mean-squared vorticity and meridional kinetic energy respectively. Various combinations of J_1, J_2 and J_3 can be employed, the properties of which have been examined numerically by Arakawa (1970). In the present work we use

$$J_A = \frac{1}{3}(J_1 + J_2 + J_3),$$

which obeys all three constraints (Arakawa 1966). In L, J_A was proposed for the vorticity equation and $J_4 = \frac{1}{2}(J_1 + J_2)$, which conserves mean zonal kinetic energy, for the zonal velocity equation. However, there is in fact no additional effort involved in using J_A for both equations, and numerical tests reveal effectively identical results from both schemes.

(ii) Time differencing: In its simplest form, the leapfrog scheme can be expressed as

$$\delta_t \bar{\theta}^t = \frac{\theta_{i,j}^{n+1} - \theta_{i,j}^{n-1}}{2\Delta t} = f_{i,j}^n \ , \qquad (29)$$

where $f_{i,j}^n$ is a specified function of the θ field at the grid point (i,j), at time $n\Delta t$. Clearly $\theta_{i,j}^{n+1}$ can be found explicitly from a knowledge of the fields at times $(n-1)\Delta t$ and $n\Delta t$, and in this manner the solutions can be integrated forwards in time from given initial conditions, the accuracy being of the order of $(\Delta t)^2$. However there are a number of stability problems associated with this

scheme which require consideration.

Firstly, if (29) is a diffusion equation, the resulting difference scheme is unconditionally unstable (Richtmyer and Morton 1967). We use a device of Platzman (1963) to overcome this difficulty: this involves calculating the diffusive terms in (26) and (27) at time $(n-1)\Delta t$ instead of $n\Delta t$ - hence the use of the subscript 'lag'. Thus the diffusive contributions to the difference equations are in fact simple forward differences from time $(n-1)\Delta t$ to $(n+1)\Delta t$. We then have the well known restriction on Δt (Richtmyer and Morton 1967):

$$\Delta t < \frac{R h^2}{8} \quad . \tag{30}$$

Alternatively, we could use the stable DuFort-Frankel Scheme which has been employed in the vortex model of Chaussee (1972).

A linear analysis of (29) when f represents the contribution of the convective terms, yields the second restriction on Δt for two space variables:

$$\Delta t < \frac{h}{\sqrt{2}\, u_{max}} \quad , \tag{31}$$

where u_{max} is the maximum velocity attained in the interior of the computational region, which, if our scaling for W_* is representative of the maximum velocities attained, will be of order unity. It is this second condition (31) which is the governing restriction for the type of highly convective flows we are considering.

There is also a weak instability which arises in connection with the leapfrog scheme due to its second order nature, used as it is to represent first order time derivatives. In this computational mode, two separate solutions appear at alternate time steps, the difference between the two gradually increasing with time until the computations become unstable (Lilly 1965). This behaviour known as 'time splitting', can be suppressed by periodic averaging of the fields (every 40 time steps is found suitable in the present case), in the following manner:

$$\theta'^{n+1}_{i,j} = \theta'^{n}_{i,j} = \frac{1}{4}(\theta^{n+1}_{i,j} + 2\theta^{n}_{i,j} + \theta^{n-1}_{i,j}) ,$$

the computations being restarted from the new (dashed) fields.

(d) *Formulation of boundary conditions.* We now obtain the boundary conditions (19) to (23) in finite-difference form. Firstly, for illustrative purposes, we derive the expression for the vorticity at the bottom boundary, assuming no slip and no flux through this surface. Thus at z=0, we have from (13), (14) and (21a),

$$\zeta=\frac{\partial u}{\partial z} = -\frac{1}{r}\frac{\partial^2 \psi}{\partial z^2} , \quad u= -\frac{1}{r}\frac{\partial \psi}{\partial z} = 0, \quad \psi=0.$$

Expansion of ψ vertically in a Taylor series yields

$$\psi(h) = \psi(0) + h\frac{\partial \psi}{\partial z}(0) + \frac{h^2}{2}\frac{\partial^2 \psi}{\partial z^2}(0) + O(h^3),$$

which with application of the above conditions, leads to

$$\zeta(0) = -\frac{2}{rh^2}\psi(h) + O(h). \qquad (32)$$

An ostensibly more accurate expression for the boundary vorticity involving both $\psi(h)$ and $\psi(2h)$ can be obtained (see Pearson 1965) and this was done in L. Notwithstanding the apparent increase in accuracy from $O(h)$ to $O(h^2)$, it has been demonstrated by Beardsley (1971), who compared his finite-difference calculations with a known exact solution, that Pearson's method gives resulting inferior to those obtained by using (32).

In terms of finite-differences, the boundary conditions (19) to (23) are:

(i) $i=0$ $(r=0)$: $\zeta_{o,j} = v_{o,j} = \psi_{o,j} = 0.$ (33)

(ii) $j=0$ $(z=0)$:

A : $\zeta_{i,o} = -\left(\frac{2}{r_i h^2}\right) \psi_{i,1}$, $v_{i,o} = \psi_{i,o} = 0$; (34a)

B : $(\zeta_{i,o}, v_{i,o})$ - see Appendix, $\psi_{i,o} = 0$; (34b)

C : $\zeta_{i,o} = 0$, $v_{i,o} = \frac{v_{i,1}}{h}$, $\psi_{i,o} = 0.$ (34c)

(iii) $i=I$ $(r=r_*)$:

a: $\zeta_{I,j} = -\left(\frac{2}{r_* h^2}\right) \psi_{I-1,j}$, $v_{I,j} = \psi_{I,j} = 0$; (35a)

b: $\zeta_{I,j} = \zeta_{I-1,j}$, $v_{I,j} = v_{I-1,j}$, $\psi_{I+1,j} = \psi_{I-1,j}$. (35b)

(iv) $j=J$ $(z=z_*)$:

$$\alpha: \quad \zeta_{i,J} = -\left(\frac{2}{r_i h^2}\right) \psi_{i,J-1} \ , \ v_{i,J} = \psi_{i,J} = 0; \tag{36a}$$

$$\beta : \quad \zeta_{i,J} = \psi_{i,J} = 0, \ v_{i,j} = v_{i,J-1} \ ; \tag{36b}$$

$$\gamma : \quad \zeta_{i,J} = \zeta_{i,J-1}, \ v_{i,J} = v_{i,J-1}, \ \psi_{i,J+1} = \psi_{i,J-1}. \tag{36c}$$

The fictitious points $(I+1,j)$ and $(i,J+1)$ outside the computational region, and introduced above in (35b) and (36c), are used to represent the normal derivatives of ψ in the numerical solution of the Poisson equation, when Neumann boundary conditions are specified. In the Appendix to this chapter, we outline the method for the numerical treatment of the nonlinear boundary condition (21b).

(e) *Steady state.* From the given initial state of solid body rotation, the vortex flow continues to develop until such time as the rate of viscous dissipation is balanced by the rate at which energy is added to the system via the body-force. It is found advantageous to partition the total kinetic energy into its zonal and meridional contributions, E_z and E_m. From Lamb (1932, §162) we have

$$E_z = \pi\rho \iint v^2 r \, dr \, dz \ , \tag{37a}$$

$$E_m = \pi\rho \iint \psi\zeta \ dr \, dz \ , \tag{37b}$$

where the region of integration is over the (r,z) cross-section $(0 \leq r \leq r_*, 0 \leq z \leq z_*)$. Steady state is assumed to have been attained when the finite-difference analogues of (37a) and (37b) remain

constant to within 1% over a specified number of time steps.

(f) *Solution of Poisson equation* (28). The method described below, dates from the introduction of algorithms designed to speed the calculation of finite Fourier series by use of the symmetry properties of trigonometric functions (Cooley and Tukey 1965). This method of direct solution, due to its high speed and accuracy, is gaining increasing favour over iterative methods for the numerical solution of elliptic differential equations (see e.g., Hockney 1966 for comparisons).

The diagnostic equation for ψ in terms of ζ at a given time $n\Delta t$, has been previously given (28) in finite-difference form as

$$\delta_r(\tfrac{1}{r}\delta_r\psi) + \tfrac{1}{r}\delta_{zz}\psi = -\zeta.$$

From (24), this is equivalent to

$$\frac{r_i}{r_i+\frac{h}{2}}(\psi_{i+1,j}-\psi_{i,j})+\frac{r_i}{r_i-\frac{h}{2}}(\psi_{i-1,j}-\psi_{i,j})+(\psi_{i,j+1}-2\psi_{i,j}+\psi_{i,j-1})=-r_i^2h^2\zeta_{i,j}, \tag{38}$$

$$(i=1,2,\ldots,I-1;\quad j=1,2,\ldots,J-1).$$

For simplicity, we consider the Dirichlet problem in which ψ is zero on all boundaries. This incorporates the cases (A,B,C; a; α,β; 1,2) defined in Section 3. These boundary conditions permit an expansion of the ψ (and consequently the ζ) fields as finite Fourier series in the z-direction (the summations below being *exact* representations of the discrete fields); we also define

$\zeta_{i,j} = r_i^2h^2\zeta_{i,j}$:

$$\psi_{i,j} = \sum_{k=0}^{J} A_{i,k} \sin \frac{\pi k j}{J} , \qquad (39)$$

$$(i=1,2,\ldots,I; \quad j=1,2,\ldots,J)$$

$$\zeta'_{i,j} = \sum_{k=0}^{J} B_{i,k} \sin \frac{\pi k j}{J} . \qquad (40)$$

The inverse transformation of (40) is

$$B_{i,k} = \frac{2}{J} \sum_{j=0}^{J} \zeta'_{i,j} \sin \frac{\pi k j}{J} . \qquad (41)$$

On substituting (39) and (40) into (38) and equating coefficients, we obtain a second order linear difference equation linking the $A_{i,k}$ and $B_{i,k}$:

$$-a_i A_{i+1,k} + b_{i,k} A_{i,k} - c_i A_{i-1,k} = B_{i,k} \qquad (42)$$

where $a_i = \frac{r_i}{r_i + \frac{h}{2}}$, $c_i = \frac{r_i}{r_i - \frac{h}{2}}$, $b_{i,k} = a_i + c_i + 2(1 - \cos \frac{\pi k}{J})$. (43)

Once calculated, the constant coefficients (43) are stored in the program for use at each subsequent time step. The solution of the tridiagonal system (42) is obtained by the efficient Thomas algorithm (see Appendix of Ch.4) to obtain the unknown $A_{i,k}$. Thus, given the interior $\zeta_{i,j}$ field, we find the $B_{i,k}$ from (41), and on solving (42) for the $A_{i,k}$, the $\psi_{i,j}$ field is recovered through the Fourier synthesis (39).

The expansions in terms of finite Fourier series facilitate a decoupling of the radial and vertical contributions in equation (28), and hence this is equivalent to separation of variables. The

mathematical basis of the method is that the expansion (39) for the $\psi_{i,j}$ field is expressed as a linear combination of the complete set of eigenfunctions of the difference operator $\delta_{zz}\psi$ (Ogura 1969).

The procedure outlined above can be modified to treat the other boundary conditions of Section 4(d). In the preliminary numerical work, the method described here was used, but in the final production version, a generalised routine POIS of Sweet (1973), capable of treating all the different boundary conditions within a single code, was incorporated.

(g) *The overall procedure.* Starting from the initial conditions of solid-body rotation at time t=0 (i.e., n=0) the body-force is applied, and the equations (26) to (28) are integrated until a steady solution is attained. This process involves three distinct operations, which are repeated consecutively at each time step. Firstly, the *interior* $\zeta_{i,j}$ and $v_{i,j}$ fields (i=1,2...,I-1; j=1,2,...,J-1) at time $(n+1)\Delta t$ are obtained from the fields of ζ, v and ψ at the two previous time steps, $(n-1)\Delta t$ and $n\Delta t$; the first time step is necessarily a simple forward difference. This is followed by calculation of the ψ field using the direct method described immediately above. Finally, by way of (19) to (23) the boundary values on ζ, v and ψ are calculated. The integration then proceeds to the next time step, and so on.

Values of certain variables at the axis, for instance ζ/r required for the Jacobian in (26), can be calculated by L'Hopital's Rule. The overall accuracy of the difference solution obtained is second order in both the spatial and time coordinates.

5. Results

In this section we specify firstly the dimensions of the rotating tank, and then consider in turn the influence of the various boundary conditions and other relevant parameters.

5.1 *Selection of flow parameters.* It is clear from the work discussed in the Introduction (e.g., the experiments of Long, the numerical studies of L and the order of magnitude analysis of Morton) that concentrated vortices are capable of forming only over a narrow range of physical parameters. Firstly, the Rossby number ε must be suitable for vortex formation; in the present case, this demands that the values of the driving force and the background rotation be 'compatible'. Secondly, the Reynolds number **R** must be sufficiently large in order that the vertical stretching of vortex lines is not dominated by radial diffusion.

As the physical dimensions of the tank itself, we choose $R_* = 7.5$ cm and $Z_* = 30$ cm, with the value of R_c being set at 1.5 cm. After a number of preliminary numerical experiments, where guidance was provided by the analysis of Morton (1969), the following values of F, Ω and ν were chosen: $F=1.5$ cm^2 sec^{-1}, $\Omega=0.1$ sec^{-1} and $\nu=2.5\nu_o$, where ν_o is the kinematic viscosity of water equal to 1.008×10^{-2} cm^2 sec^{-1}. These values were found to lead to a vortex flow which exhibits large amplification of the background rotation and also in which the region of radial inflow grows downwards from the driven region towards the bottom boundary. Hence $W_* = (F.R_c)^{\frac{1}{2}} = 1.5$ cm sec^{-1}, and we can now calculate the Reynolds and Rossby

numbers from (11) and (12) as $R = 89.3$ and $\varepsilon = 5.0$. Also $r_* = 5$, $z_* = 20$ and $T_* = 1$.

In all the numerical experiments performed, the forcing is specified along one third of the extent of the axis of rotation. Unlike the case of L which modelled the experiments of Turner and Lilly where the force was applied to the top third, the driven region in the present case is situated halfway up the axis, much as indicated in Figure 1(b). This is done in order to minimise as far as possible, the direct influence of the forcing in the vicinity of both the top and bottom boundaries. The dimensions chosen for the finite-difference mesh as described in Section 4(a), are I=15, J=60 and hence $h=r_*/I = 1/3$. That is, r_c, the radial extent of the forcing, is three grid lengths. A triangular profile for f is used over this region as shown in Figure 3, where we also indicate the specification of the term $\partial f/\partial r$, required in equation (26). A suitable dimensionless time step, ensuring computational stability is found to be $\Delta t=0.05$ and steady-state is judged to have been reached after 2500 time steps, corresponding to a total elapsed time of 125 sec. The one minor exception to the above is in the case Abα2, in which we set I=16, J=64 and hence $r_c=3.2h$. Here the time step is chosen as $\Delta t=0.04$ and an equivalent total time is attained by running the integrations out to 3125 time steps. Details of the various cases considered are presented in Table 1.

5.2 *The bottom boundary.* As previously indicated, the principal reason for considering this boundary is to determine more fully the influence of different surface conditions in atmospheric vortices.

This is carried out by testing the two cases, Aaγ2 and Caγ2 which are identical apart from the bottom boundary, which is one of no slip and zero stress (inviscid) respectively.

In Figure 6, we show the contours of ψ v, u and w for case Aaγ2 after 500 time steps, still a comparatively early stage in the development of the vortex. As can be seen, the flow is 'growing' downwards towards the bottom of the tank but there is yet no noticeable interaction with the no slip boundary there. However at steady-state (n=2500) as seen from Figure 7, this situation has altered considerably. The vortex has continued to develop until it has begun to interact with the bottom boundary. At this point the disruption of the approximate centrifugal/pressure-gradient balance by the no slip condition, induces the large radial inflow velocities near the boundary as shown most clearly in (c). The inflow boundary layer is seen in (a) to extend along the bottom of the tank and (b) shows the zonal velocity field in the mature state, with the vortex lines terminating in the bottom boundary layer. Figure 6(b) exhibits a region of negative zonal velocity near the top, which by steady-state has been carried out of the computational region. The velocities in this region are negative in the frame of the rotating tank, but are (necessarily) positive in the inertial frame. At steady-state, the maximum amplification of the zonal velocity field for this case is 39.1.

In Figure 8, we show the steady-state contours for case Caγ2, the vortex obtained with the idealised inviscid bottom boundary. The contours at 500 time steps (not presented here) are very similar

to those of Figure 6, since at this point there is no effective interaction with the bottom boundary. However this picture has altered noticeably, as expected, by the time that steady-state is attained. Because of the inviscid boundary, the centrifugal/pressure-gradient balance is maintained right to the bottom of the tank. Hence there is no strong radial inflow layer and the vortex lines terminate in the boundary itself.

In Figure 4, we show the variation of w along the axis and near the bottom boundary for these two cases. Below the driven region, the profile for the inviscid boundary is effectively linear, in line with the Burgers vortex. However in case $A a \gamma 2$, the active role of the no slip bottom boundary condition is clearly visible. Considerable disruption of the w field is observed near the bottom in the region of boundary layer eruption, but above this, the profile is also seen to be linear. In Figure 5, we show contours of v at height $z' = 10/3$, which is within the linear w region of Figure 4 for both these cases. These curves are best least-squares fits of the Burgers profile, given in the Introduction.

The two works with which we can compare the results of this particular study, are the laboratory experiments of Dessens (1969, 1972) and the numerical studies of Davies-Jones and Vickers (1971), both of whom consider the problem of the influence of boundary friction on the structure of a concentrated vortex. Dessens ...lished this by using actual physical roughness elements on the bottom boundary of his experimental setup, while Davies-Jones and Vickers incorporate the same boundary conditions as in the present case. The results which we obtain are in good qualitative

agreement with those of Dessens. The inviscid boundary results in a considerably stronger vortex, with a maximum amplification of 55.0 as against 39.1 for the no slip case. Because of the enhanced radial converge induced near the boundary by the no slip condition, the vertical velocities in Figure 4 are noticeably stronger in this case, as also found by Dessens. Furthermore, in agreement with him, the zonal velocities in Aaγ2, as well as being considerably weaker, have also a more diffuse core structure than in Caγ2, as seen from the fitted curves of Figure 5. Here, the Burgers core thicknesses are σ (dimensionless) equal to 0.38 and 0.27 respectively. The numerical vortices obtained by Davies-Jones and Vickers appear to be much more strongly influenced by the bottom boundary than those of the present study, the ratio of the maximum amplifications obtained being almost 5 for the inviscid and no slip conditions. However it is noticeable that their vortex for the no slip case, is not joined to the bottom boundary by a strong inflow boundary layer, suggesting that their choice of parameters may not be ideal. Indeed, their streamline contours show that there is even a cell of reversed circulation adjacent to the rigid boundary!

From the above discussion, we deduce that so far as the strength of the resulting vortex is concerned, the no slip bottom boundary appears to act in a purely dissipative manner, and in this we are in agreement with both Dessens and Davies-Jones and Vickers, as well as the arguments of Brooks (1951). In the present work we have not attempted to treat the intermediate boundary condition B, defined in (20b), but as indicated in the Appendix, no difficulties are foreseen

in incorporating this at a later date. In connection with actual atmospheric vortices, we have the case reported by Golden (1971), in which a tornado that formed over land, later veered over the water, inflicting severe damage on boats which were moored in this area. However, there are no estimates available of the change in strength of this vortex due to these two surface conditions.

5.3 *Influence of Rotation and Diffusion.* For purposes of comparison, we have also performed the calculations at rather different Rossby and Reynolds numbers from the cases discussed above. In Figure 9, we show the steady-state contours of ψ and w for case Caγ1, which is identical to Caγ2 except for the rotation rate which is zero, resulting in an infinite Rossby number instead of the previous value of 5. Here we can see that, as expected, there is no growth of the flow region below the driven region. In fact, in the early numerical experiments, it was found that apparently strong vortices could be formed at Rossby numbers considerably greater than 5, but that a closer examination revealed a streamline pattern much as in Figure 9(a). Here the forcing was tending to dominate the effect of rotation, and although large zonal velocities were obtained in the driven region, there was negligible vortex growth, and hence no possible interaction with the bottom boundary. This behaviour is also seen in Figure 4, where we show the vertical velocity along the axis.

The second condition obtained by Morton (1969) for the existence of concentrated vortices is that the Reynolds number must be sufficiently large, otherwise radial diffusion of the vortex lines will dominate vertical stretching to the extent that the flow is no longer a rapidly swirling vortex. To this end,

we have considered the case denoted by Aaγ2', which is identical in all respects to Aaγ2 except for the viscosity ν, which is equal to $10\nu_o$ instead of $2.5\nu_o$ as in the latter. In Figure 10 we show the steady-state contours of ψ and v for this case. Since the value of the Rossby number ε is still equal to 5, the flow fields have developed downwards with considerable inflow occurring adjacent to the bottom no slip boundary. However as seen in Figures 5 and 9(b), the zonal velocity field is much weaker and more diffuse than the case of Aaγ2, with a maximum amplification equal to 8.9 and σ equal to 1.05. These can be compared with the values of 39.1 and 0.38 found in the higher Reynolds number case. In Figure 4 the vertical velocity on the axis is seen to resemble the profile for case Aaγ2, but with only a comparatively minor disruption in the vicinity of the bottom boundary.

5.4 *The 'non-physical' boundaries.* In the Introduction, we laid considerable stress on the fact that in both the experimental and numerical studies which have been performed to date, very little consideration has been given to the effect of imposed boundaries on the flow, in models which attempt to make meaningful comparisons with atmospheric vortices. Thus in this section, we wish to examine more closely the flow resulting from different conditions imposed at the outer boundaries, $r=r_*$ and $z=z_*$.

In all the cases which have been discussed above, the same conditions have been applied on these two boundaries, namely no slip on $r=r_*$ and free flow through the boundary at $z=z_*$, as represented by (22a) and (23c) respectively. It was decided therefore, to examine the further case in which these boundary

conditions were reversed, by applying a no slip rigid lid and with free flow being permitted through the side boundary. Apart from this, the bottom boundary is one of no slip, while ε and R are maintained at the values selected in Section 5.1, this case being denoted by Abα2.

In Figure 11, we present contours of (a) zonal velocity and (b) stream function, showing the time development of this case from the initial state of solid body rotation, to the situation at time $1000\Delta t$. Now in the Introduction we mentioned that in preliminary experiments, it was found that the presence of a rigid lid led to oscillations appearing in the flow fields, and it was this problem which was one of the reasons for removing this constraint at the upper surface, by allowing free flow through the boundary of the computational domain. As can be seen in Figure 11, these oscillations have become apparent after 250 time steps, by which point the flow has begun to interact with the upper boundary. There are two possible explanations for the existence of this oscillation. The first is simply that the finite-difference mesh in the region of lid may not be capable of resolving the flow, which consists essentially of a strong narrow jet which comes into abrupt contact with a rigid boundary. The second is a physical mode, which has been observed in conjunction with confined concentrated vortices in the laboratory, by Turner (1966) and Pritchard (1970). This feature has the appearance of a solitary wave supported by the rigid boundaries, and which oscillates back and forwards along the axis much in the manner of longitudinal vibrations of a spring. This problem has also recently been considered theoretically by

Leibovich and Randall (1972).

In order to determine if it is the second mechanism exclusively which causes the appearance of these oscillations, the same case but with zero rotation (Abα1) was run out to 500 time steps, but no appreciable attenuation of these waves was observed. However regardless of the exact mechanism which causes them in association with a rigid lid, we have seen that this problem can be removed by allowing the flow to pass out of the top of the container, as in the other cases which have been calculated. If it is the first mechanism that is the cause, then removal of the lid means that the vertical core flow is not suddenly constrained to form a radial outflow region as shown in Figure 11(b). On the other hand, if the inertial oscillations are also affecting the system, they can no longer be supported, once the lid is removed. Furthermore, this leads to a steady, well-behaved situation, and one that is also much more realistic so far as comparisons with atmospheric vortices are concerned. We have not attempted at this stage to ascertain if the height z_* is sufficiently far above the driven region to justify the assumption of no radial flow, and it can be seen from the radial velocity contours of Figures 6, 7 and 8 that there is in fact not a completely smooth transition to zero at this upper boundary. In the numerical study of L in which a rigid lid was applied, these oscillations were removed by periodic smoothing of the flow fields, whereas we have seen in the present work, that this mode can be effectively suppressed by a simple change in the upper boundary conditions. The third possible boundary condition, that of zero stress - equation (23b) - has not been considered in the present study.

The effect of removing the side boundary constraint can also be seen. In the early stages of development, the fluid tends to pass unconstrained through the outer wall, but at a later time it is seen that the value of the Rossby number is sufficiently small to constrain most of the return flow within the boundaries of the region. Consequently, a cell of reversed circulation is set up as seen in Figure 11(b). In Figure 5, we show the calculated values of $v(r,z')$ after 250 time steps, and the corresponding fit of a Burgers profile. The agreement between the two is very good at this point, although at later stages the situation is altered to some extent, due to the effect of the circulating flow of the overall system, particularly at the rather low Rossby number of the present vortex. Nevertheless, it is an interesting result, and agrees with the measurements of Golden (1971) taken in an actual waterspout. The maximum amplification found for this case, $Ab\alpha 2$, is 32.2.

6. Conclusions

In this chapter, we have demonstrated by means of a number of numerical experiments, the role played by the boundaries in the overall structure of concentrated, convectively-driven vortices. One point which is immediately obvious is the ease with which the various cases can be simulated numerically, in contrast with the difficulties which are involved in the laboratory situation. As well as this, it is a simple matter to specify any required combination of the Rossby and Reynolds numbers in these numerical simulations. In detailed experiments which have been performed, such as those of Crawford (1971) and Wan and Chang (1972), it appears a comparatively simple matter to generate the vortex itself, but a prodigious number of

measurements is needed to determine the overall flow details.

The present approach differs substantially from the line adopted in many earlier works. In these, a particular model is usually proposed as being representative *per se*, of a typical tornado or waterspout. Here, we make no such strong claims; the main emphasis has been centred on obtaining information as to how different constraints at the boundaries and different physical parameters can affect the strength and structure of the resulting vortex. The use of different bottom boundary conditions has clearly demonstrated the active role of boundary friction on the resultant vortex, and thus the many models which neglect this interaction, cannot hope to provide a realistic treatment of such flows. The removal of the upper boundary constraint has been shown to lead to situation which avoids the problems caused by the imposition of an upper surface, with the resulting solution being steady and also providing an improved model of atmospheric vortices.

The fact that a genuine steady-state flow is apparently attainable, may point to considerably more work which can be performed in this area. In the following chapter, we develop a numerical method for steady two-dimensional flow which should adapt quite readily to the equations governing the present three-dimensional axisymmetric case. One of the difficulties of the approach we have used here, is the extremely large amounts of computation required in integrating out the flow from the initial conditions of solid body rotation to the final steady-state. On the other hand, since it is the steady solution which is of most interest, then the

advantages of a rapid solution of the steady equations of motion are immediately obvious, and it is anticipated that further work into concentrated vortices can be carried out along these lines.

To date we have yet to consider the effect of removing the boundary constraints on *both* $r=r_*$ and $z=z_*$ and this is one case which we hope to treat in the near future. Also needed is a much fuller investigation of the effect that variations of the Rossby and Reynolds numbers have on the flow, since we have demonstrated here to some extent just how critical these parameters are in a correct modelling of these vortices. One further point which was not investigated, is the effect of grid resolution on the finite-difference solutions obtained. This is clearly a most important consideration, yet it was felt that in the present context, it would be preferable to concentrate for the moment, solely on the boundary effects. One other interesting, and as yet unexplained feature was observed in the preliminary experiments. When the Reynolds number was increased much above the value of 89.3 used in all the cases apart from $Aa\gamma 2'$, an instability in the computed fields was observed near the bottom of the tank. Since this is not the region of the largest velocities, it is not likely to be simple numerical instability, and further, the upper constraint was removed so that the waves could not be generated there. One possibility is that we were observing the initial stages of vortex breakdown, but it would be unwise at this stage to speculate any further along these lines.

The work which we have reported in this chapter has revealed a number of important features of vortex flows, particularly the effect of the imposed boundaries. It makes it clear that in future

numerical and experimental studies, there is a much greater need than has been common in the past, to take account of the active role that these boundaries play, particularly when analogies (or direct comparisons!) are being made with tornadoes and waterspouts. Much more work is still necessary in order to gain a fuller understanding of these flows, and we have indicated a number of approaches that it is hoped will be productive in this respect.

APPENDIX

The boundary conditions (21b), with $A = \mathbb{R}C_d$, are

$$\zeta_{i,o} = A|\underline{u}|_{i,o}u_{i,o}, \tag{A.1}$$

$$\left(\frac{\partial v}{\partial z}\right)_{i,o} = A|\underline{u}|_{i,o}v_{i,o}. \tag{A.2}$$

In terms of one-sided differences at the boundary, $u_{i,o}$ is a known function of the interior ψ field; from (13), we obtain

$$u_{i,o} = -\frac{\psi_{i,1}}{r_i h}, \tag{A.3}$$

and for the normal derivative of v,

$$\left(\frac{\partial v}{\partial z}\right)_{i,o} = \frac{v_{i,1} - v_{i,o}}{h} \tag{A.4}$$

Thus the two equations (A.1) and (A.2) for $\zeta_{i,o}$ and $v_{i,o}$, are specified in terms of the known quantities A, h, r_i, $\psi_{i,1}$ and $v_{i,1}$. Now $|\underline{u}|_{i,o} = (u_{i,o}^2 + v_{i,o}^2)^{\frac{1}{2}}$, and thus from (A.4),

$$\zeta_{i,o} = A\, u_{i,o}(u_{i,o}^2 + v_{i,o}^2)^{\frac{1}{2}}, \tag{A.1'}$$

$$(v_{i,1} - v_{i,o})^2 = (Ahv_{i,o})^2(u_{i,o}^2 + v_{i,o}^2). \tag{A.2'}$$

Since $u_{i,o}$ is known from (A.3), we can solve (A.2') for $v_{i,o}$ by simple functional iteration such as Newton's method, with the value obtained at the previous time step furnishing a good initial estimate. From the value obtained for $v_{i,o}$, $\zeta_{i,o}$ is calculated directly from (A.1').

Case	Bottom boundary	Upper boundary	Side boundary	Ω	ν/ν_o	R	ε	Grid Size	Maximum Amplification	w_{max}
AaY2	No slip	No lid	No slip	0.1	2.5	89.3	5	16x61	39.1	3.37
CaY2	Stress-free	No lid	No slip	0.1	2.5	89.3	5	16x61	55.0	2.87
CaY1	Stress-free	No lid	No slip	0	2.5	89.3	∞	16x61	-	3.19
AaY2'	No slip	No lid	No slip	0.1	10.0	22.3	5	16x61	8.9	2.41
Aba2	No slip	No slip	No side	0.1	2.5	89.3	5	17x65	32.2	3.33

Table 1. Details and results of various cases computed.

Figure Captions

Figure 1(a) Sketch of the rotating tank and the coordinate system used.

(b) Corresponding cross-section in the (R,Z) plane.

Figure 2. The (r,z) finite-difference mesh.

Figure 3. Formulation of the forcing term in equation (26), when f is distributed over two mesh spacings.

Figure 4. Variation with height of the vertical velocity along the axis for cases Aaγ2, Caγ2, Caγ1 and Aaγ2'.

Figure 5. Radial variation of the zonal velocity v with radius at height z'=10/3, and fitted by least-squares Burgers profiles. Crosses indicate calculated values at time 250Δt for case Abα2; remainder are steady-state profiles.

Figure 6. Contours of (a) stream function, (b) zonal velocity, (c) radial velocity, (d) vertical velocity. The contours are equidistant, with maximum and minimum values being denoted by an overbar and underbar respectively: case Aaγ2, n=500.

Figure 7. As for Figure 6: case Aaγ2, steady-state.

Figure 8. As for Figure 6: case Caγ2, steady-state.

Figure 9. Contours of (a) stream function, (b) vertical velocity: case Caγ1, steady-state.

Figure 10. Contours of (a) stream function, (b) zonal velocity: case Aaγ2', steady state.

Figure 11. Contours of (a) zonal velocity (b) stream function: case Abα2, times as indicated.

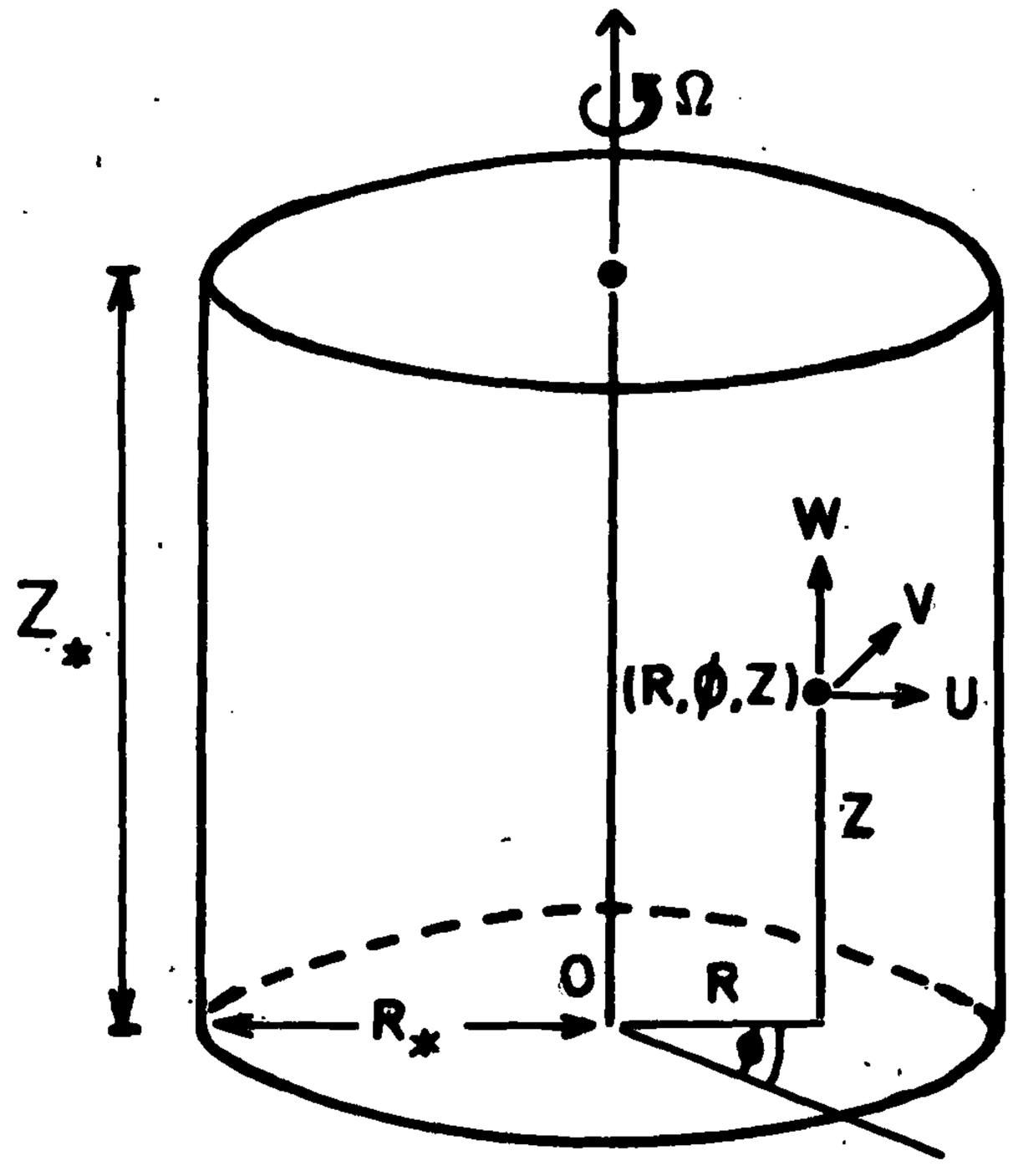

Figure 1(a)

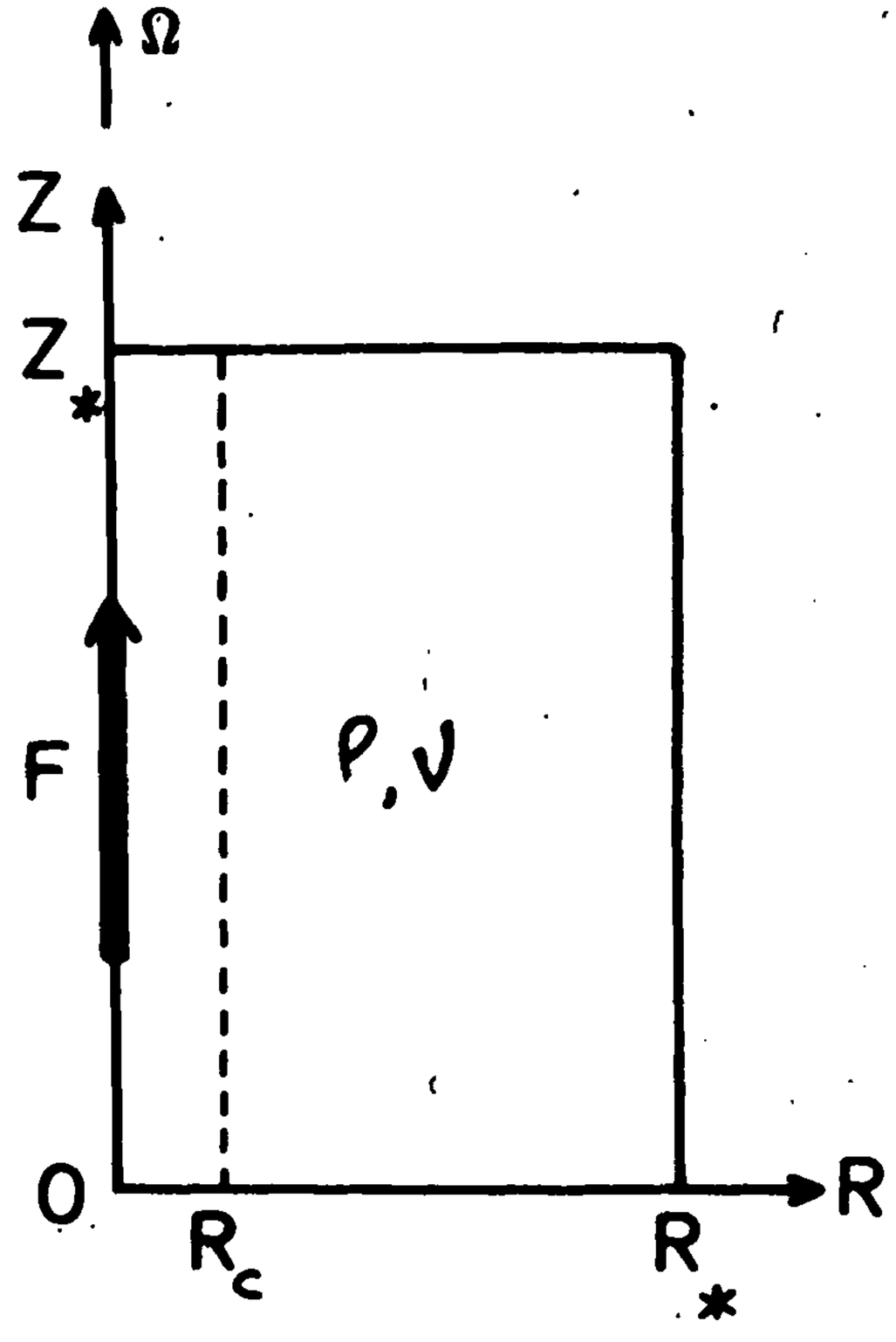

Figure 1(b)

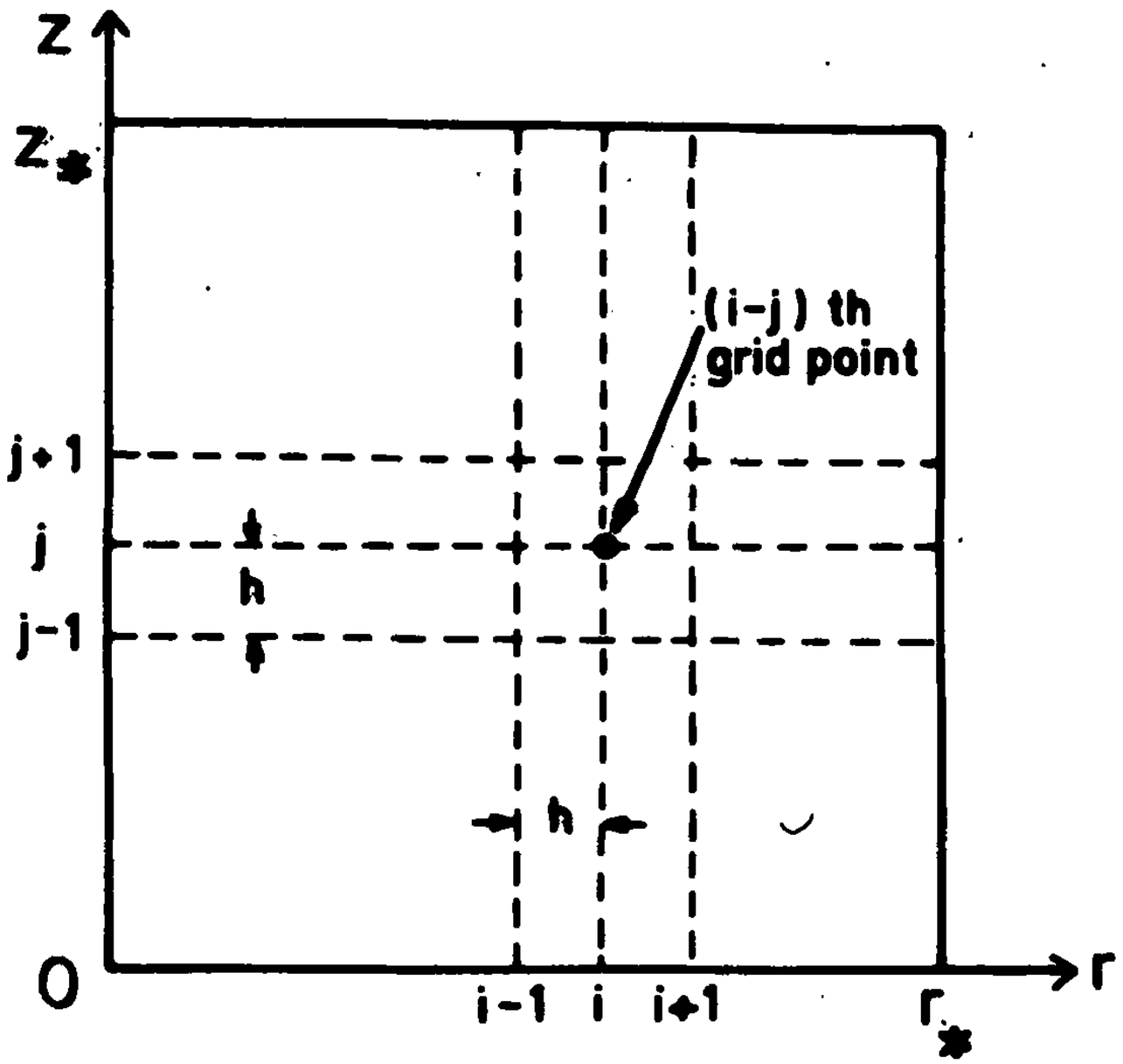

Figure 2

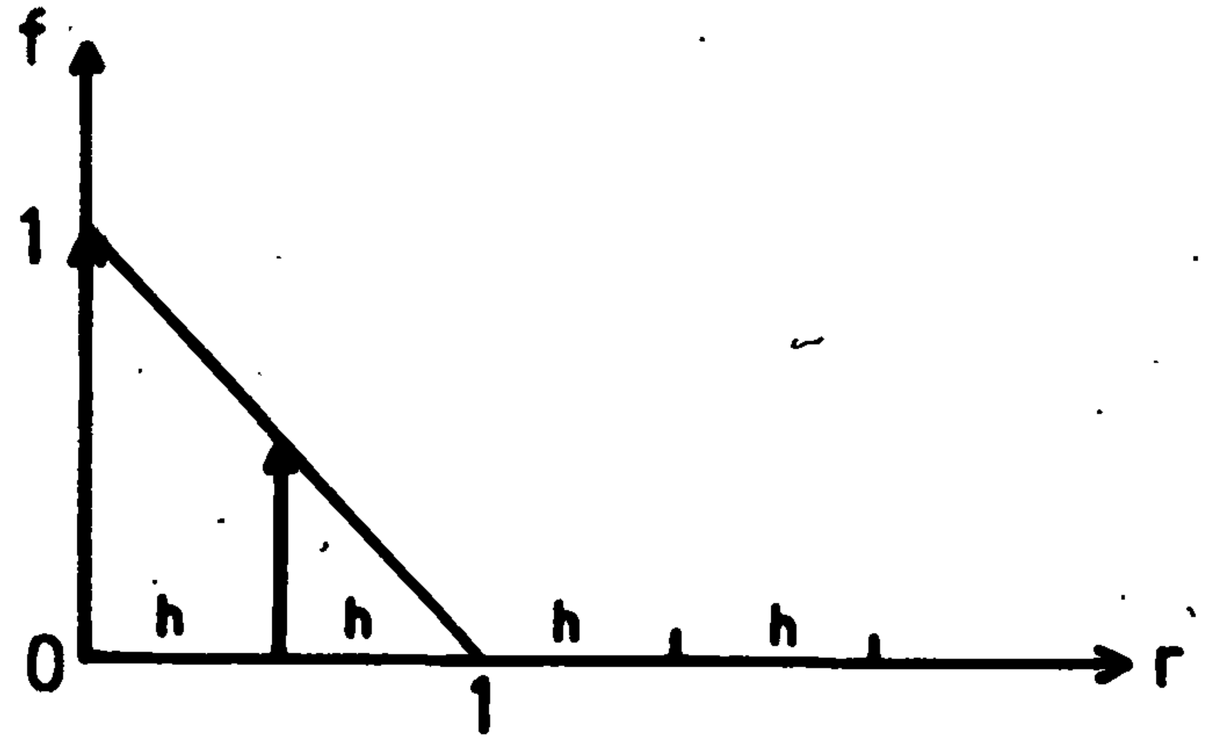

$$\frac{\partial f}{\partial r}: \quad 0 \quad -\frac{1}{2h} \quad -\frac{1}{4h} \quad 0 \quad 0 \quad \dots$$

Figure 3

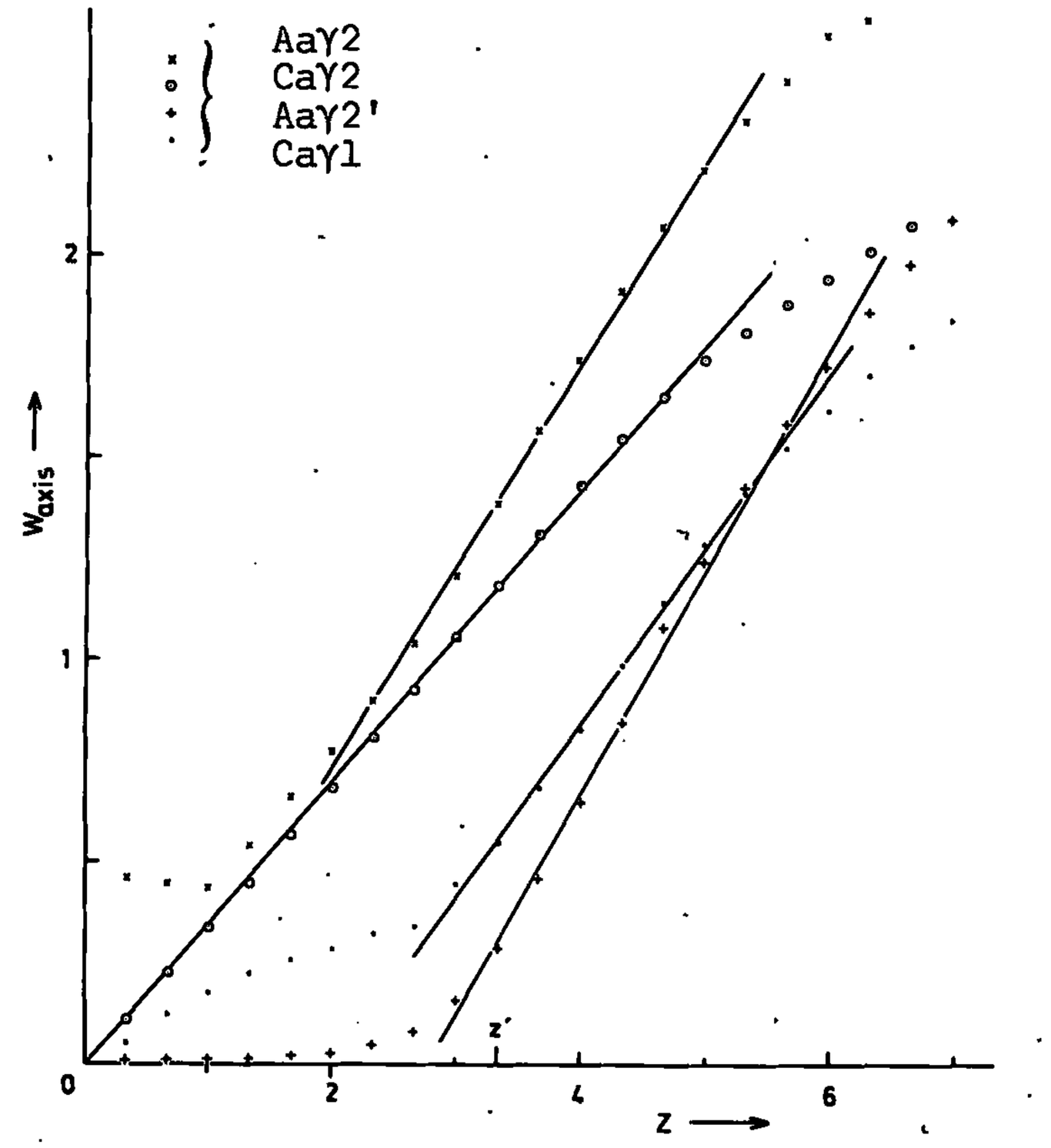

Figure 4

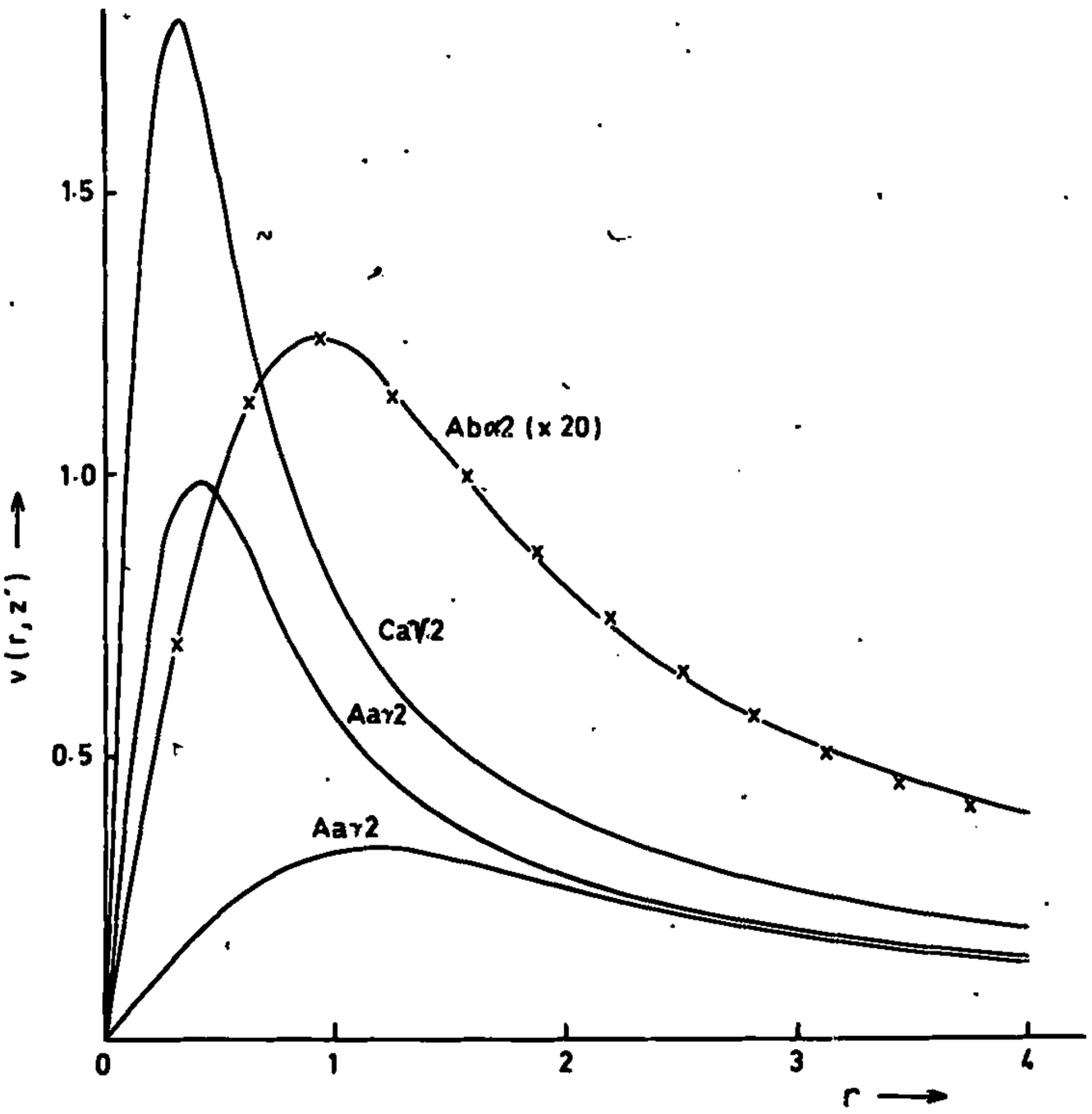

Figure 5

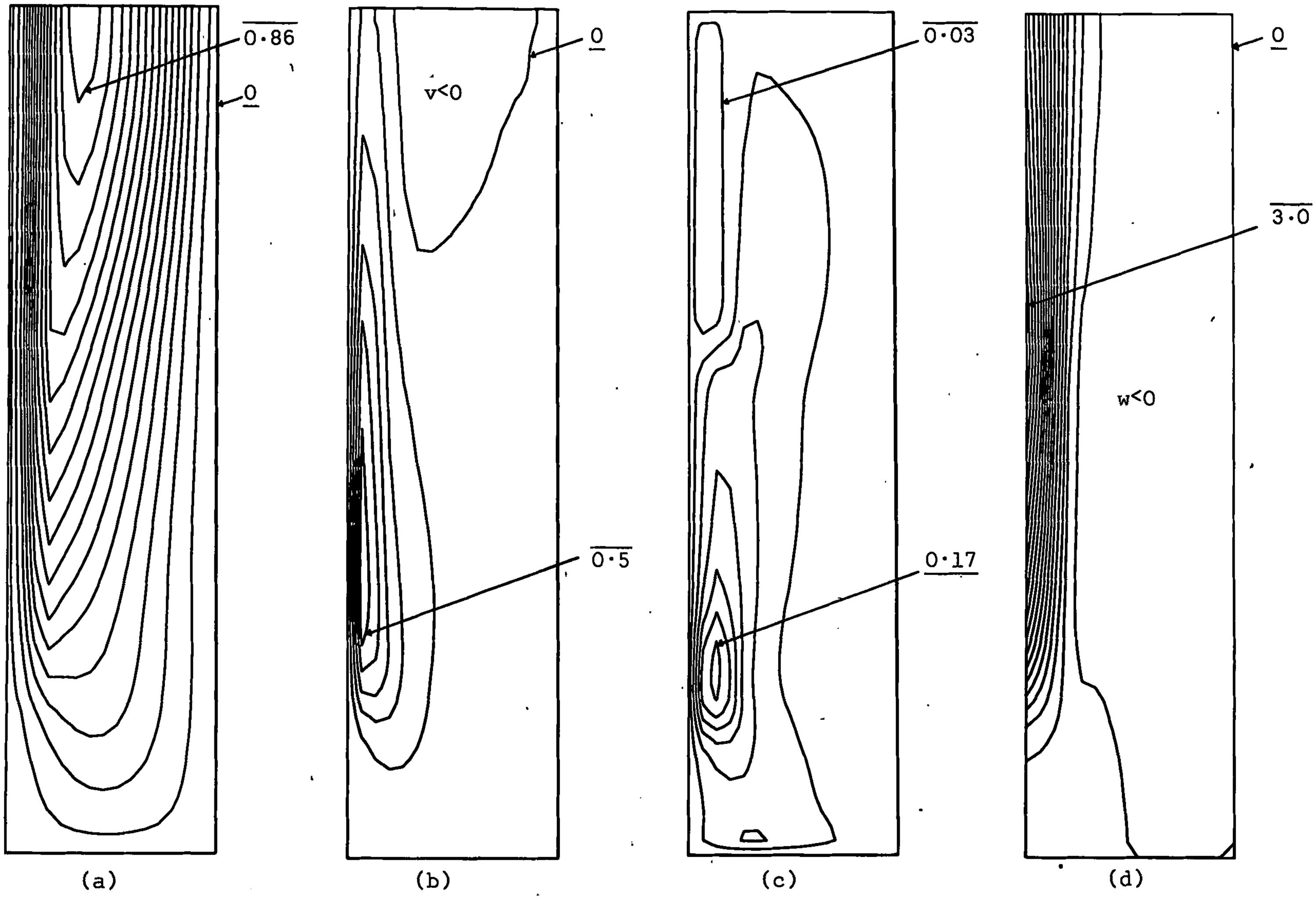

Figure 6

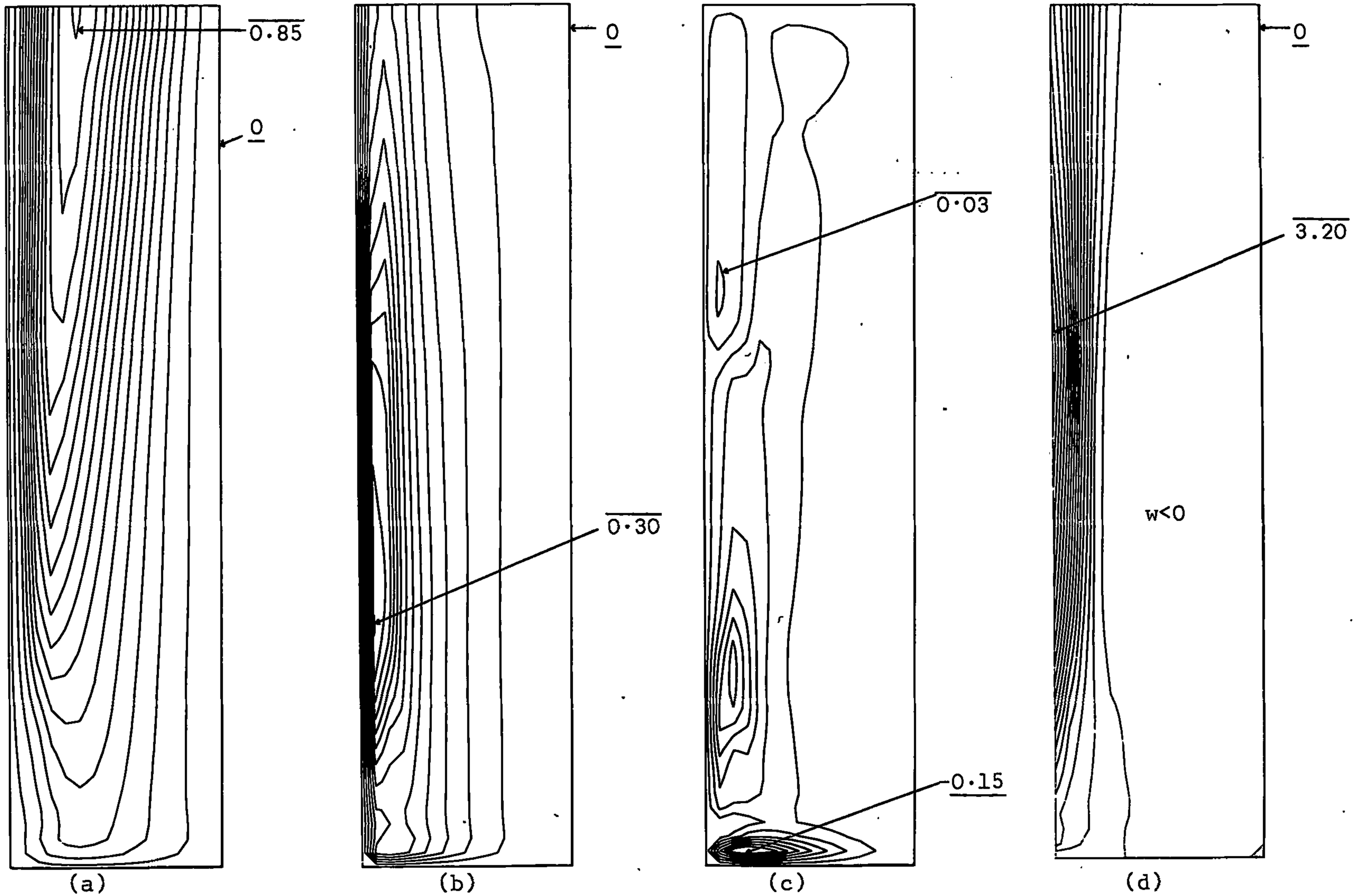

Figure 7

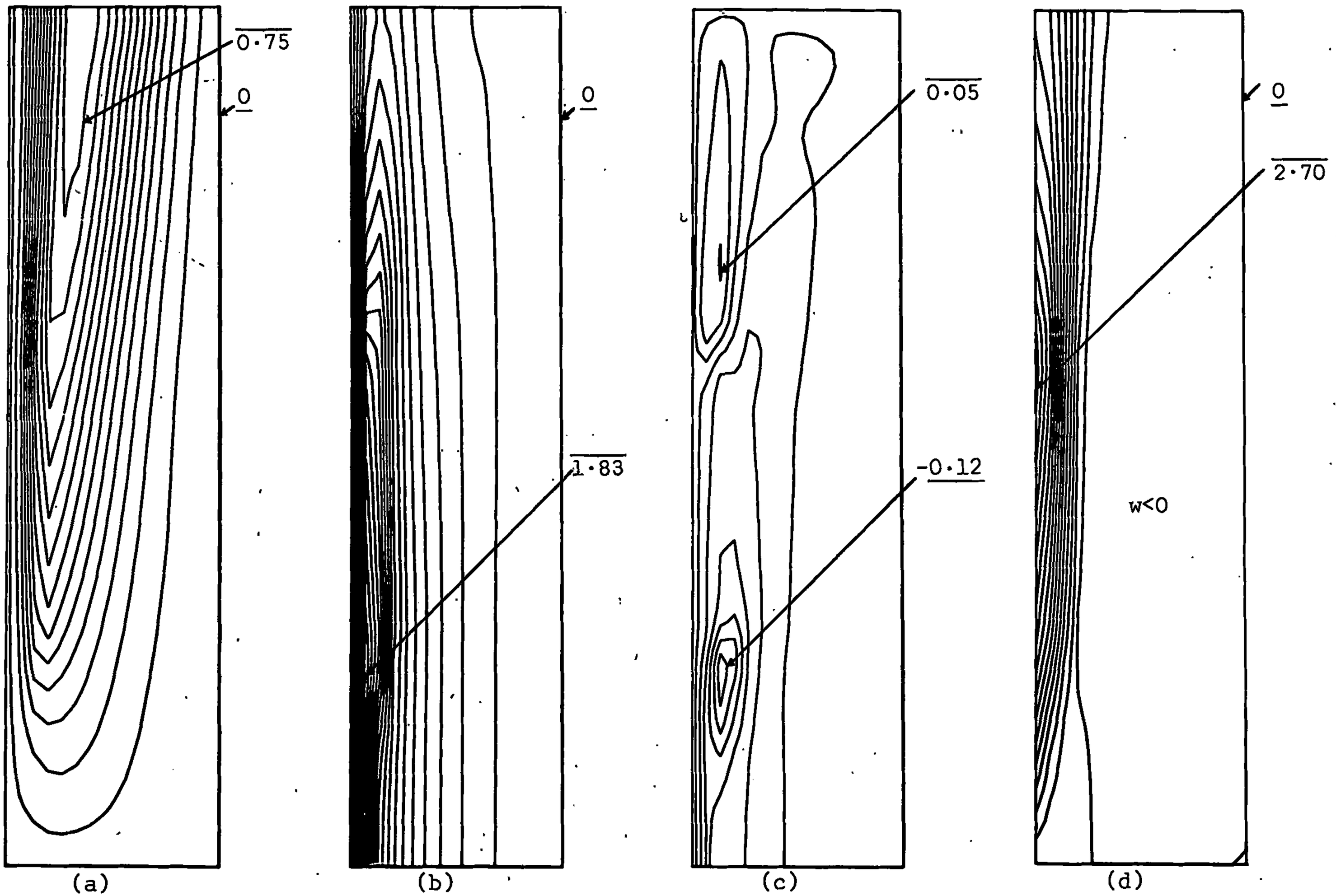

Figure 8

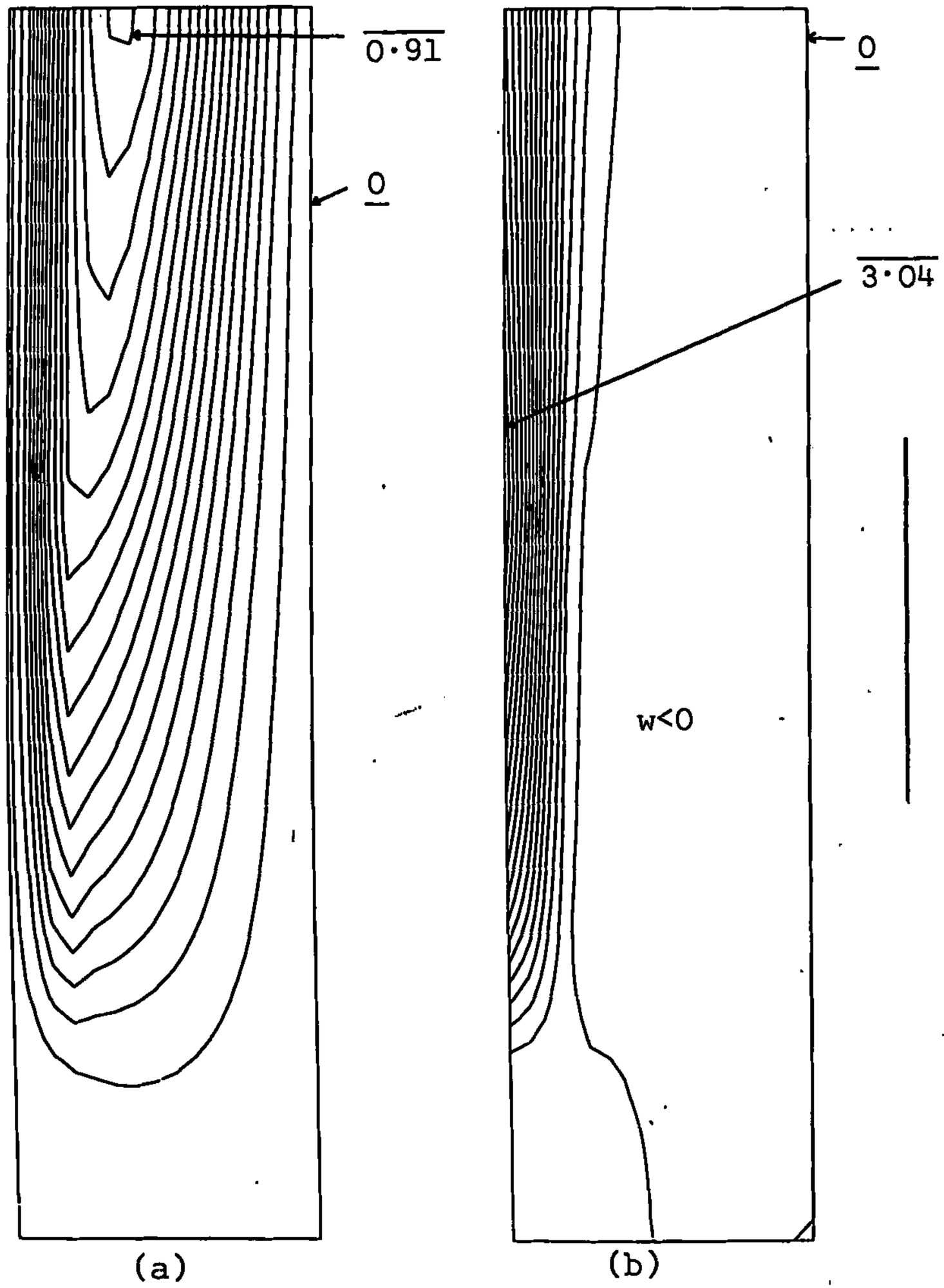

(a) (b)

Figure 9

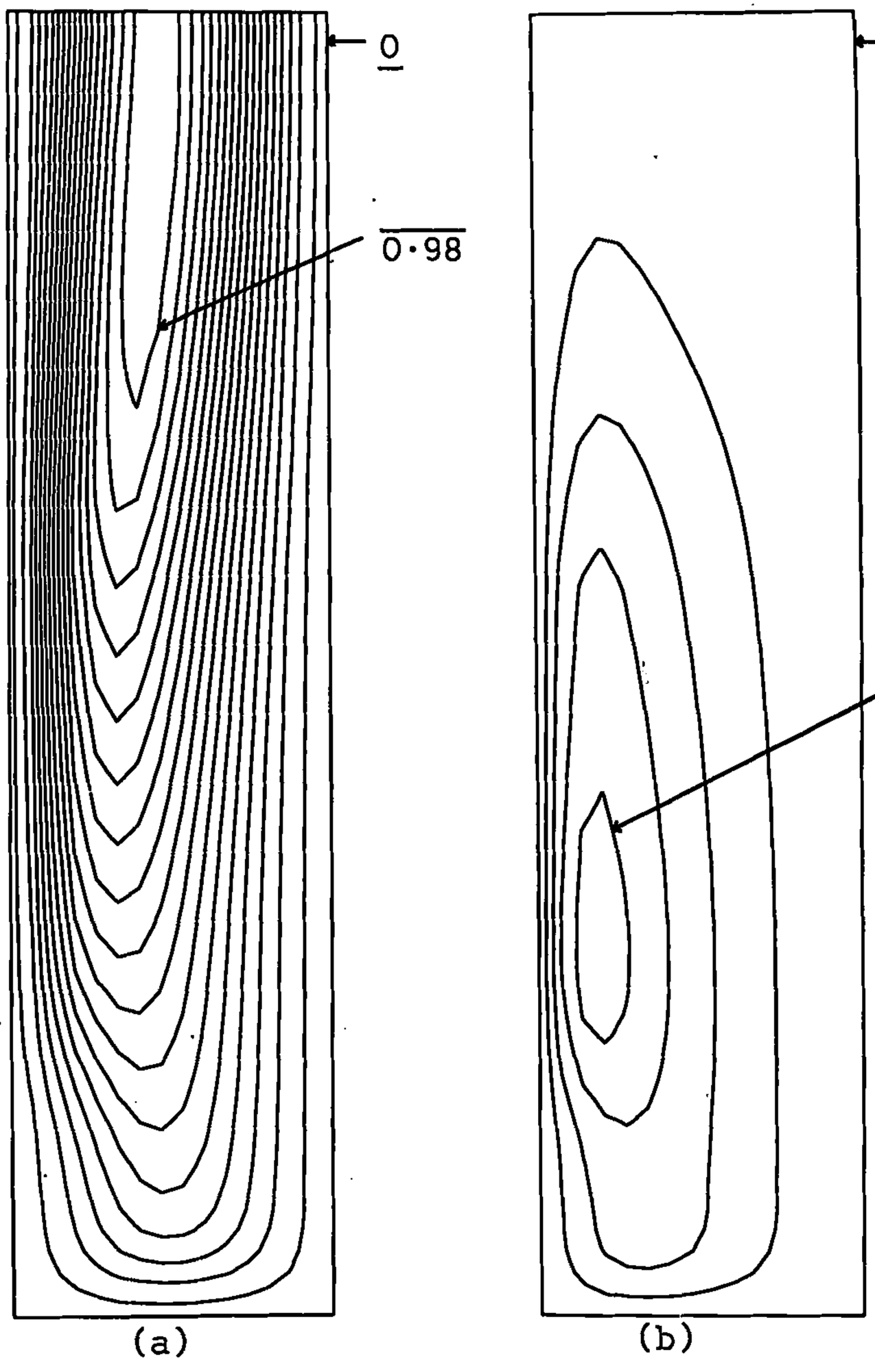

(a) (b)

Figure 10

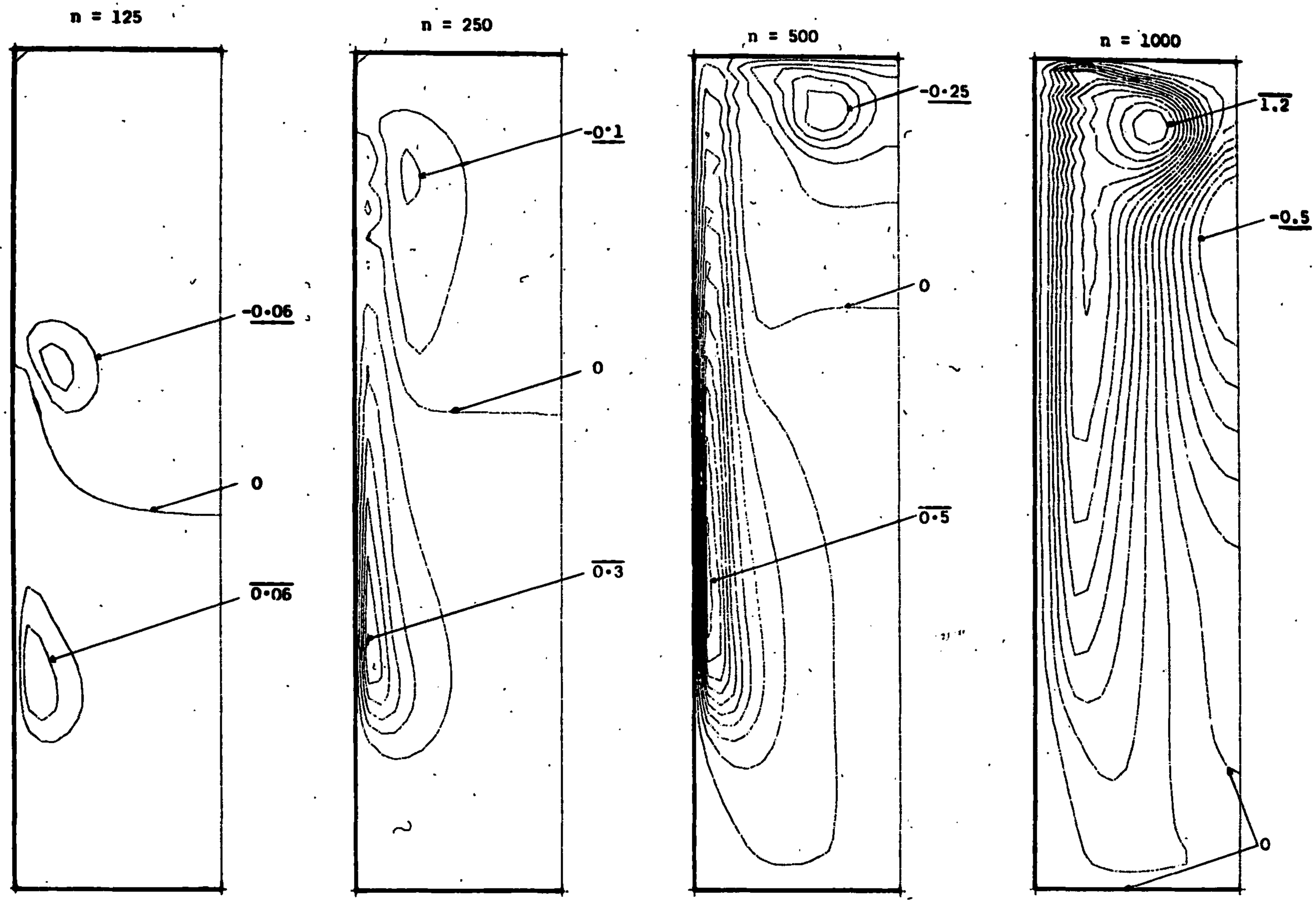

Figure 11(a)

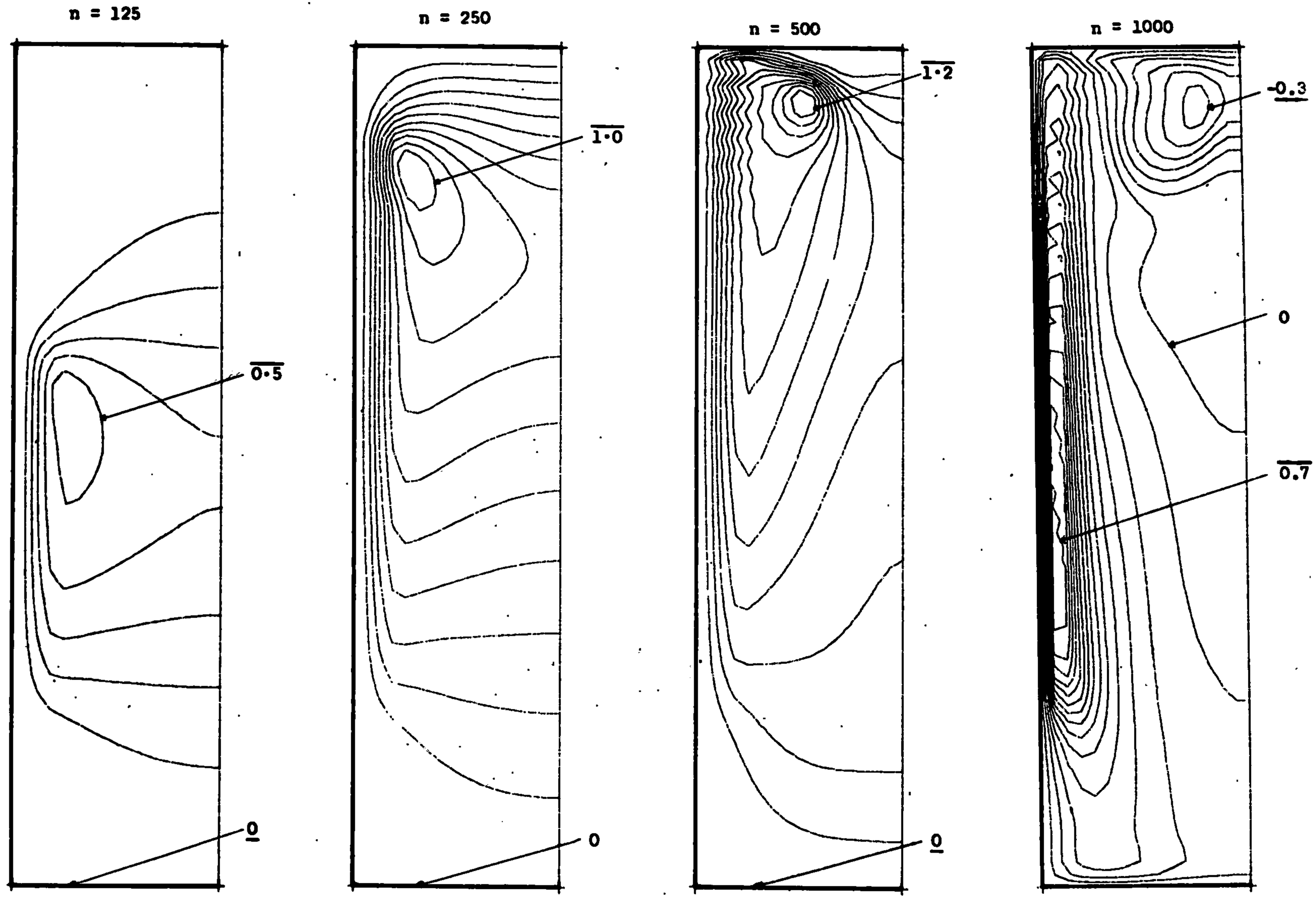

Figure 11(b)

Chapter 4

A numerical method for the steady two - dimensional Navier - Stokes equations.

ABSTRACT

A method is developed for the numerical solution of the steady, two-dimensional Navier-Stokes equations, by considering the flow in a square cavity. The stream function/vorticity approach is used, and the finite-difference equations are solved by an inner and outer iterative process. The form of both the stream function and vorticity difference equations permits the application of an alternating direction implicit method, and this is believed to be a novel approach to this type of problem. It is shown that only when the finite-difference Jacobian representing the convective terms, is formulated in a conservative manner, can rapid solutions be obtained for the case of high Reynolds number flows.

The motivation for this study arises from the work of the previous chapter, in which steady, three-dimensional axisymmetric flows are obtained by numerical integration of the time-dependent Navier-Stokes equations. However, this process is most time-consuming when compared with the method developed in the present chapter, and it is anticipated that considerable advantage will result from the use of this method in future examination of these more complicated flows.

1. Introduction

Over the last few years there has been considerable interest in the problem of the numerical solution of the steady-state Navier-Stokes equations, particularly for the case of flow in a two-dimensional square cavity. While it could not be claimed that this particular problem is in itself of great practical interest, nevertheless, it is perhaps the simplest non-trivial example of fluid flow in a confined region. It is felt therefore, that if one is able to develop a satisfactory numerical approach to the solution of this relatively simple problem, there is then some justification in attempting to extend the method to more complicated examples.

In the present context, there was some external motivation for considering the problem, other than merely an interest in developing a new numerical method for two-dimensional, steady, viscous, incompressible flows. In the previous chapter, the problem being considered ultimately concerned the steady-state numerical solution of the Navier-Stokes equations for three-dimensional axisymmetric flow in a rotating frame, and this was accomplished by solving the time-dependent equations as an initial-value problem and countinuing until a steady-state was attained. However, it can be seen there, that this approach is most time-consuming, since effectively, the computational effort per time step varies as the cube of the grid resolution, and with such flows where the Reynolds number is large, it is most important to have good resolution.

Now the steady version of the equations in the previous chapter

can in fact be expressed in a form suitable for solution by the method which we shall develop here, and therefore it was felt that the present problem of steady flow in a square cavity was indeed worthy of attention, and furthermore, could be considered within the overall aims of this thesis.

The numerical methods which will be described here, are essentially similar in many respects to the work of several other authors. The well known stream function/vorticity representation is used, in which the Navier - Stokes equations for steady, incompressible two-dimensional flow, together with the continuity equation, can be reduced to a pair of coupled partial differential equations. The method of inner and outer iterations is used to solve these two equations; the inner iteration for each equation is a single Peaceman - Rachford alternating direction implicit cycle, while the outer iterative process is of the relaxation type.

The numerical solution of steady two-dimensional flows by means of a stream function/vorticity approach has been attempted as far back as 1933 by Thom, who treated the flow around a cylinder at low Reynolds numbers. His calculations were performed completely by hand, and it is only since the advent of the high speed electronic computer, that interest in such problems has increased considerably. Kawaguti (1961) obtained certain solutions for the cavity problem, but these were of low resolution and for rather low Reynolds numbers only. The fast computational speeds and large memory capacities of modern computers can now overcome the first defect,

but as first noted by Greenspan (1968), for high Reynolds numbers, the convective terms must be formulated in terms of one-sided differences, for the problem to be a well posed one at arbitrary Reynolds number and grid spacing.

Extensive analytical and numerical work for the problem has been presented by Burggraf (1966), but he was unable to obtain solutions for Reynolds numbers larger than 400 for the reason just mentioned above. The problem has also been considered by Spalding and his co-workers (see e.g., Gosman *et al.* (1969), Runchal and Wolfshtein (1969) and Runchal (1972)), who have obtained large Reynolds number flows by use of the one-sided formulation. The steady-state cavity flows have also been obtained as large-time solutions to the time-dependent Navier - Stokes equations, as carried out for instance, by Fortin, Peyret and Teman (1971), Torrance *et al.* (1973), Leal (1973) and by Marshall and Van Spiegel (1973); the equations solved by Fortin *et al.* have pressure and the velocity components as their dependent variables instead of the more common stream function and vorticity. Numerous references to other works considering the present problem may be found in the papers cited above. Laboratory experiments to simulate such motions have been reported by Pan and Acrivos (1967).

As stated above, the principal motivation in considering the present problem, is ultimately to employ it as a basis for extending the method to more complicated and physically significant flows. One class of such problems is that of steady two-dimensional flow past a circular cylinder, where, as shown by Takami and Keller (1969), the use of a conformal transformation reduces it to

a rectangular cavity flow, with the far-field solution being used to provide some of the boundary conditions.† Gosman *et al.* (1969) present a number of examples of other idealised two-dimensional flows. As stated above, an immediate extension can generally be made to treat steady three-dimensional axisymmetric flows such as those considered by Rasmussen (1969), Textor, Lick and Farris (1969) and by Gosman and Spalding (1971). The vector potential method as outlined by Aziz and Hellums (1967), suggest the possibility of obtaining solutions to fully three-dimensional cavity flows by methods very similar to those which we shall describe, such as the scheme formulated by Douglas (1962).

Apart from the interest in using the square cavity problem as a prototype to develop a general numerical method for steady flows, one could also use this example to investigate the viscous corner eddies of Moffatt (1964) and the flow that is obtained at very high Reynolds numbers, the theory for which has been presented by Batchelor (1956). Burggraf (1966) for example, gives quite an extensive discussion of both these aspects, within the context of square cavity flows.

---

†The interest in such flows is considerable, as can be seen from the number of papers treating them in Supplement II, Physics of Fluids 12 (1969), and in the Proceedings of the Second International Conference on Numerical Methods in Fluid Dynamics, University of California, Berkeley, 1970 (Springer - Verlag 1971, 462 pp.).

2. The equations of motion

We consider motion in an idealised two-dimensional square cavity in a Cartesian coordinate system (X,Y) with corresponding velocity components (U,V) as depicted in Figure 1. The length of a side of the cavity is L, and the lid is moved in the negative X-direction with speed U, thus setting up a principally anti-clockwise circulation within the cavity. The Navier - Stokes equations and the equation of continuity for steady, incompressible flow in this situation, have the form

$$U\frac{\partial U}{\partial X} + V\frac{\partial U}{\partial Y} = -\frac{1}{\rho}\frac{\partial P}{\partial X} + \nu\left(\frac{\partial^2 U}{\partial X^2} + \frac{\partial^2 U}{\partial Y^2}\right), \qquad (1)$$

$$U\frac{\partial V}{\partial X} + V\frac{\partial V}{\partial Y} = -\frac{1}{\rho}\frac{\partial P}{\partial Y} + \nu\left(\frac{\partial^2 V}{\partial X^2} + \frac{\partial^2 V}{\partial Y^2}\right), \qquad (2)$$

$$\frac{\partial U}{\partial X} + \frac{\partial V}{\partial Y} = 0, \qquad (3)$$

where ρ is the density of the fluid, P is the pressure and ν the kinematic viscosity.

The boundary conditions for the flow are clearly

$X = 0,L$; $Y = 0$: $U = V = 0$.

$Y = L$: $U = -U, V=0$.

The equations are now non-dimensionalised in the natural manner, namely using L and U as the scales of length and velocity respectively. Thus we define

$$x = \frac{X}{L}\ ,\ y = \frac{Y}{L}\ ,\ u = \frac{U}{U}\ ,\ v = \frac{V}{U}\ ,\ p = \frac{P}{\rho U^2}\ .$$

In terms of these dimensionless variables, the continuity equation (3) is unchanged in form, and in the normal manner, we define the Stokes stream function ψ so that (3) is satisfied:

$$u = \frac{\partial \psi}{\partial y} , \quad v = - \frac{\partial \psi}{\partial x} , \qquad (4a)$$

and also the vorticity component ζ, by

$$\zeta = \frac{\partial v}{\partial x} - \frac{\partial u}{\partial y} , \qquad (4b)$$

Clearly, we have

$$\nabla^2 \psi = - \zeta, \qquad (5)$$

where ∇^2 is the two-dimensional Cartesian Laplacian operator. If we now cross - differentiate the two momentum equations (1) and (2) to eliminate the pressure, we obtain in terms of the dimensionless variables,

$$\nabla^2 \zeta + R.J(\zeta) = 0, \qquad (6)$$

where $R = UL/\nu$ is the appropriate Reynolds number for the flow. J is the Jacobian operator, used as a shorthand notation for representing the convective terms. For a given flow variable A,

$$J(A) = \frac{\partial \psi}{\partial x} \frac{\partial A}{\partial y} - \frac{\partial \psi}{\partial y} \frac{\partial A}{\partial x} .$$

It can be seen that the boundary conditions can now be expressed as

$$\left.\begin{array}{lll} x = 0,1 & : & \psi = \dfrac{\partial \psi}{\partial x} = 0. \\ y = 0 & : & \psi = \dfrac{\partial \psi}{\partial y} = 0. \\ y = 1 & : & \psi = 0, \quad \dfrac{\partial \psi}{\partial y} = -1 \end{array}\right\} \qquad (7)$$

With some manipulation, the non-dimensional pressure p can be obtained as the solution to the following Poisson equation:

$$\nabla^2 p = 2\left[\frac{\partial^2 \psi}{\partial x^2} \frac{\partial^2 \psi}{\partial y^2} - \left(\frac{\partial^2 \psi}{\partial x \partial y} \right)^2 \right]$$

with appropriate Neumann boundary conditions.

3. The finite-difference equations

In this section, we shall discuss the setting up of the finite-difference mesh, and then obtain the difference equations corresponding to equations (5) and (6) for the stream function and vorticity. We shall also obtain difference expressions for the boundary conditions, and consider the necessity of a one-sided formulation, as mentioned above, for the convective terms.

On the square cavity, whose sides in dimensionless units are of unit length, we superimpose a square mesh with grid spacing $h = 1/N$, where N is a predetermined positive integer. If we let $A(x,y)$ be any continuous function defined on the cavity region, then we approximate this function by $A_{i,j}$, its corresponding discrete representation, defined at the mesh points (i,j), where $x=ih$ and $y=jh$ $(i,j = 0,1,2,\ldots, N)$ as represented diagramatically in Figure 2. In the usual manner, we define the following first order difference operators:

$$\delta_x A_{i,j} = \frac{1}{h} (A_{i+1,j} - A_{i,j}),$$

$$\delta_{\bar{x}} A_{i,j} = \frac{1}{h} (A_{i,j} - A_{i-1,j}),$$

$$\delta_{\hat{x}} A_{i,j} = \frac{1}{2h} (A_{i+1,j} - A_{i-1,j}),$$

all of which are finite - difference representations at the mesh point (i,j), of the derivative $\partial A/\partial x$, and have discretisation errors of the order of h,h and h^2 respectively. The above operators are usually referred to as the forward, backward and centred differences respectively. In a similar fashion, analogous expressions can be written down for $\partial A/\partial y$.

If we now transform equations (5) and (6) to second order centred difference form, we arrive at the following equations:

$$-\nabla^2 \psi_{i,j} = h^2 \zeta_{i,j} \quad , \tag{8}$$

$$-\frac{\varepsilon}{h^2} \nabla^2 \zeta_{i,j} - (\delta_{\hat{x}} \psi_{i,j})(\delta_{\hat{y}} \zeta_{i,j}) + (\delta_{\hat{y}} \psi_{i,j})(\delta_{\hat{x}} \zeta_{i,j}) = 0, \tag{9}$$

where $\varepsilon = 1/R$ and ∇^2 is the second order finite - difference analogue of the Laplacian, namely

$$\nabla^2 A_{i,j} = h^2 (\delta_{\bar{x}x} + \delta_{\bar{y}y}) A_{i,j}$$

$$= (A_{i+1,j} + A_{i-1,j} + A_{i,j+1} + A_{i,j-1} - 4A_{i,j}).$$

The above two equations (8) and (9) were deduced by Kawaguti (1961) and Burggraf (1966), amongst others, as being the obvious forms of the difference equations to use; yet these authors found that above a certain Reynolds number (for a given h), no solution could be obtained. Soon afterwards, it was realised by Greenspan (1968), that the actual nature of the finite - difference equations is altered for large *R* under this formulation. In order for there to be a unique solution to the set of difference equations, it can be shown (see e.g., Forsythe and Wasow 1960) that they must necessarily be of *positive* type. With respect to the present

equations, this condition is violated in a centred difference formulation, once the contribution from the convective terms (in terms of the finite - differences) exceeds that arising from the diffusive terms anywhere within the computational region.

In order to overcome this problem, we resort to the use of one-sided or 'upstream' differencing for the convective terms of equation (6). Physically, what is meant by upstream differencing at a mesh point (i,j), is that the derivatives of the vorticity are calculated in such a way as to ensure that vorticity is always convected towards the point (i,j). For instance, if $\partial\psi/\partial y$ $(=u) \geq 0$ at the point (i,j), then we use the points (i,j) and (i-1,j) which is clearly upstream of (i,j) (since $u \geq 0$), to evaluate $(\partial\zeta/\partial x)_{i,j}$ as $(\zeta_{i,j} - \zeta_{i-1,j})/h$ in the vorticity equation. Alternatively, if $u<0$, the upstream point is now (i+1,j), and similarly for the second convective term.

A paper by Dorr (1970) who treats the one-dimensional version of equations (5) and (6), clearly illustrates the nature of the problem. As an analogue of the vorticity equation, he considered the equation

$$\varepsilon \frac{d^2 v}{dx^2} + g(x) \frac{dv}{dx} = 0,$$

with appropriate boundary conditions. In accordance with the above, we can represent the term dv/dx by a one-sided difference expression, depending on the sign of g(x), and in so doing, we ensure that the matrix representation of the difference equations becomes diagonally dominant and positive (see Forsythe and Wasow

1960 for definitions). That is,

$$\left(g(x)\frac{dv}{dx}\right)_i = \begin{cases} g(x_i)\delta_x v_i \ , & g(x_i) \geq 0, \\ g(x_i)\delta_{\bar{x}} v_i \ , & g(x_i) < 0. \end{cases}$$

Dorr showed that if one used a centred difference representation instead, there would be a solution to the equations, only if the condition

$$\frac{2\varepsilon}{h} > \max \mid g(x_i) \mid$$

was satisfied, and clearly for high Reynolds numbers (small ε), the mesh spacing h would have to be prohibitively small in order to obtain a solution. Numerical experiments of Runchal (1972) illustrate dramatically the nature of this cutoff criterion.

Hence we must rewrite equation (9) so that it is of positive type. At each interior mesh point (i,j), let

$$\alpha = h\delta^{\wedge}_x \psi_{i,j} \quad \text{and} \quad \beta = h\delta^{\wedge}_y \psi_{i,j} \qquad (10)$$

The new form of equation (9) will now depend on the signs of α and β, and can be written as:

$$\begin{aligned}
(-\varepsilon \nabla^2 - \alpha \delta_y + \beta\delta_{\bar{x}})\ \zeta_{i,j} &= 0, \qquad (\alpha,\beta \geq 0), \\
(-\varepsilon \nabla^2 - \alpha \delta_y + \beta\delta_x)\ \zeta_{i,j} &= 0, \qquad (\alpha \geq 0, \beta < 0), \\
(-\varepsilon \nabla^2 - \alpha \delta_{\bar{y}} + \beta\delta_{\bar{x}})\ \zeta_{i,j} &= 0, \qquad (\alpha < 0, \beta \geq 0), \\
(-\varepsilon \nabla^2 - \alpha \delta_{\bar{y}} + \beta\delta_x)\ \zeta_{i,j} &= 0, \qquad (\alpha,\beta < 0).
\end{aligned}$$

This may be written in the following single form in which the positive, diagonally dominant nature of the equations is clearly illustrated:

$$\Phi\zeta_{i,j} - \varepsilon\Sigma_{i,j} - |\alpha|\zeta_{i,j+J} - |\beta|\zeta_{i+I,j} = 0, \qquad (11)$$

where $\Phi = 4\varepsilon + |\alpha| + |\beta|,$

$$\Sigma_{i,j} = \zeta_{i+1,j} + \zeta_{i-1,j} + \zeta_{i,j+1} + \zeta_{i,j-1},$$

$$J = \text{sgn}(\alpha), \quad I = -\text{sgn}(\beta),$$

and the function sgn is defined by

$$\text{sgn}(x) = \begin{cases} +1 & , \quad x \geq 0, \\ -1 & , \quad x < 0. \end{cases}$$

Equations (8) and (11) are now our difference analogues of (5) and (6), and we shall discuss the method of solution in the following section. Although we now have difference equations which should theoretically have a solution for all Reynolds numbers, there are nevertheless some disadvantages arising from the use of one-sided differences. Firstly the discretisation error in the convective terms is increased from h^2 to h, and also there is a computational diffusive effect which is introduced, but for the moment we will defer any discussion of these effects.

To date, we have yet to discuss the incorporation of the boundary conditions (7) into the finite-difference scheme. In the original formulation of the equations of motion, the boundary conditions (7) were pre-specified values of the stream function ψ and its normal derivative on the boundaries, but we are now required to solve two second order equations for ψ and the vorticity ζ.

The boundary condition for ψ in the difference scheme, is obviously

$$\psi_{i,j} = 0 \quad \text{at all boundary mesh points } (i,j) \qquad (12)$$

The boundary conditions we shall use for the $\zeta_{i,j}$ field were first formulated by Thom (1933) and have since been used widely in many similar problems. We shall consider the boundary y=1, where the boundary conditions (7) are

$$\psi = 0 \quad \text{and} \quad \frac{\partial \psi}{\partial y} = -1.$$

The situation as it occurs in the finite - difference formulation is depicted in Figure 3, where from above, we have that

$$\psi_B = 0 \quad \text{and} \quad \frac{\psi_A - \psi_C}{2h} = -1. \qquad (13)$$

Here the fictitious point A has been introduced so that we may use a centred difference approximation to the derivatives at the boundary. We now proceed to eliminate A so that it does not appear in the difference scheme itself. If we apply equation (8) at the boundary point B, we obtain after a little manipulation,

$$\zeta_B = \frac{4\psi_B - (\psi_A + \psi_C + \psi_D + \psi_E)}{h^2}$$

Since the points D and E are also on the boundary, $\psi_D = \psi_E = 0$, and by use of (12), we obtain from the above-equation,

$$\zeta_B = \frac{2}{h} - \frac{2}{h^2} \psi_C$$

In a similar fashion, we apply this procedure to the other boundaries, and with the inclusion of condition (12), we thus have

as the boundary conditions in finite-difference form,

$$\left.\begin{aligned} \psi_{i,o} &= \psi_{i,N} = 0 \\ \zeta_{i,o} &= -\frac{2}{h^2}\psi_{i,1} \\ \zeta_{i,N} &= \frac{2}{h}\left(1 - \frac{1}{h}\psi_{i,N-1}\right) \end{aligned}\right\} \quad (i=1,2\ldots,N-1)$$

$$\left.\begin{aligned} \psi_{o,j} &= \psi_{N,j} = 0 \\ \zeta_{o,j} &= -\frac{2}{h^2}\psi_{1,j} \\ \zeta_{N,j} &= -\frac{2}{h^2}\psi_{N-1,j} \end{aligned}\right\} \quad (j=1,2,\ldots,N-1) \qquad (14)$$

where we note that the four corner points do not enter physically into the finite-difference calculations.

4. The method of solution

The procedure which we shall adopt for the solution of equations (8) and (11) under the boundary conditions (14), is known as the method of inner and outer iterations. Different variations on this method have been used to obtain solutions to the cavity flow problem by, for example, Burggraf (1966), Greenspan (1968, 1969) and Gosman *et al.* (1969).

Firstly, we define a sequence of 'outer iterates' $\bar{\psi}_{i,j}^{(n)}$ and $\bar{\zeta}_{i,j}^{(n)}$, and a similar sequence of 'inner iterates' $\psi_{i,j}^{(n)}$ and $\zeta_{i,j}^{(n)}$, where the superscript n denotes the number of outer iterations which have been performed. For convenience, we write equation (11) in the shorthand form

$$\left[L(\psi_{i,j})\right]\zeta_{i,j} + M\psi_{i,j} = 0 ,$$

where L and M are finite-difference operators. The first term indicates the contribution of the $\psi_{i,j}$ field to the vorticity equation via the convective terms, while the second term represents the contribution of the boundary vorticity, which, as can be seen from (14), is defined in terms of the interior stream function values.

We now define the inner and outer iteration scheme to be used, in the following manner:

$$\left[L(\bar{\psi}^{(n)}_{i,j})\right]\zeta^{(n+1)}_{i,j} + M\overset{*}{\psi}{}^{(n)}_{i,j} = 0, \qquad (15a)$$

$$\bar{\zeta}^{(n+1)}_{i,j} = \omega_2\,\zeta^{(n+1)}_{i,j} + (1-\omega_2)\bar{\zeta}^{(n)}_{i,j} , \qquad (15b)$$

$$-\nabla^2\psi^{(n+1)}_{i,j} = h^2\,\bar{\zeta}^{(n+1)}_{i,j} , \qquad (15c)$$

$$\bar{\psi}^{(n+1)}_{i,j} = \omega_1\psi^{(n+1)}_{i,j} + (1-\omega_1)\bar{\psi}^{(n)}_{i,j} , \qquad (15d)$$

where

$$\overset{*}{\psi}{}^{(n)}_{i,j} = \omega_2\,\bar{\psi}^{(n)}_{i,j} + (1-\omega_2)\bar{\psi}^{(n-1)}_{i,j} \qquad (15e)$$

The numerical solution of (15a) and (15c) is known as the inner iterative process, and we shall defer discussion on the method which we are proposing for this step until the following section. The outer iterative process is described by (15b), (15d) and (15e), and is that used by Greenspan (1968), being basically a global relaxation process (or 'filtering' as it is called by him).

The steps involved in one overall iteration are as follows: We begin with two initial fields $\bar{\psi}^{(o)}_{i,j}$ $(= \overset{*}{\psi}{}^{(o)}_{i,j})$ and $\bar{\zeta}^{(o)}_{i,j}$, these specified

initial fields being either arbitrary values (usually zero) or else, a linear interpolation of the solution to the equations at a different value of R or h. Using the values of $\bar{\psi}^{(o)}_{i,j}$ and $\bar{\zeta}^{(o)}_{i,j}$, we solve equation (15a) for the next inner iterate $\zeta^{(1)}_{i,j}$ which is then combined with the $\bar{\zeta}^{(o)}_{i,j}$ field through equation (15b) to obtain $\bar{\zeta}^{(1)}_{i,j}$. In a similar fashion, we then solve (15c) and (15d) for $\bar{\psi}^{(1)}_{i,j}$ using the values of $\bar{\psi}^{(o)}_{i,j}$ and $\bar{\zeta}^{(1)}_{i,j}$. The boundary vorticity values are obtained from the previous outer iterate of the stream function by means of (14), but are then filtered *again* via equation (15e), as though they were in fact actual vorticity values. This two-step filtering used by Greenspan, has been found to be essential for convergence of the iterations. The above steps complete the first iteration and the whole process is repeated until the outer iterates are judged to have converged. The convergence criterion which we have found to be suitable, is that the following two conditions are satisfied:

$$\frac{|\bar{\psi}^{(n+1)}_{i,j} - \bar{\psi}^{(n)}_{i,j}|}{\max |\bar{\psi}^{(n+1)}_{i,j}|} < \varepsilon_1 , \qquad (16a)$$

$$\frac{|\bar{\zeta}^{(n+1)}_{i,j} - \bar{\zeta}^{(n)}_{i,j}|}{\max |\bar{\zeta}^{(n+1)}_{i,j}|} < \varepsilon_2 , \qquad (16b)$$

$$(i,j=1,2,\ldots,N-1)$$

where ε_1 and ε_2 are prescribed small (in some meaningful sense) positive numbers. Checks are also made to ensure that the individual difference equations (8) and (11) are satisfied by the final solution.

In work such as this, there is unfortunately almost no theoretical guidance to be found in the literature, and one has to rely upon, in general, so-called 'numerical experiments' in order to find optimum values of the filtering parameters ω_1 and ω_2 for particular values of R and h. The problems which are encountered in obtaining convergence would appear to be at least partly caused by the changing values of the boundary vorticity (which depend on the interior stream function field) as we proceed from one iteration to the next. This is not unlike the problem encountered in the numerical solution of parabolic systems with time-dependent boundary conditions, if we consider the advance from one iteration to the next as analogous to a time step. In such cases, just as in the present, it has been found necessary to weight the values of the boundary vorticity with the values at the previous time step in order to prevent the growth of instabilities (Pearson 1965). Without the filtering of (15b), (15d) and (15e), the iterates rapidly diverge except at very small Reynolds numbers.

The problem of solving numerically the biharmonic equation (to which our equations (5) and (6) together reduce for zero Reynolds number) as a pair of coupled elliptic equations, has been considered theoretically by Smith (1968, 1970) and by Ehrlich (1971), both of whom use the concept of inner and outer iterations, with the outer process being similar, but not identical to that used in the present work. However, the rates of convergence which they are able to predict for the outer iterations, are not appreciably smaller than unity except for the case of large h, which is of no practical interest. In spite of the fact that some small theoretical progress

has been made by these authors in the simple case of R=0, it is clear that a satisfactory treatment for the nonlinear Navier - Stokes equations poses many more difficulties, and that numerical experiments are the sole effective method presently available.

5. The inner iterations

Other authors who have treated the steady cavity flow problem, and who have used methods similar to those so far described here (Burggraf, Greenspan, Gosman *et al.*) have all solved equations (8) and (11) in the same manner for the inner iterations; that is, Successive Overrelaxation for (8) and Gauss-Seidel for (11).* However, none appear to have considered the generally more powerful alternating direction implicit (ADI) methods, and therefore it seemed worthwhile to investigate whether or not an ADI method could be employed profitably to solve these two difference equations.

We shall present a brief outline below of the principles of the method; a more detailed description may be found for instance, in the comprehensive review article by Birkhoff, Varga and Young (1962).

If we consider the difference equation (8), for example, it may be written in the block matrix form

$$A\underline{z} = \underline{k} \qquad (17)$$

---

*A very recent paper by Bozeman and Dalton (1973) is a notable exception.

where A is the $(N-1)^2 \times (N-1)^2$ block matrix representing the difference operator $-\nabla^2$:

$$A = \begin{bmatrix} L & I & & & O \\ I & L & I & & \\ & \ddots & \ddots & \ddots & \\ & & I & L & I \\ O & & & I & L \end{bmatrix}$$

Here L is an $(N-1) \times (N-1)$ matrix, and I is the unit matrix of the same order, with

$$L = \begin{bmatrix} 4 & -1 & & & O \\ -1 & 4 & -1 & & \\ & \ddots & \ddots & \ddots & \\ & & -1 & 4 & -1 \\ O & & & -1 & 4 \end{bmatrix}$$

The column matrices $\underline{z}$ and $\underline{k}$ represent the unknown field $\psi_{i,j}$ and the given field $h^2 \zeta_{i,j}$ respectively. The basis of all ADI methods for solving a sparse matrix system such as the above, is that one can decompose A into

$$A\underline{z} = (H+V)\underline{z} = \underline{k} \, , \qquad (17')$$

where the matrix H is the (horizontal) difference operator, given by

$$\begin{aligned} Hz_{i,j} &= -h^2 \zeta_{x\bar{x}} z_{i,j} \\ &= -z_{i+1,j} + 2z_{i,j} - z_{i-1,j} \end{aligned}$$

which is the finite-difference analogue of the expression $-h^2(\partial^2 z/\partial x^2)_{i,j}$. Similarly for the (vertical) difference operator, we have

$$Vz_{i,j} = -z_{i,j+1} + 2z_{i,j} - z_{i,j-1}$$

In what follows, we shall employ the following convention: the operators in the ψ - equation (8), will be denoted by a subscript 1, and those for the ζ - equation (11) by a subscript 2. Thus, we have

$$\left.\begin{aligned} H_1\psi_{i,j} &= -\psi_{i+1,j} + 2\psi_{i,j} - \psi_{i-1,j} \\ V_1\psi_{i,j} &= -\psi_{i,j+1} + 2\psi_{i,j} - \psi_{i,j-1} \end{aligned}\right\} \qquad (18)$$

while for the vorticity equation, it can be seen from (11) that the horizontal and vertical operators have the form

$$\left.\begin{aligned} H_2\zeta_{i,j} &= \varepsilon(-\zeta_{i+1,j} + 2\zeta_{i,j} - \zeta_{i-1,j}) - |\beta|(\zeta_{i+I,j} - \zeta_{i,j}) \\ V_2\zeta_{i,j} &= \varepsilon(-\zeta_{i,j+1} + 2\zeta_{i,j} - \zeta_{i,j-1}) - |\alpha|(\zeta_{i,j+J} - \zeta_{i,j}) \end{aligned}\right\} \qquad (19)$$

where as previously defined, $J = \mathrm{sgn}(\alpha)$ and $I = -\mathrm{sgn}(\beta)$.

The matrix operators H_1, V_1 and H_2, V_2 which we have defined above, can be seen to possess the following properties:

(i) The matrix $A=H + V$ is non-singular.

(ii) For any $\rho>0$, the matrices $H + \rho I$ and $V + \rho I$ are non-singular

(iii) The matrices H and V are tridiagonal, or are permutationally similar to tridiagonal matrices. By this, we mean that if the mesh points are numbered consecutively by rows, H_1 and H_2 are tridiagonal, but if numbered by columns, V_1 and V_2 are.

(iv) The matrices H and V are diagonally dominant and positive definite (see Birkhoff, Varga and Young 1962).

Property (i) is clearly essential for the solution of the original equation (17), while it will soon be apparent that (ii) is necessary for a solution to be obtained by the ADI method used. Property (iii) is in fact not essential for a solution, but the efficiency of ADI methods, as will be seen below, depends on finding rapid solutions to linear equations in which the matrices $H + \rho I$ and $V + \rho I$ are required to be inverted. Property (iv) is also essential to the ADI method; equation (8) for the stream function has this property inherently and it arises in equation (11) for the vorticity, through the necessary use of a one-sided formulation of the convective terms. The particular ADI we shall use to solve (17') is the well known Peaceman - Rachford (P-R) method (see Birkhoff, Varga and Young for variations on this procedure). The P-R method is defined by the following two-step procedure:

$$(H + \rho_{n+1} I)\underline{z}_{n+\frac{1}{2}} = \underline{k} - (V - \rho_{n+1} I)\underline{z}_n \qquad (20)$$

$$(V + \rho_{n+1} I)\underline{z}_{n+1} = \underline{k} - (H - \rho_{n+1} I)\underline{z}_{n+\frac{1}{2}} \qquad (21)$$

Here the ρ_{n+1} $(n \geq 0)$ constitute a finite sequence of positive parameters, designed to accelerate the convergence of the iterations. The procedure is started with an initial iterate $\underline{z}_0$, and it can be seen that both of the above equations are equivalent to (17') in the limit of convergence, where $\underline{z}_n = \underline{z}_{n+\frac{1}{2}} = \underline{z}_{n+1}$. The method consists of two essentially identical steps: in the first, we solve (20) implicitly for $\underline{z}_{n+\frac{1}{2}}$ along the rows, using the previous

iterate $\underline{z}_n$ and the inverse of the matrix $(H + \rho_{n+1} I)$; in the second, these operations are performed along the columns to obtain the subsequent iterate $\underline{z}_{n+1}$. On the first double-sweep we use ρ_1 as the acceleration parameter, on the second, ρ_2, and so on up to the final parameter, this sequence being known as a cycle. If further iterations are necessary, we perform additional cycles. The various methods of choosing the ρ's and deciding the optimum number of sweeps per cycle in solving such an elliptic system numerically, may be found in Birkhoff, Varga and Young (1962). The solution for $\underline{z}_{n+\frac{1}{2}}$ is required only as an intermediate result and is not retained from one iteration to the next.

The tridiagonal nature of the matrices $(H + \rho_{n+1} I)$ and $(V + \rho_{n+1} I)$, noted in (iii) above, permits us to use the efficient Thomas algorithm to invert them. This algorithm is outlined in the Appendix. By subtracting equation (20) from (21) we obtain a different, but equivalent form of the latter, which saves a number of operations each sweep, since the matrix $(V - \rho_{n+1} I)\underline{z}_n$ has been previously calculated in solving (20):

$$(V + \rho_{n+1} I)\underline{z}_{n+1} = (V - \rho_{n+1} I)\underline{z}_n + 2\rho_{n+1} \underline{z}_{n+\frac{1}{2}} \qquad (21')$$

It now remains for us to calculate the acceleration parameters ρ_n. As stated above in (iv), the matrices H and V are positive definite, and thus each has a spectrum of positive eigenvalues. Let a be the min of the greatest lower bounds of the eigenvalues of H and V, and b be the corresponding max of the least upper bounds.

For an ADI cycle of just one double-sweep, it can be shown (see Birkhoff, Varga and Young) that the optimum value for a single acceleration parameter, is

$$\rho = (ab)^{\frac{1}{2}} \qquad (22)$$

If a cycle of m double-sweeps is used, then the most common choice involves the so-called Wachspress parameters:

$$\rho_i = b\left(\frac{a}{b}\right)^{(i-1)/(m-1)} \qquad (i=1,2,\ldots, m;\ m>1)$$

Thus we are presented with two problems: the first is to calculate the range of the eigenvalues for both the ψ and ζ difference operators, while the second is to decide the number of ADI cycles and the number of sweeps per cycle during one iteration on each equation. As there is no theory to guide us in considering this second point, we shall have to resort to numerical experiments to provide the answer, and thus we defer the relevant discussion until the following section where the results are presented.

In considering the first problem, this is no real difficulty with the ψ - equation, since the matrices H_1 and V_1, given by (18) are constant, arising from the Laplacian operator. The resulting calculation of the eigenvalues, and hence the acceleration parameters is then very much a standard exercise. However, in the ζ - equation, as can be seen from (19), the operators H_2 and V_2 are not constant, but are functions of both $\varepsilon(= 1/R)$ and of the magnitudes of the quantities α and β, which in turn represent the gradients of the stream function field. On appealing to the physics of the problem, we anticipate that the largest stream function gradients

(i.e., the largest velocities), will occur in the vicinity of the moving boundary y=1. Here, we know from (7), that $\partial\psi/\partial y = -1$, and hence from (10), the maximum possible magnitudes of α and β will be h. Clearly, their minimum possible magnitudes will arise from regions where there is no contribution from the convective terms, and thus these values are zero.

Use of Gerschgorin's Theorem (Varga 1962) permits us to calculate b for H and V of both equations, as the maximum of the sum of the moduli of the matrix elements along any row or column. From what has been discussed above, and from (18) and (19), we arrive at

$$b_1 = 4 , \quad b_2 = 2(2\varepsilon + h), \tag{23}$$

where as before, the subscripts 1 and 2 refer to the ψ - and ζ - equations respectively. The lower bounds a, are also immediately obtained by use of a result of Varga (1962), namely that the greatest lower bound of the eigenvalues of an (N-1)x(N-1) matrix of the form

$$\begin{bmatrix} 2k & -k & & & 0 \\ -k & 2k & -k & & \\ & \ddots & \ddots & \ddots & \\ & & -k & 2k & -k \\ 0 & & & -k & 2k \end{bmatrix}$$

is

$$a = 2k\left(1 - \cos\frac{\pi}{N}\right) > 0.$$

Thus, in the present case we obtain, since h = 1/N,

$$a_1 = 2(1 - \cos \pi h), \quad a_2 = 2\varepsilon(1 - \cos \pi h). \qquad (24)$$

In works such as those of Burggraf (1966), Greenspan (1968, 1969) and Gosman *et al.* (1969), relaxation methods were the procedure adopted for the inner iterations. In the case of the ψ - equation, Successive Overrelaxation was used by these authors, since the optimum overrelation factor for the Laplacian is a standard result (Varga 1962). However, for the ζ - equation the above authors were obliged to resort to the Gauss-Seidel iterative method, since no such optimum relaxation factor could be calculated. Yet we have shown here that it is a relatively simple matter to obtain the eigenvalue bounds which are required when *both* equations are treated by an ADI method.

6. Results

As stated in the previous section, the first problem to be considered is the number of sweeps per cycle and the number of cycles required for each inner iteration. That is, we are required to determine the necessary accuracy of the inner iterations for each outer iteration, a familiar problem in numerical methods of this type.

Heuristically, one can imagine that if the $\psi_{i,j}$ field, say, is not known to any great degree of accuracy, then there is unlikely to be any advantage in calculating the $\zeta_{i,j}$ field from this $\psi_{i,j}$ through

equation (11), with much accuracy. In fact, it is more likely to be disadvantageous in terms of computer time. On the other hand, when $\psi_{i,j}$ and $\zeta_{i,j}$ have almost converged, then one will also require only a small number of inner iterations to obtain the desired accuracy. This point is made for example, by Osborne (1967), who used an inner/outer iterative process to solve a nonlinear eigenvalue equation arising from a problem in hydrodynamic stability. Accordingly, one would expect to perform only a few inner iterations per outer iteration for optimum convergence.

With respect to the relevant literature, the works cited earlier of Smith (1968, 1970) and Ehrlich (1971), who treat the inner/outer problem theoretically, give no indication of the procedure one should adopt here. The authors who deal specifically with the numerical solution of the steady cavity problem, adopt quite different approaches: Greenspan (1968, 1969) solves for his inner iterates to the *same* precision as the outer iterates; Burggraf (1966) performs just one inner iteration on each of the two equations per outer iteration, while Gosman *et al.* (1969) in fact present no information at all on the procedure they used.

In order to resolve this problem, it was necessary to perform numerical experiments, most of which used a Reynolds number of 200, in which it was found that the optimum method involved taking just *one* double ADI sweep on each equation per outer iteration. Not only did increasing the number of sweeps within an inner iteration naturally increase the computer time, but perhaps surprisingly, it was found in all the cases tested, that this actually increased

the number of outer iterations required for convergence!

The remaining problem is to find suitable values of the filtering parameters ω_1 and ω_2 used in the outer iterations, as functions of R and h. These were obtained by performing several outer iterations with a number of pairs (ω_1,ω_2), and from the resulting rates of convergence, a suitable pair giving approximately optimum convergence could be selected. In order to calculate the position of the vortex centre and the values ψ_c and ζ_c of the stream function and vorticity at this point, a further routine was added to the program. This selected several points near the centre (the point at which ψ takes its maximum value) which were then fitted with a least-squares paraboloid, the maximum value of which was chosen to be ψ_c. The coordinates (x_c,y_c) of this maximum were thus also immediately available, and from these, the value ζ_c could be found by interpolation of the calculated vorticity field. A value of 10^{-4} was in most cases found to be suitable for ε_1 and ε_2, defined by (16a,b).

The calculations were performed at values of R equal to 10, 50, 100, 200, 500, 1000 and 2000, the details of which are presented in Table 1. In all cases except R = 1000 and 2000, the fields were calculated for h = 1/10, 1/20 and 1/40. With h=1/10, the initial fields were set to zero, and in this case it was found that slightly faster convergence was obtained if the first two iterates of the ψ and ζ fields were combined in a single Aitken del-squared step, followed by filtering for the remaining outer iterations. For h = 1/20 and 1/40, the initial fields were those calculated previously for h = 1/10 and 1/20 respectively, the values at the intermediate

grid points being obtained by linear interpolation. The quantity in Table 1 called the 'eddy size' is defined as the y-coordinate on the axis x = o where the separation streamline of the main Moffatt eddy meets the wall. This has been measured experimentally as a function of R by Pan and Acrivos (1967). The time taken for a complete inner/outer step was approximately $7.3 \times 10^{-4}/h^2$ seconds on an IBM 370/155.

It can be seen from Table 1 that for Reynolds numbers up to 200, relatively few iterations are required for convergence, and the filtering parameters ω_1 and ω_2 vary quite regularly with R and h. However this situation alters as R is further increased, and many more iterations become necessary. This behaviour is by no means unexpected, since physically, as the Reynolds number is increased, the diminishing effect of viscous damping means that the time for steady-state flow to be reached from given inital conditions will be correspondingly increased. The present method used to find steady solutions to the Navier - Stokes equations, is in fact analogous to an accelerated solution of the time-dependent equations, and thus we can expect the computational time to increase with R. Furthermore, with h = 1/40, it was found that in order to improve the convergence rates at R = 200 and 500, ω_1 and ω_2 had to be altered after a certain number of iterations, as indicated in Table 1.

In Figures 4 to 8, we present contours of the stream function and vorticity fields for R = 10, 50, 100, 200 and 500 respectively, with h = 1/40. At R = 10, the fields of ψ and ζ are seen to be approximately symmetrical about $x = \frac{1}{2}$, since here the equations are

approaching those of Stokes flow. As R is further increased, the effect of the convective terms becomes more important and the position of the vortex centre moves downstream. At $R = 500$, convection is dominating the flow, except in the thin boundary layers at the walls of the cavity. The position of the vortex centre has now moved in the direction of the centre of the cavity and the situation is more closely approaching that envisaged by Batchelor (1956), in which at high Reynolds numbers, the flow, except in the boundary layers is an effectively inviscid core of constant vorticity, calculated by Burggraf to have a value of 1.89 in the limit of infinite R.

The accuracy of the finite-difference solutions obtained can be assessed for example, from the value of ψ_c, and it can be seen from Table 1 that for $R \leq 200$, $h = 1/40$ affords sufficient resolution. However as R is increased, the velocity gradients in the boundary layers increase and hence more grid points are needed to resolve the flow details there. Unfortunately, since the computing time varies as $1/h^2$ (and the total number of iterations is also considerably increased), it is evident that there are a number of difficulties involved in obtaining steady solutions numerically for high Reynolds number flows, and hence there is a need for improved methods to be further developed.

Greenspan (1968, 1969) has approached this problem by taking the first interior grid point as the boundary in solving (5), and claims to have obtained solutions up to $R = 10^5$ with $h = 1/20$. However, this method effectively ignores the structure of the boundary layer region across which vorticity is transferred between

the walls and the interior flow, and thus it is difficult to gauge the value of these solutions. Furthermore, it is scarcely conceivable that steady flows will physically exist at such large values of R; indeed, Pan and Acrivos (1967) report that in their experiments, turbulence has already set in at $R = 4000$.

An alternative approach lies in the use of a non-uniform finite difference mesh as employed for instance by Gosman *et al.* (1969) for the present problem, where the distribution of the grid points is concentrated near the walls and is relatively sparse in the interior. There are no inherent difficulties in formulating this problem, since by use of the 'integral method' (e.g., Varga 1962), equations (5) and (6) can be converted to a finite-difference form suitable for the application of the present ADI method. This in fact has been carried out as a preliminary case, for $R = 200$, with 10 mesh spacings in each coordinate direction, and as seen from Table 1, a certain improvement is apparent in the value of ψ_c.

Nevertheless, it can be seen from Table 1, that the method as presented, while giving excellent results for low to moderate Reynolds numbers, is not nearly so satisfactory as R is increased. For example, at $R = 1000$, the fields at h=1/20 are converging very slowly in an oscillatory manner. However an alternative approach has been advocated by Gosman and Spalding (1971) who have used a type of conservative difference scheme for the vorticity equation, and satisfactory results for large R using a similar approach have also recently been reported by Bozeman and Dalton (1973).

Instead of the vorticity equation (6), we can combine this equation with the continuity equation to obtain the 'flux' form

$$\nabla^2 \zeta - \nabla \cdot (\underline{u}\, \zeta) = 0, \qquad (25)$$

where $\underline{u}$ is the velocity vector (u,v). In centred difference form, the Jacobian for equation (6), the 'advective' form, is

$$J_1 = (\delta_{\hat{x}} \psi_{i,j})(\delta_{\hat{y}} \zeta_{i,j}) - (\delta_{\hat{y}} \psi_{i,j})(\delta_{\hat{x}} \zeta_{i,j}),$$

while that for the above equation (25) can be seen to be

$$J_2 = \delta_{\hat{y}}(\zeta_{i,j}\, \delta_{\hat{x}} \psi_{i,j}) - \delta_{\hat{x}}(\zeta_{i,j}\, \delta_{\hat{y}} \psi_{i,j})$$

Now it has been shown theoretically, and in accompanying numerical studies (Arakawa 1966, 1970), that J_2 conserves mean kinetic energy in time-dependent calculations, assuming dissipation is neglected, while J_1 fails to do so. Since, as we have previously noted, there are analogies between the present method and time-dependent treatments, it can be realistically expected that use of J_2 instead of J_1, will lead to more reliable results. Both J_1 and J_2 fail to conserve mean-square vorticity, although Bozeman and Dalton (1973) incorrectly claim this as a property of their difference scheme. A third form of the Jacobian has been shown by Arakawa (1966) to conserve mean-square vorticity, but its particular difference formulation prevents it being split into horizontal and vertical operators, as required here for the ADI formulation.

It is a relatively simple matter to incorporate J_2 (with upstream differencing) instead of J_1, into the numerical scheme, particularly since the eigenvalue bounds (23) and (24) will be unaltered. In Table 2 we list results for the flux form with

R = 200, 500 and 1000, and in Figure 9 we present contours of ψ and ζ at h = 1/40 for R = 1000. The results of these calculations are most encouraging, and clearly show that through the use of J_2, the number of outer iterations required for large R is not substantially greater than that for values of R an order of magnitude or so lower. The values of ζ_c obtained with J_2 are considerably small than those of J_1, and this is consistent with the conservative properties of the former.

Since the main interest of the work in this chapter lies in the development of a specific numerical method, rather than in the study of the square cavity problem itself, other results of interest, such as the velocity profiles across the cavity have not been detailed. Also, no effort has been made to increase grid resolution above h = 1/40, although an interesting outcome of such a step could be the possible appearance of further nested viscous corner eddies as predicted by Moffatt (1964). The numerical solutions can be seen to exhibit the behaviour determined experimentally by Pan and Acrivos (1967), where the eddy size is seen to increase with R to a maximum near R = 500 and then decrease as viscous effects gradually become less important.

7. Conclusions

In this chapter we have presented a method for the solution of the steady two-dimensional Navier - Stokes equations, which differs from previously published methods through its use of the Peaceman-Rachford alternating direction implicit method for both the stream

function and vorticity equations. The method can be seen to be general enough to be extended to cases of steady three-dimensional axisymmetric motion (with rotation if required) and to non-uniform finite-difference meshes. Indeed, no conceptual difficulties are foreseen in extending the method to fully three-dimensional problems, although considerations of computer time and storage required for such a calculation would tend to place considerable restrictions on the viability of such an approach.

In particular, the use of the flux form J_2 has been shown to give rapidly converging solutions at high resolution ($h = 1/40$) for the more interesting and difficult case of high Reynolds number flow. It would therefore be advantageous in later studies, to combine the flux form with a non-uniform mesh distribution, thus benefitting from the resulting faster convergence and the improved resolution of the boundary layers. Following Greenspan (1968), upstream differencing in the convective terms has been used so that a solution to the difference equations is theoretically attainable. However it should be noted that the use of upstream differencing does lead to a false diffusive effect (Molenkamp 1968) whose magnitude is proportional to the mesh size h, and hence this point must also be taken into account when assessing the worth of a particular solution.

The calculations performed, and the results presented, are by no means extensive, since the main interest was in the overall numerical method. Nevertheless, the results obtained indicate that the method itself has considerable promise, and is sufficiently versatile to be worthy of further attention at a later date.

APPENDIX

We discuss here the method, usually known as the Thomas algorithm, to solve the tridiagonal system of equations

$$A\underline{x} = \underline{k}, \qquad (A.1)$$

where A is an (n-1)x(n-1) matrix of the general form

$$A = \begin{bmatrix} b_1 & -c_1 & & & 0 \\ -a_2 & b_2 & -c_2 & & \\ & \ddots & \ddots & \ddots & \\ & & -a_{n-2} & b_{n-2} & -c_{n-2} \\ 0 & & & -a_{n-1} & b_{n-1} \end{bmatrix}$$

which in our case has arisen in the numerical solution of an elliptic equation through reduction, either by an alternating direction implicit, or a direct Fourier method. A method for the solution of the above equation is given by Varga (1962), the basic idea being to utilise the particular properties of the tridiagonal matrix A to greatly reduce the number of operations required.

Alternatively, we can write the above system as the equivalent second order difference equation

$$-a_i x_{i-1} + b_i x_i - c_i x_{i+1} = k_i \qquad (A.2)$$

where $i=1,2,\ldots,n-1$ and we are assuming the simplest boundary conditions

$$x_o = x_n = 0 \qquad (A.3)$$

The method we shall employ to solve equations (A.2) and (A.3) has been presented by Richtmyer and Morton (1967), and is as follows. Firstly, we assume that the solution can be written in the form

$$x_i = E_i\, x_{i+1} + D_i \qquad (A.4)$$

Now, if the boundary conditions (A.3) are to be consistent with this form, we must have that

$$E_o = D_o = 0 \qquad (A.5)$$

From (A.4) we can set $x_{i-1} = E_{i-1}\, x_i + D_{i-1}$, and on substituting this in equation (A.2) and rearranging, we obtain

$$x_i = \frac{c_i}{b_i - a_i E_{i-1}}\, x_{i+1} + \frac{k_i + a_i D_{i-1}}{b_i - a_i E_{i-1}} \qquad (A.6)$$

If equation (A.6) is to be consistent with the assumed form of the solution (A.4), it means we require that

$$E_i = \frac{c_i}{b_i - a_i E_{i-1}} \qquad (A.7)$$

and

$$D_i = \frac{k_i + a_i D_{i-1}}{b_i - a_i E_{i-1}} \qquad (A.8)$$

for $i \geq 1$. Thus, using the boundary conditions (A.5), we can use the recurrence relations (A.7) and (A.8) to calculate the E_i and D_i for $i \geq 1$. From (A.3) we have the other boundary condition that $x_n = 0$ and therefore we can calculate the $x_i (i = n-1, n-2, \ldots, 2, 1)$ backwards, using the values of the E_i and D_i just obtained. A count of operations involved shows this is of order N, as against N^3 for normal Gaussian elimination.

Table Captions

Table 1. Details of the numerical solutions.

Table 2. Corresponding results to those of Table 1 but obtained with difference equations in flux form.

Figure Captions

Figure 1. Dimensional sketch of cavity.

Figure 2. Sketch of finite-difference mesh.

Figure 3. Region involved in the formulation of the boundary vorticity values - equation (14).

Figure 4. Stream function and vorticity contours, with contour values depicted for h = 1/40. R = 10.

Figures 5 to 8. Caption as for Figure 4. R = 50, 100, 200, 500 respectively.

Figure 9. Caption as for Figure 4 but with fields obtained from the flux form (25) of the vorticity equation. R = 1000.

Table 1.

R	h^{-1}	ε_1	ε_2	ω_1	ω_2	Iterations	x_c	y_c	ψ_c	ζ_c	Eddy size
10	10	10^{-4}	10^{-4}	0.90	0.75	22	0.4752	0.7596	0.0978	3.0726	0
	20	10^{-4}	10^{-4}	0.95	0.50	24	0.4831	0.7628	0.0998	3.1822	0.071
	40	10^{-4}	10^{-4}	0.95	0.30	30	0.4836	0.7644	0.1002	3.2025	0.084
50	10	10^{-4}	10^{-4}	0.90	0.80	22	0.4222	0.7612	0.0952	2.9148	0
	20	10^{-4}	10^{-4}	0.95	0.50	20	0.4247	0.7592	0.1004	3.2058	0.096
	40	10^{-4}	10^{-4}	0.95	0.30	40	0.4262	0.7593	0.1014	3.2445	0.105
100	10	10^{-4}	10^{-4}	0.85	0.50	38	0.3738	0.7639	0.0854	2.7637	0
	20	10^{-4}	10^{-4}	0.95	0.60	30	0.3857	0.7556	0.0986	3.1954	0.126
	40	10^{-4}	10^{-4}	0.95	0.30	60	0.3864	0.7463	0.1024	3.2112	0.144
200	10	10^{-4}	10^{-4}	0.85	0.50	24	0.3399	0.7730	0.0781	2.6018	0.120
	10*	10^{-4}	10^{-4}	0.925	0.30	86	0.3262	0.7912	0.0838	3.0870	0.118
	20	10^{-4}	10^{-4}	0.95	0.30	58	0.3529	0.7524	0.0918	3.0307	0.230
	40	10^{-4}	10^{-4}	0.96	0.15	50					
				0.96	0.10	80	130	0.3704	0.7167	0.1013	2.9047	0.256
500	10	10^{-4}	10^{-4}	0.85	0.60	38	0.2850	0.7923	0.0584	2.3633	0.231
	20	10^{-4}	10^{-4}	0.92	0.30	100	0.3161	0.7691	0.0727	2.7355	0.416
	40	10^{-4}	10^{-4}	0.95	0.05	300					
				0.97	0.02	120	420	0.3809	0.6985	0.0893	2.5108	0.417

Table 1. (cont.)

R	h^{-1}	ε_1	ε_2	ω_1	ω_2	Iterations	x_c	y_c	ψ_c	ζ_c	Eddy size
1000	10	10^{-4}	10^{-4}	0.85	0.70	38	0.2387	0.8150	0.0442	2.6518	0.308
	20	10^{-4}	10^{-4}	0.98	0.01	700†	0.2494	0.8276	0.0618	3.4810	0
2000	10	10^{-4}	10^{-4}	0.90	0.80	78	0.1727	0.8598	0.0304	2.8291	0.352

*Non-uniform finite-difference mesh; †Solution oscillating with very slow convergence.

Table 2

R	h^{-1}	ε_1	ε_2	ω_1	ω_2	Iterations	x_c	y_c	ψ_c	ζ_c	Eddy size
200	10	10^{-4}	10^{-4}	0.15	0.50	28	0.3823	0.7217	0.0729	1.9075	0
	20	10^{-4}	10^{-4}	0.05	0.70	44	0.3698	0.7322	0.0849	2.2916	0.154
	40	10^{-4}	10^{-4}	0.04	0.85	115	0.3782	0.7107	0.0939	2.5108	0.207
500	10	10^{-4}	10^{-4}	0.15	0.40	28	0.3563	0.6796	0.0568	1.1486	0
	20	10^{-4}	10^{-4}	0.05	0.75	74	0.3757	0.6658	0.0723	1.6083	0.213
1000	10	10^{-4}	10^{-4}	0.15	0.30	32	0.3708	0.6236	0.0467	0.9698	0
	20	10^{-4}	10^{-4}	0.05	0.80	60	0.3917	0.6041	0.0614	1.1485	0.173
	40	10^{-4}	10^{-4}	0.03	0.80	105	0.4374	-0.5838	0.0761	1.3748	0.320

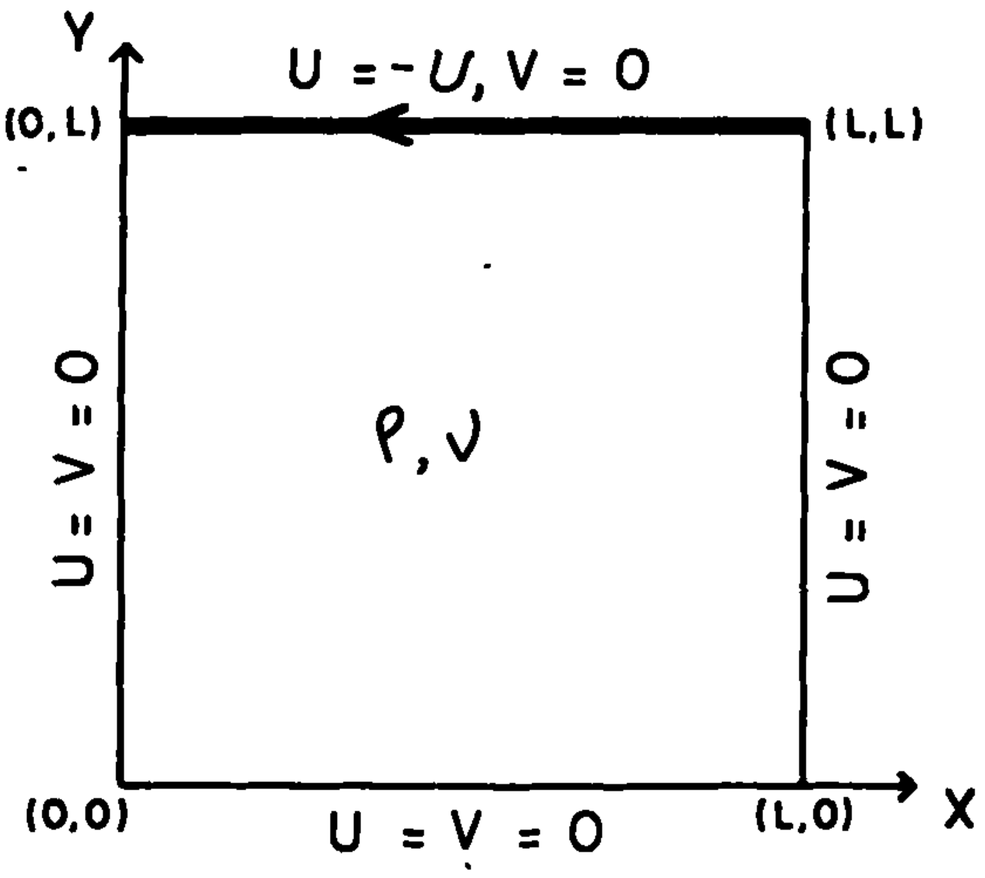

Figure 1

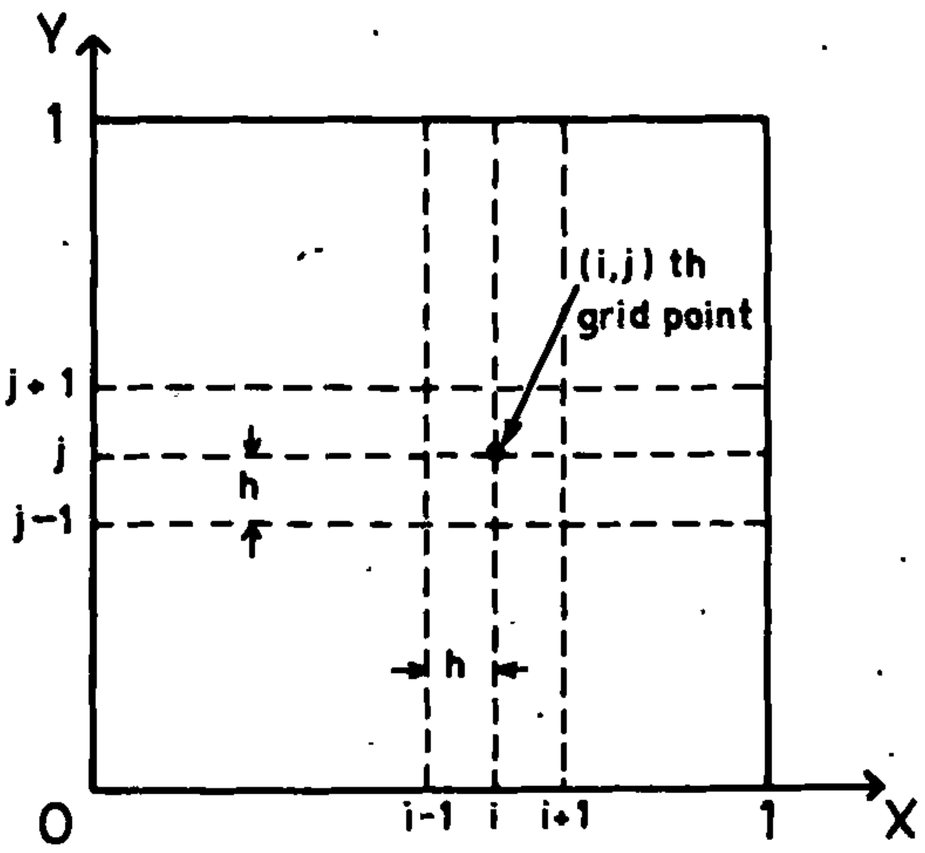

Figure 2

Figure 3

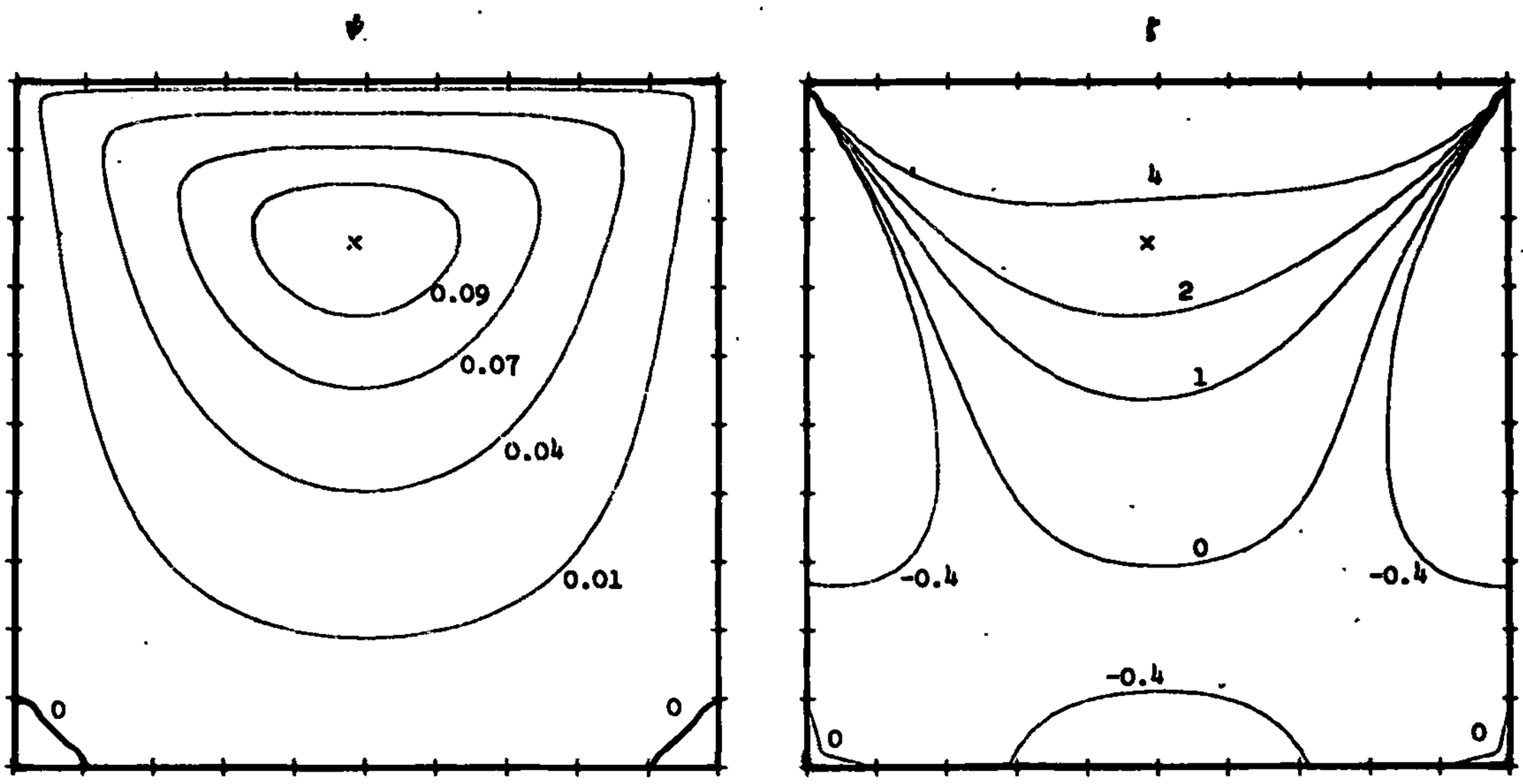

Figure 4

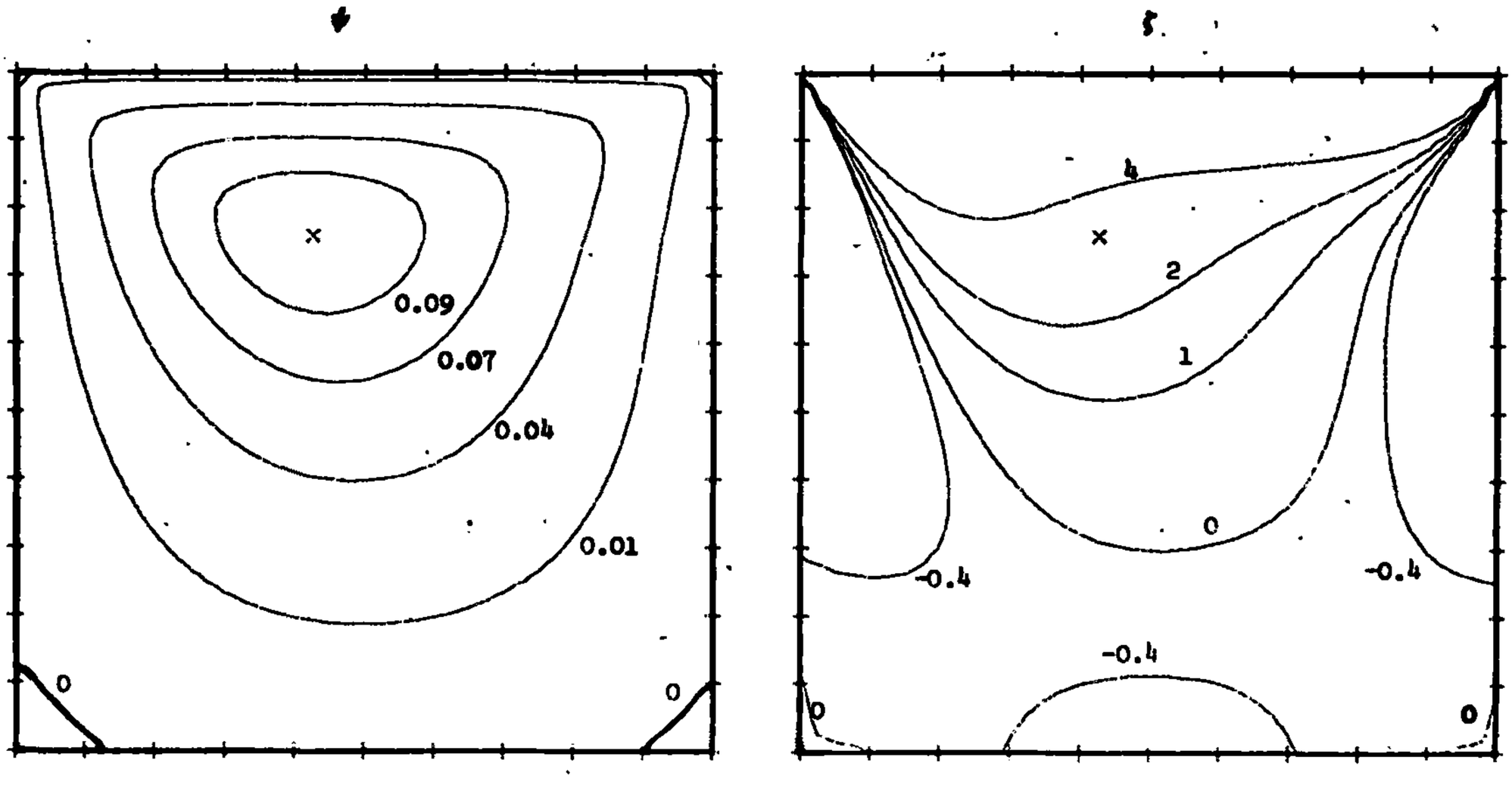

Figure 5

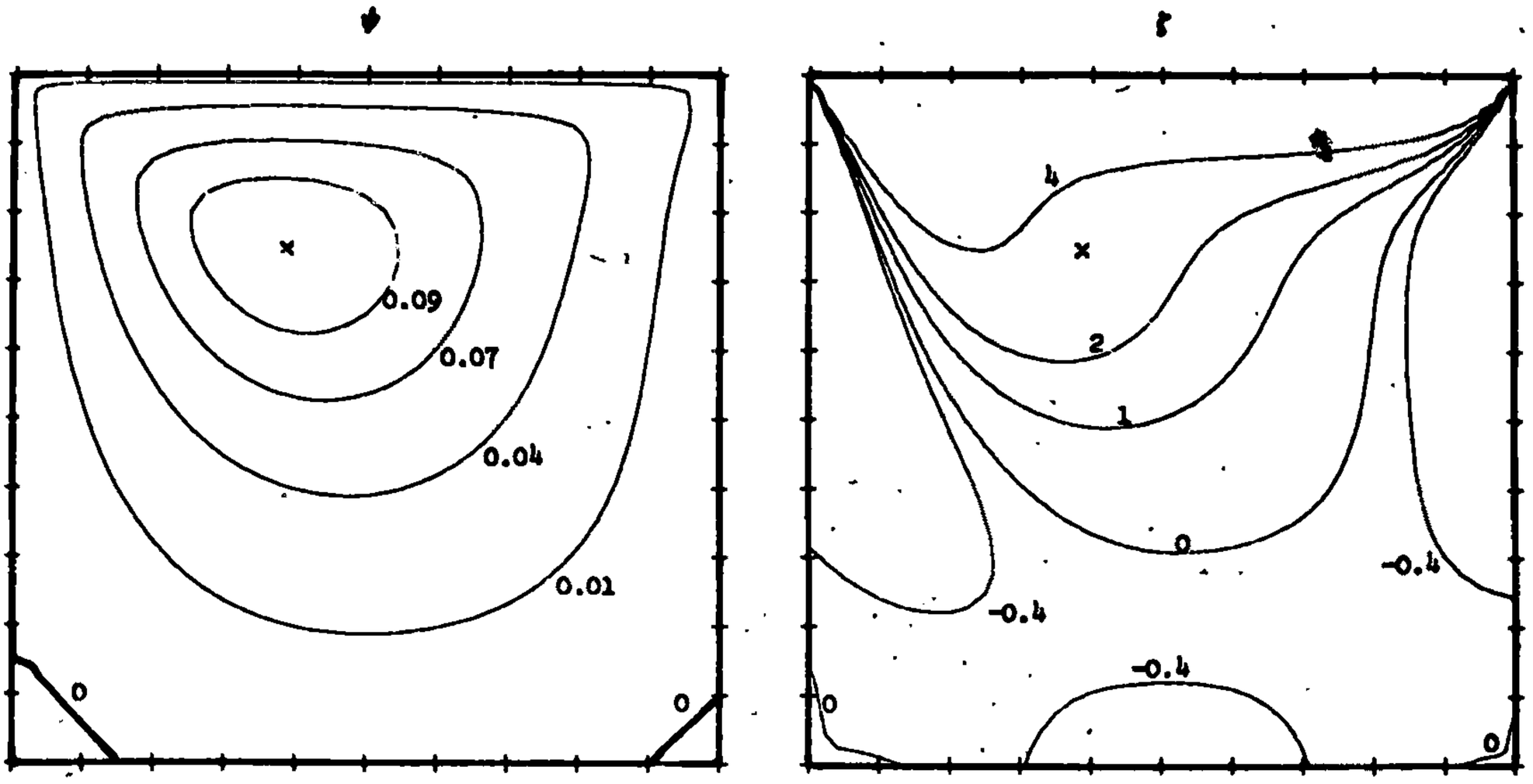

Figure 6

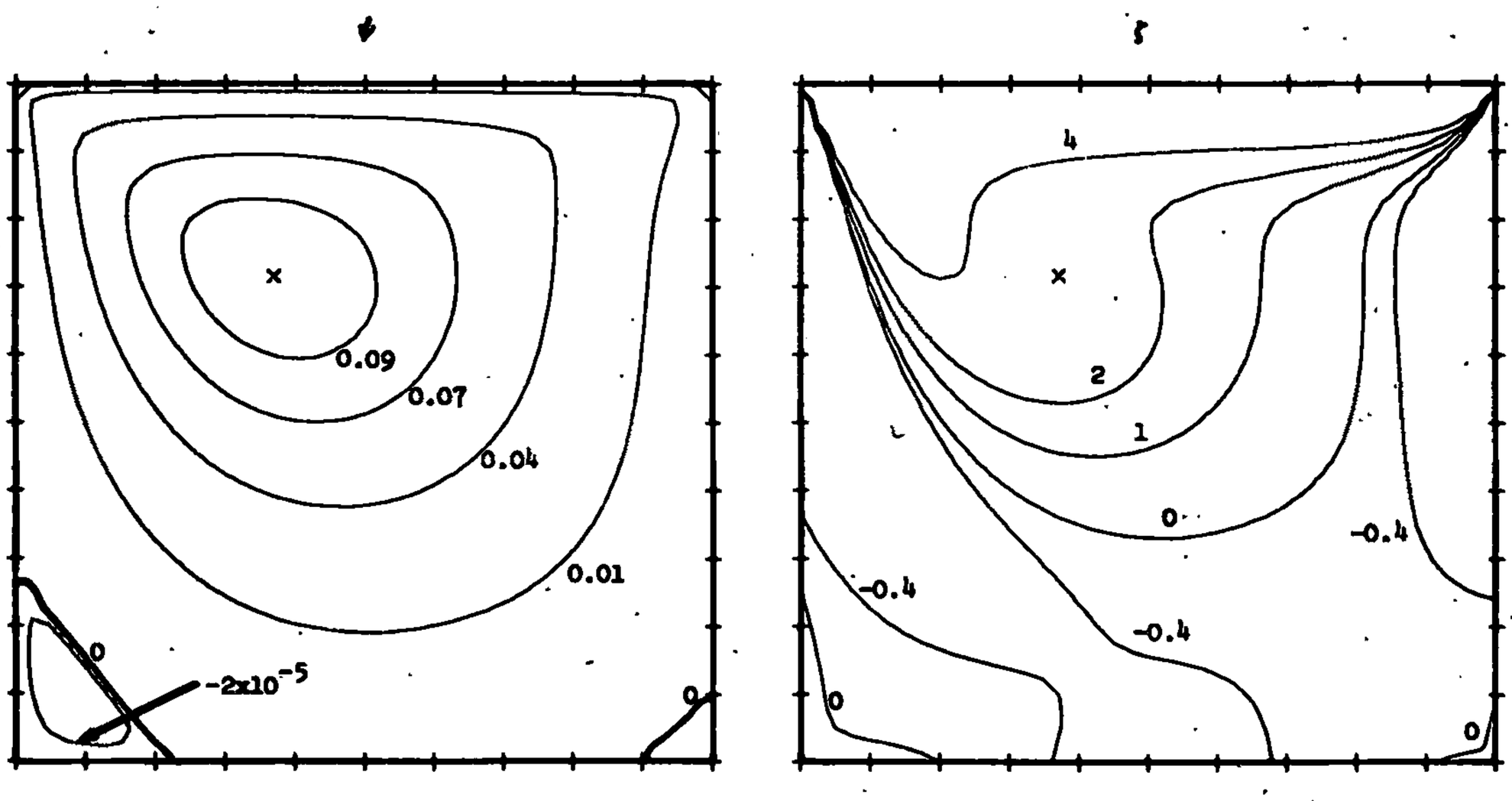

Figure 7

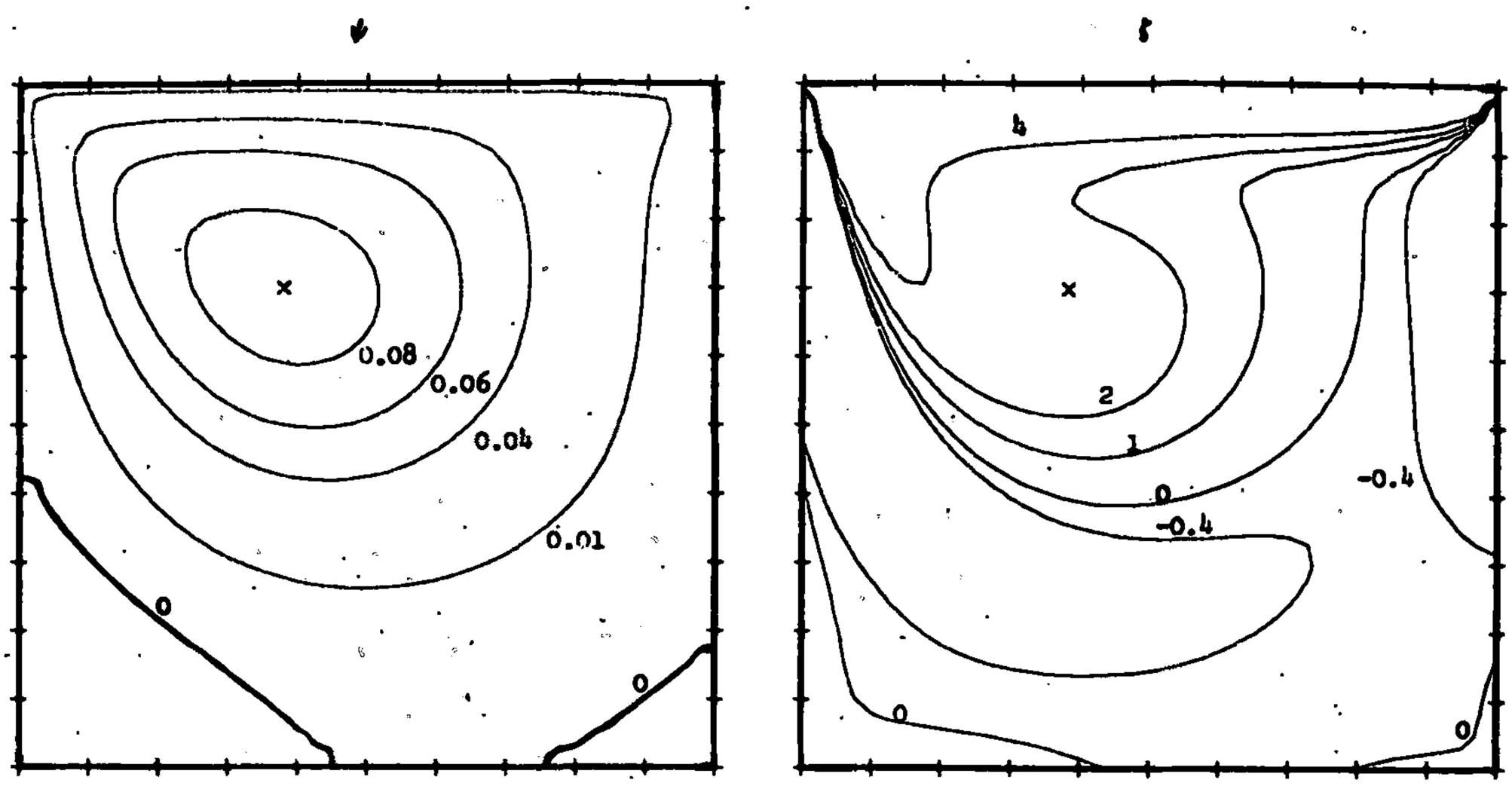

Figure 8

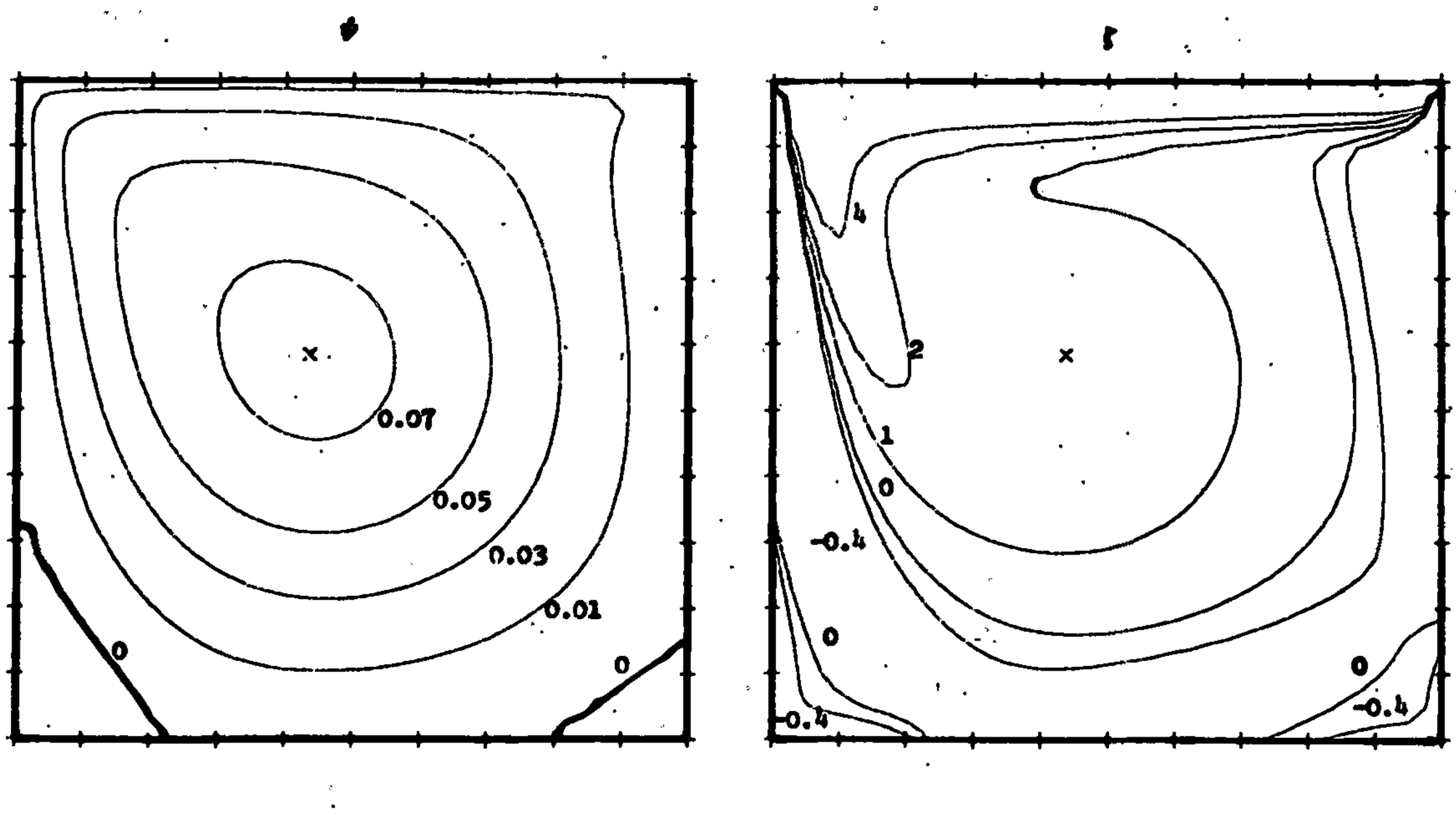

Figure 9

REFERENCES†

ANDERSON, O.L. 1966 Ph.D. Thesis, Rensselaer Polytechnic Institute. {1}

ARAKAWA, A. 1966 J. Comput. Phys. 1, 119-143. {3,4}

ARAKAWA, A. 1970 Numerical Solution of Field Problems in Continuum Physics 2, SIAM-AMS Proceedings, 24-40. {3,4}

AZIZ, K. & HELLUMS, J.D. 1967 Phys. Fluids 10, 314-324. {4}

BARCILON, A. 1967a J. Atmos. Sci. 24, 453-466. {3}

BARCILON, A. 1967b J. Fluid Mech. 27, 155-175. {3}

BARCILON, A. 1968 Report R68SD59, Gen. Electric Space Sci. Lab. {1}

BATCHELOR, G.K. 1956 J. Fluid Mech. 1, 177-190. {4}

BEARDSLEY, R.C. 1971 Mon. Weather Rev. 99, 387-392. {3}

BELCHER, R.J., BURGGRAF, O.R. & STEWARTSON, K. 1972 J. Fluid Mech. 52, 753-780. {1}

BELLAMY-KNIGHTS, P.G. 1970 J. Fluid Mech. 41, 673-687. {3}

BELLAMY-KNIGHTS, P.G. 1971 J. Fluid Mech. 50, 1-16. {3}

BETHEL, H.E. 1968 AIAA J. 6, 220-225. {1}

BIRKHOFF, G., VARGA, R.S. & YOUNG, D.M. 1962 Adv. Comput. 3, 187-273. {4}

BLACKADAR, A.K. 1962 J. Geophys. Res. 67, 3095-3102. {2}

BLACKADAR, A.K. & TENNEKES, H. 1968 J. Atmos. Sci. 25, 1015-1020. {2}

BLACKADAR, A.K. & PANOFSKY, H.A. 1969 US Army Final Report DA-28-043-AMC-01388(E). {2}

BOZEMAN, J.D. & DALTON, C. 1973 J. Comput. Phys. 12, 348-363. {4}

BUJATTI, K. & BLACKADAR, A.K. 1957 Quart. J. R. Met. Soc. 83, 486-500. {2}

BURGERS, J.M. 1948 Adv. Appl. Mech. 1, 171-199. {3}

BURGGRAF, O.R. 1966 J. Fluid Mech. 24, 113-151. {4}

BURGGRAF, O.R., STEWARTSON, K. & BELCHER, R. 1971 Phys, Fluids 14, 1821-1833. {1}

---

†Numbers in brackets after reference denote chapters in which it is cited.

BUSINGER, J.A., WYNGAARD, J.C., IZUMI, Y. & BRADLEY, E.F. 1971 J. Atmos. Sci. 28, 181-189. {2}

CARRIER, G.F. 1965 SIAM J. 13, 68-95. {1}

CARRIER, G.F. 1971a J. Fluid Mech. 49, 133-144. {1}

CARRIER, G.F. 1971b J. Fluid Mech. 49, 145-158. {1}

CARRIER, G.F., HAMMOND, A.L. & GEORGE, O.D. 1971 J. Fluid Mech. 47, 145-170. {1}

CHAM, T.S. & HEAD, M.R. 1969 J. Fluid Mech. 37, 129-147. {1}

CHANG, C.C. 1969 Proc. Sixth Annual Local Severe Storms Conf., Chicago. {1,3}

CHARNEY, J.G. 1971 *Mathematical Problems in the Geophysical Sciences. Volume 1, Geophysical Fluid Dynamics.* American Mathematical Society, Lectures in Applied Mathematics 13, 355-368. {1}

CHARNEY, J.G. & ELIASSEN, A. 1949 Tellus 1, 38-54. {1}

CHAUSSEE, D.S. 1972 Ph.D. Thesis, Iowa State University. {3}

CHI, S.W., YING, S.J. & CHANG, C.C. 1969 Tellus, 21, 693-700. {3}

CLARKE, R.H. 1970 Quart. J. R. Met. Soc. 96, 91-114. {2}

COOKE, J.C. 1952 J. Aeronaut. Sci. 19, 486-490. {1}

COOLEY, J.W. & TUKEY, J.W. 1965 Math. Comp. 19, 297-301. {3}

CRAWFORD, L.J. 1971 Ph.D. Thesis, Catholic University of America. {1,3}

CSANADY, G.T. 1967 J. Atmos. Sci. 24, 467-471. {2}

CSANADY, G.T. 1972 J. Atmos. Sci. 29, 488-496. {2}

DAVIES-JONES, R.P. & VICKERS, G.T. 1971 NOAA Tech. Memo. ERL NSSL-57. {3}

DEARDORFF, J.W. 1972 J. Atmos. Sci. 29, 91-115. {1,2}

DERGARABEDIAN, P. & FENDELL, F. 1967 Phys. Fluids 10, 2293-2299. {3}

DERGARABEDIAN, P. & FENDELL, F. 1970 J. Astronaut. Sci. 17, 218-236. {3}

DERGARABEDIAN, P. & FENDELL, F. 1972a Report 18524-6001-RO-01, TRW Systems, California. {1}

DERGARABEDIAN, P. & FENDELL, F. 1972b J. Astronaut. Sci. 20, 9-34. {1}

DESSENS, J. 1969 Doctoral Thesis, University of Paris. {3}

DESSENS, J. 1972 J. Appl. Meteorol. 11, 72-75. {3}

DONALDSON, C.D. & SULLIVAN, R.D. 1960 Proc.(1960) Heat Transf. & Fluid Mech. Inst., 16-30. {3}

DORR, F.W. 1970 SIAM J. Num. Anal. 7, 281-313. {4}

DOUGLAS, J. 1962 Numer. Math. 4, 41-63. {4}

EINSTEIN, H.A. & LI, H. 1955 Houille Blanche, 10, 483-496. {3}

EHRLICH, L.W. 1971 SIAM J. Num. Anal. 8, 278-287. {4}

ELLISON, T.H. 1956 *Surveys in Mechanics* (ed. G.K. Batchelor & R.M. Davies, Cambridge University Press), 400-430. {2}

ESTOQUE, M.A. 1967 Tellus 19, 560-565. {2}

FENDELL, F. & COATS, D. 1967 Proc. (1967) Heat Transf. & Fluid Mech. Inst., 341-360. {3}

FINLAYSON, B.A. & SCRIVEN, L.E. 1966 Appl. Mech. Rev. 19, 735-748. {1}

FITZJARRALD, D.E. 1973 J. Atmos. Sci. 30, 894-902. {3}

FORSYTHE, G.E. & WASOW, W.R. 1960. *Finite-Difference Methods for Partial Differential Equations* (Wiley). {3}

FORTIN, M., PEYRET, R. & TEMAN, R. 1971 J. de Mécanique 10, 357-390. {4}

GEORGE, O.D. 1971 Ph.D. Thesis, Harvard University. {1}

GOLDEN, J.H. 1971 Mon. Weather Rev. 99, 146-154. {3}

GOLDEN, J.H. 1973 New Scientist, 58(850), p. 665. {3}

GOL'DSHTIK, M.A. 1960 J. Appl. Math. Mech. 24, 913-929. {3}

GOSMAN, A.D., PUN, W.M., RUNCHAL, A.K., SPALDING, D.B. & WOLFSHTEIN, M. 1969 *Heat and Mass Transfer in Recirculating Flows* (Academic Press). {4}

GOSMAN, A.D. & SPALDING, D.B. 1970 Proc. Second International Conf. on Num. Methods in Fluid Dynamics, University of California, Berkeley, 67-72. {4}

GRANGER, R. 1966 J. Fluid Mech. 25, 557-576. {3}

GRANGER, R. 1972 Geophys. Fluid Dyn. 3, 45-88. {3}

GRAY, W.M. 1966 J. Atmos. Sci. 23, 278-288. {1,2}

GRAY, W.M. 1966 Proc. Sixth Annual Local Severe Storms Conf., Chicago. {3}

GREENSPAN, D. 1968 *Lectures on the Numerical Solution of Linear, Singular and Nonlinear Differential Equations* (Prentice-Hall). {4}

GREENSPAN, D. 1969 Comput. J. 12, 89-94. {4}

GUTMAN, L.N. 1957 Bull. Acad. Sci. USSR (Geophysics Series) 1, 87-103. {3}

HALTINER, G.J. 1971 *Numerical Weather Prediction* (Wiley). {3}

HALTINER, G.J. & MARTIN, F.L. 1957 *Dynamical and Physical Meteorology* (McGraw-Hill). {2}

HANNA, S.R. 1969 ESSA Tech. Memo. ERLTM-ARL 8. {2}

HAURWITZ, B. 1935 Beitr. Geophys. 45, 243-267. {1}

HERBERT, D.M. 1965 J. Fluid Mech. 23, 65-75. {3}

HIDE, R. 1968 J. Fluid Mech. 32, 737-764. {1}

HIDE, R., IBBETSON, A. & LIGHTHILL, M.J. 1968 J. Fluid Mech. 32, 251-272. {1}

HOCKNEY, R.W. 1966 Methods Comput. Phys. 9, 135-211. {3}

HOECKER, W.H. 1960 Mon. Weather Rev. 88, 167-180. {3}

KAISER, J.A.C. 1973 J. Atmos. Sci. 30, 950-953. {3}

KAWAGUTI, M. 1961 J. Phys. Soc. Japan 16, 2307-2315. {4}

KAZANSKII, A.B. & MONIN, A.S. 1961 Bull. Acad. Sci. USSR (Geophysics Series) 5, 786-788. {2}

KESSLER, E. 1970 Bull. Amer. Met. Soc. 51, 926-936. {3}

KRAUS, E.B. 1968 Bull. Amer. Met. Soc. 49, 247-253. {2}

KRAUS, E.B. 1972 *Atmosphere-Ocean Interactions* (Oxford Monographs on Meteorology). {2}

KUO, H.L. 1966 J. Atmos. Sci. 23, 25-42. {3}

KUO, H.L. 1967 J. Atmos. Sci. 24, 95-97. {3}

KUO, H.L. 1971 J. Atmos. Sci. 28, 20-41. {1}

LAIKHTMAN, D.L. 1964 *Physics of the Boundary Layer of the Atmosphere* (Israel Program for Scientific Translations). {2}

LAMB, H. 1932 *Hydrodynamics* (Cambridge University Press). {3}

LEAL, L.G. 1973 J. Fluid Mech. 59, 513-535. {4}

LEIBOVICH, S. & RANDALL, J.D. 1972 J. Fluid Mech. 51, 625-635. {3}

LESLIE, L.M. 1971 J. Fluid Mech. 48, 1-21. {3}

LESLIE, L.M., MORTON, B.R. & SMITH R.K. 1970 Quart. J. R. Met. Soc. 96, 544-549. {3}

LESLIE, L.M. & SMITH, R.K. Tellus 22, 288-297. {1,2}

LETTAU, H.H. 1962 Beitr. Phys. Atmos. 35, 195-212. {2}

LEWELLEN, W.S. 1962 J. Fluid Mech. 14, 420-432. {3}

LIGHTHILL, M.J. 1966 J. Fluid Mech. 26, 411-431. {1}

LILLY, D.K. 1965 Mon. Weather Rev. 93, 11-26. {3}

LILLY, D.K. 1969 NCAR Manuscript 69-117. {3}

LONG, R.R. 1956 Quart. J. Mech. Appl. Math. 9, 385-393. {3}

LONG, R.R. 1958 J. Meteorol. 15, 108-112. {3}

LONG, R.R. 1961 J. Fluid Mech. 11, 611-624. {3}

MACDONALD, D.A. 1966 Ph.D. Thesis, University of Manchester. {1}

MACDONALD, D.A. 1970 J. Inst. Math. Applic. 6, 115-130. {1}

MACK, L.M. 1962 Jet Propulsion Lab. Caltech Report 32-224. {1}

MACK, L.M. 1963 Jet Propulsion Lab. Caltech Report 32-366. {1}

MACWILLIAMS, J.C. 1971 Ph.D. Thesis, Harvard University. {1}

MARSHALL, G. & VAN SPIEGEL, E. 1973 J. Engng. Math. 7, 173-188. {4}

MILDNER, P. 1932 Beitr. Phys. frei. Atmos. 19, 151-158. {2}

MILLER, B.I. 1965 Nat. Hurr. Res. Lab. Report 75. {1}

MOFFATT, H.K. 1964 J. Fluid Mech. 18, 1-18. {4}

MOLENKAMP, C.R. 1968 J. Appl. Meteorol. 7, 160-167. {4}

MONIN, A.S. 1970 Ann. Rev. Fluid Mech. 2, 225-250. {2}

MONIN, A.S. & OBHUKOV, A.M. 1954 Trans. Inst. Acad. Sci. USSR (Geophysics Series) No. 24(151), 163-187. {2}

MORTON, B.R. 1966 Progress in Aeronautical Sciences 7, 145-194. {3}

MORTON, B.R. 1969 J. Fluid Mech. 38, 315-333. {3}

MORTON, B.R. 1971 GFDL Paper 36, Monash University. {1}

O'BRIEN, J.J. 1970 J. Atmos. Sci. 27, 1213-1215. {2}

OGURA, M. 1969 J. Met. Soc. Japan 47, 319-323. {3}

OHMSTEDE, W.D. & APPLEBY, J.F. 1964 Met. Res. Note 8, DA Task 1-A-0-11001-B-021-08. USAERDAA-MET-5-64. {2}

OOYAMA, K. 1969 J. Atmos. Sci. 26, 3-40. {1}

OSBORNE, M.R. 1967 SIAM J. Appl. Math. 15, 539-557. {4}

PALMEN, E. & NEWTON, C.W. 1969 *Atmospheric Circulation Systems* (Academic Press). {1}

PAN, F. & ACRIVOS, A. 1967 J. Fluid Mech. 28, 643-655. {4}

PAO, H.P. & LONG, R.R. 1966 Quart. J. Mech. Appl. Math. 19, 1-26. {3}

PAO, H.P. & KAO, T.W. 1969 Phys. Fluids 12, 1536-1546. {3}

PAO, H.P. & SHIH, H.H. 1973 J. Fluid Mech. 57, 459-480. {3}

PEARSON, C.E. 1965 J. Fluid Mech. 21, 611-622. {3,4}

PHILLIPS, N.A. 1959 *The Atmosphere and the Sea in Motion* (Oxford University Press), 501-504. {3}

PLATZMAN, G.W. 1963 Meteor. Monog. 4, No. 26. {3}

PRIESTLEY, C.H.B. 1959 *Turbulent Transfer in the Lower Atmosphere* (University of Chicago Press). {2}

PRITCHARD, W.G. 1970 J. Fluid Mech. 42, 61-83. {3}

RASMUSSEN, H. 1969 GFDL Paper 24, Monash University. {4}

RAYLEIGH, LORD 1916 Proc. Roy. Soc. A93, 148-154. {1}

RICHTMYER, R.D. & MORTON, K.W. 1967 *Difference Methods for Initial-Value Problems* (Wiley Interscience). {3,4}

ROGERS, M.H. & LANCE, G.N. 1960 J. Fluid Mech. 7, 617-631. {3}

ROSENTHAL, S.L. 1962 Nat. Hurr. Res. Proj. Report 56. {1}

ROSENZWEIG, M.L., LEWELLEN, W.S. & ROSS, D.H. 1964 AIAA J. 2, 2127-2134. {3}

ROSSBY, C.-G. 1932 M.I.T. Met. Papers I (No. 4). {2}

ROSSBY, C.-G. & MONTGOMERY, R.B. 1935 M.I.T.-Met. Papers III(No.3). {2}

ROTT, N. 1958 ZAMP 9b, 543-553. {3}

ROTT, N. 1959 ZAMP 10, 73-81. {3}

ROTT, N. & LEWELLEN, W.S. 1966 Progress in Aeronautical Sciences 7, 111-144. {1}

RUNCHAL, A.K. 1972 Int. J. Num. Meth. Engng. 4, 541-550. {4}

RUNCHAL, A.K. & WOLFSHTEIN, M. 1969 J. Mech. Engng. Sci. 11, 445-453. {4}

SERRIN, J. 1972 Phil. Trans. Roy. Soc. A271, 325-360. {3}

SHIH, H.S. & PAO, H.P. 1971 J. Fluid Mech. 49, 509-527. {3}

SMITH, J. 1968 SIAM J. Num. Anal. 5, 323-339. {4}

SMITH, J. 1970 SIAM J. Num. Anal. 7, 104-111. {4}

SMITH, R.C. & SMITH, P. 1965 Tellus 17, 213-219. {1}

SMITH, R.K. 1968 Tellus 20, 473-484. {1,2}

SMITH, R.K. 1969 GFDL Paper 12, Monash University. {1,2}

SULLIVAN, R.D. 1959 J. Aero/Space Sci. 26, 767-768. {3}

SWEET, R. 1973 SIAM J. Num. Anal. 10 (to appear). {3}

TAKAMI, H. & KELLER, H.B. 1969 Phys. Fluids 12, Suppl. II, 51-56. {4}

TAYLOR, G.I. 1915 Phil. Trans. Roy. Soc. A215, 1-26. {2}

TENNEKES, H. 1968 AIAA J. 6, 1735-1740. {2}

TEXTOR, R.E., LICK, D.W. & FARRIS, G.J. 1969 J. Comput. Phys. 4, 258-269. {3,4}

THOM, A. 1933 Proc. Roy. Soc. A141, 651-669. {4}

TORRANCE, K., DAVIS, R., EIKE, K., GILL, P., GUTMAN, D., HSUI, A., LYONS, S. & ZIEN, H. 1972 J. Fluid Mech. 51, 221-231. {4}

TURNER, J.S. 1966 J. Fluid Mech. 25, 377-400. {3}

TURNER, J.S. & LILLY, D.K. 1963 J. Atmos. Sci. 20, 468-471. {3}

VARGA, R.S. 1962 *Matrix Iterative Analysis* (Prentice-Hall). {4}

WAGNER, N.K. 1966 Hawaii Inst. Geophys. Report HIG-66-16, 1-80. {2}

WAN, C.A. & CHANG, C.C. 1972 J. Atmos. Sci. 29, 116-127. {3}

WARD, N.B. 1972 J. Atmos. Sci. 29, 1194-1204. {3}

WILKINS, E.M., SASAKI, Y. & SCHAUSS, R.H. 1971 Mon. Weather Rev. 99, 577-592. {3}

WIPPERMAN, F., BERKOFSKY, L. & SZILLINSKY, A. 1969 Quart. J. R. Met. Soc. 95, 689-702. {3}

YANAI, M. 1964 Rev. Geophys. 2, 367-414. {1}

YING, S.J. & CHANG, C.C. 1970 J. Atmos. Sci. 27, 3-14. {3}

YUDIN, M.I. & SHVETS, M.E. 1940 Trudy Glav. Geofiz. Obs. 31, 42-52. {2}

ZILITINKEVICH, S.S., LAIKHTMAN, D.L. & MONIN, A.S. 1967 Izv. Atmos. Ocean. Phys. 3, 297-333. {2}

BROOKS, E.M. 1951 Compendium of Meteorology, 673-680. {3}